Faculty of Science and Engineering
Department of Petroleum Engineering

Simulations of Hydraulic Fracturing Initiation in Perforated Boreholes

Seyed Hassan Fallahzadeh Abarghooei

This thesis is presented for the Degree of
Doctor of Philosophy
of
Curtin University

December 2015

Declaration

To the best of my knowledge and belief this thesis contains no material previously published by any other person except where due acknowledgment has been made. This thesis contains no material which has been accepted for the award of any other degree or diploma in any university.

Name: Seyed Hassan Fallahzadeh Abarghooei
Signature:
Date: 2 December 2015

Copyright

Name: Seyed Hassan Fallahzadeh Abarghooei
Signature:
Date: 2 December 2015

Abstract

While hydraulic Fracturing becomes most viable stimulation technique to enhance production of oil and gas especially from low permeable unconventional reservoirs, there are many problems associated with the complicated nature of the state of the stresses near a cased hole perforated wellbore. The fracture initiation, propagation, and complex behaviour of fracture geometry are not very well understood in such wellbores. This study has been focused on the understanding of the mechanism, and identification of various causes of these issues through analytical modelling, numerical simulation and experimental studies, particularly in the case of hydraulic fracturing through cased hole perforated wellbore.

In this study a new analytical model is developed to simulate the mechanism of hydraulic fracture initiation from the arbitrarily oriented cased hole perforated wellbores. The developed analytical model is validated against experimental study conducted using a true tri-axial stress cell. The model has the capacity to simulate the stress profile along perforations' tunnel with different orientations analytically, and investigate the near wellbore fracture geometry. Results of this model are presented for different in situ stress regimes, cement and rock properties, perforation orientation and wellbore trajectory parameters. Additionally, the effects of the casing as well as poro-elasticity and thermo-elasticity effects on the wellbore and perforation stress distribution and accordingly fracture initiation mechanism are studied. The developed analytical models are then applied to three different cased perforated wellbores to simulate fracture initiation in theses wellbores and to investigate the reasons of past failed fracturing operation in one of them.

It is demonstrated that the fracture breakdown pressure and hydraulic fracture geometry are significantly impacted by all these considered parameters. Cement sheath micro-annulus creation could be avoided, and less tortuous near wellbore fracture could be created with a relatively lower fracture breakdown pressure, if the optimum wellbore trajectory and perforation orientation is designed. In addition, comparing the analytical elastic approach with uncoupled thermos-poro-elastic methodology, it is demonstrated that fracture initiation pressure reduces as the formation temperature decreases and pore pressure increases.

This research also simulated near wellbore hydraulic fracturing through laboratory experiments and numerical simulations. Scaled hydraulic fracturing tests were conducted on synthetic cubic samples to simulate field representative fracturing mechanisms using a true tri-axial stress cell. Several scenarios of vertical and horizontal wells with different stress regimes were modelled. ABAQUS software was also used to numerically simulate a set of the experiments in order to achieve a better understanding of fracture initiation mechanism. The results of the numerical model showed good agreement with the experimental results. Moreover, three different fracturing fluids with distinct viscosities were considered to investigate the effects of varying fracturing fluid viscosities and fluid injection rates on fracturing mechanism. New parameters, namely fracturing energy and fracturing power are introduced to address the complex behaviour of near wellbore fracture geometry, and effectively interpret the results.

Acknowledgements

This work could not have been completed without the help and support of many individuals during these three years. I would like to express my gratitude to my supervisors Associate Professor Mofazzal Hossain and Professor Vamegh Rasouli for their continuous and timely support towards my project. Their unlimited support and guidance made this project complete. I would also like to express my gratitude to my associate supervisors Dr. Robert Jeffery and Dr Masood Mostofi for their supervision and support. I would like to acknowledge Dr Ali Saeedi, Curtin University Department of Petroleum Engineering, Dr Maxim Lebedev, Curtin University Department of Exploration Geophysics, and Mr Bruce Maney, CSIRO Earth Science and Resource Engineering, for their guidance in running the experimental tests.

It is also my pleasure to thank Professor Brian Evans, the head of Department of Petroleum Engineering, for his constant support during the course of my studies. I would like to express my appreciations to the Department of Petroleum Engineering for providing me with a scholarship towards my PhD studies. I also would like to appreciate the support of all my colleagues and friends at the Department of Petroleum Engineering in various occasions. A very special recognition goes to my friends Dr Amin Chamani, Dr Ahmad Reza Younessi, Dr Mohammad Sarmadivaleh, Dr Mohammadreza Kamyab, Mr Ashton James Cornwell, and Mr Junxian He for their endless supports and helps.

Above all, I praise God who gave me the courage and strength to go through this phase of my life successfully.

To

To my wife Zahra, and our parents for their support, understanding and encouragement.

Preface

The research presented in this thesis is the outcome of more than three years of analytical, laboratory and numerical studies for the purpose of simulating hydraulic fracturing initiation and near wellbore propagation in perforated wellbores. The main objective of this research was to improve the knowledge of fracture initiation mechanism and fracture propagation geometry in perforations' tunnels. Therefore, extensive analytical study was performed to investigate the state of stress distribution around a perforation hole with the consideration of the effects of wellbore inclination and azimuth, perforation orientation, and rock and cement sheath properties. Thereafter, a set of laboratory experiments were conducted to validate the analytical results. Additionally, numerical modelling was utilized to strengthen the validation of both analytical and experimental outcomes. Subsequently the experimental study was further expanded to investigate the effects of casing, fracturing fluid viscosity and flow rate.

Over the course of this study, several papers were published in different journals and conference proceedings. At least two expert reviewers peer-reviewed every paper and their comments were implemented to improve this research. These papers almost cover most parts of this study; however, some other parts are not yet published. Consequently this PhD thesis is presented based on the published papers which are explained briefly in Part I of the thesis report and in more detailed in Part II where the published papers are presented. The sections that have not been published yet are explained in more details in the thesis report (Part I). The following list provides the published papers in the order of their appearance in Part I:

Paper 1 *Fallahzadeh, S. H., and V. Rasouli. "The impact of cement sheath mechanical properties on near wellbore hydraulic fracture initiation." In ISRM International Symposium-EUROCK 2012. International Society for Rock Mechanics, 2012.*

Paper 2 *Gotti, A., S. H. Fallahzadeh, and V. Rasouli. "An experimental study to investigate hydraulic fracture reorientation with respect to the principal stresses." Petroleum and Mineral Resources 81 (2012): 197.*

Paper 3 *Fallahzadeh, S. H., V. Rasouli, and M. Sarmadivaleh. "An investigation*

of hydraulic fracturing initiation and near-wellbore propagation from perforated boreholes in tight formations." Rock Mechanics and Rock Engineering 48, no. 2 (2015): 573-584.

Paper 4 *Fallahzadeh, S. H., V. Rasouli, "Challenges in hydraulic fracturing from perforated boreholes in unconventional reservoirs." Australian Petroleum Production & Exploration Association Journal, 2014.*

Paper 5 *Fallahzadeh, S. H., A. James Cornwell, V. Rasouli, and M. Hossain. "The Impacts of Fracturing Fluid Viscosity and Injection Rate on the Near Wellbore Hydraulic Fracture Propagation in Cased Perforated Wellbores." In 49th US Rock Mechanics/Geomechanics Symposium. American Rock Mechanics Association, 2015.*

At the beginning of each chapter the papers referred to in that chapter are named in the footnote on the first page. In addition, the papers are referred to where needed within each chapter.

Chapter 1 presents an introduction to hydraulic fracturing; more specifically, hydraulic fracturing in cased hole perforated wellbores is discussed and the operation challenges are argued. A review of the past studies in fracturing of perforated wellbores is also presented in this chapter. At the end of this chapter the objectives, framework, methodologies and significance of the research work of this study are summarized.

In Chapter 2, an analytical modelling is developed for studying the mechanism of fracture initiation in a perforation hole. Elastic theory is applied to analyse the stress concentration in the vicinity of a wellbore with arbitrary inclination and azimuth, then a new methodology is introduced to calculate the stress distribution on the surface of a perforation. This perforation stress analysis is performed for the whole length of the perforation hole while the effect of the wellbore stress concentration is superimposed on the perforation stress modelling. Tensile criterion is implemented to study fracture initiation on the surface of the perforation. Next, an iterative numerical method is applied in order to calculate the FIP. In addition, the location and initiation angle of the starter fracture is identified along the perforation hole.

Then in Chapter 3 the analytical model developed in Chapter 2 is further advanced to account for the formation pore pressure and temperature variations. Wellbore and perforation stress distribution equations are modified to adjust the

stress analysis for poro-elasticity and thermo-elasticity effects. Darcy's law is used to model the pore pressure variation, and superposition principal is implemented to include the effect of this pressure variation in the elastic model. As a result, wellbore and perforation general poro-elastic stress analysis equations are derived, which could be used for various wellbore and perforation orientations.

Then the correspondence between thermo-elasticity and poro-elasticity is used to derive perforation stress equations which account for formation temperature variations. Next, the numerical method presented in Chapter 2 is applied to study perforation fracture initiation using the developed poro-elastic and thermo-elastic models. Various aspects and results of the developed models are presented in the rest of the chapter.

In Chapter 4, some field case studies using the analytical models developed in Chapter 2 and Chapter 3 are presented. Required input parameters are obtained from several raw field data and then applied to the developed models to simulate the fracture initiation mechanism in three different wellbores (wells A, B and C). These cased perforated wells are selected from Ahwaz oil field, which is located in Iran.

The results of several series of scaled fracturing experiments are presented in Chapter 5. In the first series of experiments, two parallel notches were created in the borehole of each sample to simulate the perforations. In the second series of experiments, various scenarios of vertical and horizontal wells and in situ stress regimes were modelled in perforated borehole. It is noteworthy that some of the tests performed in the second set were conducted for the purpose of validating the analytical model (see Section 2.5.2). Furthermore, the initiation of hydraulic fracturing from a perforated tunnel was studied numerically using a finite element method. The numerical model was generated to represent a laboratory experimental test, which has been carried out on tight concrete cubic samples. And, in the last series of the experiments, three different fracturing fluids were used to investigate the effects of varying fracturing fluid viscosities and fluid injection rates on fracturing mechanism in cased perforated wellbores.

Contents

List of Figures

List of Tables

1 Introduction and literature review

In this chapter an introduction to hydraulic fracturing is presented; more specifically, hydraulic fracturing in cased hole perforated wellbores is discussed and the operation challenges are argued. A review of the past studies in fracturing of perforated wellbores is also presented in this chapter. At the end of this chapter the objectives, framework, methodologies and significance of the research work of this study are summarized.

1.1 Introduction

Hydraulic fracturing has played a key role in developing oil and gas underground resources since 1947. It has been primarily used as an effective stimulation technique to create a high permeable conduit in the pay zone in order to increase the production of oil and gas. The recovery of unconventional resources has introduced a new and motivating source of energy for future supply all around the world and specifically in Australia.

In recent years, hydrocarbon production from shale gas and shale oil has exponentially increased in many countries. U.S. Energy Information Administration (EIA) has estimated that Australia is technically capable of producing almost 20 billion barrels of shale oil from its underground shale formations (Figure 1-1). In the U.S., tight oil production has increased to 4.3% of total crude oil production by the fourth quarter of 2013 (U.S. EIA). In addition, shale gas production is also becoming increasingly vital to gas production all over the world. Based on the U.S. EIA estimation, Australia could be among the top countries in shale gas production by having 11.2 trillion cubic meters of shale gas reserves. The U.S. EIA has also predicted that by development of shale gas resources over the next decades, shale gas recovery may contribute to 50% of U.S. dry gas production in 2040.

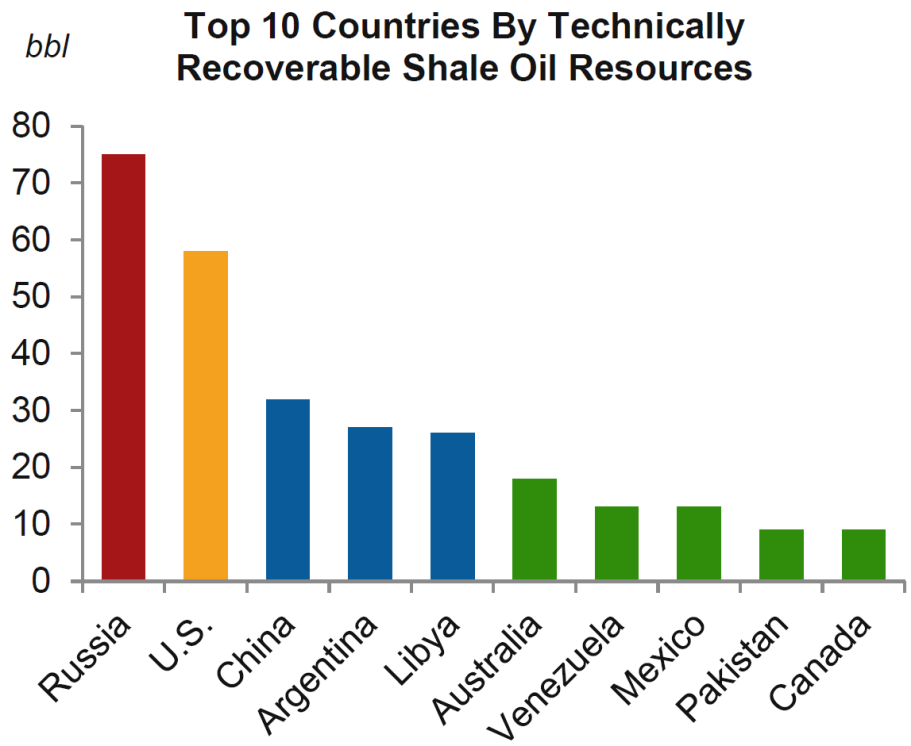

Figure 1-1 Recoverable shale oil resources in billion barrels for top 10 Countries (U.S. Energy Information Administration, 2013).
(http://www.eia.gov/conference/2014/pdf/presentations/webster.pdf).

Based on some recent studies, it has been found that unconventional oil and gas basins have been continuously discovered more and more in many countries (Figure 1-1). Russia has the largest recoverable unconventional oil resources of about 75 billion barrels, and the United State, which is ranked as the second country in shale oil reservoirs, could technically recover about 60 billion barrels of oil from these resources. The predicted unconventional gas reserve in United States is 861.7 Tcft (trillion cubic feet), China is forecasted to have 1274.3 Tcft, and Argentina 773.1 Tcft. Therefore, unconventional oil and gas will continue to have an important role in supplying the world's energy demands.

Since unconventional reservoirs generally consist of very low-permeable formations, hydrocarbon flow rate is normally very low in these formations. Therefore, it is vitally important to increase the wellbore and formation contact area by drilling deviated and horizontal wellbores (Fisher et al., 2004; Wiley et al., 2004), and apply a proper stimulation method in order to increase the productivity of these reservoirs and accordingly increase the production rate. Over the past few decades, it has been realized that hydraulic fracturing is the sole method to make it economically worthwhile to produce form low-permeable formations such as shale gas and tight

sandstones (Britt et al., 2006; Valk & Economides, 1995; Waters et al., 2009; Watson et al., 2008).

Deviated and horizontal drilling methodologies are used frequently all over the world to improve the oil and gas production from the formations which are not possible to recover effectively by vertical boreholes. Most of these drilling operations are then completed by a cemented casing across the pay zone, and consequently they are perforated to create a pathway between the borehole and the formation. The presence of the casing, cement sheath, and the perforation holes along with the deviated trajectory of the wellbore significantly impact the stress distribution around the wellbore. As a result, the process of hydraulic fracturing initiation and near wellbore propagation will be relatively complex in such wellbores, in comparison to an open hole (Alekseenko et al., 2012; Atkinson & Eftaxiopoulos, 2002; Behrmann & Nolte, 1999; Hossain et al., 2000; J Romero et al., 1995; Weng, 1993). Consequently, it is essentially important to accurately understand and analyse the process of hydraulic fracturing in unconventional formations, and particularly in deviated cased hole perforated wellbores.

Therefore, this research was conducted in order to expand the knowledge of fracture initiation and near wellbore propagation in such wellbores. Elastic, poro-elastic and thermo-elastic analytical models were developed to simulate the stress profile along perforations' tunnel with different orientations, and investigate the near wellbore fracture geometry. Results of this model are presented for different in situ stress regimes, cement, casing and rock properties, perforation orientation and wellbore trajectory parameters. The developed model is capable of investigating the optimum wellbore trajectory and perforation orientation as well as identifying the best cement properties to minimize the near wellbore fracture challenges.

In addition, scaled hydraulic fracturing tests were conducted on tight cubic samples to simulate field representative fracturing mechanisms using a true tri-axial stress cell. Several scenarios of vertical and horizontal wells with different stress regimes were studied. ABAQUS software was also used to numerically simulate a set of the experiments; the experimental results showed good agreement with the numerical and analytical models. Moreover, the effects of varying fracturing fluid viscosities and injection rates on fracturing mechanism were studied. As a result, new parameters, namely fracturing energy and fracturing power are introduced to address the complex behaviour of near wellbore fracture geometry.

1.2 Hydraulic fracturing overview

The first Hydraulic fracturing operation took place during the 1930's when an American company called Dow Chemical increased the downhole pressure in an acidizing operation, and consequently the formation rock was fractured and finally a more efficient reservoir stimulation was resulted. In 1947, a gas well in Kansas was stimulated by the first hydraulic fracturing operation, which was done using fluids other than acid, in order to compare it with oxidization technology (Veatch Jr et al., 1989). Currently, hydraulic fracturing is being operated extensively to improve the productivity of oil and gas wells, particularly in tight reservoirs. Hydraulic fracturing has been used for several applications other than tight formations too. It has been implemented to stimulate a wide variety of different geological formation including weakly consolidated sandstones, naturally fractured carbonate layers, lenticular and coal bed methane resources (Adachi et al., 2007). In addition, it has been widely used in geothermal energy extraction and waste disposal applications (Berumen et al., 2000; Hainey et al., 1999). Also it has been applied in mining and geotechnics industry for in-situ stress measurement, fault reactivation, and remediation projects for underground water aquifers (Hayashi & Haimson, 1991; Murdoch & Slack, 2002; Raaen et al., 2001).

1.2.1 The process of hydraulic fracturing

A hydraulic fracture operation consists of several stages. In a cased wellbore, initially a series of perforations are made into the casing and through the cement sheath and formation rock in order to create a pathway for the fracturing fluid to initiate fractures in the formation. Then a viscous fluid, generally termed as, "pad fluid", is pumped downhole with a predesigned flow rate so that the bottom hole pressure and simultaneously the perforations' pressure increases to a specific level at which the first cracks are initiated in the perforations (Veatch Jr et al., 1989). Until this point, which is called fracture initiation pressure (FIP), the wellbore pressurization rate is almost constant; and as the very first cracks initiate, the pressurization rate decreases while the wellbore pressure is still increasing (Figure 1-2). Once the maximum wellbore pressure is reached, which is known as fracture break down pressure (FBP), some major fracture(s) will be formed in the formation and accordingly the wellbore pressure will decrease. Since the formations are always porous, there is always some fluid dissipation into the porous rock or natural fractures and fissures; therefore, the fluid injection flow

rate should be enough high to compensate for these fluid losses and build up the bottom hole pressure to FBP (Wong et al., 1993).

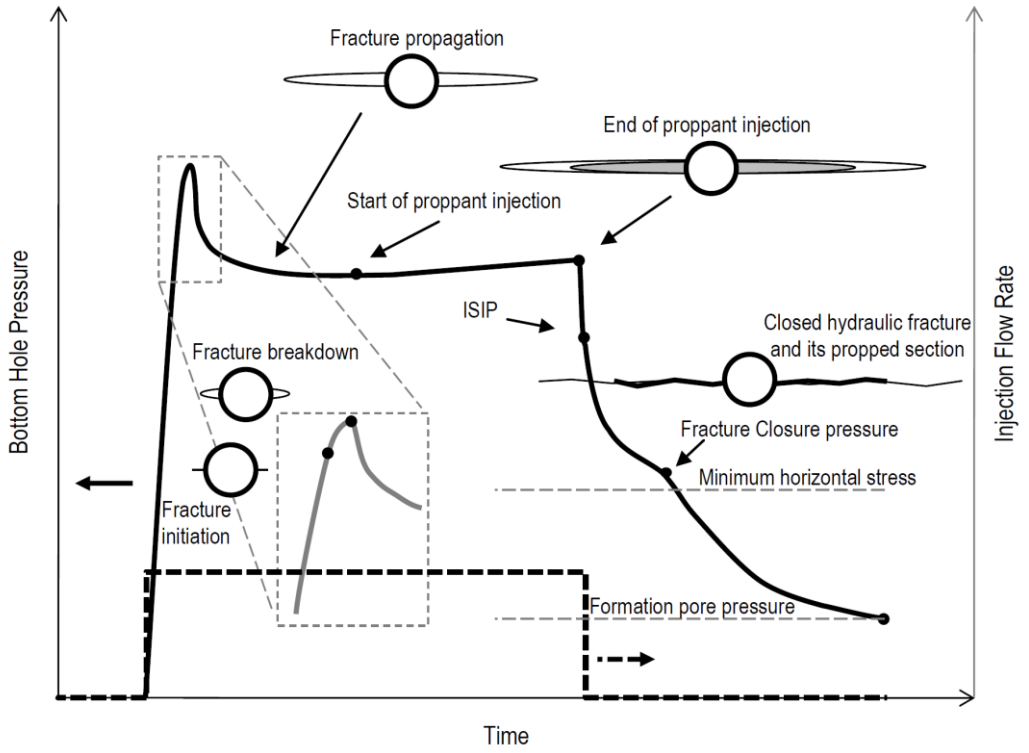

Figure 1-2 A schematic of typical fracturing operation pressure curve (Sarmadivaleh, 2012)

After the breakdown point, the fracture(s) will grow in the formation rock away from the wellbore and perforations, and consequently the wellbore pressure decreases. This is because some new volume is being developed, and therefore, the pressurized fracturing fluid expands into the newly developed fractures resulting in wellbore pressure reduction (S. Fallahzadeh et al., 2015). However, the wellbore pressure reaches to an almost stabilized pressure called fracture propagation pressure (FPP), when the fracture keeps growing and propagating into the formation (see Figure 1-2).

In the next stage, proppant slurry is injected after the pad fluid. This slurry is prepared by mixing some vicious fluid with sorted high strength granular particles such as sand, which are known as proppants. As the proppant slurry is injected, the hydraulic fracture continues to propagate and at the same time the proppant grains are transported into the created fracture. The slurry may be pumped into the wellbore in several continuous batches with different proppant concentrations; this is to ensure that proppants are placed at the right location inside the fracture. The final slurry batch may contain the highest proppant concentration (Veatch Jr et al., 1989).

As it is depicted in Figure 1-2, where a schematic of typical fracturing operation pressure curve is shown, FIP, FBP, and FPP are among the main fracturing operation parameters. All these pressures are larger than the formation pore pressure and minimum in-situ stress component, since the main body of the fracture is generally propagated perpendicular to this stress direction as there is least resistance for the fracture to grow in such direction (Ali Daneshy, 2004). Typically, the underground petroleum reservoirs are quite deep so that the minimum in-situ stress is in horizontal direction, resulting in a vertical hydraulic fracture. However, the fracture growth should be constrained to the boundary of the petroleum bearing layer.

Accordingly, there is some other important pressure parameter in a hydraulic fracturing operation known as containment pressure which reflects the mechanical ability of the upper and lower formations to prevent the fracture propagating into these formations. It is not generally an easy task to predict all these fracturing-related pressures, since many other parameters significantly influence these pressures. The main influencing parameters include, but not limited to wellbore and perforations' orientations, casing, cement and rock mechanical and elastic properties, characteristics of natural fractures, pore pressure and in-situ stresses (S. H. Fallahzadeh et al., 2013; M. Sarmadivaleh & Rasouli, 2010; Weijers, 1995).

The fracture generally continues to grow until the time at which either fluid leak off becomes almost equal to the injection flow rate or the injection stops. Once the fluid injection stops, the bottom hole pressure drops suddenly to a point known as instantaneous shut in pressure (ISIP), as shown in Figure 1-2. This sudden reduction in pressure is due to the fact that by stopping the injection flow rate, the fluid flow through fracture stops and accordingly the frictional pressure loss will be eliminated, resulting in abrupt pressure reduction. Then the remaining fluid inside the fracture will continue leaking off, and consequently the fracture closes as the pressure is reducing by fluid dissipation. This will approach a point at which the fracture pressure would become equal to the minimum in-situ stress, and as the dissipation continues, the fracture pressure reduces to formation pore pressure.

As the fracture closes down by the pressure reduction, the high strength proppants would prevent the fracture from being closed completely and therefor, providing a high permeable conduit. Also the remaining slurry fluid chemically breaks down, normally due to high formation temperature, and therefore its viscosity reduces. As a result, once the wellbore is put on production by lowering the bottom hole pressure,

the remaining slurry fluid will flow back along with hydrocarbon. Consequently, a high permeable and conductive propped fracture will be left for the oil and gas to flow through (Veatch Jr et al., 1989).

This high permeable fracture might be very narrow but it could be quite long depending on the design of the fracturing operation. On average, a hydraulic fracture may have a width of about 0.25 inch or even less; however, the fracture length could be 1500 ft on one wing. And in terms of time-scale, a hydraulic fracturing treatment could be operated within tens of minutes or a few hours, depending on the size and geometry of the fracture and the volume of the fluids and slurry that should be injected. A successful hydraulic fracturing stimulation could improve the production flow rate several times, and additionally could increase the ultimate reservoir production.

1.3 Hydraulic fracturing in cased wellbores

Generally, the main objective of hydraulic fracturing and most of other stimulation techniques is to improve the wellbore and reservoir communication through creating a high conductive flow pathway between the reservoir rock and the wellbore. However, the implication of such a technique in perforated boreholes is still a challenging subject due to the complexity of parameters involved in this operation. When performing a hydraulic fracturing operation in a cased perforated wellbore, many problems may arise such as micro-annulus creation, near wellbore fracture tortuosity, and multiple fracturing. These problems may lead to high frictional pressure loss near the wellbore, and consequently would result in significant increase in the operating pressures, and may eventually cause premature screen outs (Aud et al., 1994; Cleary et al., 1993; A. A. Daneshy, 2011; Davidson et al., 1993).

Additionally, because of some near wellbore problems, a complex conduit develops around the perforations, connecting the wellbore to the main part of the fracture. Several different fracture geometries may be created in this complicated conduit, which may eventually result in premature screen out. Many multiple fracturing and near wellbore fracture tortuosity have been encountered during the implication of the hydraulic fracturing operation in cased hole perforated completions (Cipolla et al., 2008; Lehman & Brumley, 1997; Narendran, 1983). Such complex near wellbore fracture geometry significantly increases the fracturing fluid

frictional pressure loss. Moreover, multiple and tortuous fractures, which are developed around the perforations, typically have a narrower width with respect to the main body of the fracture. This is mainly due to higher stress concentration around a cased perforated wellbore. The narrow width of the fractures may prevent the proppant slurry to flow through easily, and this may eventually result in low proppant concentration in the main body of the fracture (Cleary et al., 1993).

The quality of a hydraulic fracturing operation could be negatively impacted by these issues, and consequently the fracturing treatment may not improve the production of the wellbore effectively. Such kinds of challenges are mainly due to the existence of the perforations cavities which complicate the fracture initiation and near wellbore propagation (Abass et al., 1994; Behrmann & Elbel, 1991; Guangqing & Mian, 2009). The presence of the perforations' holes considerably affect the near wellbore stress profile, and accordingly the fracturing mechanism is significantly impacted. There are several other parameters that may restrict the hydraulic fracturing treatment in establishment of an effective wellbore and reservoir connection. The existence of the steel casing along with cement sheath, which is filling the annulus between the casing and the wellbore, could also greatly influence the stress distribution around the wellbore and thereby impact the fracture initiation and near wellbore propagation (S. Fallahzadeh & Rasouli, 2012). In addition, the deviation of the wellbore could impact the FIP and near wellbore fracturing mechanism (Chen & Economides, 1995; Soliman, 1990). These impacting parameters are all interrelated and one may influence the other one and cause a more complicated issue. Therefore, a strong knowledge of all these major parameters could improve the quality of a hydraulic fracturing operation.

Many researchers have tried to analyse and model the mechanism of hydraulic fracturing operation in cased perforated wellbores. Numerical simulations, analytical solutions and experimental studies have been proposed and performed in the past to understand and mitigate the fracture initiation and near wellbore propagations' challenges. Additionally, field operational procedures have been designed and implemented in order to reduce the high treatment pressures and thereby prevent screen outs. In the following sections, a summary of the main previous studies, available in the open literature, is presented; the strengths and weaknesses of each study are analysed. And accordingly, appropriate research objectives, methodologies

and strategies are proposed in order to further expand the knowledge of hydraulic fracturing in cased hole perforated wellbores.

1.4 Literature review

As it is mentioned earlier in this chapter, hydraulic fracturing consists of four main steps:

- Fracture initiation and breakdown,
- propagation of the fracture,
- laden proppants to keep the fracture open,
- flow back & production.

Various studies have been performed to understand different parts of hydraulic fracturing and consequently some models (both 2D & 3D) have been developed for designing a hydraulic fracturing operation. Generally these models predict the fracture propagation pressure as well as fracture shape/geometry, while they are not able to accurately estimate the fracture initiation and break down pressures. In addition, such models generally do not consider the near wellbore propagation and its complex geometry, since they normally assume that a symmetric bi-wing planar fracture initiates directly from the wellbore and perforations (Economides, 2000; C. H. Yew & Weng, 2014).

Therefore, many studies have been done in order to provide some new insight into this complex problem, so that the fracturing simulators could be modified by incorporating the fracture initiation and near wellbore propagation (Alekseenko et al., 2012; Hossain et al., 2000; Van Ketterij & De Pater, 1999). Reviewing the past studies would better clarify the statement of the problem, and would help proposing effective research methodologies. It is quite valuable to study the field scale researches in the first stage, since the actual geometry and complexity of the problem could be identified. Field studies typically conclude with suggesting some practical techniques to mitigate the operational challenges. In the next stage numerical, experimental and analytical studies could be reviewed to understand the problem in more depth.

Typically, numerical models are adjusted via obtaining a reasonable match with field or experimental data. Then the adjusted model could be used to study the effects of various parameters on the FIP, for example. However, dimensional analysis is

required to be carried out for the experimental part of the study, so that the main impacting parameters could be scaled down to laboratory scale and accordingly these parameters could be studied systematically. Otherwise, the experimental results and its corresponding numerical analysis could not be rationally compared with field data. In fact, dimensional analysis provides some scaling laws that make it plausible to study field scale physical phenomena in the laboratory environment. Fracturing scaling analysis concept will be briefly presented in this chapter along with a review of the past experimental as well as analytical studies.

Analytical solutions are typically based on several simplifying assumptions, for instance, the formation rock may be considered as a non-porous elastic material and some specific fracture geometries may be assumed to develop an analytical model. However, such models are very useful for performing sensitivity analysis to investigate the effect of various parameters, and also comparison purposes. A review of previously developed analytical solutions, numerical models, experimental attempts as well as field data interpretation studies are presented in the next sections of this chapter.

1.4.1 Field studies

Abnormally high downhole pressures have been recorded in the first step of hydraulic fracturing, which is fracture initiation and formation break down; followed also by high treating pressure for the propagation of the fracture around the wellbore. Such high treating pressures are more encountered in fracturing operations of deviated wellbores and particularly where the perforations are either not adequate or not designed properly. Several field studies have been carried out to analyse the influence of near wellbore fracturing mechanism on the overall success of the hydraulic fracturing operations, and accordingly some operational procedures were suggested to reduce the high treating pressures and prevent screen outs (Aud et al., 1994; Cleary et al., 1993; Stadulis, 1995). High fracture initiation and near wellbore propagation pressures are generally supposed to be directly related to the perforations, which provide a communication pathway from the wellbore to the formation rock. The misalignment of the perforations may lead to fracture turning and twisting (tortuosity) and micro-annulus creation as well as multiple fracturing, which eventually result in high fracturing pressure (Cherny et al., 2009; J Romero et al., 1995; Stadulis, 1995).

Several studies have reported field observations in vertical and deviated cased wellbore to study the effects of perforation orientation on the hydraulic fracturing operation. Pearson et al. (1992) presented a field study and stated that the key parameters for a proper perforation design are the size, number, phasing, and orientation of the perforations. They also indicated that the main goal of perforation design for a fracturing treatment is to control and minimize the perforation friction pressure loss over the course of the fracturing operation. The results of one of the first applications of stress-oriented perforating of deviated wellbores at Kuparuk River field, Alaska is analysed in this study. Perforation parameters are designed for each wellbore in a way that starter fractures from each perforation is promoted to join other fractures and form a single main fracture along the wellbore wall. This study concluded that aligned perforation strategy could greatly reduce the perforation pressure loss, allowing the development of a larger far field fracture with higher productivity.

Venditto et al. (1993) pointed out an increase of 500 psi in the break down pressure for a wellbore in which the perforations were 90 degrees off the direction of the main body of the fracture. This pressure increases was reported in comparison to some other wellbore at which the perforations were aligned with the direction of the preferred fracture plane. Pearson et al. (1992) also reported that the perforation pressure friction loss was significantly reduced when the wellbore was perforated along its tensile zone; the tensile zone was obtained using the starter fracture link-up concept which was based on the elastic theory. They also stated that larger fractures were developed as a result of having the perforations within the tensile zone.

Cleary et al. (1993) investigated the fracture tortuosity around the wellbore and proposed some field procedures to mitigate the negative impacts a tortuous near wellbore fracture may have on the overall fracturing treatment. They analysed the injection of what they called “proppant slug” in the near wellbore area along with some immediate injection shut-ins. Accordingly, they concluded that by implementing the proppant slugs, some near wellbore fracture tortuosity can be eliminated, and therefore, the response of the fracture around the wellbore can be better characterized. This would, in turn, help to more accurately determine the behaviour of the far field fracture-reservoir response.

Aud et al. (1994) proposed that the main cause for low effectiveness of most hydraulic fracturing treatments is due to improper placement of the proppants, and

this is mainly because of complex fracture geometry around the wellbore. They analysed some fracturing field data in order to understand the impacts of near wellbore fracture geometry on the overall success of hydraulic fracturing operation and the proper transportation and placement of the proppants. As a result, they suggested using more viscous fluids to initiate the fracture in the near wellbore area, and thereby improving the geometry of the fracture in this region. Additionally, they discussed that a more viscous carrying fluid could improve the proppant transportation through the near wellbore fracture and could eventually prevent screen out and improve the final placement of the proppants. However, high viscous fracturing fluid may increase the overall frictional pressure loss significantly, especially through the tortuous part of the fracture, up to a point which may exceed the pumping pressure rating. Additionally, the authors did not theoretically address the mechanism of tortuous fracture development around the wellbore.

Stadulis (1995) also studied fracturing screen outs in three different oil and gas fields in Texas and Oklahoma. He found that the main cause of these screen outs were the near wellbore multiple fractures. Therefore, he proposed a completion design in order to reduce the chance of creating multiple fractures. This design consisted of a set of un-oriented zero-degree phased perforations with some specific shots that create big holes on one side of the wellbore. And then he suggested injecting several batches of high concentration proppant slugs and cleaning spacer in the early stage of the hydraulic fracturing operation. The proppant slugs may stop the propagation of several small fractures and promote the development of a main fracture; however, the idea of un-oriented perforation may not be very appropriate; since the perforations may be formed not along the preferred fracture plane, resulting in creation of a much curved narrow fracture around the wellbore.

Several methods of mitigating pinching effects were suggested by (Gulrajani & Romero, 1996) to practically prevent or mitigate problems related to the near-wellbore fracture tortuosity. They have discussed that when there is a risk of multiple fracture development, high concentration slugs of small size proppant can be used to plug small fractures. Also, low concentration slugs may be applied to erode the perforation channels and initial fracture and thus remove pinching. Based on step-rate or constant rate test they also discussed how to assess the presence of near-wellbore (NWB) problems (tortuosity or bad perforation), and their results were compared with the treatment decline analysis and theoretical estimations.

Based on the study done by McDaniel et al. (2001), casing-hole entry problems, perforation tunnel entry problems, fracture plane twisting, and multiple fractures accepting fluid are among the main NWB issues in hydraulic fracturing initiation. They tried to understand various practical methods for reducing the risks associated with NWB problems. Based on the field case analysis, they mentioned that the method most frequently used to mitigate NWB issues (proppant slug and gel slug) does not always give expected results. The best method is first to recognize the type of NWB problem, and then applying proppant or gel slugs, or basically modifying the completion of the wellbore by re-perforating the well in order to mitigate the NWB problems.

By reviewing these field observations it can be generally concluded that the near wellbore fracture complexity could be remedied using higher viscous fracturing fluids and high concentration proppant slugs. There is typically a routine practice in the industry to initially inject a fluid stage in order to break down the formation and measure the perforation pressure loss; this also examines whether there is enough connection between the wellbore and the formation to operate the main fracturing treatment (Gidley, 1989; Hallam & Last, 1991). However, it should be practically possible to inject such fluids and proppant slurries, since pumping these fluids may significantly increase the treating pressure.

It is also noteworthy that multiple fracturing may happen in naturally fractured formations, where the shear slippage of the natural cracks and the offsetting of the hydraulic fracture could lead to fracture complexity (Murphy & Fehler, 1986). Nevertheless, multiple fracturing is quite rare in the far field fracture in isotropic and homogeneous formations (Freund, 1998; Valk & Economides, 1995). Although fracture branching is not desirable from the fracturing point of view, it may increase the reservoir productivity locally (Cipolla et al., 2008).

1.4.2 Laboratory experimental studies

Several investigators have experimentally studied the fracture initiation mechanisms in both open and cased vertical and deviated wellbores. Some experimental studies showed that when the perforations are directed almost close to the proposed fracture plane, which is vertical to the direction of minimum in-situ stress, the starter fractures will be initiated from the perforations (Behrmann & Elbel, 1991; Abbas Daneshy, 1973). Other studies stated that non-planar or s-shaped fractures may initiate and propagate around the wellbore when the wellbore is deviated and the perforations are not oriented along the direction of main fracture body (El Rabaa,

1989; Weijers, 1995). However, the near wellbore fracture geometry is such complicated that it is very difficult to predict the frictional pressure loss in this part of the fracture.

The first experimental study investigating the impacts of perforation on hydraulic fracturing was done by Abbas Daneshy (1973). He prepared cubic samples with hydrostone (gypsum cement) and placed a steel casing at the centre of each sample while molding the perforations. After running his hydraulic fracturing experiments, he found that fracture break down pressure decreases by increasing the number of perforations. In addition, he concluded that the presence of the casing and perforation do not affect the direction of the far field fracture propagation, since he observed that in several samples the fracturing fluid flowed from the perforations through an annulus behind the casing to initiate a fracture perpendicular to the direction of the minimum stress. Several other studies also showed that the orientation of the perforations should be along a plane, where the main body of the fracture is anticipated to be developed (Behrmann & Elbel, 1991; El Rabaa, 1989; Hallam & Last, 1991; King, 1989).

Similar results have also been reported by Abass et al. (1994). In their study, laboratory experiments were carried out on shale and hydrostone samples to investigate the effect of perforation orientation on hydraulic fracturing operations in vertical and horizontal wellbores. The application of oriented perforation for mitigating sand production is also discussed in this study. They found that in vertical wells, lower fracture break down pressure and wider fractures could be achieved, if the perforations are oriented in the direction of maximum horizontal stress. They also stated that multiple fracturing could be avoided in vertical wellbores when the perforations are oriented appropriately. Moreover, for horizontal wellbores, they concluded that the use of gravity oriented clustered perforations is the best strategy to eliminate the near wellbore multiple fracturing.

Behrmann and Nolte (1999) also conducted an experimental study and found that when the perforation gun orientation is not properly selected or when the directions of the in-situ stresses are not accurately known, the width of the fracture near the wellbore would be mostly less than that of the main body of the fracture. This is due to the fact that the magnitudes of induced stresses are larger near the wellbore compared to in-situ stresses. Almost the same results were obtained through a theoretical and numerical investigation conducted by Jean Romero et al. (2000). In

another experimental study done by Behrmann and Elbel (1991), they recognised that there are three major factors influencing the fracturing mechanism in cased holes; formation pore-pressure, pressurisation of the annulus, and perforation orientation in relation to the preferred fracture plane (PFP) (the minimum in-situ stress is perpendicular to this plane). In their experiments, they observed that when the perforation phasing was deviated more than 10° away from the direction of the PFP, the fracture plane may not initiate from the perforations and the fracturing fluid would break down the cement sheath behind the casing, which in turn results in the formation of a pinch point.

In addition to the orientation of the perforation, the frictional pressure loss inside the perforation hole may also affect the fracturing treatment pressure. Crump and Conway (1988) analysed field and laboratory data to calculate the perforation entry friction loss in order to evaluate its effect on the fracturing treatment design. They stated that when the perforations are properly sized and oriented, the impact of the perforation friction could be typically insignificant. Otherwise, a constant pressure loss may be considered for the perforations that could be calculated through the following equation;

$$\Delta P_{perf} = 0.2369 \frac{q^2 \rho}{n^2 \, d^4 \, C^2} \tag{1.1}$$

where q is the total flow rate, ρ is the density of the fracturing fluid, n is the number of perforations, d is the perforation diameter, and C is called discharge coefficient. The authors indicated that the perforation friction pressure loss may vary significantly due to the erosion that may be caused by the passage of the proppant slurry. When proppant slurry is injected at high differential pressure through the perforations, it enlarges the diameter and erodes the entrance of the perforations, resulting in an increase in the discharge coefficient as shown in Figure 1-3.

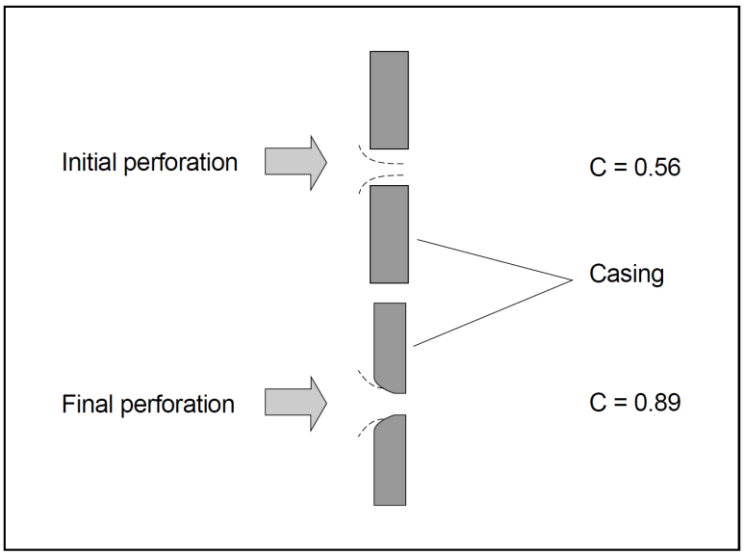

Figure 1-3 Erosion of the entrance of the perforations by passage of proppant slurry (Crump & Conway, 1988).

The rate of perforation erosion increases in smaller perforations when higher concentrated proppant slurries are pumped at higher differential pressure. The authors of this study showed that the perforation erosion may cause misinterpretation of the true bottom hole pressure during a fracturing operation; therefore, they presented some guidelines to help indicating when to modify the pumping schedules according to proppant perforation erosion. The effect of perforation friction becomes more critical when the fracture is propagating, and large volume of fluid is pumped through the perforations. However, in the initiation phase of the hydraulic fracturing, one may ignore this effect, because the flowrate of fracturing fluid in this stage is not significant.

1.4.3 Scaling analysis

As it is briefly presented in the previous section, several experimental studies have been carried out in order to physically model and analyse the mechanism of fracture development in perforated boreholes (Abass et al., 1994; Behrmann & Elbel, 1991; Abbas Daneshy, 1973; El Rabaa, 1989; Hallam & Last, 1991); however they have not scaled down the real field fracturing processes to experimental test samples. These sets of experimental research could have been greatly improved by the application of proper scaling analysis.

In order to have a reasonable correspondence between the results of lab experiments to field scale operations, dimensional analyses should be performed which are known as scaling laws. The scaling laws discuss various fracture

propagation regimes, which consist of the main fracturing mechanisms. The energy of fracturing dissipates through different mechanisms. At each specified time, the main dissipating mechanism is the fracturing propagation regime. In fact, an infinite number of mechanisms may be considered for each fracturing case; however, the main dissipation mechanism is considered for the propagation mechanism (Bunger, 2005). For designing a laboratory hydraulic fracturing experiment, the injection rate, fluid viscosity, and the total fracture propagation time must be obtained from the scaling analysis. By knowing the sizes of the sample and the wellbore, and also sample hydro-mechanical properties, one would be able to calculate the required viscosity, flow rate, and injection time for running a hydraulic fracturing test.

Basically the initiation and propagation of a real fracture in the field can generally be considered under the influence of three extreme boundaries of viscosity, toughness, and leak-off-dominated propagation regimes (Bunger, 2005). In field fracturing operations, during the initiation phase the fracture development is toughness-dominated; however, it becomes viscous-dominated quickly (Mack & Warpinski, 2000), and for a radial fracture, it becomes once more toughness dominated at the final stage of fracture extension (Detournay, 2004).

Van Ketterij and De Pater (1999) were probably the first researchers that developed and implemented the scaling laws in their fracturing experiments. They investigated the effects of perforation phasing and orientation on fracturing pressure. The experiments were scaled based on the study done by De Pater et al. (1994), and the sample material had very low permeability and fracture toughness. This study was carried out to investigate the relation between the cased perforated completions and the fracturing treatment parameters in deviated wellbores; nevertheless, only a deviated wellbore with an azimuth of 60° from the preferred fracture plane and an inclination angle of 49° was modelled. Additionally, special instruments were mounted on the external wall of the casing to indicate if fracturing fluid made a channel behind the casing.

The authors observed that, when the perforation phasing is 90°, mostly the perforations on top section of the borehole were initially fractured; however, in this phasing arrangement, the link-up of the initiated fractures was hampered, since the spacing between the perforations increases in 90° phasing. On the other hand, it was observed that when perforation phasing was 180°, more started fractures linked up to develop one single larger fracture, as the perforations' spacing was smaller in this

case. It was also concluded that when the initiation pressure increases, the possibility of fracture link-up also increases. Higher initiation pressures were achieved by increasing the product of fracturing fluid viscosity and flow rate.

1.4.4 Numerical simulations

Generally, there are two main reasons for analysing the fracture initiation and near wellbore propagation. Firstly, to understand the complexity of the fracture around the wellbore; so that methodologies could be proposed to prevent and eliminate the near wellbore causes of screen outs. And secondly, to estimate the total near wellbore pressure loss, in order to deduct it from the total fracturing pressure; therefore, the net fracturing pressure could be analysed to characterize the geometry of the far field fracture. It is noteworthy that the high FIP and the complicated near wellbore fracture geometry may not have any significant influence on the main body of the fracture, if the high treating pressures could be supplied by the pumping equipment and the proppants could be properly place at the right position within the fracture body. In contrary, the geometry of the main body of the fracture may be adversely impacted by the fracture tip effects (Economides, 2000).

Jean Romero et al. (2000) performed numerical fracture simulations considering three probable near wellbore pressure loss mechanisms, namely perforation pressure drop, perforation phasing misalignment and fracture reorientation (tortuosity). They have stated that these pressure losses are additive;

$$\Delta P_{near\ wellbor} = \Delta P_{perforation} + \Delta P_{tortuosity} + \Delta P_{misalignment} \quad (1.2)$$

They specified typical signs of these three main pressure loss sources in the fracturing pressure records, and proposed some methodologies in order to differentiate them. They pointed out that fracture tortuosity defines a convoluted conduit connecting the far field fracture to the wellbore. Figure 1-4 shows a schematic of a tortuous fracture in the vicinity of a deviated wellbore. As it is seen from this figure, the initiated fracture from the wellbore wall has turned and twisted to become aligned with the direction of preferred fracture plane. It is noteworthy that Figure 1-4 is depicting the tortuous fracture for an open hole, where the fracturing fluid has access to whole circumference of the wellbore and could initiate the fracture wherever more tensile stress exists. However, when the deviated wellbore is cased, cemented and perforated, the near wellbore fracture could be more

complicated, since the fracturing fluid has access to the formation rock only through the perforations, and this may result in the creation of narrower width fractures.

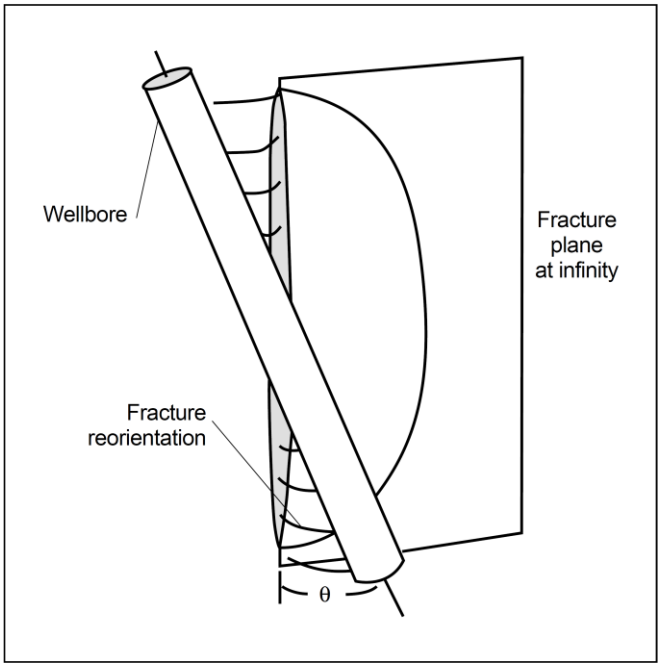

Figure 1-4 Fracture tortuosity around a deviated wellbore (Economides, 2000).

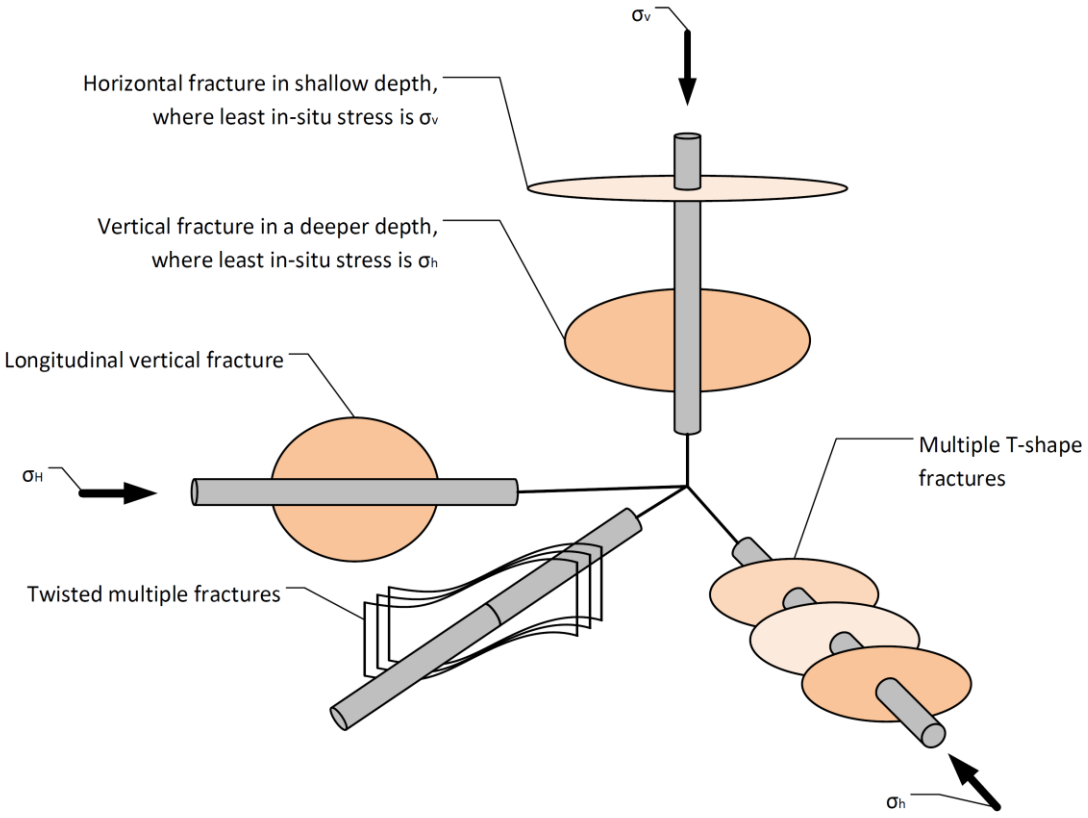

Figure 1-5 A schematic showing the effect of the relative direction of the borehole and in-situ principal stresses on the near wellbore fracture geometry; after (Economides et al., 1998).

Another important parameter, which affects the geometry of the fracture around a wellbore, is the in situ stress orientation which significantly determines the stress distribution around the borehole. Figure 1-5 illustrates schematically the importance of the relative direction of the borehole and in-situ principal stresses.

The width of a fracture may also vary greatly in the near wellbore region. Basically, the width of a fracture is indicated by the difference between the fracture pressure and the normal stress which is perpendicular to the plane of the fracture (Veatch Jr et al., 1989). Therefore, the tortuous fracture around the wellbore is narrower than the main body of the fracture. This is because it is opening against some stress components that are larger than the minimum in-situ stress. As the ratio of the near wellbore stress, applied on the tortuous fracture to the minimum in-situ stress increases, the fracturing fluid would experience more frictional pressure drop as it flows through the near wellbore fracture, which may eventually lead to screen out (Economides, 2000).

In addition, the fracture may not always initiate from the perforation hole, especially if the perforation is not oriented properly; therefore, a narrow channel will be developed around the wellbore, which is called micro-annulus. This channel provides the pathway for the fracturing fluid to flow through and develop the main body of the fracture. This is what has been observed in several experimental studies (Behrmann & Elbel, 1991; Behrmann & Nolte, 1999; Abbas Daneshy, 1973).

Jean Romero et al. (2000) found that as the fracturing fluid flows through the micro-annulus and propagate the main fracture, a Poisson's effect (elastic response) happens. Basically, the propagation and opening of the fracture, which typically takes place perpendicular to the direction of the minimum in-situ stress, will compress the rock in this direction, and as a result the rock elongates in the other two directions. This results in some displacement of the rock towards the cement sheath. Figure 1-6 shows the displacement of the rock, due to fracture opening, around the wellbore when the fluid pressure is equal both in the micro-annulus and the fracture.

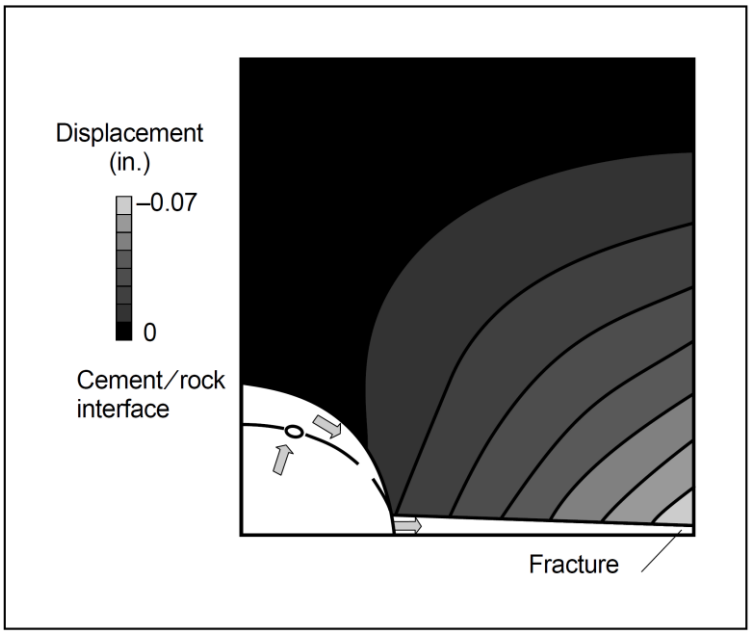

Figure 1-6 The rock displacement caused by fracture opening (Jean Romero et al., 2000).

Nolte (1988) also performed several case studies and pointed out that if the perforations parameters are not appropriate for the fracture to initiate from the perforations' holes then the fracturing fluid must make a narrow channel behind the casing to communicate with the main body of the fracture. According to (Jean Romero et al., 2000), the creation of this narrow channel (micro-annulus) causes an increase in the contact stress between the cement sheath and the formation rock which result in width restriction at the interface of cement and rock, which is known as pinching effect.

The micro-annulus can increase the fracture treating pressure significantly, similar to the near wellbore tortuosity effect. This may lead to screen out because of proppant bridging, although proppant may erode the restrictions. The fracturing fluid and proppants flow at high velocity through the pinch points; therefore, pinch point smoothing may occur by the proppant slurry, provided that smoothing happens before proppant bridging. The amount of erosion is a function of the fluid viscosity, the size and concentration of the proppants, and the strength of the rock and cement (Economides, 2000). This erosion is possibly why the proppant slugs have been reported effective to reduce the near wellbore fracturing pressure drop (Cleary et al., 1993; Stadulis, 1995). The slugs do not bridge the restrictions, since they consist of small sized particles; therefore, they keep eroding the narrow channels as the fluid is injected at high flow rate. It has also been common to inject low concentration proppant slurries to mitigate the high FIPs.

Nevertheless, in order to continue the flow of fracturing fluid through the micro-annulus, it is required to pressurize the pinch point to some higher level than the far field fracture. But this would then increase the net fracture pressure and accordingly increase the rock displacement. Figure 1-7 shows pinch point displacement for a typical case when the net fracture pressure increases to 1000 psi.

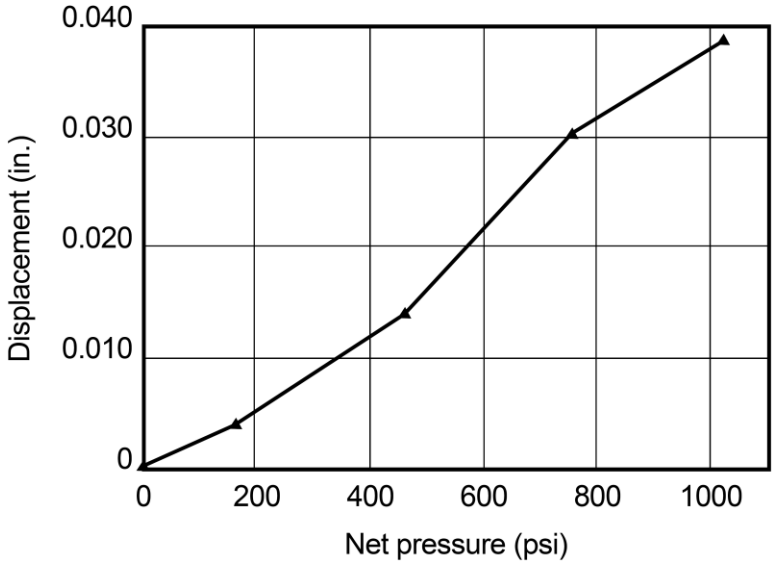

Figure 1-7 Increase in rock displacement by fracturing net pressure, resulting in more pinching of the micro-annulus (Economides, 2000).

Therefore, in contrast to tortuosity, larger pad fluids and higher fracturing pressure may increase the pinching effect before the pinch points are eroded. This is due to the fact that higher fracturing pressure propagate the main body of the fracture and increase the fracture width, resulting in more Poisson's effect and higher stress at the rock and cement interface (Jean Romero et al., 2000).

(Cherny et al., 2009) also conducted a numerical study to investigate the near wellbore fracture initiation mechanism. They developed a 2D model to analyse the interaction of the casing, cement and the formation rock considering a curved fracture path. The geometric theory used in this modelling is analogous to the concept used in plane strain models, similar to the Khristinaovic-Geertsma-de Klerk, KGD model (C. H. Yew & Weng, 2014); however, it allows for a curved fracture connecting the wellbore to the far field fracture as shown in Figure 1-8.

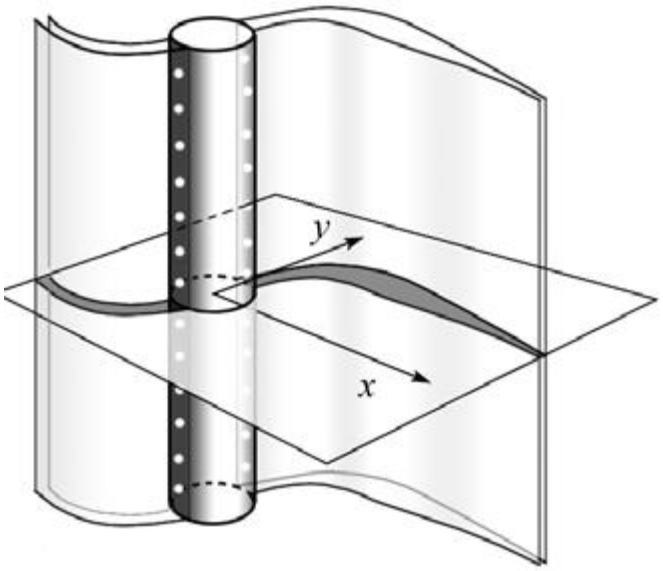

Figure 1-8 2D geometry of a curved fracture initiating from a vertical perforated wellbore (Cherny et al., 2009).

Coupled differential equations are considered to model fluid flow and rock linear elasticity behaviour. This model estimates and evaluates the pinching effects in the near wellbore fracture incorporating the perforation orientation angle, cement and rock properties and fracturing fluid parameters. Several scenarios of fracture initiation and near wellbore propagation through the cement-rock micro-annulus are studies using this model. However, this model did not take into account the effect of the formation pore pressure; additionally, the perforation stress distribution is not properly implemented in this modelling.

Recently, Alekseenko et al. (2012) conducted a numerical investigation, applying a 3 dimensional boundary element method (BEM), to study the FIP in perforations' holes for arbitrary deviated non-cemented borehole. Using the linear elastic theory and the tensile failure criterion, this model is capable of predicting the location and direction of the initial fracture. The authors stated that there are several applications for this numerical modelling, but it is particularly implemented for oriented perforations in multistage fracturing of the horizontal wellbores. It is also indicated that the key parameter, that could be applied to regulate FIP, is the angle between the orientation of the perforation and the preferred main body of the fracture. This is what has also been observed in several experimental studies (Behrmann & Elbel, 1991; Behrmann & Nolte, 1999; Abbas Daneshy, 1973).

1.4.5 Analytical modelling

Many studied have been carried out over the last decades to analytically study the fracture initiation in oil and gas wellbores. Most of these studies have considered the formation rock as an elastic material, and by considering the plane strain condition for the wellbores, have developed fracture break down pressure solutions for a vertical wellbore. This has been basically achieved by equating the wellbore tangential stress to the tensile strength of the formation rock (Howard & Fast, 1970). The effect of pore pressure was also implemented in the modelling by applying poro-elasticity concepts in the solutions (Haimson & Fairhurst, 1967, 1969). However, in these studies the wellbore axis was assumed to be parallel to one the in-situ principal stresses.

C. Yew and Li (1988) performed one of the first analytical studies for fracture initiation in deviated wellbores. They have applied the elasticity theory in three dimensions in order to analyse the induced fracture plane on the wall of a deviated open borehole by deriving a set of equations for the borehole stress distributions. It is shown in this study that because of the impacts of off-plane shear and normal stress components, the initiated fracture on the surface of the well makes an angle with the axis of the wellbore, and then the fracture would deviate from this initial crack as it propagates away from the wellbore. In addition, it was demonstrated that the off-plane stress values have significate effect on the fracture break down pressure.

C. Yew et al. (1989) continued the previous study through analytical methodologies and identified the width and location of the tensile zone on the wall of deviated wellbores, where the circumferential stress is tensile, and therefore, is the right zone for the initial fractures to initiate. They showed that the starter fractures initiated on the wellbore wall would then turn towards a plane which is normal to the direction of the minimum in-situ stress. They also established a linking up criterion for the initiated fractures which was based on the relative magnitude of stress intensity factor at the tip of each fracture. This study specified that for a cased hole, it is preferred to have the perforation on the tensile zone of the wellbore, so that the initiated fractures from each perforation link up easier and less near wellbore fracture tortuosity results. However, the authors did not address how the initial fracture is initiated from the perforation; in fact they ignored the impact of the perforation hole on the near wellbore stress distribution.

This study was further expanded by C. Yew et al. (1993). They studied the behaviour of the starter fractures on a plane tangent to the wellbore in order to analyse the link-up of the fractures initiated at perforation holes of a cased deviated wellbore. The displacement resulted from the opening of the fractures along with the external loads were analysed to obtain the solution. It was shown that, when the perforation spacing is small, the starter fractures will link to each other to form a larger fracture close to the wellbore. However, for a cased wellbore they found that the linked up fracture surface is rough and large quantity of rock are trapped by the linking cracks. The authors stated that this rough fracture surface could be one of the reasons for high near wellbore frictional pressure loss. In this study also, the researchers did not take into account the effect of perforation stress profile on the fracture initiation mechanism.

Weng (1993) also investigated fracture initiation and propagation from deviated and cased perforated wellbores using an analytical modelling analysis. He studied the interaction and link-up of initiated fractures from perforations by developing a criterion incorporating the in-situ stresses and wellbore parameters. He also investigated the near wellbore multiple fracturing by studying the fracture width reduction and its corresponding frictional pressure loss, and he found that the initiated fracture plane has a tortuous path in a distance, not more than few wellbore radii, close to the wellbore. However, he did not also considered the effect of the perforations' holes on the wellbore stress distribution. Since all fractures are initiated from the perforations, it is essential to analyse the perforation stress profile for having a better understanding of the fracture initiation mechanism.

Perhaps the first study which included the perforation hole in the near wellbore stress profile was carried out by Hossain et al. (2000). They initially developed an analytical model for analysing the fracture initiation in an open hole with arbitrary deviation. This model incorporated the in-situ stress components and the inclination and azimuth of a deviated wellbore to estimate the FIP and its geometry initiated from wellbore wall for non-perforation case. In addition, they developed analytical equations to study the initiation of transverse, longitudinal, and multiple fractures from horizontal and vertical open wellbore.

For the case of a perforated wellbore, the authors considered a perforation hole to be perpendicular to the wellbore as shown in Figure 1-9. Accordingly, a closed-form analytical equation was developed by superimposing the stress concentrations to

calculate the tangential stress at the base of the perforation, where it intersects with the wellbore;

$$\sigma_{\theta\theta'} = (\sigma_x + \sigma_y + \sigma_{z\theta}) + 2\,(\sigma_x + \sigma_y - \sigma_{z\theta})cos2\theta'$$
$$-2(\sigma_x - \sigma_y)(cos2\theta + 2cos2\theta cos2\theta') - 4\tau_{xy}(1 + 2cos2\theta)sin2\theta \quad (1.3)$$
$$- 4\tau_{z\theta}sin2\theta' - P_w(2cos2\theta' + 2)$$

where τ_{xy} and $\tau_{z\theta}$ are shear stress components on the wellbore wall in Cartesian and cylindrical coordinate system respectively, and P_w is the wellbore pressure. All other parameters are shown in Figure 1-9. Equation (1.3) was then used to calculate the initiation pressure of a fracture which is formed perpendicular to the perforation tangential stress ($\sigma_{\theta\theta'}$). However, this is only applicable when the perforation axis is parallel to one of in-situ principal stresses. Otherwise, the fracture may initiate along a direction which makes an angle with the axis of the perforation; therefore, it would not initiate against $\sigma_{\theta\theta'}$.

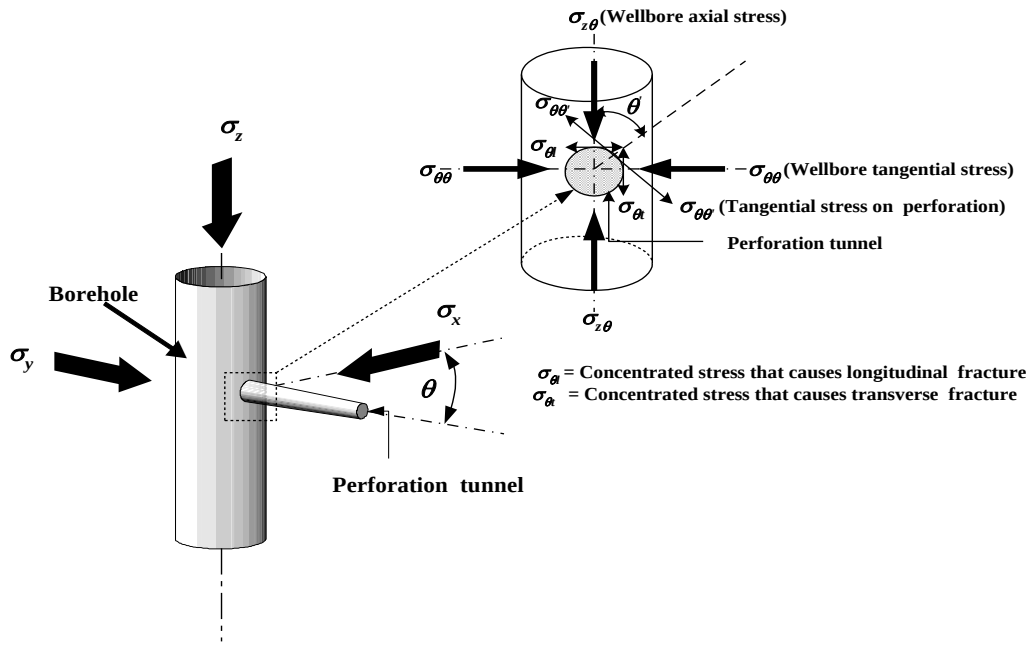

Figure 1-9 A schematic of a wellbore and perforation showing the stress components (Hossain et al., 2000).

In addition, this approach is only applicable for the base of the perforation, since it assumes that the fracture does not initiate anywhere else along the length of the perforation. Although it is generally believe that the starter fracture typically initiates at the interface of the perforation and wellbore, it has been numerically showed that,

depending on the orientation of the perforation and deviation of the wellbore, the fracture could initiate at any location along the perforation hole (Alekseenko et al., 2012). Therefore, a more sophisticated perforation stress analysis is required to study the fracture initiation in the perforations.

Van Ketterij and De Pater (1999) also presented a set of analytical equations to analyse the wellbore stress distribution. Moreover, an equation was presented to calculate the tangential stress on the surface of the perforation. This was also similar to the equation developed by Hossain et al. (2000) (Equation (1.3)), and therefore, has some limitations in predicting the fracture initiation in a perforation's hole. As explained earlier, because a fracture may initiate at an angle in the perforation; therefore, the perforation tangential stress could not interpret the fracture initiation mechanism. Basically, all stress components along the perforation hole are required to analytically analyse the moment of fracture initiation.

Atkinson and Eftaxiopoulos (2002) also applied analytical and numerical methods to study fracture propagation in a cased cemented wellbore. Using a two-dimensional plane model, they concluded that when the cement sheath bonding to the casing and rock fails, no fracture turning would occur and higher pressure is required.

1.4.6 Summary

After reviewing the literature, it is understood that, for designing a hydraulic fracturing treatment, it is critically important to consider the effects of the near wellbore parameters. These parameters significantly affect the FIP and the geometry of the fracture around the wellbore. Particularly, in cased hole perforated wellbores, where the communication of the wellbore and the formation rock is only through the perforations' holes; therefore, the perforations' quality is vital.

Economides (2000) stated that "ideal perforation for fracture initiation would have a minimum injection pressure drop, initiate only a single bi-wing fracture, and generate a fracture with minimum tortuosity (turning smoothly from the plane containing the perforation axes into the Preferred hydraulic Fracture Plane, PFP) at an achievable FIP". To design such an ideal perforation, it is necessary to understand the fracture initiation mechanism in the perforation's hole, while considering the effects of all impacting parameters. In the next step the near wellbore fracture propagation and geometry should be studied.

As it is indicated in most of past studies, the tortuosity of the fracture around the wellbore is a challenging issue. It may cause high frictional pressure loss and proppant bridging; therefore, leading to unsuccessful fracturing treatment by creating premature screen outs. The other troublesome issue is the formation of micro-annulus that may also lead to screen outs. Generally, near wellbore fracture tortuosity is less challenging than a micro-annulus. Since, when there is a micro-annulus behind the casing, by increasing the fracturing pressure the micro-annulus will become narrower at the pinch points; accordingly, causing proppant bridging and possibly early screen out. In contrary, the tortuous fracture width could be increased by increasing the fracturing fluid viscosity and pressure. Therefore, it is critically important to improve the cement sheath properties, as well as perforation parameters, so that the fracturing fluid does not develop any micro channel behind the casing. This would ensure that the fracture will be created in the formation rock rather than cement.

Several analytical modelling have been performed in the past to establish analytical solutions for the problem of fracture initiation and propagation in vertical and deviated open wellbores (Haimson & Fairhurst, 1967, 1969; Li, 1991; Van Poollen, 1957; C. Yew & Li, 1988). Whereas only a few analytical studies have been performed to provide solution for the mechanism of fracture initiation in cased perforated wellbores (Hossain et al., 2000; Weng, 1993; C. Yew et al., 1989), while none of them took into account the effect of wellbore and perforation stress distributions simultaneously. Since, in a cased hole, all fractures are initiated from the perforations, it is essential to analyse the perforation stress profile along with the wellbore stress concentration in order to have a better understanding of the fracture initiation mechanism. In addition, experimental tests should be carried out for the purpose of validating the analytical solutions.

Several laboratory fracturing studies have been performed in the past to investigate various features of fracturing in perforated wellbores (Abass et al., 1994; Behrmann & Elbel, 1991; Abbas Daneshy, 1973; El Rabaa, 1989; Hallam & Last, 1991); however, they have not carried out any dimensional analysis. Dimensional analysis makes the experimental results more reliable as it takes into account the relative dimensional aspects of a laboratory fracturing experiment with respect to the physical phenomenon occurring in field fracturing operations.

1.5 Research objectives and methodology

Although many studies have been carried out in the past to investigate various aspects of hydraulic fracturing in perforated wellbores, still there are many knowledge gaps in regard to the mechanism of fracture initiation along perforations' holes. The physical effects of wellbore, casing, cement, and perforation parameters on the fracture initiation are not well analysed yet. Considering the previous sections, one may question how to design the ideal perforation parameters, or how to prevent the possible micro-annulus development, or how to reduce the tortuosity of the near wellbore fracture. To find realistic solutions for these questions, it is essential to theoretically understand the fracture initiation mechanism in cased perforated wellbores. Therefore, the main objective of this research thesis is to investigate the fracture initiation and near wellbore propagation through analytical modelling and laboratory experiments. Additionally, numerical simulations are developed, where necessary, to validate the experimental and analytical results. The details of the objectives of this research and their corresponding methodologies applied to achieve these objectives are presented as follow:

- Developing an analytical model simulating the wellbore stress distribution at different well azimuths and inclinations and also various in situ stress regimes. The model will then be further advanced to simulate the stress profile on the surface of a perforation all along its length, while considering the effects of wellbore stress concentration, as well as cement and rock properties.
- Predicting the FIP in the perforation hole at various conditions. In addition, establishing maximum tension zone of the wellbore at different wellbore orientations, and stress regimes, this is then set as the reference point on the wall of the wellbore for investigating the effects of the perforation orientation.
- Estimating the likelihood of micro-annulus creation and near wellbore fracture tortuosity by estimating the location and angle of fracture initiation with respect to perforation axis.
- Further advancing the analytical model by incorporating the effects of pore pressure and temperature variations which take place in the formation rock due to injection of fracturing fluid.
- Applying the developed analytical model to some case studies and real field data.

- Performing scaled hydraulic fracturing experiments on a series of synthetically made cube samples in a true tri-axial cell (TTSC). The results of the experiments are used to initially validate the analytical model and to further investigate the effects of perforation orientation and wellbore orientation on FIP and near wellbore propagation geometry.
- Developing three dimensional numerical model using ABAQUS software for validating the experimental results obtained from the fracturing tests, which were done using the TTSC.
- Conducting further fracturing experiments to investigate the effects of varying fracturing fluid viscosities and fluid injection rates on fracturing mechanism.

In summary, this research developed a new analytical model, while incorporating the poro-elastic and thermo-elastic effects, in order to predict the FIP and the initiation angle and location along the perforation hole. The developed model is capable of analysing the fracture initiation mechanism in perforated wellbores by applying various parameters related to wellbore and perforation orientations as well as casing, cement and rock properties. This analytical model was validated with scaled fracturing experiments, and implemented for field case studies. In addition, through experimental studies, further new knowledge were developed on how perforation fracture initiation and propagation are affected by relative wellbore and perforation orientations, in-situ stresses, and fracturing fluid viscosity and injection rate.

1.6 Research significance

According to the objectives which have been defined for this research, the following reasons make it significant and unique:

- An elastic analytical model was developed to analyse the wellbore and perforation stress concentrations simultaneously. This means that the model is capable of estimating the stress profile on the surface of the whole length of the perforation. This stress analysis was done at different wellbore deviations with varying perforation orientations.
- FIP in the perforation hole was predicted using the analytical model. In addition the location of the initial fracture and its angle with respect to the perforation axis was determined. Consequently, the near wellbore fracture

tortuosity and possible micro-annulus creation were analysed qualitatively at various conditions.

- The effect of pore pressure and temperature variation of the formation was also developed in the model by incorporating the poro-elasticity and thermo-elasticity theories. In addition, the impacts of the steel casing, and cement sheath properties on the FIP were analysed.
- The analytical model was successfully applied to analyse several field-scale case studies.
- A set of scaled hydraulic fracturing tests were performed on cubic samples in a true tri-axial stress cell (TTSC) to validate the results of the analytical model. In addition, the effects of in-situ stress regime, and perforation orientation were studied in vertical and horizontal wellbores.
- A numerical 3D modelling was developed using ABAQUS software to simulate a set of the laboratory fracturing experiments, and thereby validating the results.
- The impacts of fracturing fluid viscosity and injection rate on the fracture initiation and near wellbore propagation geometry were studied experimentally.

1.7 Summary

In this Chapter an overview of hydraulic fracturing was presented. The process of fracturing in cased wellbores was discussed and the corresponding challenges were explained. Then, a comprehensive literature survey was presented. Past field studies, laboratory experimental observations, and analytical and numerical modellings were reviewed to study the strengths and weaknesses of the previously performed investigates. Accordingly, the main influencing parameters were recognized and effective research objectives and corresponding methodologies were identified to further expand the knowledge of fracture initiation in cased perforated wellbores.

2 Elastic analytical modelling*

2.1 Introduction

As it is stated in Chapter 1, various parameters can influence the initiation of a fracture in perforated wellbore. Wellbore orientation, perforation parameters, in-situ stress regime, steel casing, cement sheath and rock properties are among the main impacting parameters. To investigate the effects of these parameters, an analytical model is developed and presented in this chapter for studying the mechanism of fracture initiation in a perforation hole. Elastic theory is applied to analyse the stress concentration in the vicinity of a wellbore with arbitrary inclination and azimuth, then a new methodology is introduced to calculate the stress distribution on the surface of a perforation. This perforation stress analysis is performed for the whole length of the perforation hole while the effect of the wellbore stress concentration is superimposed on the perforation stress modelling.

After modelling the wellbore and perforation stress distributions, tensile criterion is implemented to study fracture initiation on the surface of the perforation. Next, an iterative numerical method is applied in order to calculate the FIP. In addition, the location and initiation angle of the starter fracture is identified along the perforation hole.

2.2 Wellbore Stress distribution

All underground formations are generally in compression due to the weight of the overlaying layers; therefore, when a wellbore is drilled in a formation, it causes stress variation. This is generally because a cylindrical column of rock is being replaced by drilling fluid. Since the drilling fluid could not support the wellbore wall similar to the removed rock, stress redistribution occurs around the wellbore. This stress redistribution induces tangential and radial stress components on the wall and vicinity of the wellbore, resulting in stress concentration in specific directions. Rock

*Some of the contents given in this chapter are based on the material presented in:
Paper 3. An investigation of hydraulic fracturing initiation and near-wellbore propagation from perforated boreholes in tight formations.

mechanical theories could be used to calculate stress concentration around a cylindrical wellbore.

Several mathematical models are available in the literature for calculating wellbore stress distribution. One of the first studies performed in this area was presented by Westergaard (1940), he developed an elasto-plastic model to analyse the stress profile around a deep wellbore. Many other elasto-plastic modelling have been presented after the first one (Crook et al., 2002; Mitchell et al., 1987; Roshan & Rahman, 2011). However, some other researchers have studies and developed mathematical models based on the linear elastic theory (Aadnoy, 1989; Bradley, 1979). Linear elastic models typically do not require many input parameters; therefore, they are used widely in the stress analysis studies.

In this analytical study, linear elastic stress analysis is used. The main reason for implementing a linear elastic approach is because in a hydraulic fracturing operation, the wellbore and perforation pressure is increased, accordingly, the stress components around the wellbore and perforations are at low levels of tension or compression. Since typically formation rocks behave linearly elastic under low stress magnitudes, it is reasonable to apply linear elastic models for analysing fracture initiation mechanism. To do so, firstly, wellbore stress distribution should be studied.

A vertical wellbore could be simply considered to be a hallow cylinder with an external radius much larger than its internal radius. In addition, since the length of a wellbore is much larger than its radius, an infinite long wellbore could be assumed; therefore, the plane strain condition could be used. Considering equal horizontal stresses of σ_h, a vertical stress of σ_v, and a wellbore pressure of P_w, the following equation have been derived for the wellbore stress components (Fjar et al., 2008):

$$\sigma_r = \sigma_h \left(1 - \frac{{R_w}^2}{r^2}\right) + P_w \frac{{R_w}^2}{r^2}$$

$$\sigma_\theta = \sigma_h \left(1 + \frac{{R_w}^2}{r^2}\right) - P_w \frac{{R_w}^2}{r^2} \tag{2.1}$$

$$\sigma_z = \sigma_v$$

In Equations (2.1), σ_r is radial stress, σ_θ is tangential stress, σ_z is axial stress, R_w is the wellbore radius, and r is the distance between an point in the formation and the centre of the wellbore. Figure 2-1 shows a diagram of a wellbore stress distribution based on the hollow cylinder linear elastic equations. Radial and

tangential stresses are plotted at two different wellbore pressures of 5000 and 7500 psi, while the isotropic horizontal stresses are 7000 psi in both cases. As it is depicted in this figure, at a P_w of 5000 psi, the radial stress at the wellbore wall is as low as the wellbore pressure, and as it moves away from the wellbore, the radial stress increases and approaches to the horizontal stress value. However, the tangential stress at this P_w is 9000 psi at the wellbore wall, and it decreases as it moves away from the wellbore and reaches to the level of horizontal stress at a distance of about $6\times R_w$.

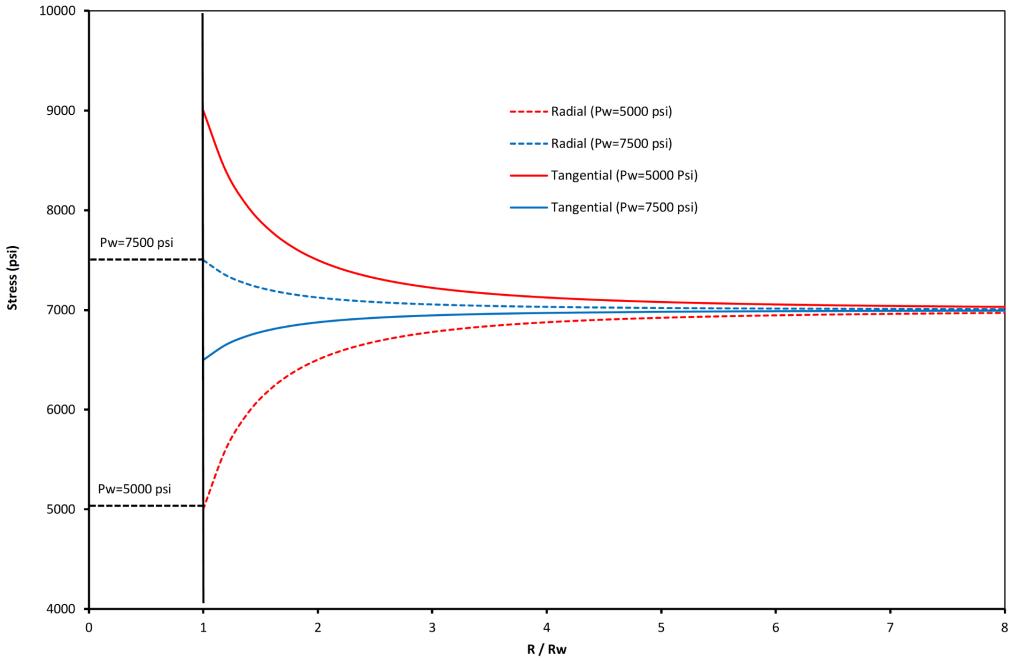

Figure 2-1 Wellbore stress distribution in a linear elastic formation with isotropic horizontal stresses of 7000 psi.

Nevertheless, when the wellbore pressure increases to 7500 psi, tangential stress drops to 6500 psi on the surface of the wellbore, while radial stress increases to 7500 psi. This confirms that, when a wellbore is subject to hydraulic fracturing, as the wellbore pressure increases, typically the level of compressive stress components reduces. The wellbore pressure increases to a point where some tensile stress develops at a point on the surface of the wellbore, and once this tensile stress overcomes the tensile strength of the formation, a starter fracture will be initiated. Since rocks normally have quite low tensile strengths, therefore, in a fracturing operation, the tensile stresses are typically low. Consequently as it is mentioned earlier, linear elastic theory could be applied to accurately model the rock behaviour for fracturing treatments.

2.2.1 Elastic stresses around inclined wellbores

In the last section, the simple equations for the stress distribution around a vertical wellbore, in an isotropic horizontal stresses formation, were discussed. However, because of great advances in drilling operations, deviated wellbores have been drilled for many years; therefore, it is of great interest to analyse the stress profile of a deviated wellbore. In addition, not many underground formations have isotropic horizontal stresses; thus, the effect of stress anisotropy should also be considered in wellbore stress analysis.

Kirsch (1898) presented one of the early solutions for analysing the stress distribution in the vicinity of a circular hole which is located in an infinite plate. The Kirsch equations were then expanded to be used for a vertical wellbore with anisotropic horizontal stresses. Bradley (1979) studied Kirsch equations and developed the wellbore stress distribution formulas, which are widely applied in oil and gas literature.

To study the general arrangement of these formulas, at first, principal in-situ stress components are proposed to define a Cartesian coordinate system denoted by $x', y', and\ z'$, as shown in Figure 2-2. The vertical stress σ_v, is considered to be along z' axis, and the minimum and maximum horizontal stresses are denoted by σ_h and σ_H, and are supposed to be along y' and x' axes, respectively. Then, since the general formulas are used for inclined wellbores, inclination and azimuth angles of a wellbore are used to transform the in-situ principal stresses to be aligned with the wellbore oriented coordinate system.

This second Cartesian coordinate system has three axes, namely $x, y, and\ z;$ the wellbore is parallel to z axis, the x axis is towards the lowest point of the well, and the y axis is obviously perpendicular to the $z - x$ plane (see Figure 2-2). Now, the stresses could be transformed from the in-situ stresses coordinate system to the wellbore coordinate system. This is done using the inclination (i) and azimuth (a) angles of the wellbore.

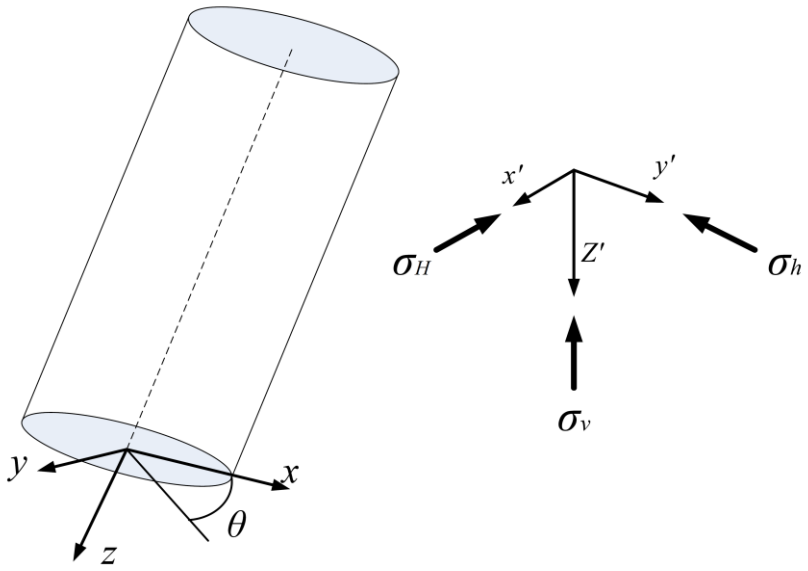

Figure 2-2 In-situ principal stresses and wellbore Cartesian coordinate systems.

Direction cosines could be used to mathematically derive the transformation equations as follows (Fjar et al., 2008):

$$\begin{aligned} l_{xx'} &= \cos a \times \cos i & l_{xy'} &= \sin a \times \cos i & l_{xz'} &= -\sin i \\ l_{yx'} &= -\sin a & l_{yy'} &= \cos a & l_{yz'} &= 0 \\ l_{zx'} &= \cos a \times \sin i & l_{zy'} &= \sin a \times \sin i & l_{zz'} &= \cos i \end{aligned} \tag{2.2}$$

where, for instance, $l_{xx'}$ is the cosine of the angle between the x and x' axes. Having the transformation equations, the in-situ stress components could be calculated along the wellbore coordinate system through the following formulas (Fjar et al., 2008) :

$$\begin{aligned} \sigma_x^o &= l_{xx'}^2\sigma_H + l_{xy'}^2\sigma_h + l_{xz'}^2\sigma_v \\ \sigma_y^o &= l_{yx'}^2\sigma_H + l_{yy'}^2\sigma_h + l_{yz'}^2\sigma_v \\ \sigma_z^o &= l_{zx'}^2\sigma_H + l_{zy'}^2\sigma_h + l_{zz'}^2\sigma_v \end{aligned} \tag{2.3}$$

$$\begin{aligned} \tau_{xy}^o &= l_{xx'}l_{yx'}\sigma_H + l_{xy'}l_{yy'}\sigma_h + l_{xz'}l_{yz'}\sigma_v \\ \tau_{yz}^o &= l_{yx'}l_{zx'}\sigma_H + l_{yy'}l_{zy'}\sigma_h + l_{yz'}l_{zz'}\sigma_v \\ \tau_{zx}^o &= l_{zx'}l_{xx'}\sigma_H + l_{zy'}l_{xy'}\sigma_h + l_{zz'}l_{xz'}\sigma_v \end{aligned} \tag{2.4}$$

In these formulas, $\sigma_x^o, \sigma_y^o,$ and σ_z^o stand for wellbore in-situ normal stresses, whereas τ_{xy}^o, τ_{yz}^o, and τ_{zx}^o are the corresponding shear stresses. Since the wellbore has a cylindrical geometry, it is routine to express the stress components in cylindrical coordinate system. In such coordinate system, any point around the wellbore is defined with three components $r, \theta, and\ z$, where r is the shortest distance of the point to the centre of the wellbore, θ is an angle (azimuth) measure relative to the x axis, and z is a distance measured along the z axis. Accordingly, the cylindrical wellbore stress distribution could be calculated, at any point around the wellbore, using the below equations;

$$\sigma_r = \frac{\sigma_x^o + \sigma_y^o}{2}\left(1 - \frac{R_w^2}{r^2}\right) + \frac{\sigma_x^o - \sigma_y^o}{2}\left(1 + 3\frac{R_w^4}{r^4} - 4\frac{R_w^2}{r^2}\right)\cos 2\theta + \tau_{xy}^o\left(1 + 3\frac{R_w^4}{r^4} - 4\frac{R_w^2}{r^2}\right)\sin 2\theta + P_w\frac{R_w^2}{r^2} \tag{2.5}$$

$$\sigma_\theta = \frac{\sigma_x^o + \sigma_y^o}{2}\left(1 + \frac{R_w^2}{r^2}\right) - \frac{\sigma_x^o - \sigma_y^o}{2}\left(1 + 3\frac{R_w^4}{r^4}\right)\cos 2\theta - \tau_{xy}^o\left(1 + 3\frac{R_w^4}{r^4}\right)\sin 2\theta - P_w\frac{R_w^2}{r^2} \tag{2.6}$$

$$\sigma_z = \sigma_z^o - \vartheta\left(2\left(\sigma_x^o - \sigma_y^o\right)\frac{R_w^2}{r^2}\cos 2\theta + 4\tau_{xy}^o\frac{R_w^2}{r^2}\sin 2\theta\right) \tag{2.7}$$

$$\tau_{r\theta} = \frac{\sigma_x^o - \sigma_y^o}{2}\left(1 - 3\frac{R_w^4}{r^4} + 2\frac{R_w^2}{r^2}\right)\sin 2\theta + \tau_{xy}^o\left(1 - 3\frac{R_w^4}{r^4} + 2\frac{R_w^2}{r^2}\right)\cos 2\theta \tag{2.8}$$

$$\tau_{\theta z} = \left(-\tau_{xy}^o \sin\theta + \tau_{yz}^o \cos\theta\right)\left(1 + \frac{R_w^2}{r^2}\right) \tag{2.9}$$

$$\tau_{rz} = \left(-\tau_{xz}^o \cos\theta + \tau_{yz}^o \sin\theta\right)\left(1 - \frac{R_w^2}{r^2}\right) \tag{2.10}$$

In the above equations, σ_r stands for radial stress and based on Equation (2.5), σ_r is equal to the wellbore pressure on the surface of the wellbore where $r = Rw$. σ_θ is tangential (hoop) stress, σ_z is axial stress, which is parallel to the direction of the wellbore axis, and $\tau_{r\theta}, \tau_{\theta z}\, and\, \tau_{rz}$ are shear stress components. These stress components are all functions of θ, which is an angle indicating the location of a point relative to the x axis. This shows that the various stress components change with angular position around the wellbore.

Also, as it could be seen from these equations, the wellbore stress concentration vanishes quickly as the point of interest moves away from the wellbore, since the wellbore effect is given by r^2 and r^4 terms in the equations' denominators. Therefore, as it was also depicted in Figure 2-1, the wellbore does not have any significant influence after a distance of about $6\times R_w$ away from the centre of the wellbore.

2.3 Analytical solution for perforation stress concentration

As it is mentioned earlier, underground layers are generally under compressive stress; therefore, the wellbore stress concentration is compressive too. However, in the early stages of hydraulic fracturing, when the pad fluid is injected, the wellbore and perforations' stress concentrations change. This is due to the fact that by increasing the wellbore pressure, the perforations' pressure concurrently increases, since before any fracture is initiated, there is no significant frictional pressure loss in the perforation entry. As a result, compressive stresses reduce, and as the pressure increases some tensile stress will be imposed in specific directions. Once, the tensile stress at a specific point overcomes the tensile strength of the formation, the first fracture initiates.

In the case of an open wellbore, the fracture may initiate anywhere on the surface of the well; however, when the wellbore is cased and perforated, it could only be developed somewhere along the perforation hole. Therefore, it is critical to evaluate the stress distribution on the surface of the perforation hole in order to study the fracture initiation. In this way, the FIP, its location and the angle at which the fracture would make with the axis of the perforation could be analysed. The pressure and geometrical study of the initial fracture would then help to enhance investigating the near wellbore fracture link-up and propagation geometry.

As it was reviewed in Chapter 1, a few researchers have tried to analytically analyse the perforation stress concentration for the purpose of hydraulic fracturing modelling (Hossain et al., 2000; Van Ketterij & De Pater, 1999). However, Hossain et al. (2000) developed an equation to predict the perforation tangential stress merely at the perforation and wellbore interface (Equation (1.3)). This equation could only predict a fracture, which initiates right at the wellbore wall and perforation edge, and is opening parallel to the perforation axis (i.e. fracture opening perpendicular to the perforation tangential stress). Van Ketterij and De Pater (1999) also only developed the perforation tangential stress equation, and did not analyse any other stress components along the perforation hole. But, since a fracture may initiate anywhere along the perforation tunnel and at any angle with respect to the perforation hole, there is significant limitations using these formulas. Therefore, it is essential to carry out a full stress analysis all along the perforation tunnel, evaluating tangential, radial and axial stresses to accurately study the mechanism of fracture initiation.

In order to model perforation stress concentration, it is assumed that the perforation tunnel is a micro-cylindrical hole, which is perpendicular to the surface of the well as shown in Figure 2-3. Although, some perforations may have a conical shape typically at the end of their hole, it is reasonably acceptable to simulate a perforation hole as a cylinder. This is because most experimental fracturing studies have revealed that starter fractures normally initiate at the first half of the perforation hole, and very rarely a fracture may initiate at the end of the perforation tunnel (Behrmann & Elbel, 1991; Behrmann & Nolte, 1999; Abbas Daneshy, 1973).

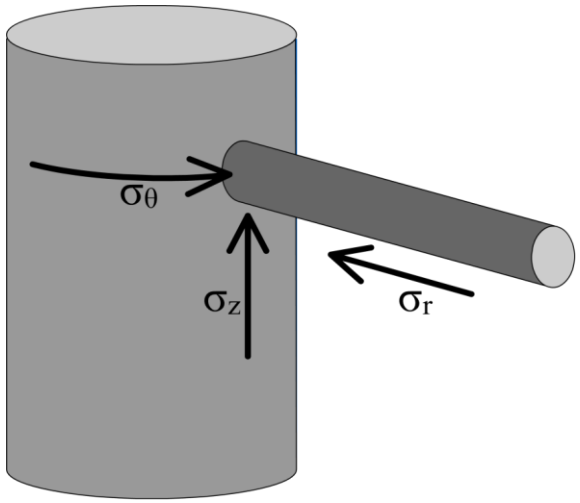

Figure 2-3 Wellbore and perforation model geometry.

In this model the perforation length is supposed to be six times the wellbore radius (a radial distance away from the well, where the wellbore stress concentration after this distance is really negligible). Even if the real perforation length is less than this distance, it does not affect the results, because, as it is mentioned earlier, fractures always initiate in a short distance away from the wellbore.

As it is depicted in Figure 2-3, since the perforation is located in the vicinity of the wellbore, the wellbore stress concentration greatly influences the stress distribution on the surface of the perforation. However, if there was no wellbore, perforation hole could have been supposed as a small cylindrical hole under direct effects of the in-situ stresses, and accordingly, Equations (2.2) to (2.10) could have been directly used for estimating the perforation stress concentration. Therefore, the stress distribution around the wellbore should be incorporated in the analysis of the perforation stress concentration.

In this analytical study, wellbore stress components ($\sigma_z, \sigma_\theta, and\ \sigma_r$) are used to calculate the perforation stress distribution. Referring to Figure 2-3, it is realized that the wellbore tangential and axial stresses, σ_θ and σ_z, are perpendicular to the axis of the perforation, while the wellbore radial stress, σ_r, is along the perforation axis. Therefore, these wellbore normal stresses along with their corresponding shear components ($\tau_{r\theta}, \tau_{\theta z}\ and\ \tau_{rz}$) are assumed as the input stress parameters to calculate the stress distribution on the surface of the perforation. It is noteworthy that, all wellbore normal and shear stresses are functions of r, the distance between any point of interest and the centre of the wellbore. Therefore, wellbore stress components should be calculated at any point along the length of the perforation using Equations (2.5) to (2.10) in order to calculate the perforation stress concentration all along its hole (i.e. the length of the perforation is equivalent to the radial distance away from the wellbore).

Since perforation is also a cylindrical hole, Equations (2.5) to (2.10) could be rearranged to calculate the cylindrical stress components of the perforation. To do so, perforation radius (R_p) and pressure (P_p) should replace wellbore radius (R_w) and pressure (P_w), respectively. Also, wellbore stress components should be used instead of the in-situ stresses. As a result the following equations are obtained:

$$\sigma_{rp} = \frac{\sigma_z + \sigma_\theta}{2}\left(1 - \frac{R_p^2}{r^2}\right) + \frac{\sigma_z - \sigma_\theta}{2}\left(1 + 3\frac{R_p^4}{r^4} - 4\frac{R_p^2}{r^2}\right)\cos 2\theta_p$$
$$+\tau_{\theta z}\left(1 + 3\frac{R_p^4}{r^4} - 4\frac{R_p^2}{r^2}\right)\sin 2\theta_p + P_p\frac{R_p^2}{r^2} \quad (2.11)$$

$$\sigma_{\theta p} = \frac{\sigma_z + \sigma_\theta}{2}\left(1 + \frac{R_p^2}{r^2}\right) - \frac{\sigma_z - \sigma_\theta}{2}\left(1 + 3\frac{R_p^4}{r^4}\right)\cos 2\theta_p$$
$$-\tau_{\theta z}\left(1 + 3\frac{R_p^4}{r^4}\right)\sin 2\theta_p - P_p\frac{R_p^2}{r^2} \quad (2.12)$$

$$\sigma_{zp} = \sigma_r - \vartheta\left(2(\sigma_z - \sigma_\theta)\frac{R_p^2}{r^2}\cos 2\theta_p + 4\tau_{z\theta}\frac{R_w^2}{r^2}\sin 2\theta_p\right) \quad (2.13)$$

$$\tau_{r\theta p} = \frac{\sigma_z - \sigma_\theta}{2}\left(1 - 3\frac{R_p^4}{r^4} + 2\frac{R_p^2}{r^2}\right)\sin 2\theta_p$$
$$+\tau_{z\theta}\left(1 - 3\frac{R_p^4}{r^4} + 2\frac{R_p^2}{r^2}\right)\cos 2\theta_p \quad (2.14)$$

$$\tau_{\theta zp} = \left(-\tau_{z\theta}\sin\theta_p + \tau_{r\theta}\cos\theta_p\right)\left(1 + \frac{R_p^2}{r^2}\right) \quad (2.15)$$

$$\tau_{rzp} = \left(-\tau_{rz}\cos\theta_p + \tau_{r\theta}\sin\theta_p\right)\left(1 - \frac{R_p^2}{r^2}\right) \quad (2.16)$$

where subscript P indicates that the corresponding parameter is a perforation parameter such as σ_{rp}, which is the perforation radial stress, and r is radial distance of the point of interest from the centre of the perforation. Equations (2.11) to (2.16) estimate the stress concentration in the vicinity of a perforation hole, while the wellbore stress concentration is superimposed. However, it should be noted that the effects of the neighbouring possible perforations are not included, since each perforation radius and zone of influence is supposed to be such small that it does not affect any other perforation stress profile.

2.4 Fracture initiation analysis

The topic of fracture initiation in open wellbores has been studied by many researchers. Tensile failure criterion has been used in most of these studies to

analyse the process of fracture initiation (C. H. Yew & Weng, 2014). According to this criterion, the fracture opens up against the minimum principal stress (σ_3); mathematically speaking, the fracture initiates when:

$$\sigma_3 \leq -TS \tag{2.17}$$

In this equation, σ_3 is a negative stress, since it is a tensile component, and TS stands for the tensile strength of the formation. However, since most formations are typically porous, there might be some formation pore pressure (P_f); therefore, effective minimum principal stress (σ_3') should be used in the failure criterion;

$$\sigma_3' = \sigma_3 - \alpha P_f \leq -TS \tag{2.18}$$

The simplest application of this theory is to study hydraulic fracturing in a vertical open hole which is located in a normal stress regime area. Applying the elastic theory, the wellbore stress distribution is analysed, and accordingly a vertical fracture is supposed to initiate on the surface of the wellbore. Based on the stress analysis, in this particular case, the fracture initiates against the minimum tangential stress, which is parallel to the direction of maximum horizontal stress. Therefore, Equation (2.6) could be simplified to calculate this tangential stress component on the surface of the wellbore (i.e. wellbore wall) at $r = R_w$, and $\theta = 0°$;

$$\sigma_\theta = 3\sigma_h - \sigma_H - P_w \tag{2.19}$$

As it is seen in this equation, by increasing the wellbore pressure, tangential stress reduces and it becomes a negative (tensile) stress at high wellbore pressure. Also, it is noteworthy that the poro-elastic effect is not included in Equation (2.19). Applying tensile failure criterion, when this tangential stress overcomes the tensile strength (TS) of the formation, the first fracture will be initiated; therefore, the FIP could be calculated using the following equation (C. H. Yew & Weng, 2014);

$$P_{FI} = 3\sigma_h - \sigma_H + TS \tag{2.20}$$

Similarly, the tensile failure criterion is applied in this study to investigate the fracture initiation in a perforation tunnel. To do so, first of all, the stress distribution on the surface of the perforation should be calculated. This is done by simplifying

Equations (2.11) to (2.16) through replacing r by R_p; consequently, the below formulas are obtained;

$$\sigma_{rp} = P_p$$
$$\sigma_{\theta p} = \sigma_z + \sigma_\theta - 2(\sigma_z - \sigma_\theta)\cos 2\theta p - 4\tau_{z\theta} sin2\theta p - P_p$$
$$\sigma_{zp} = \sigma_r - \vartheta(2(\sigma_z - \sigma_\theta)\cos 2\theta p + 4\tau_{z\theta} sin2\theta p) \quad (2.21)$$
$$\tau_{r\theta p} = \tau_{rzp} = 0$$
$$\tau_{\theta zp} = 2(-\tau_{rz} sin\theta p + \tau_{r\theta} cos\theta p)$$

Having the stress distribution on the surface of the perforation, principal stresses should be studied, so that the minimum principal stress could be used in the tensile failure criterion. As it is seen in Equation (2.21), since the perforation surface is a free surface, two of the shear stress components are always zero; therefore the radial perforation stress (σ_{rp}) is a principal stress. However, as the other shear stress component ($\tau_{\theta zp}$) is a non-zero value; therefore, the other normal perforation stresses ($\sigma_{\theta p}$ and σ_{zp}) could not be principals.

Nevertheless, since σ_{rp} is a principal stress, and it is always in the radial direction, (i.e. perpendicular to the surface of the perforation), the other two principal stress components should locate on a plane tangent to the perforation surface (see Figure 2-4). This is because principal stresses are always perpendicular to each other (Jaeger et al., 2009). Recalling that at the moment of fracture initiation, the perforation pressure is typically very high; thus σ_{rp} should be the maximum principal stress (σ_1). Therefore, intermediate and minimum principal stresses (σ_2, and σ_3) should be the ones on the tangent plane, as shown in Figure 2-4.

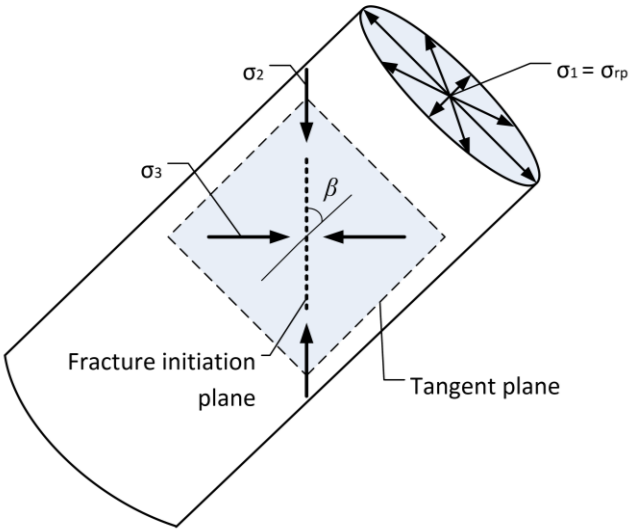

Figure 2-4 A schematic of a perforation hole and tangent plane where the fracture initiates.

In order to calculate these two principal stress components, stress transformation rules could be applied; accordingly the following equations are obtained:

$$\sigma_2 = \frac{1}{2}\left[\left(\sigma_{\theta p} + \sigma_{zp}\right) + \sqrt{\left(\sigma_{\theta p} - \sigma_{zp}\right)^2 + 4\tau^2{}_{\theta zp}}\ \right]$$
$$\sigma_3 = \frac{1}{2}\left[\left(\sigma_{\theta p} + \sigma_{zp}\right) - \sqrt{\left(\sigma_{\theta p} - \sigma_{zp}\right)^2 + 4\tau^2{}_{\theta zp}}\ \right] \quad (2.22)$$

Since the fracture always initiates perpendicular to the direction of minimum principal stress, the starter fracture will be initiated parallel to the direction of σ_2 as depicted in Figure 2-4. However, the initiated fracture plane may make an angle β with the axial direction of the perforation. Since, every single perforation may have an initial fracture; therefore, knowledge of this angle could be very useful for the analysis of starter fractures link-up and near wellbore fracture propagation. The initiation angle (β) could be calculated through the following equation, which was derived based on the stress transformation formulas:

$$\beta = \frac{1}{2} tan^{-1}\left(\frac{2\tau_{z\theta_{cr}p}}{\sigma_{\theta_{cr}p} - \sigma_{z_{cr}p}}\right) \quad (2.23)$$

where the notation cr stands for a critical angle (θ_{cr}) on the surface of the perforation, where the smallest minimum principal stress is located. Generally, based on stress theories, any specific point in a material has its own stress matrix, and accordingly principal stresses. Therefore, when the perforation surface stress

distribution is analysed, there is some minimum principal stress at any point on the surface of the perforation hole. However, the fracturing fluid will initiate the first fracture wherever the smallest principal stress exists; consequently, it is important to locate the starter fracture on the surface of the perforation.

2.4.1 Fracture initiation from perforated vertical wellbore

In this section a simple application of the developed analytical model is presented. A common example of a fracturing operation is when the borehole is vertical as shown in Figure 2-5. In this case, the axis of the wellbore is parallel to the direction of vertical in-situ principal stress, and the other two principal stresses are perpendicular to the wellbore axis.

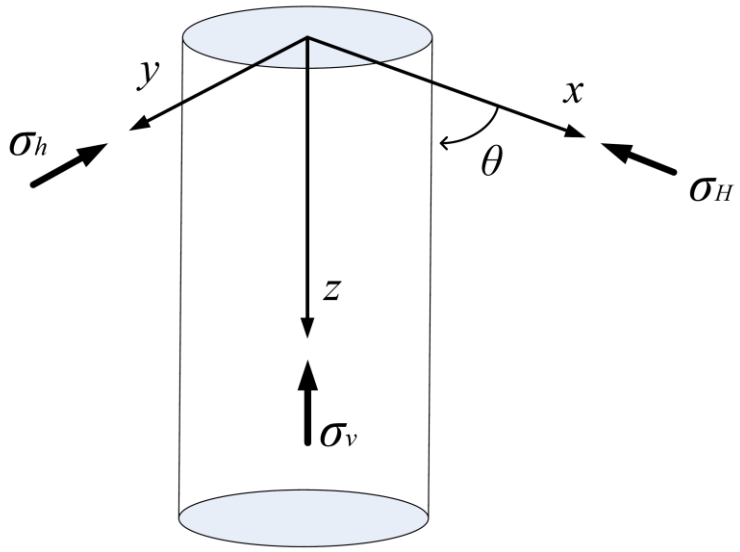

Figure 2-5 A vertical wellbore and in-situ stress components.

When this vertical wellbore is perforated, the perforations are along horizontal directions. In order to study the fracture initiation in such perforations, first of all the wellbore stress distribution should be calculated. Since the axis of a vertical wellbore is parallel to the direction of in-situ vertical stress, the two coordinate systems shown in Figure 2-2 coincide; therefore, Equations (2.5) to (2.10) could be simplified as follow to calculate the stress distribution around the wellbore;

$$\sigma_r = \frac{\sigma_H + \sigma_h}{2}\left(1 - \frac{R_w^2}{r^2}\right) + \frac{\sigma_H - \sigma_h}{2}\left(1 + 3\frac{R_w^4}{r^4} - 4\frac{R_w^2}{r^2}\right)\cos 2\theta + P_w\frac{R_w^2}{r^2} \tag{2.24}$$

$$\sigma_\theta = \frac{\sigma_H + \sigma_h}{2}\left(1 + \frac{R_w^2}{r^2}\right) + \frac{\sigma_H - \sigma_h}{2}\left(1 + 3\frac{R_w^4}{r^4}\right)\cos 2\theta - P_w \frac{R_w^2}{r^2} \tag{2.25}$$

$$\sigma_z = \sigma_v - 2\vartheta(\sigma_H - \sigma_h)\frac{R_w^2}{r^2}\cos 2\theta \tag{2.26}$$

$$\tau_{r\theta} = -\frac{\sigma_H - \sigma_h}{2}\left(1 - 3\frac{R_w^4}{r^4} + 2\frac{R_w^2}{r^2}\right)\sin 2\theta \tag{2.27}$$

$$\tau_{rz} = \tau_{\theta z} = 0$$

When the wellbore and perforation are pressurized in a fracturing operation, the starter fracture will initiate somewhere on the surface of the perforation, where the tensile failure criterion (Equation (2.18)) is satisfied. Therefore, all the points on the perforation surface should be analysed. However, in this section, to study a simple fracture initiation problem, it is assumed that the fracture initiates at the interface of the wellbore and perforation.

Accordingly, in order to analyse the perforation stress concentration at the wellbore interface, the stress distribution on the surface of the wellbore is required. This could be calculated by substituting R_w for r in Equations (2.24) to (2.27);

$$\begin{aligned}
&\sigma_r = P_w \\
&\sigma_\theta = \sigma_H + \sigma_h - 2(\sigma_H - \sigma_h)\cos 2\theta - P_w \\
&\sigma_z = \sigma_v - 2\vartheta(\sigma_H - \sigma_h)\ \cos 2\theta \\
&\tau_{r\theta} = \tau_{rz} = \tau_{\theta z} = 0
\end{aligned} \tag{2.28}$$

Having the wellbore stress distribution, in the next step, the perforation stress concentration should be studied. A perforation hole could be made in any orientation on the surface of the wellbore. In the simplest case, a perforation orientation is assumed to be in the direction of x axis (parallel to σ_H). Therefore, wellbore surface stress components at $\theta = 0°$ are required (see Figure 2-5), which could be calculated through the following equation:

$$\begin{aligned}
&\sigma_r = P_w \\
&\sigma_\theta = 3\sigma_h - \sigma_H - P_w \\
&\sigma_z = \sigma_v - 2\vartheta(\sigma_H - \sigma_h) \\
&\tau_{r\theta} = \tau_{rz} = \tau_{\theta z} = 0
\end{aligned} \tag{2.29}$$

The wellbore stress components in Equation (2.29) could now be substituted into Equation (2.21) to obtain the perforation surface stresses. However, perforation stress

components could be calculated at various circumferential positions around the perforation hole (θ_p). Therefore, to further simplify this specific analysis, the perforation stresses are only calculated at the top and bottom ($\theta_p = 0° \; or \; 180°$); and middle sides of the perforation hole ($\theta_p = 90° \; or \; 270°$). For $\theta_p = 0° \; or \; 180°$, Equation (2.21) is simplified as follow:

$$\sigma_{rp} = P_p$$
$$\sigma_{\theta p} = 3\sigma_\theta - \sigma_z - P_p$$
$$\sigma_{zp} = \sigma_r - 2\vartheta(\sigma_z - \sigma_\theta) \tag{2.30}$$
$$\tau_{r\theta p} = \tau_{rzp} = 0$$
$$\tau_{\theta zp} = 2(\tau_{r\theta})$$

Knowing that $P_p = P_w$, substituting the wellbore stress components obtained from Equation (2.29) will result in the following formulas:

$$\sigma_{rp} = P_w$$
$$\sigma_{\theta p} = (9 - 2\vartheta)\sigma_h - (3 - 2\vartheta)\sigma_H - \sigma_v - 4P_w$$
$$\sigma_{zp} = -2\vartheta(\sigma_v) - (2\vartheta - 4\vartheta^2)\sigma_H + (6\vartheta - 4\vartheta^2)\sigma_h + (1 - 2\vartheta)P_w \tag{2.31}$$
$$\tau_{r\theta p} = \tau_{rzp} = \tau_{\theta zp} = 0$$

As it is seen in these equations, all perforation shear stress components are zero at this point; therefore, the normal components are principal stresses. Among these three principal stresses, $\sigma_{\theta p}$ will be the minimum principal stress when the wellbore pressure is increased, since it will be reduced by a factor of $4P_w$. However, at the same time, the minimum principal stresses at $\theta_p = 90° \; or \; 270°$ would also decrease by increasing wellbore pressure; thus, it should likewise be calculated. To do so, for $\theta_p = 90° \; or \; 270°$ Equation (2.21) is simplified as follow:

$$\sigma_{rp} = P_p$$
$$\sigma_{\theta p} = 3\sigma_z - \sigma_\theta - P_P$$
$$\sigma_{zp} = \sigma_r + 2\vartheta(\sigma_z - \sigma_\theta) \tag{2.32}$$
$$\tau_{r\theta p} = \tau_{rzp} = 0$$
$$\tau_{\theta zp} = 2(\tau_{rz})$$

Substituting P_w for P_p, and the wellbore stress components obtained from Equation (2.29) into Equation (2.32);

$$\sigma_{rp} = P_w$$
$$\sigma_{\theta p} = 3\sigma_v - (1 + 6\vartheta)\sigma_H + (3 + 6\vartheta)\sigma_h - 2P_w$$
$$\sigma_{zp} = 2\vartheta(\sigma_v) + (2\vartheta - 4\vartheta^2)\sigma_H - (6\vartheta - 4\vartheta^2)\sigma_h + (1 + 2\vartheta)P_w \quad (2.33)$$
$$\tau_{r\theta p} = \tau_{rzp} = \tau_{\theta zp} = 0$$

Again in these equations, the shear stresses are all zero; therefore, the normal stress components are all principal stresses. In order to find the smallest minimum principal stress at the two positions on the perforation surface, a normal stress regime is assumed. The in-situ stresses are supposed to be 9000, 8000, and 7000 psi for σ_v, σ_H, and σ_h respectively, and a Poisson's ration of 0.28 is used for the formation rock. The perforation tangential and axial stress components obtained for Equations (2.31) and (2.33) are plotted versus wellbore pressure in Figure 2-6.

As it is seen from this figure, the axial stresses increase, while the tangential stresses are decreasing. Assuming a zero tensile strength for formation rock, the first fracture initiates at $\theta_p = 0° \; or \; 180°$, since the tangential stress at these points approach zero at a wellbore pressure of 7700 psi, which is the FIP. Since the initiated fracture plane is opening up perpendicular to the perforation tangential stress, the fracture initiation angle β is zero. Therefore, a longitudinal fracture will be propagated at top and bottom sides of the perforation, which in this case, is right at the PFP.

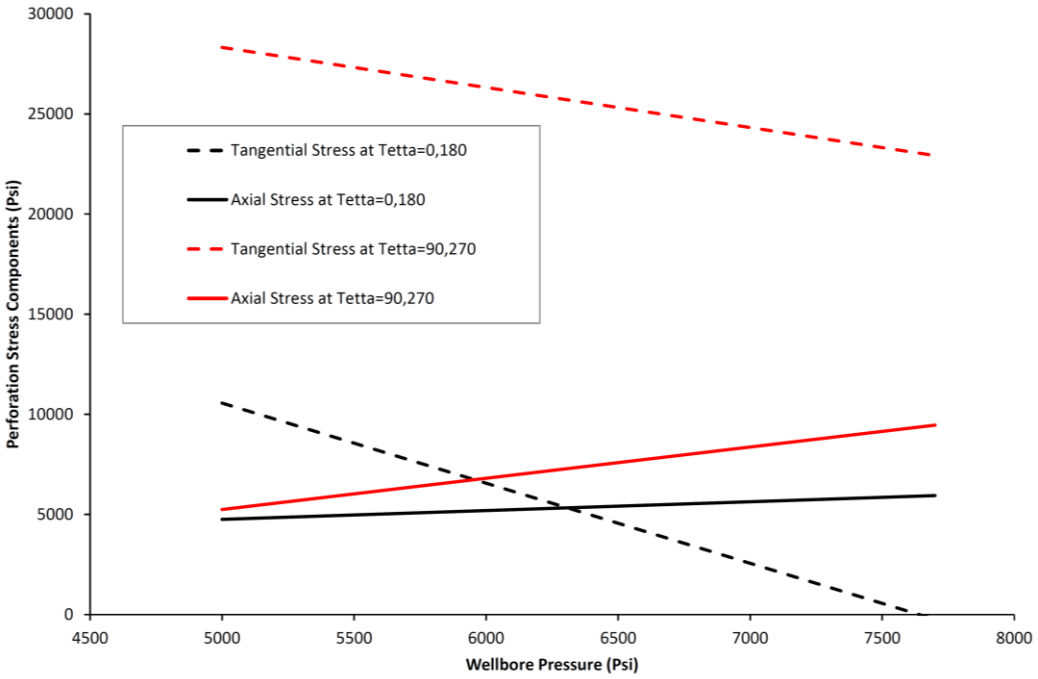

Figure 2-6 Comparing perforation principal stresses while the wellbore pressure in increasing.

2.4.2 Numerical solution for FIP in perforation hole

Since this modelling is developed for a general case of a deviated wellbore plus the point that the perforation could also be oriented in any direction around the wellbore; hence, it is not easy to analytically derive some equations to predict the FIP and the angle of the initial fracture.

Therefore, a numerical method is applied to resolve the problem and calculate the desired parameters. In this method, the wellbore pressure is raised stepwise by some specific pressure increment, and at the same time the perforation pressure is also increased. In every step, first, the wellbore stress distribution is calculated, and then this stress information is used to calculate the perforation stress distribution. Next, the critical point (θ_{cr}) with the smallest minimum principal stress is found, and then the results are calculated.

To carry out this numerical method, a program is developed using Matlab programming software to perform the calculations (Appendix A). The main steps in this program are summarized below; these steps are applied for a specific stress regime, formation pore pressure, and wellbore azimuth and inclination.

1. Divide the perforation length into some increments and select the first one (the number of the increments could be chosen by user, since increasing the perforation increment would increase the accuracy of the result, however, the program running time may increase significantly).
2. Choose the formation pore pressure as the first well pressure.
3. Increase the well pressure by a predetermined value (increment).
4. Calculate the stress components of the wellbore at the perforation orientation, and at r equal to the distance of the centre of the current perforation increment to the centre of the wellbore (using Equations (2.2)-(2.10)).
5. Divide the cylindrical perforation increment into some circumferential increments.
6. Calculate the perforation stress components at the centre of each circumferential increment (using Equation (2.21)).
7. Obtain the value of σ_3 for all the increments on circumference of the perforation (using Equation (2.22)) and find the smallest value.
8. Apply the tensile failure criterion to the smallest σ_3 (using Equation (2.18)),
9. If the criterion satisfies;

a. Record the well pressure as the fracturing pressure for that specific point of the perforation,
b. Record the specific fracture point on the circumference of the perforation (θ_{cr}),
c. Calculate and record the value of angle β (using Equation (2.23)),
d. Select the next perforation increment and go to step (2), if there is no more perforation increment go to step (10),

10. If the criterion does not satisfy go to step (3),
11. Find the minimum value of fracturing pressures which have been recorded at different perforation increments and record it as the FIP, and also record the corresponding value of angle β.

2.4.3 Micro-annulus creation

As it was discussed in Chapter 1, the perforation hole is made through the casing, cement, and some distance into the rock, as shown in Figure 2-7. As a result, when the perforation is pressurized for fracturing, the fluid may initiate a fracture in the cement sheath rather than the formation rock, and accordingly a detrimental micro-annulus may be created. In order to predict the creation of the micro-annulus, in this modelling, the cement elastic and strength properties including Biot's constant, Poisson's ratio, and tensile strength are used for the first few perforation increments, equivalent to the thickness of the cement sheath (see Figure 2-7). Therefore, based on the cement sheath properties, if the initial fracture develops at these first few perforation increments, an undesirable micro-channel may from behind the casing.

In some cemented wellbore, because of poor cement qualities or improper cementing operation, there may not be a proper casing-cement or cement-rock bonding. Such loose bonding may result in the formation of small cracks in these interfaces. Therefore, to incorporate these existing cracks in the modelling, the tensile strength of the cement sheath could be set to be zero at these boundaries. Consequently, there would be a higher chance for the pad fluid to create a micro-annulus in such situation.

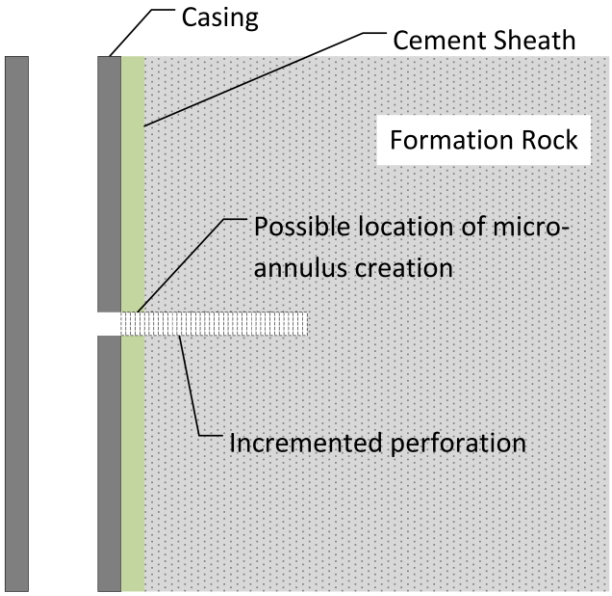

Figure 2-7 A schematic showing a perforation (incremented) on one side of a wellbore passing through the casing, cement sheath and formation rock.

2.5 Results and discussion

2.5.1 Introduction

As it is already mentioned, the major objective of this analytical modelling is to estimate the FIP in perforated wellbores. Therefore, in order to carry out the numerical modelling program, a set of data are required which includes;

- in-situ stress components (σ_v, σ_H, and σ_h),
- azimuth and inclination of the wellbore (a, and i),
- formation rock elastic and mechanical properties (P_f, ν, TS),
- cement thickness and its elastic and mechanical properties (t_c, ν, TS),
- And the orientation of the perforation.

In addition to FIP, this analytical-numerical model could also provide some further useful results as listed below;

- the stress distribution around the wellbore,
- location of the highest tensile stress area (maximum tension zone) on the wellbore surface,
- the most appropriate perforation orientation with respect to maximum tension zone,
- the analysis of the creation of micro-annulus in the cement sheath, and

- the location of the starter fracture and its angle relative to the perforation axis; this would then help in predicting the near wellbore fracture link-up and tortuosity.

Basically this fracture initiation model could be used in two main different stages of a well life;

- Firstly, when a wellbore is not drilled yet and it is still in the planning phase. If the production engineers are supposing to perform fracturing treatment when the wellbore is drilled and completed, then they could apply this modelling in order to propose the best wellbore orientation (inclination and azimuth angles), and gain an idea of proper cement sheath properties. Therefore, designing appropriate cement slurry, so that the chance of micro-annulus formation could be eliminated. In addition, the best perforation orientation could be selected to have an achievable FIP and reduce the near wellbore fracture tortuosity.
- Secondly, for a wellbore that is already drilled and completed. In this case, the wellbore and perforation orientations are almost permanent. While it is possible to re-perforate the wellbore in some other orientations, in contrary, there is almost no way to adjust the wellbore orientation and also modify the cement sheath properties. Therefore, this analytical model could be used in the fracturing treatment design phase, so that the FIP and the probability of micro-annulus creation could be analysed based on the current conditions. Additionally, the near wellbore fracture propagation geometry could be predicted.

Nevertheless, to apply this analytical model, it is primarily essential to check the validity of the model. Therefore, scaled hydraulic fracturing experiments are carried out to compare and confirm the match between the analytical and experimental results; this comparison is presented in Section 2.5.2. When the model is validated, it is then used for various applications in the subsequent sections

First of all, in Section 2.5.3, numerous wellbores are considered with various orientations in different in-situ stress regimes in order to locate the maximum tension zone for each wellbore. Next, the effects of wellbore orientation on the initiation pressure of a starter fracture is investigated and presented in Section 2.5.4. Moreover, the initiation pressure is studied at various stress regimes and stress anisotropies are studied in this section.

Then, the FIP is studied at various perforation orientations. It is noteworthy that the perforation orientation is investigated relative to the maximum tension zone of the wellbore. After that, the fracture initiation angle (β) is calculated in various conditions to predict the near wellbore fracture tortuosity. And finally, cement sheath and formation rock properties are studied to see how they impact the creation of micro-annulus and the FIP.

2.5.2 Model validation

When an analytical or numerical model is developed, it is initially necessary to ensure that the model is generating accurate results. Therefore, in this section, the results of four hydraulic fracturing experiments are compared with the results obtained from this model. The comparison confirms the accuracy of this analytical-numerical model.

For evaluation of the analytical model, hydraulic fracturing tests are conducted on cubic synthetically manufactured tight mortar samples. The use of cube samples allows application of three independent stresses to mimic real in-situ stress conditions. A true tri-axial stress cell is used for this purpose. The lab test parameters are scaled to simulate the operations at field scale. The hole and perforations were made into the sample after casting and curing were completed; more details on this experimental study could be found in Chapter 5 and Paper 3.

Since the mortar samples were tested dry, the term related to pore pressure is ignored in Equation (2.18) for this comparison. This would ensure that the analytical model is simulating the experimental samples more accurately. In addition, the mortar hydro-mechanics properties (see Paper 3) and the amount of applied experimental stresses were the input data into the analytical simulator.

Figure 2-8 presents the results of analytical modelling for these four experiments, where the changes in FIP along the perforation tunnel length are calculated. As it is seen in this figure, the minimum pressure for initiating a fracture in test 1-4 is 20 MPa which is very close to the FIP that was measured in the lab (i.e., 19.3 MPa); the experimental results are shown in Table 2.1. Also it should be mentioned that, the plot corresponding to test 1-4 in Figure 2-8 shows that fracture has not been initiated at the intersection point of the perforation and wellbore, but at a distance away, inside the perforation hole. The experimental breakdown pressure (BDP) in test 1-4 was 21.16 MPa. And according to Figure 2-8, when the wellbore pressure reaches

this BDP, it appears that some additional fracture planes should have been initiated along the perforation tunnel; this is because the BDP is larger than the FIP at some other sections of the perforation hole. This has resulted in multiple fracturing, which was observed in this test.

Table 2.1 Experimental results for validating the analytical modelling.

Test	σ_1(MPa)	σ_2(MPa)	σ_3(MPa)	Number of Perforations / Orientation	Initiation Pressure (MPa)	Break down Pressure (MPa)
1-4	20.68	13.79	6.89	1 / Minimum Stress	19.30	21.16
1-5	20.68	13.79	6.89	1 / Intermediate Stress	6.82	7.58
2-2	20.68	10.34	6.89	4 / Minimum Stress	12.41	14.47
2-3	20.68	10.34	6.89	4 / Intermediate Stress	6.89	7.62

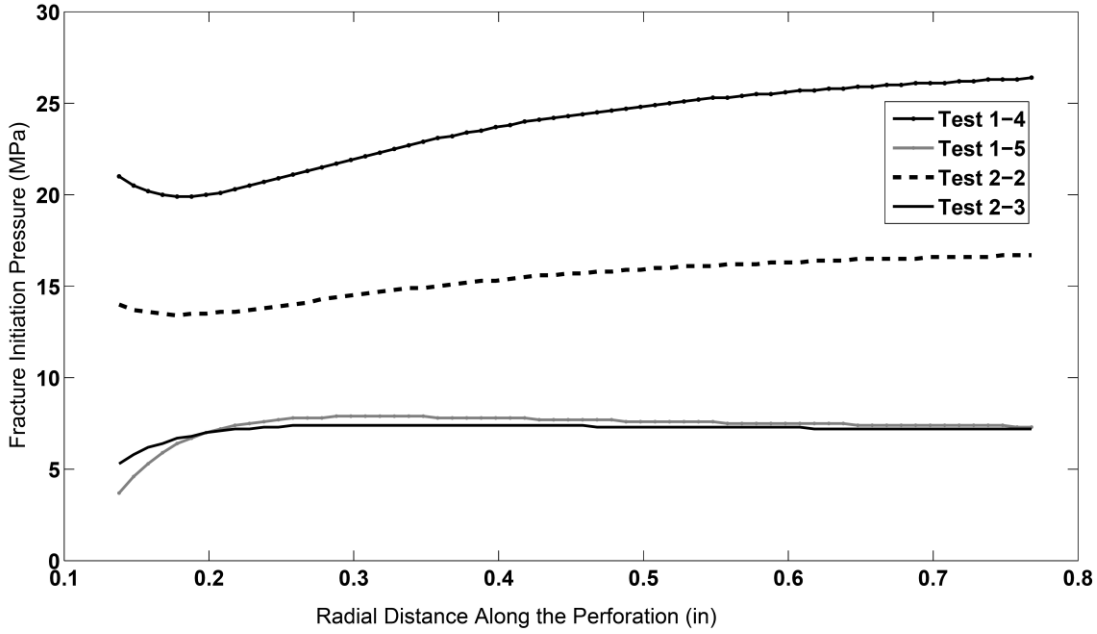

Figure 2-8 Analytical FIP along the perforation tunnel for four different tests.

From the analytical result (Figure 2-8) the FIP for test 1-5 is 5.3 MPa which is close to the experimental outcome (i.e., 6.82 MPa). In addition, the analytical results for this test shows that the fracture was initiated at the intersection of the perforation hole and wellbore wall.

In test 1-4 the perforation was aligned with the direction of minimum stress; therefore, two the maximum and intermediate stresses were perpendicular to the axis of perforation tunnel. This caused a very high-stress concentration around the perforation and, consequently, the fracturing pressure increased significantly. In test 1-5, where the perforation was run along the intermediate stress direction, the

minimum and maximum stresses were perpendicular to the axis of perforation. So, the fracture was initiated and propagated at much lower pressure. The same results are obtained from the analytical simulation (Figure 2-8).

An evaluation of the results of tests 2-2 and 2-3 yields similar conclusions. The FIP in test 2-2, where the perforations are oriented towards the minimum stress direction, is 12.41 MPa, whereas it is 6.89 MPa for test 2-3, in which the perforations are in the direction of intermediate stress. The analytical modelling also resulted in almost the same FIPs for these two tests. This close agreement confirms that the developed analytical model is capable of predicting accurate FIPs and fracture initiation location for hydraulic fracturing applications. It also emphasises the benefits of using analytical models as a starting point when studying hydraulic fracturing from a perforated wellbore. In the following sections, various applications of this modelling are discussed.

2.5.3 Wellbore maximum tension zone

The wellbore tangential (hoop) stress, σ_θ, determines the wellbore maximum tension zone. Based on Equation (2.6), σ_θ depends on θ, the angular position around the wellbore measured relative to the x axis, as depicted in Figure 2-2. This wellbore normal stress component is typically a compressive stress which may become tensile, when the wellbore pressure increases to some high level. However, because of horizontal stress anisotropy, all tangential stresses around the wellbore do not become tensile at the same wellbore pressure. Accordingly, as the wellbore pressure is increasing in a fracturing treatment, the first point on the wellbore circumference that would experience tensile tangential stress is known as the wellbore maximum tension zone (tensile zone).

The tensile zone of a wellbore is shown in Figure 2-9, which is created by evaluating the tangential stress (TS), and minimum principal stress (MPS) on the circumference of the wellbore at two wellbore pressures. As it is shown in this figure, TS and MPS tend to more tensile (positive) values as the wellbore pressure is increased. The highest tensile stress area indicates the tensile zone of the wellbore. The position of the tensile zone is normally very important for a fracturing operation, since in open boreholes, the first fractures typically initiate at this zone. However, in cased wellbores, the relative orientation of a perforation with respect to the tensile zone may influence the FIP of that perforation.

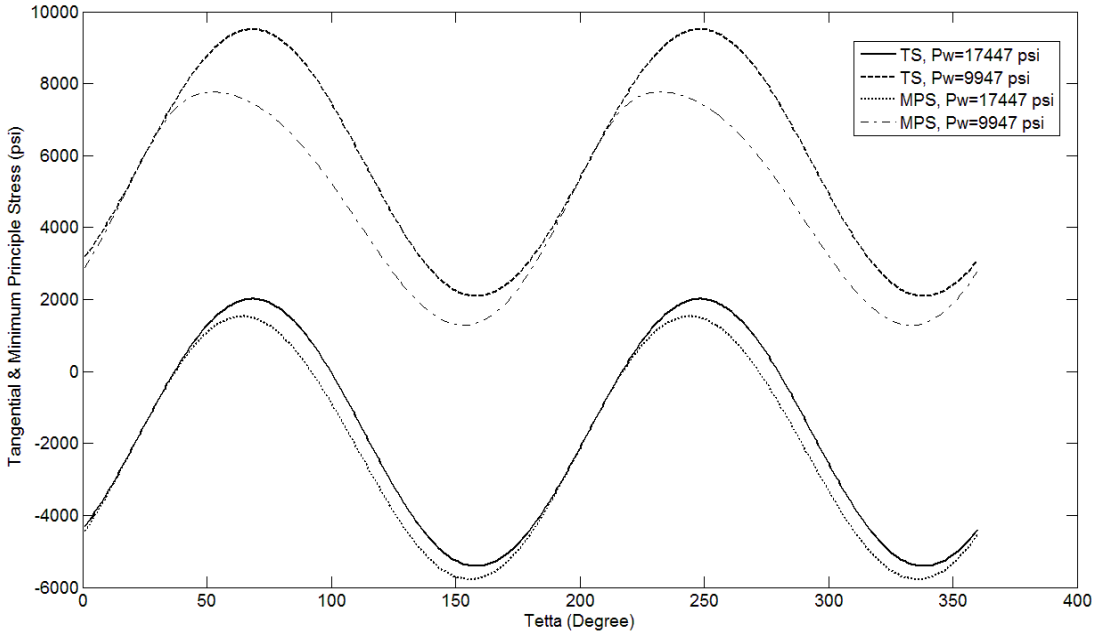

Figure 2-9 The effect of wellbore pressure on tangential and minimum principal stress on the surface of a wellbore.

The location of the tensile zone on the circumference of a wellbore also depends on the wellbore orientation as well as the prevailing in-situ stress regime. Therefore, before any fracture initiation analysis, it is of great importance to locate this zone for different wellbores at various deviation and stress conditions. The following figures present the situation of tensile zone at three different stress regimes and varying wellbore inclination and azimuth.

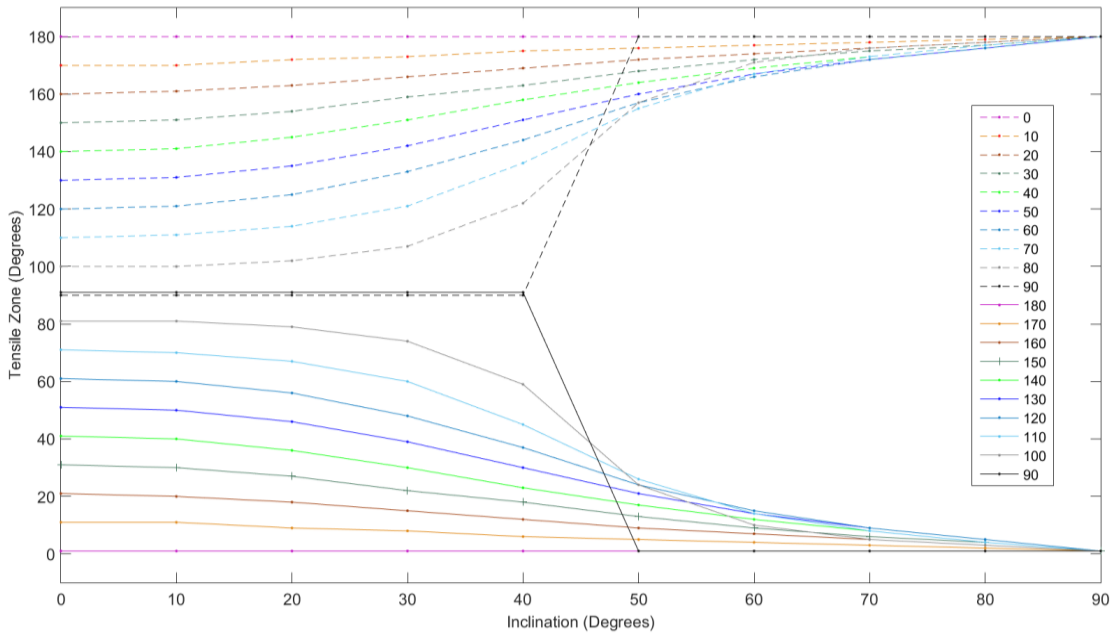

Figure 2-10 The effects of wellbore inclination and azimuth on the tensile zone position around a wellbore in a normal stress regime area.

Figure 2-10 presents the effects of wellbore inclination and azimuth $(0^{\circ}, 180^{\circ})$ on the tensile zone position around a wellbore which is located in a normally stressed regime field. As it is depicted in this figure, the influence of wellbore inclination is more significant when the wellbore is inclined towards the direction of the minimum in-situ horizontal stress σ_h $(A = 90^{\circ})$. However, when the wellbore is parallel with the maximum in-situ horizontal stress σ_H $(A = 0^{\circ}, 180^{\circ})$, the inclination angle does not have any effect and in this situation, tensile zone is always at a position making an angle of 0° or 180° with the wellbore x axis (refer to Figure 2-2). This means that the tensile zone is located on the top or bottom side of the wellbore. This makes sense when imagining an inclined wellbore in the direction of σ_H, since the wellbore is drilled in a plane perpendicular to the direction of σ_h (PFP), the fracture will always initiate on the top and bottom sides of the wellbore, regardless of the well inclination. It is helpful to recall that in a normal stress regime $\sigma_v > \sigma_H > \sigma_h$.

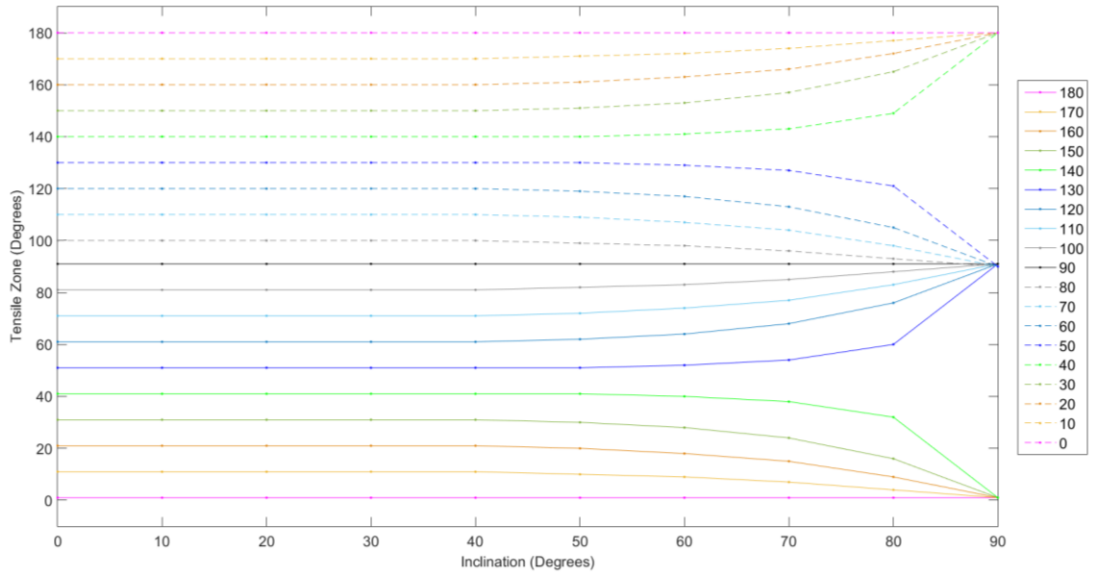

Figure 2-11 The effects of wellbore inclination and azimuth on the tensile zone position around a wellbore in a strike slip stress regime area.

However, for a strike slip stress regime $\sigma_H > \sigma_v > \sigma_h$; therefore still the PFP is perpendicular to the direction of σ_h. Figure 2-11 shows the position of tensile zone for various wellbore orientations in such stress regime. The significant changes in the pattern of most curves, in comparison to the ones in Figure 2-10, emphasize the general effect of the prevailing stress regime on the tensile zone location. However, if a borehole is drilled parallel to σ_H direction in a strike slip stressed region, the tensile zone position would be the same as a σ_H-oriented wellbore in the normal stress regime. This is due to the fact that in both stress regimes σ_h is vertical to PFP.

Further analysis of Figure 2-11 shows that, when a well is drilled along the direction of σ_h, the zone of maximum tension is always positioned at an angle of 90˚ away from the lowermost side of the wellbore (x axis direction). This indicates that the tensile zone is located on the sides of the borehole. Therefore, considering an open hole drilled in this orientation (σ_h), the starter fractures initiates on the middle sides of the wellbore, opening mostly against σ_h and σ_v for low and high inclined wellbores respectively. Thus, if the wellbore is horizontal in this direction, horizontal fractures are supposed to initiate from the tensile zone of the wellbore. But this may not occur in the field, as in this case transverse vertical fractures would initiate from the wellbore wall, opening up perpendicular to σ_h direction. Therefore, one may conclude that hydraulic fractures may not always initiate from the tensile zones of the wellbore. The reason behind this is that the tensile zone is only evaluated based on the tensile tangential stress around the wellbore. However, it is still a good reference for the purpose of analysing the perforation orientation effects.

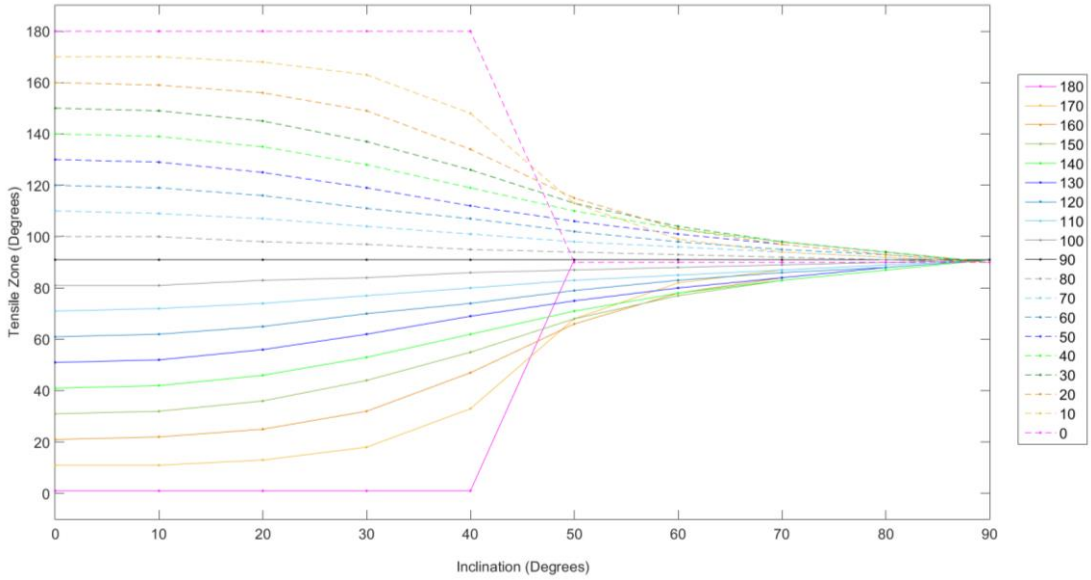

Figure 2-12 The effects of wellbore inclination and azimuth on the tensile zone position around a wellbore in a reverse fault stress regime area.

For a reverse fault stress regime, the relative magnitude of the principal stress components is $\sigma_H > \sigma_h > \sigma_v$; therefore, as it is depicted in Figure 2-12, the location of maximum tension zone for this stress regime is not similar to other two stress regimes. As an example, for a borehole, which is oriented towards σ_H, and when the inclination angle is below 40˚, the tensile zone is nearly positioned on the top and bottom side of the wellbore (0˚ and 180˚ away from the x axis). This is because at such well azimuth and inclinations, the intermediate principal stress (σ_h) makes a

prevailing effect on the fracture initiation. However, when the wellbore becomes more inclined, for inclination angles larger than 50˚, the minimum principal stress (σ_v) would have a dominant influence; consequently, the position of the tensile zone would move to 90˚. This means that the starter fractures would mostly initiates on the side of the wellbore and open up generally against the vertical stress.

2.5.4 Impacts of borehole orientation and stress regime on FIP

After analysing the maximum tension zone position in different wellbore orientations under three different in-situ stress regimes, the FIP in perforation hole is studied in this section. The effects of wellbore orientation, prevailing stress regime, and stress anisotropy are analysed using the developed analytical model. In order to specifically study these parameters, the perforation orientation is always located in the direction of the tensile zone of the wellbore, so that the impact of each parameter could be analysed properly. The tensile zone orientation of each wellbore is obtained from the graphs presented in Section 2.5.3. The perforation orientation effect is investigated in Section 2.5.5.

Table 2.2 Modelling input parameters, their units and assigned magnitudes.

Parameter	Unit	Magnitude
Wellbore true vertical depth	ft	10000
Wellbore radius	in	3.5
Maximum principal stress	psi	11000
Intermediate stress gradient	psi	10000
Minimum stress gradient	psi	9000
Pore pressure	psi	4560
Cement thickness	in	1
Cement Biot's constant	-----	0.6
Cement Poisson's ratio	-----	0.2
Cement tensile strength	psi	500
Formation rock Biot's constant	-----	0.7
Formation rock Poisson's ratio	-----	0.25
Formation rock tensile strength	psi	500

According to Section 2.5.1, some input parameters are required in order to run this analytical-numerical model; therefore, some common magnitudes for these parameters are considered, which are listed in Table 2.2.

Entering these values in the developed Matlab program, a series of graphs are generated to analyse FIP in various in-situ stress and wellbore direction conditions.

For each specific stress regime, two extreme wellbore azimuth are investigated, one wellbore parallel to the direction of σ_h and the other one parallel to σ_H; this is done for various inclinations. In addition, the effect of stress anisotropy is studied by varying the relative magnitudes of the in-situ principal stresses through the following graphs.

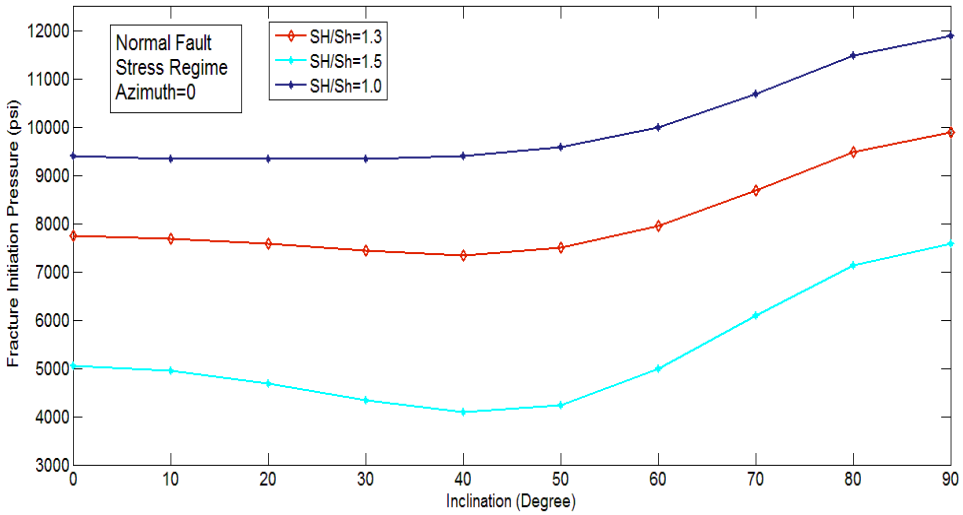

Figure 2-13 FIP for wellbores drilled parallel to σ_H in a normal stress regime area.

Figure 2-13 presents perforation FIP for different wellbores with various inclinations locating in PFP (parallel to σ_H) in a normal stress regime area. As it is shown in this figure, generally the FIP increases as the wellbores are becoming more inclined. This feature is more significant when the wellbore inclination is greater than 50˚. This is mainly due to perforation stress distribution which is varying as the inclination of the wellbore is increasing. Based on Figure 2-10, the tensile zone of all wellbores examined in Figure 2-13 is 180˚, meaning that it is located on the top side of the wellbore. Therefore, the perforation orientation is always kept in this position for the results presented in Figure 2-13.

However, as the wellbore is becoming more inclined, the 3D position of the perforation is changing relative to the in-situ stress components. As a result, σ_H will have more dominant effect on the perforation of a more inclined wellbore, in comparison to σ_v; consequently, the perforation stress profile would change and higher FIPs are resulted. In addition to the inclination effect, Figure 2-13 also illustrates that as the horizontal stress anisotropy increases; it would result in lower FIPs.

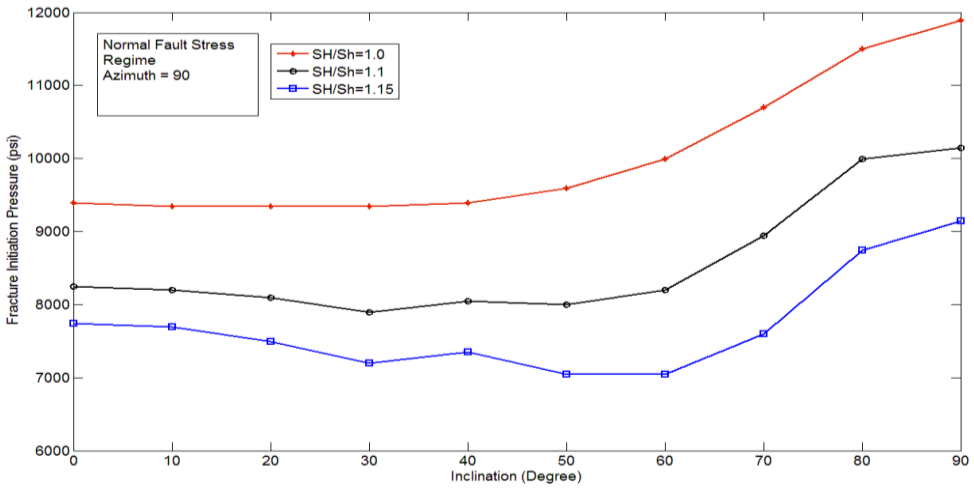

Figure 2-14 FIP for wellbores drilled parallel to σ_h in a normal stress regime area.

The graph presented in Figure 2-14 is almost similar to the one in Figure 2-13; however, the wellbore azimuth for this figure is parallel to the direction of σ_h. As it is seen from this figure, again by increasing the horizontal stress anisotropy, lower FIP are required. But it should be noticed that according to Figure 2-10, the tensile zone position for an azimuth angle of 90° varies by the wellbore inclination. Therefore, to keep the perforation orientation in the direction of tensile zone, the relative phasing of the perforation with respect to the lower side of the wellbore (x axis) is specified for every inclination angle.

The other outcome that could be drawn from Figure 2-14 is that, similar to Figure 2-13, as the wellbore inclination angle increases, generally higher pressure is required to initiate a starter fracture in the perforation. This effect is more pronounced for the wellbore inclinations larger than 60°. This is basically due to the fact that as the wellbore inclination is changing, the perforation surface stress would redistribute and this may change the stress concentration in various points on the circumference and along the perforation hole.

Nevertheless, the graph shown in Figure 2-15 indicates that the effect of wellbore inclination on FIP is a function of the prevailing stress regime. As it is shown in this figure, by increasing the wellbore inclination, the FIP reduces, overall. The main reason causing such result is the fact that σ_v is the least principal in-situ stress in a reverse fault stress area; therefore, as the wellbore becomes more inclined in this condition, the starter fracture may initiate almost perpendicular to the direction of vertical stress. This would result in lower FIP.

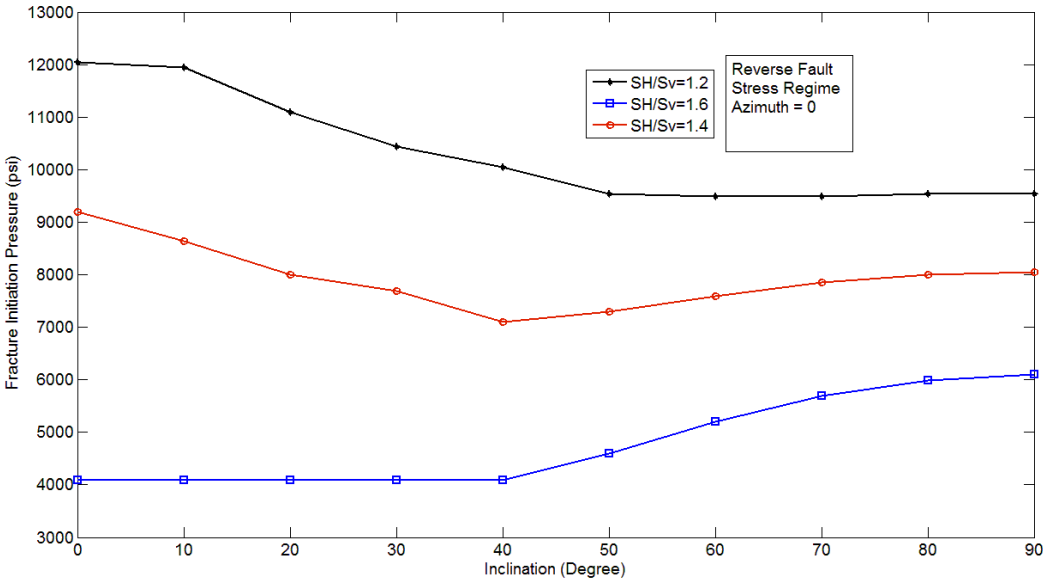

Figure 2-15 FIP for wellbores drilled parallel to σ_H in a reverse fault stress regime area.

However, such general feature may not come true in all stress anisotropy situations. Since, as Figure 2-15 depicts, when the stress ratio σ_H/σ_v increases to 1.6, the wellbore inclination angle plays a different effect. It should also be noticed that based on Figure 2-12, the tensile zone position and accordingly the orientation of the perforation is a varying parameter for the analysis of the results presented in Figure 2-15.

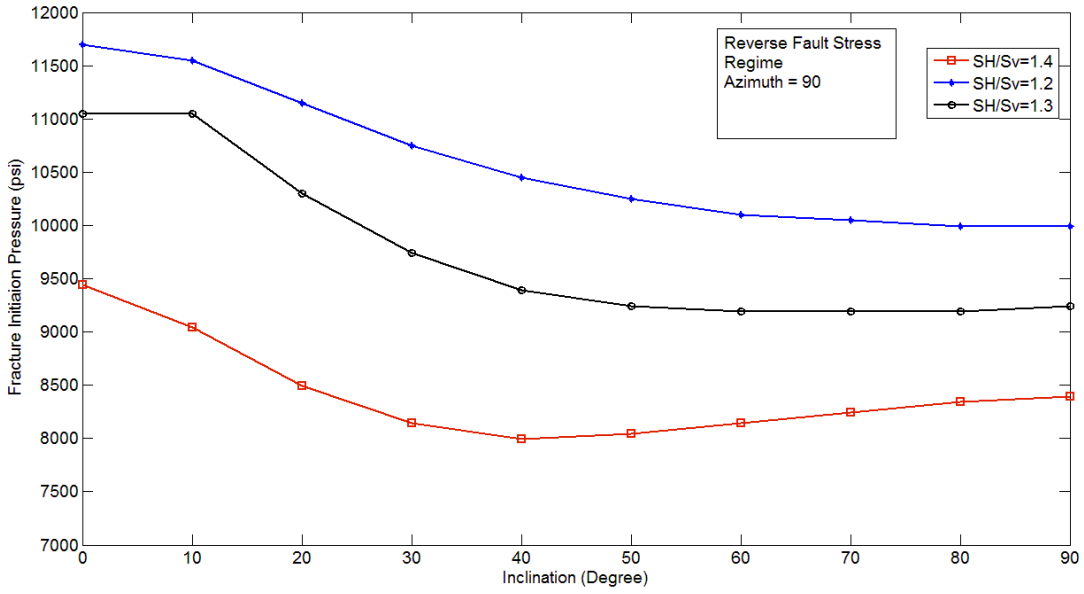

Figure 2-16 FIP for wellbores drilled parallel to σ_h in a reverse fault stress regime area.

Figure 2-16 is presenting more or less similar trends to the previous figure, as the FIP generally decreases by wellbore inclination. In addition, for similar level of stress anisotropy, the quantities of the initiation pressures are almost identical to the case when wellbore is oriented towards σ_H. This reveals that the FIP is not a strong

function of wellbore azimuth when the prevailing stress regime is reverse fault. However, it should be remarked that all these graphs are generated for a perforation orientation being in the direction of the wellbore tensile zone. Therefore, if the perforation orientation changes, the perforation stress concentration may change significantly and as a result the FIP trends might change too. Hence, every particular wellbore, perforation, and in-situ stress conditions should be analysed specifically.

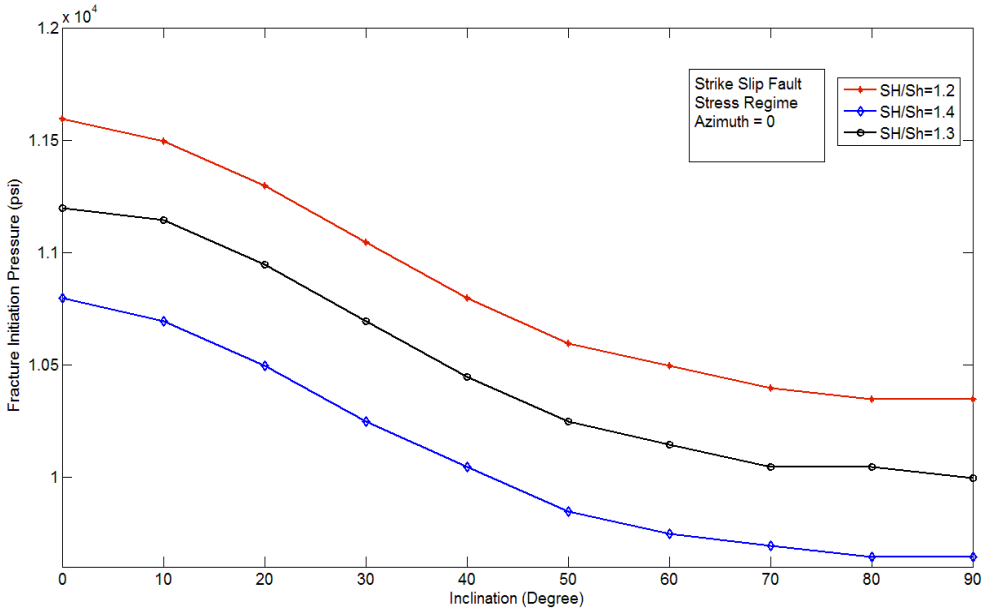

Figure 2-17 FIP for wellbores drilled parallel to σ_H in a strike slip stress regime area.

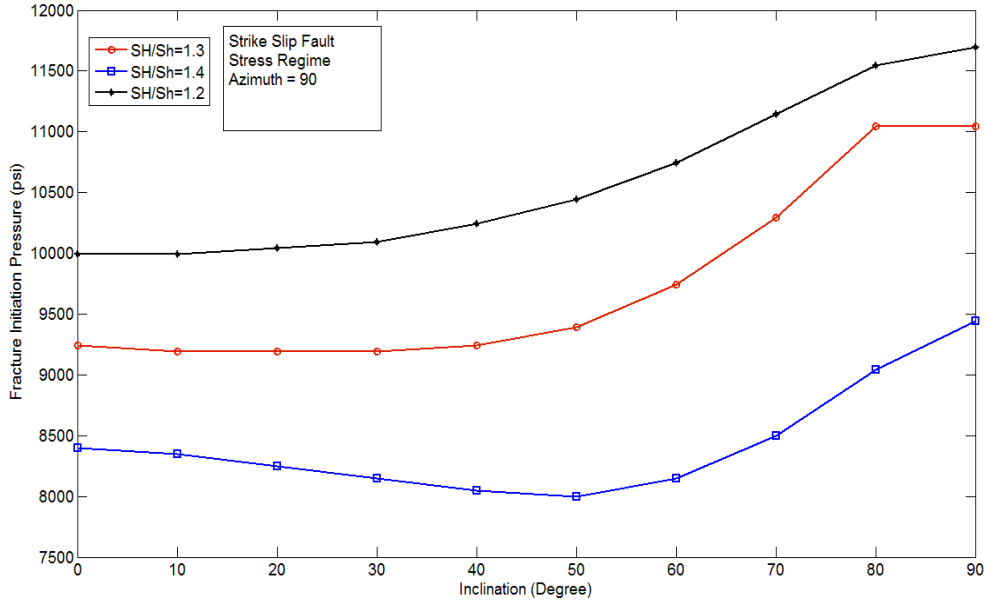

Figure 2-18 FIP for wellbores drilled parallel to σ_h in a strike slip stress regime area.

FIP is also analysed for inclined wellbores in strike slip stress regime. As Figure 2-17 shows, when the wellbore is oriented parallel to σ_H direction, by increasing the inclination angle, the FIP decreases. On the other hand, when the

orientation of the wellbore is towards σ_h direction, higher inclined wellbores generally require higher pressure to initiate a fracture in their perforation, according to Figure 2-18. This means that when the in-situ stress regime is strike slip, the azimuth angle of a wellbore has a great influence on its perforation FIP. Such significant azimuth influence was not observed for the other two stress regimes. Yet, it is noteworthy to again recall that, for all these FIP analyses done so far, the perforation orientation is kept along the direction of the maximum tension zone. As it was presented previously in Section 2.5.3, the maximum tension zone position is always a function of the wellbore orientation and prevailing stress regime. Therefore, these results may change, if the perforation orientation moves away from the maximum tension zone of the wellbore.

The other remarkable result, which is discovered from both Figure 2-17 and Figure 2-18, is the point that by increasing the stress anisotropy, the FIP of the perforation reduces. The same result was more or less observed in all other stress regimes and wellbore orientations. However, it should be noted that, in all these cases, the stress anisotropy was imposed by decreasing the smaller stress component, while the other stress value was kept constant. This has resulted in a reduction in the first stress invariant (I_1), therefore, generally less in-situ stress magnitudes were applied on the wellbore and perforation, resulting in lower FIPs.

However, according to experimental studies (see Paper 3), when the stress anisotropy is imposed by increasing one of the stress components, while keeping the other one constant; this will lead to an increase in the first stress invariant, and the FIP generally increases. In addition, the perforation orientation plays an important effect on the role of the stress anisotropy. In other words, depending on the perforation direction, if the stress anisotropy is associated with the values of those stress components which are perpendicular to the axis of the perforation, the perforation stress distribution will be affected to some extent; therefore, the fracturing pressure will also be influenced.

2.5.5 Impacts of perforation orientation on FIP

In Section 2.5.4, the perforation orientation for all FIP analyses were kept in the tensile zone of the wellbore; however, in the field operations, the perforations may have various phasing orientations as shown in Figure 2-19. As it is already stated, the perforation orientation has a significant effect on the FIP and the geometry of the fracture around the wellbore. To further investigate this effect, various perforation orientations are analysed in this section.

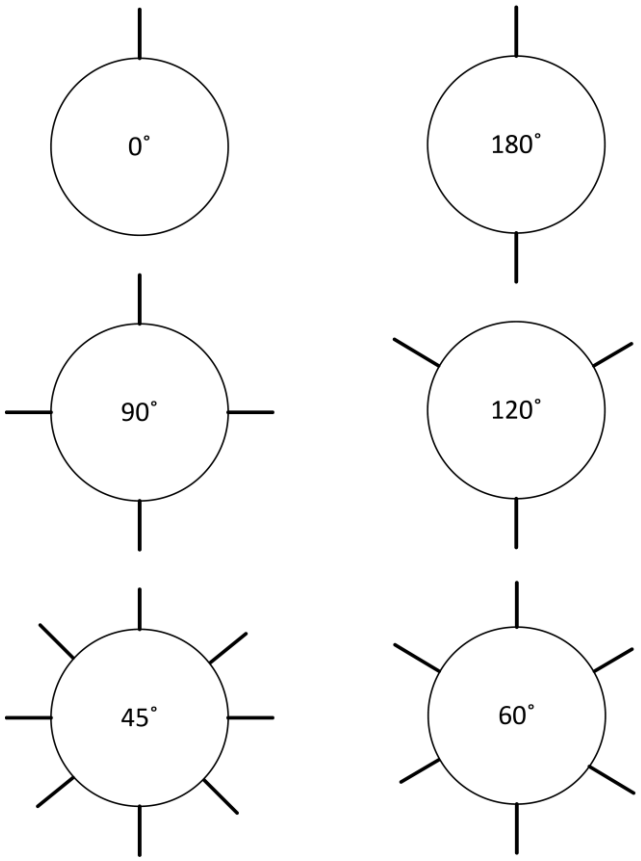

Figure 2-19 A schematic of various perforation phasing patterns.

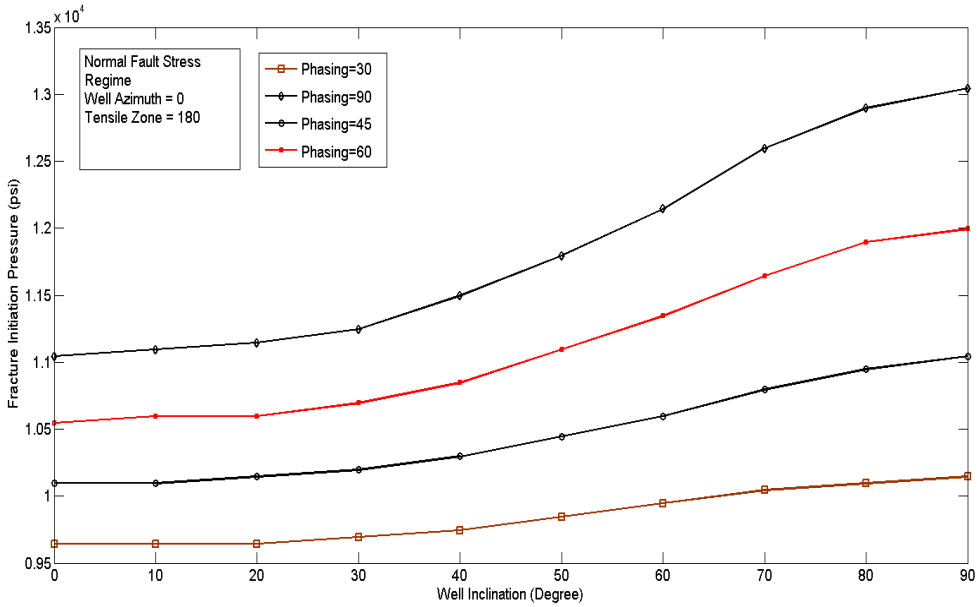

Figure 2-20 FIP for wellbores drilled parallel to σ_H in a normal stress regime with different perforation orientations.

The graph presented in Figure 2-20 illustrates the influence of perforation phasing orientation for various wellbores drilled in a normal stress regime area. All wellbores have an azimuth of 0° with varying inclinations; accordingly based on Figure 2-10, they all have a similar tensile zone on the top and bottom sides of the borehole. Consequently, in Figure 2-20, the perforation orientation is examined according to the tensile zone direction. This figure shows that, as the perforation phasing is moving further away from the tensile zone direction, higher FIPs are experienced.

This is generally in good agreement with the previous studies presented in the open literature (C. H. Yew & Weng, 2014). However, similar result has not been observed over the course of this study. In fact there are some other cases of wellbore orientations and in-situ stress regimes where lower FIPs could be achieved by making the perforation orientation further away from the tensile zone of the wellbore. Some of these observations are presented in the next graphs.

Figure 2-21 presents one of the cases in which tensile zone is not always the right place for perforating. As it is seen in this figure, for this particular wellbore azimuth and stress regime, perforation orientation effect on FIP varies as the wellbore inclination angle increases. When the inclination angle is below 45°, the lowest FIP is achieved by placing the perforation in the tensile zone of the wellbore, and as the perforation orientation moves away from the tensile zone, the FIP increases. The

same result is discovered for the wellbores with inclination angles larger than approximately 75˚.

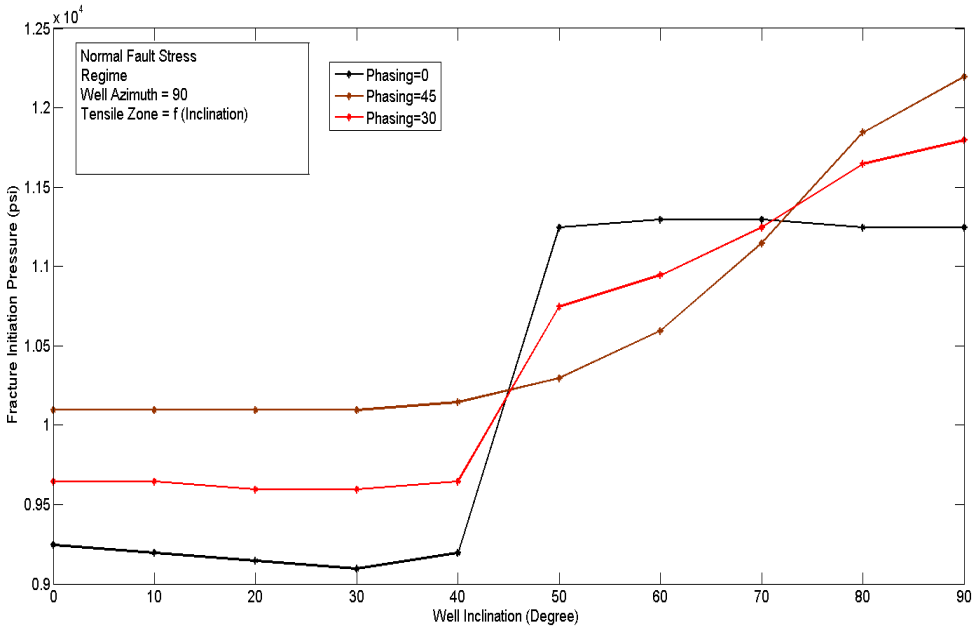

Figure 2-21 FIP for wellbores drilled parallel to σ_h in a normal stress regime with different perforation orientations.

However, when the wellbore has an inclination angle in the range of 45˚ to 75˚, the FIP trends change. In fact, for this range of inclination angle, it is easier to initiate a fracture in a perforation that is more deviated with respect to the direction of the wellbore tensile zone. Similar results are obtained in some other cases as well.

As an example, the graph shown in Figure 2-22 also presents similar trends. This graph is generated for wellbores drilled in the direction of σ_H, while the prevailing stress regime is reverse fault. As per the presented trends, lower FIPs are required to initiate a fracture in a perforation, which is made further away from the maximum tension zone of the wellbore. This outcome is relevant to wellbores having inclination angles ranging from 18 to 45 degrees.

Such remarkable result emphasizes that it is not always appropriate to perforate a wellbore in the direction of its maximum tension zone. Since, the FIP in a perforation hole is not directly a dependent of the wellbore stress concentration; however, it is primarily a function of the perforation stress concentration, though wellbore stress distribution has substantial influence on the perforation stress profile. This is while some previous studies available in the literature had almost analysed the wellbore stress concentration, virtually ignoring the perforation effect, and had concluded that

it is the best practice to always perforate along the tensile zone of the wellbore (Pearson et al., 1992; C. Yew et al., 1989; C. H. Yew & Weng, 2014).

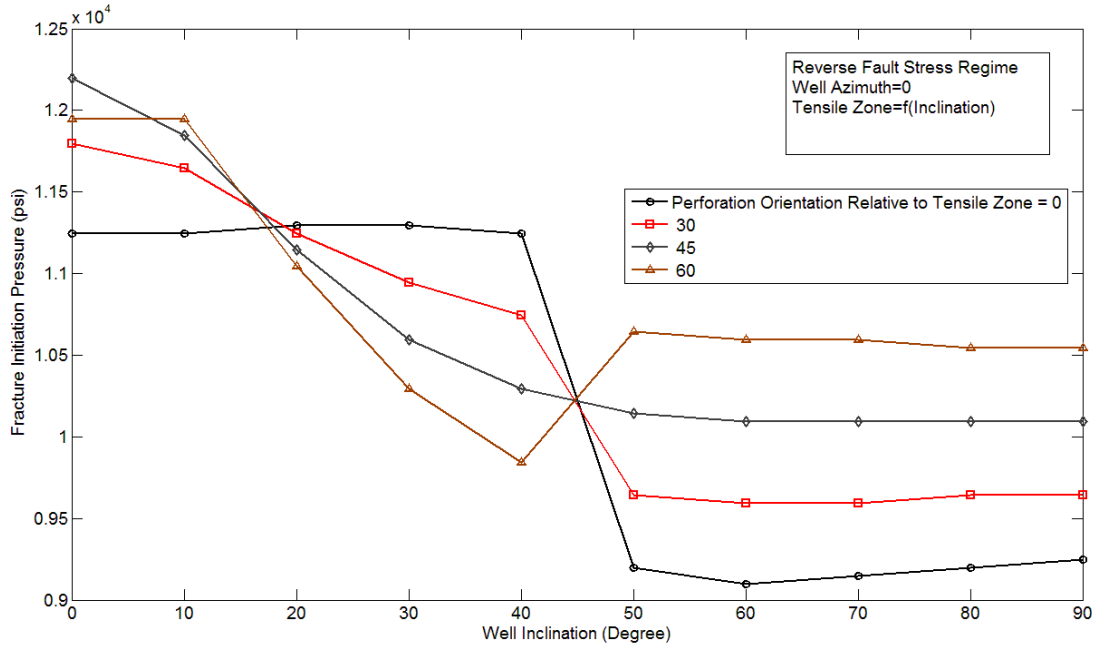

Figure 2-22 FIP for wellbores drilled parallel to σ_H in a reverse fault stress regime with different perforation orientations.

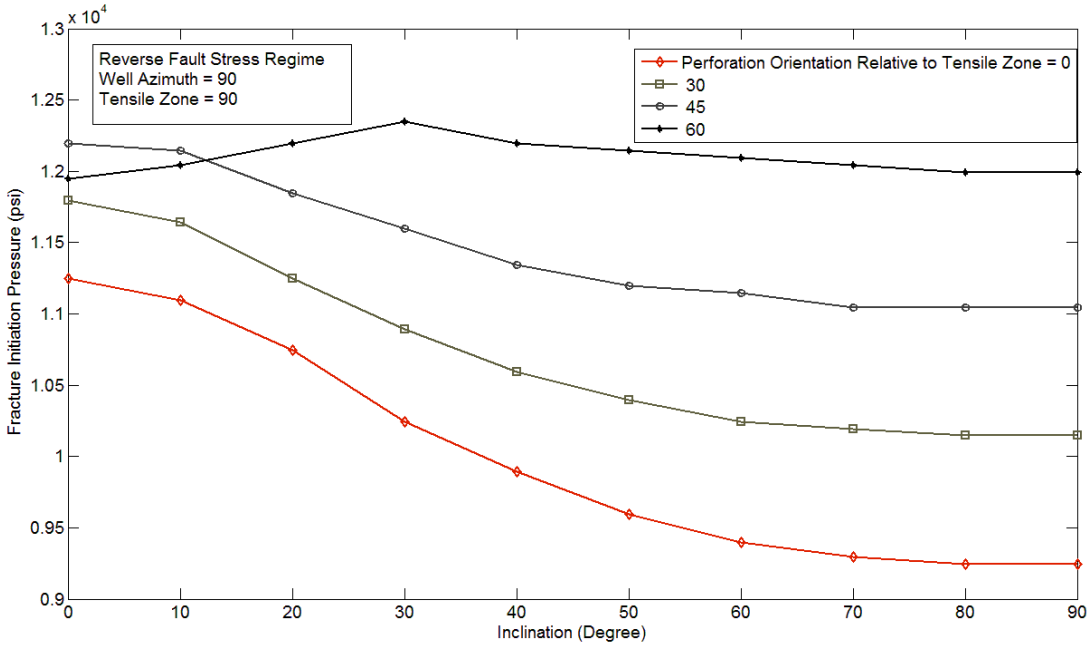

Figure 2-23 FIP for wellbores drilled parallel to σ_h in a reverse fault stress regime with different perforation orientations.

Figure 2-23 shows a general trend of increase in FIP as the perforation orientation is moving further away from the maximum tension zone. In addition, as the wellbore inclination increases, the FIP reduces. However, when the perforation orientation is

60˚, a reverse trend is observed. In this case, for the inclination angles ranging from 0 to about 30 degrees, more inclined wellbores would experience higher FIP in their perforations. Even when the inclination angle is less than about 12˚, a 60˚ oriented perforation will have lower FIP in comparison to a 45˚ oriented perforation. This observation confirms that the best practice is not always to perforate along the wellbore tensile zone. Therefore, it is essential to analyse the wellbore and perforation stress concentrations simultaneously to obtain the best fracturing-aimed perforating orientation.

The other important feature that could be observed from this modelling result is that, regardless of the prevailing stress regime and the wellbore orientation, when the wellbore is perforated in all directions (45, 60 or 90 degrees phasing), it is more probable to have multiple fracturing. Considering the first stage of a hydraulic fracturing treatment, when the wellbore pressure is increasing, as soon as the wellbore pressure reaches the lowest FIP in a perforation hole, the first fracture may initiate (see Figure 2-23). Then, the wellbore pressure should further increase to propagate that starter fracture. Accordingly, the next perforation FIP may be satisfied, so another starter fracture will be initiated in this perforation. As the wellbore pressure is increasing, further fractures will be initiated in the other neighbouring perforations, which have a different orientation with respect to the first fractured perforation. This would increase the probability of near wellbore fracture complexity.

However, if the wellbore is perforated according to a greater phasing pattern (180˚ phasing), providing that the perforation orientations are properly selected, less multiple fracturing and fracture complexity may occur. This improves the near wellbore fracture geometry and lessens the chance of having premature screen out.

2.5.6 Fracture tortuosity

As it is illustrated in Figure 2-4, the starter fracture develops on a plane tangent to perforation surface and perpendicular to minimum principal stress direction. According to Section 2.4, this starter fracture plane is not necessarily parallel with perforation axis and may make an angle β with this axis. Such initial fracture plane may not be aligned with the direction of PFP too, since the initiation mechanism is dominantly dictated by the wellbore and perforation stress concentrations, rather than the minimum far field stress. Therefore, as the starter fracture propagates in the

vicinity of wellbore, it may develop a curved path, in some distance away from the wellbore and perforations, to become aligned with the PFP direction (see Figure 1-4).

The curvature of the near wellbore fracture geometry could be studied by comparing the fracture initiation angle β with the PFP direction. This should be done while the relative orientations of wellbore, perforation and PFP are considered. As it is explained in Section 2.4, the angle β could be calculated using Equation (2.23). Accordingly, the following graphs are produced for some stress conditions and various wellbore and perforation orientations to better study this feature of the presented model.

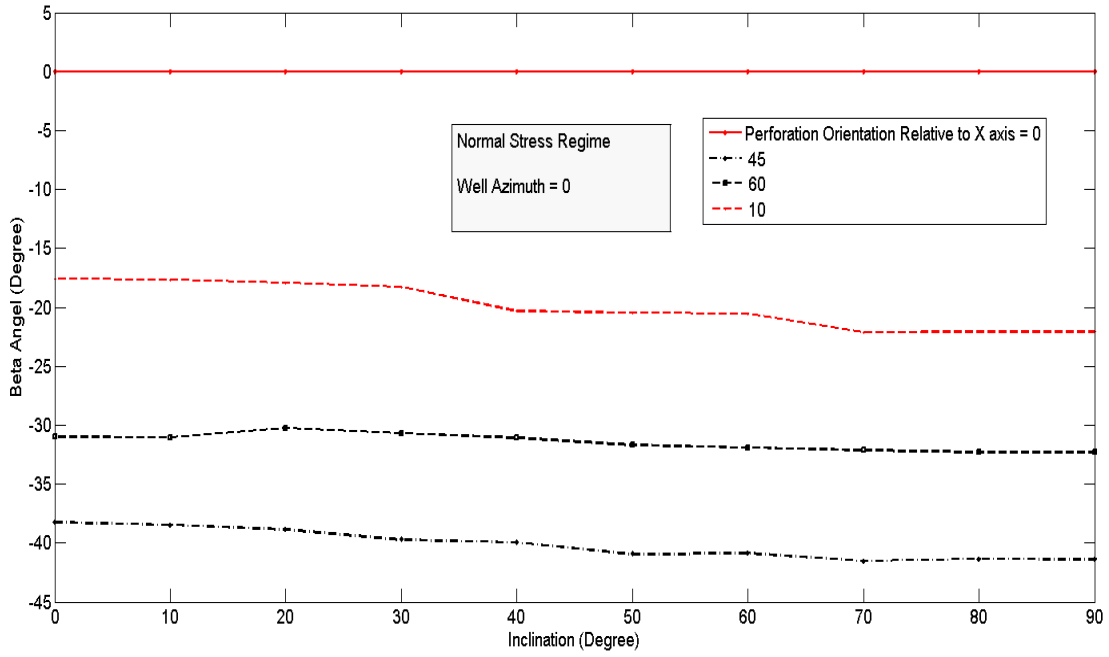

Figure 2-24 Fracture initiation angle for wellbores drilled parallel to σ_H in a normal stress regime.

Figure 2-24 shows the fracture initiation angle versus wellbore inclination, while a fixed wellbore azimuth of 0° is assumed. Different perforation orientations are considered to generate this figure. For example, when the perforation is located at the bottom side of the well, aligned with wellbore x axis (see Figure 2-2), the initiation angle is not a function of wellbore inclination, and it is constantly zero. Meaning that, the starter fracture is opening up against the perforation tangential stress component, which in this case is the perforation minimum principal stress. Accordingly, the initiated fracture is parallel to the perforation axis. Such modelling result is physically justifiable, since, in this specific wellbore and perforation orientations, both wellbore and perforation are located in PFP. Therefore, regardless

of the wellbore inclination, the initiated fracture will always be parallel to perforation axis and accordingly to the PFP. This will result in a planar near wellbore fracture propagation.

However, when the perforation orientation deviates away from the x axis, the initiation angle is no longer equal to zero; this is clearly shown in Figure 2-24. Such non-zero initiation angle may result in tortuous near wellbore fracture, depending on the relative direction of initiated fracture and PFP in 3D.

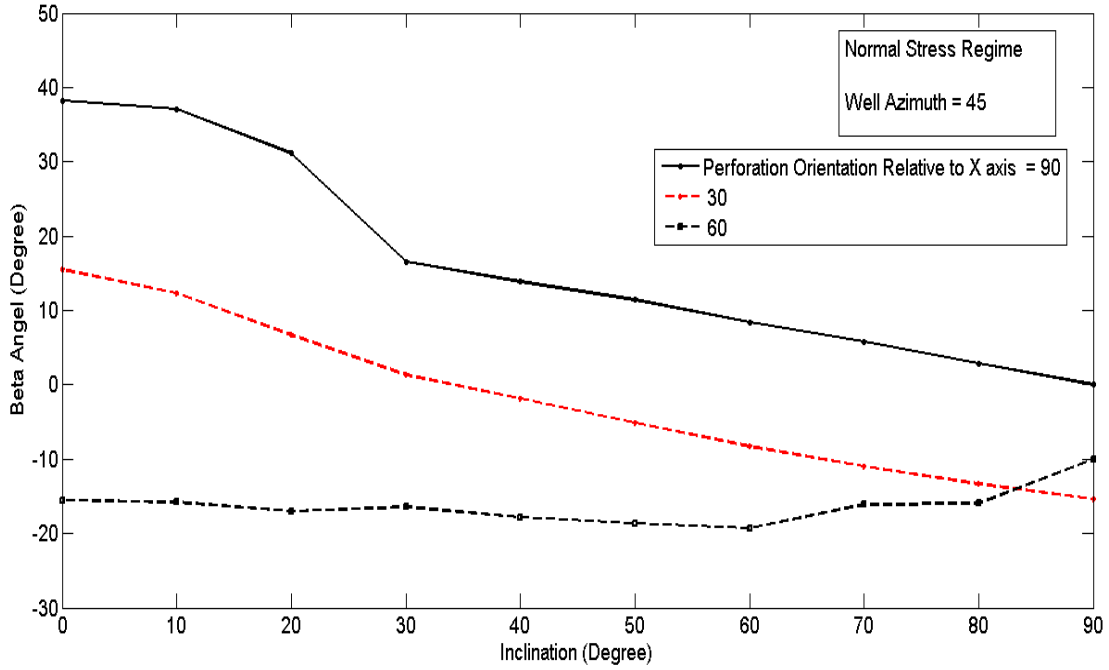

Figure 2-25 Fracture initiation angle for wellbores drilled in an azimuth of 45˚ in a normal stress regime.

When the azimuth angle of the wellbore is tuned from 0 to 45 degrees, different initiation angles are observed as presented in Figure 2-25. For various perforation orientations, the initiation angle is no longer zero, and it is also significantly dependent on the wellbore inclination. As an example, for a perforation orientation of 90˚ apart from the x axis (i.e. the perforation is on the middle side of the wellbore), as the wellbore is becoming more inclined, the initiation angle decreases. This is basically due to the fact that as the wellbore inclination changes, the perforation stress redistributes, and accordingly, the initiation angel is affected. In this case, the relative 3D angle between the initiated fracture plane and PFP increases as the wellbore is becoming more inclined, making the near wellbore fracture more complex.

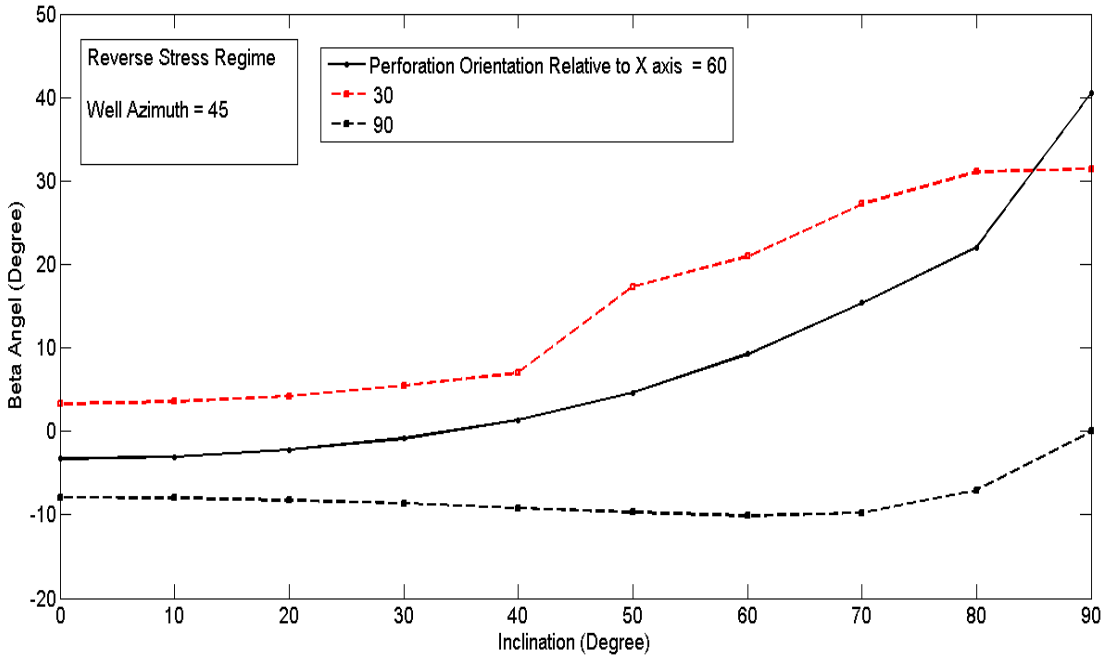

Figure 2-26 Fracture initiation angle for wellbores drilled in an azimuth of 45˚ in a reverse fault stress regime.

Nevertheless, in a reverse fault stress regime, the vertical stress σ_v is the minimum in-situ stress; consequently, the PFP is a horizontal plane. Therefore, any starter fracture should turn and twist to get aligned with a horizontal plane. As it is displayed in Figure 2-26, for wellbores having an azimuth angle of 45˚, the initiation angle generally increases by wellbore inclination angle. For example, for a perforation with an orientation of 60˚, the fracture initiation angle may increase to a value of about 40˚, when the wellbore is horizontal.

Based on the developed analytical model, the fracture initiation angle could be obtained for various wellbore, perforation, and in-situ stress conditions. Therefore, the fracturing engineer could analyse the near wellbore fracture geometry through studying the starter fracture orientation. This has to be done while considering the FIP for various perforation orientations, so that the best practice could be designed for an effective fracturing treatment.

2.6 Sensitivity analysis

As it is discussed in Section 2.5.1, several formation rock and cement parameters like, Biot's constant, tensile strength, pore pressure, and Poisson's ratio are included in this modelling. Each parameter plays its own role, while different parameters may

interact with each other. In this part the effects of some of these parameters are investigated to see how much the model is sensitive to each of them.

2.6.1 Biot's constant

Biot's constant is a poro-elastic parameter ranging from 0 to 1; the lower boundary typically is used for very low porosity and stiff rocks, while a compliant rock may have a Biot's constant as large as one. It is defined by the following simple equation:

$$\alpha = 1 - \frac{Bulk\ modulus\ of\ rock}{Bulk\ modulus\ of\ grain} \tag{2.34}$$

Generally the cement sheath is considered to have smaller Biot's constant in comparison to formation rock, because it is typically less porous. The effects of cement and formation Biot's constants are demonstrated in Figure 2-27.

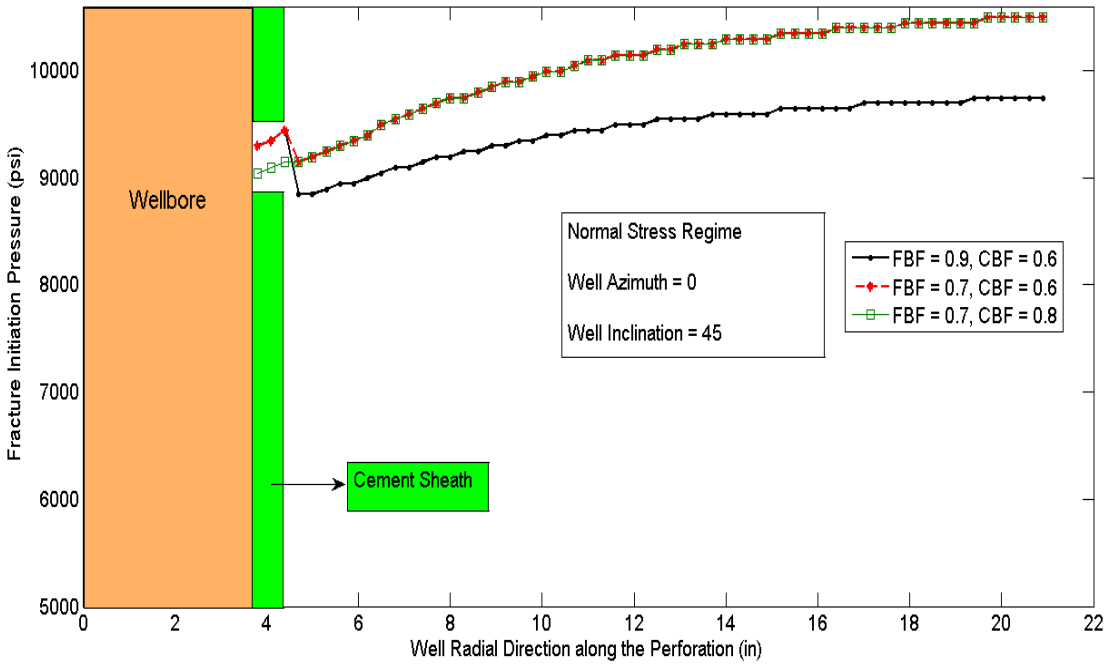

Figure 2-27 The effect of Biot's constant of formation (FBF) and cement sheath (CBF) on FIP.

As it is depicted in the above figure, by an increase in Biot's constant, less pressure is required to fracture the formation rock. This is due to a decrease in the effective stress. Based on Equation (2.18), a higher formation Biot's factor (FBF) increases the effect of the formation pore pressure, therefore decreasing the value of effective stress.

Cement sheath Biot's Factor (CBF) plays a similar role. A bigger Biot's constant for a cement rock means lower effective stress in the cement rock, as a result increasing the chance of micro-annulus creation. As is it depicted in Figure 2-27,

when the CBF is 0.6, and FBF is 0.9, the initiation pressure in the formation rock is more than 500 psi lower than that of the cement sheath. Therefore, it could be concluded that it is essential to design cement slurry and perform the cementing operation in such a way that low porosity stiff cement rock results. Accordingly the Biot's factor of such cement rock would be very low.

2.6.2 Formation pore pressure

As it is explained in the previous section, an increase in the formation pore pressure can lead to lower effective stress; thereby reducing the fracture initiation pressure. The sensitivity of the fracture initiation pressure to formation pore pressure is illustrated in Figure 2-28.

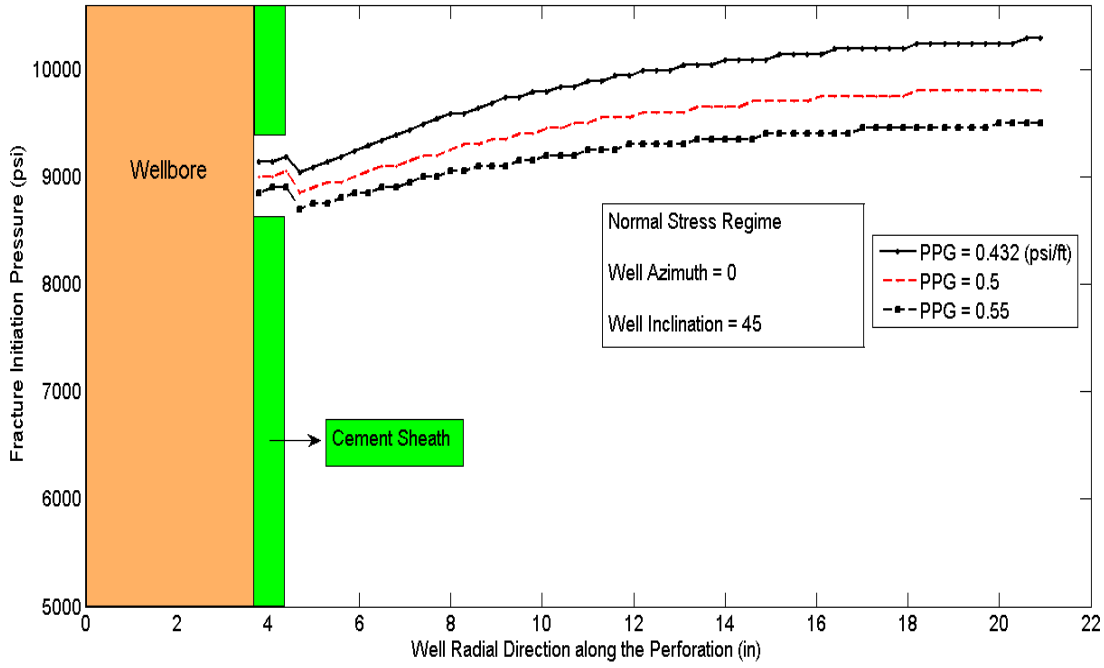

Figure 2-28 The effect of formation pore pressure gradient (PPG) on FIP.

Having a look on the graph in Figure 2-28, it is clear that a formation with a pore pressure gradient (PPG) of 0.55 psi/ft needs lower fracturing pressure in comparison to a formation having a PPG of 0.5 psi/ft. Therefore this graph confirms the previous discussion. Considering above graph, one can conclude that, a reservoir with a higher pore pressure is easier to be hydraulically fractured. This result is in contrary to fluid injection processes, such as water flooding, where it requires more injection pressure when the formation pore pressure is higher.

One parameter which is not included in this modelling is the effect of fluid leak off. Generally when a high pressure fluid is exposed to a lower pressure porous

medium, the fluid will leak into the porous space. Consequently the local pore pressure will increase, resulting in a lower effective stress. But this effect is not considerable in the process of fracture initiation in this chapter; however, this effect is discussed and covered in Chapter 3.

2.6.3 Tensile strength

The process of fracture initiation is a tensile failure of the rock or cement; therefore, the cement and rock tensile strengths are two essential parameters. The following graph illustrates the effect of these two parameters on fracture initiation pressure and location.

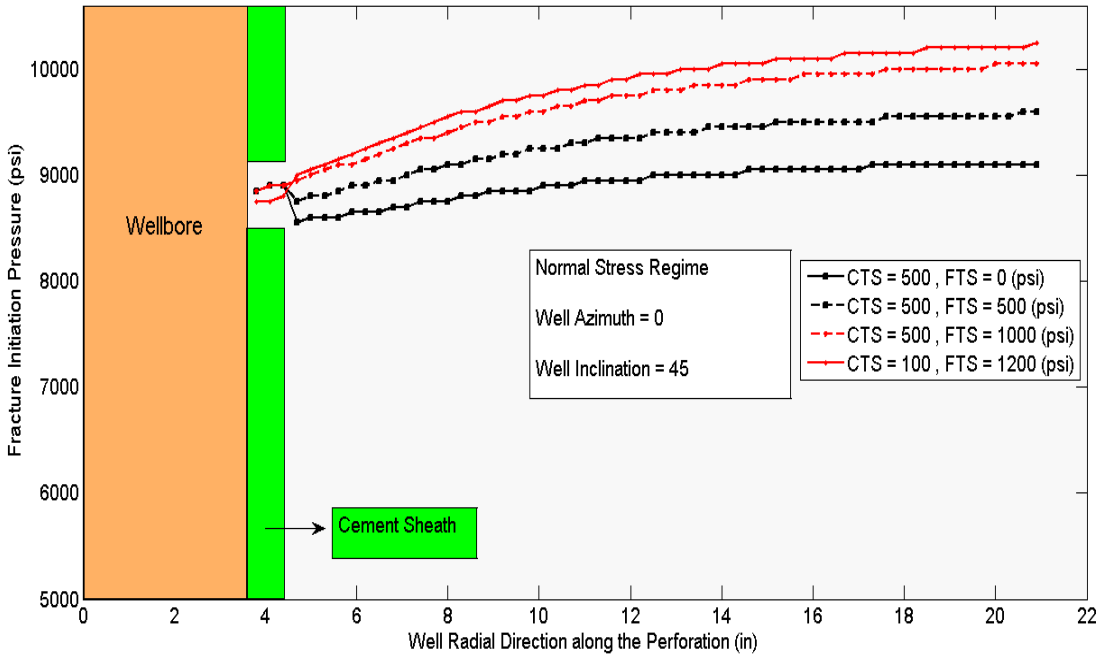

Figure 2-29 The effect of tensile strength of formation (FTS) and cement sheath (CTS) on FIP.

Figure 2-29 shows clearly the influence of tensile strength. As it is depicted, higher fracturing pressure is required to break down a formation with higher tensile strength. In most of occasions, it is reasonable to apply zero formation tensile strength for naturally fractured rocks, which already have some natural fissures. The other feature of Figure 2-29 is that, as the ratio of formation to cement sheath tensile strengths increases, the possibility of micro-annulus creation also increases. This emphasises the importance of designing high strength cement sheath to prevent the creation of micro-channel behind the casing.

2.6.4 Poisson's ratio

Poisson's ratio is an important parameter, which affects the magnitudes of in situ stresses, since the horizontal stresses directly depend on this parameter. Generally, as the Poison's ratio increases, larger horizontal stresses are expected (Fjar et al., 2008). The effect of the Poisson's ratio on FIP is shown in Figure 2-30.

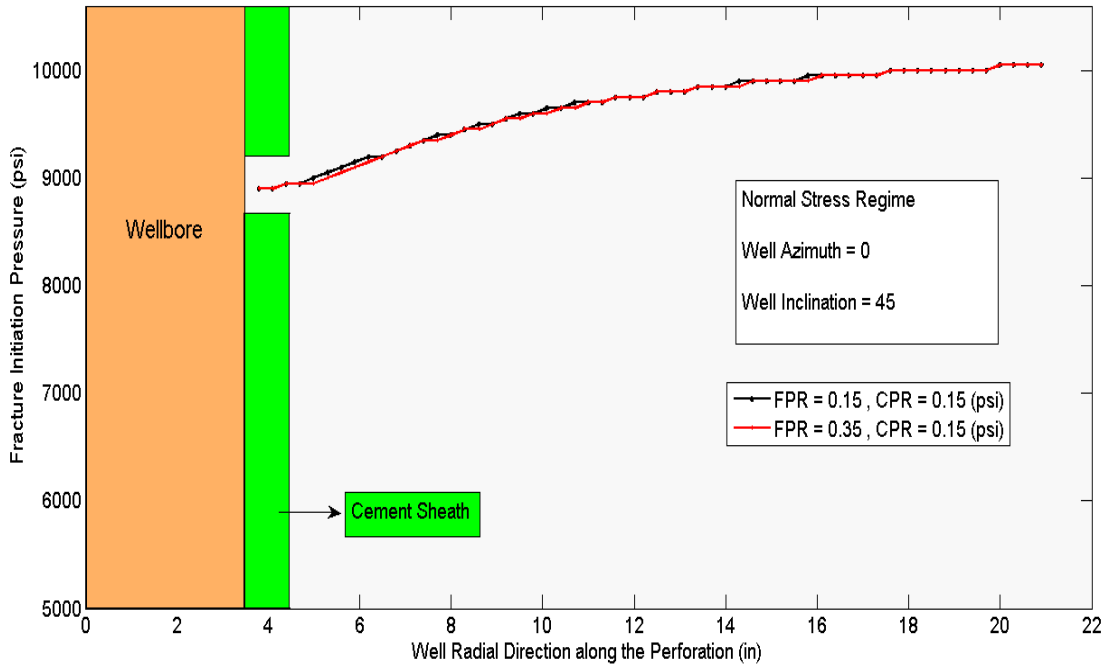

Figure 2-30 The effect of Poisson's ratio on FIP.

The graph presented in Figure 2-30 is obtained for two different formation Poison's ratios (FPR) of 0.15 and 0.35, while, a constant cement Poison's ratio (CPR) of 0.15 in considered. As it is seen in this graph, the effect of Poisson's ratio on FIP is negligible. Although Poisson's ratio is an important factor in determining in situ horizontal stresses, the effect of this parameter on wellbore and perforation stress profiles is not significant. It is noteworthy that, to produce the graph in Figure 2-30, the magnitudes of horizontal stresses were considered constants (as per Table 2.2) at various Poisson's ratios.

2.7 Summary

An elastic analytical model was developed in this chapter for studying the mechanism of fracture initiation in a perforation hole. The model is capable of analysing the stress distribution around an arbitrary deviated wellbore. Then a new analytical methodology was established to analyse the stress distribution around a

perforation hole, all along its length; this was done while the wellbore stress components were superimposed on the perforation stress modelling. Next, the tensile failure criterion was used to establish the fracture initiation model in perforations.

An application of the developed model was presented for a simple vertical perforated wellbore. And then a numerical method was introduced to apply the analytical solution for every possible wellbore and perforation orientations. The presented model was then validated with some scaled experimental fracturing results. In the next sections, maximum tension zone was located for each condition. It was found that the location of the tensile zone on the circumference of a wellbore depends on the wellbore orientation as well as the prevailing in-situ stress regime. Therefore, the location of this zone was identified for different wellbores at various deviations and stress conditions. Basically, in cased holes, the relative direction of the perforation orientation and the wellbore tensile zone, is a main factor influencing both the FIP and near wellbore fracture propagation. In contradiction to what is supposed in literature, this study showed that, it is not a general rule to have lower FIP when the perforations are aligned with the tensile zone of the well.

Then FIPs were calculated for different in-situ stress regimes while numerous wellbore inclination and azimuth angles were considered. Accordingly, it was found that when the regional stress regime is normal, the fracture initiation pressure increases as the well gets more inclined. However generally, the situation is vice versa in a reverse stress regime area, where FIP mostly reduces with well inclination increase. The impact of well azimuth on FIP is also significant, when the areal prevailing stress regime is strike slip, though it does not greatly affect the fracturing pressure for wells which are drilled in other stress regime areas.

It was also found that stress anisotropy is an important factor, influencing the fracture initiation pressure. Generally more anisotropic stress state will lead to lower fracture initiation pressure, and this effect does not depend on the prevailing stress regime and on the well direction.

Next, the effect of perforation orientation was studied and fracture initiation angle was investigated in various wellbore and perforation orientations. By using the modelled perforation stress distribution, the angle (β), which is the angle between the initiated fracture plane and the perforation axis, was calculated. Knowing this angle, and comparing it with the PFP, while considering the wellbore and perforation orientations, the near wellbore fracture tortuosity could be analysed.

At the end of this chapter, various parameters were studied to see how each one could impact the process of fracture initiation in a perforation hole. The effects of cement tensile strength, Biot's constant and Poisson's ratio were also included in the developed model, so that the possibility of micro-annulus creation can be specifically inspected. An increase in the cement and formation Biot's constant will result in less FIP. Also, any increase in formation pore pressure implies similar effect.

3 Poro-Elastic and thermo-elastic analytical modelling*

3.1 Introduction

An elastic analytical model was developed in Chapter 2 for analysing the fracture initiation mechanism in perforated wellbores, in which the formation rock was considered as a non-permeable medium. However, most underground formations are porous and permeable; therefore, high pressure fracturing fluid may flow through the rock, resulting in pore pressure increase. In addition, since fracturing fluid is normally cooler than underground formations, temperature variations may also occur locally by the injection of the fluid. The increase in pore pressure and reduction in formation temperature affect the wellbore and perforation stress distribution, thereby, the FIP may change. Several early experimental studies have revealed that in permeable rocks, pore pressure variations influence the fracture break down pressure (Haimson & Fairhurst, 1967, 1969; Medlin & Masse, 1979).

Therefore, in this chapter, the analytical model developed in Chapter 2 is further advanced to account for the formation pore pressure and temperature variations. Wellbore and perforation stress distribution equations are modified to adjust the stress analysis for poro-elasticity and thermo-elasticity effects. Darcy's law is used to model the pore pressure variation, and superposition principal is implemented to include the effect of this pressure variation in the elastic model. As a result, wellbore and perforation general poro-elastic stress analysis equations are derived, which could be used for various wellbore and perforation orientations.

Then the correspondence between thermo-elasticity and poro-elasticity is used to derive perforation stress equations which account for formation temperature variations. Next, the analytical method presented in Chapter 2 is applied to study perforation fracture initiation using the developed poro-elastic and thermo-elastic

*Some of the contents given in this chapter are based on the material presented in:
Paper 1. The impact of cement sheath mechanical properties on near wellbore hydraulic fracture initiation.

models. Various aspects and results of the developed models are presented in the rest of the chapter.

Some other results of this modelling, in regards to the properties of the cement sheath, are presented in Paper 1. In addition, this paper studies the effect of the casing on wellbore and perforation stress distributions through a simple method. And accordingly, the impact of the casing on FIP is analysed in the paper, which is included at the end of this thesis.

3.2 Model development

In this section, the linear elastic model, which was presented in Chapter 2, is further expanded to simulate the wellbore and perforation stress distributions for porous and permeable formations. Then the developed model is applied to study the fracture initiation in a perforation hole. One of the first poro-elastic models, which was used for predicting FIP, was presented by Schmidt and Zoback (1989). In this model, they proposed two different conditions. Firstly, a formation rock was supposed to be porous but not permeable to the fracturing fluid, accordingly the following equation was derived in which φ is formation porosity;

$$P_{FI} = 3\sigma_{min} - \sigma_{max} + TS - \varphi P_f \tag{3.1}$$

In this equation σ_{min} and σ_{max} are the minimum and maximum in-situ principal stresses, respectively, which are perpendicular to the axis of the wellbore. However, when the formation rock is both porous and permeable to the fracturing fluid, the following equation was developed to predict FIP (Schmidt & Zoback, 1989);

$$P_{FI} = \frac{3\sigma_{min} - \sigma_{max} + TS - \alpha P_f(\frac{1-2\vartheta}{1-\vartheta})}{1 + \varphi - \alpha(\frac{1-2\vartheta}{1-\vartheta})} \tag{3.2}$$

Nevertheless, these equations are only applicable when the wellbore is parallel to one of the in-situ principal stresses. Since the fracturing treatment may be operated in oriented wellbores, it is essential to derive poro-elastic fracture initiation equations for arbitrarily deviated wellbores. The other problem of Equation (3.2) is that, it does not consider a varying formation pore pressure. While in a fracturing treatment, since the fracturing fluid pressure is higher than formation pore pressure, there is a continuous leak off of fluid into the permeable rock, resulting in pore pressure

increase. Hence, more accurate stress analysis could be obtained by developing a model which accounts for pore pressure variations.

3.2.1 Poro-Elastic stress distribution around inclined wellbores

Pore pressure variations should be studied first in order to establish the wellbore poro-elastic stress model. A common approach is to consider a constant radial flow from the wellbore into the formation rock. Assuming a non-transient flow behaviour, the formation fluid pressure could be evaluated by Darcy's law;

$$Q = \frac{2\pi rhk}{\mu}\frac{dP}{dr} \tag{3.3}$$

where Q is assumed to be a constant flow rate, h and k are the thickness and permeability of the formation, respectively, and μ is the viscosity of the flowing fluid. Since it is common in petroleum engineering to assume an average constant reservoir pressure (P_a) at the outer boundary of the reservoir (R_e), Equation (3.3) could be solved to find the formation pore pressure at any distance from the wellbore;

$$P_f = P_w + (P_a - P_w)\frac{ln\frac{r}{R_w}}{ln\frac{R_e}{R_w}} \tag{3.4}$$

Risnes et al. (1982) considered the analogy of a hollow cylinder to a vertical wellbore with isotropic horizontal stresses, and applied the Darcy's radial flow solution to derive the following equations;

$$\sigma_r = \sigma_h + (\sigma_h - P_w)\left(1 - \left(\frac{R_e}{r}\right)^2\right)\frac{{R_w}^2}{{R_e}^2 - {R_w}^2} - (P_a - P_w)\eta\left[\left(1 - \left(\frac{R_e}{r}\right)^2\right)\frac{{R_w}^2}{{R_e}^2 - {R_w}^2} + \frac{ln\frac{R_e}{r}}{ln\frac{R_e}{R_w}}\right] \tag{3.5}$$

$$\sigma_\theta = \sigma_h + (\sigma_h - P_w)\left(1 + \left(\frac{R_e}{r}\right)^2\right)\frac{{R_w}^2}{{R_e}^2 - {R_w}^2} - (P_a - P_w)\eta\left[\left(1 + \left(\frac{R_e}{r}\right)^2\right)\frac{{R_w}^2}{{R_e}^2 - {R_w}^2} + \frac{ln\frac{R_e}{r} - 1}{ln\frac{R_e}{R_w}}\right] \tag{3.6}$$

$$\sigma_z = \sigma_v + 2\vartheta(\sigma_h - P_w)\frac{{R_w}^2}{{R_e}^2 - {R_w}^2} - (P_a - P_w)\eta\left[\frac{2\vartheta {R_w}^2}{{R_e}^2 - {R_w}^2} + \frac{2ln\frac{R_e}{r} - \vartheta}{ln\frac{R_e}{R_w}}\right] \quad (3.7)$$

In these equations, η is a function of formation Poisson's ratio and Biot's constant, and is known as Poro-elastic stress coefficient;

$$\eta = \frac{1 - 2\vartheta}{2(1 - \vartheta)}\alpha \quad (3.8)$$

As in an underground formation, the external radius is typically much larger than the wellbore radius; the above equations could be presented in the following simpler form;

$$\sigma_r = \sigma_h - (\sigma_h - P_w)\left(\frac{R_w}{r}\right)^2 + (P_a - P_w)\eta\left[\left(\frac{R_w}{r}\right)^2 - \frac{ln\frac{R_e}{r}}{ln\frac{R_e}{R_w}}\right] \quad (3.9)$$

$$\sigma_\theta = \sigma_h + (\sigma_h - P_w)\left(\frac{R_w}{r}\right)^2 - (P_a - P_w)\eta\left[\left(\frac{R_w}{r}\right)^2 + \frac{ln\frac{R_e}{r}}{ln\frac{R_e}{R_w}}\right] \quad (3.10)$$

$$\sigma_z = \sigma_v - (P_a - P_w)\eta\left[\frac{2ln\frac{R_e}{r} - \vartheta}{ln\frac{R_e}{R_w}}\right] \quad (3.11)$$

Comparing Equations (3.9)-(3.11) with Equation (2.1), in which elastic stress solutions for a vertical wellbore are presented, it is realized that an extra term is appeared in each of the above equations to account for the poro-elastic effect. Therefore, based on superposition principle, poro-elastic stress solutions for inclined wellbores could also be obtained by including the same poro-elastic terms in the basic elastic solutions. Accordingly, Equations (2.5)-(2.7) are used to develop the following poro-elastic solutions for an arbitrarily oriented wellbore;

$$\sigma_r = \frac{\sigma_x^o + \sigma_y^o}{2}\left(1 - \frac{R_w^2}{r^2}\right) + \frac{\sigma_x^o - \sigma_y^o}{2}\left(1 + 3\frac{R_w^4}{r^4} - 4\frac{R_w^2}{r^2}\right)\cos 2\theta$$
$$+\tau_{xy}^o\left(1 + 3\frac{R_w^4}{r^4} - 4\frac{R_w^2}{r^2}\right)\sin 2\theta + P_w\frac{R_w^2}{r^2}$$
$$+ (P_a - P_w)\eta\left[\left(\frac{R_w}{r}\right)^2 - \frac{ln\frac{R_e}{r}}{ln\frac{R_e}{R_w}}\right] \quad (3.12)$$

$$\sigma_\theta = \frac{\sigma_x^o + \sigma_y^o}{2}\left(1 + \frac{R_w^2}{r^2}\right) - \frac{\sigma_x^o - \sigma_y^o}{2}\left(1 + 3\frac{R_w^4}{r^4}\right)\cos 2\theta$$
$$-\tau_{xy}^o\left(1 + 3\frac{R_w^4}{r^4}\right)\sin 2\theta - P_w\frac{R_w^2}{r^2}$$
$$-(P_a - P_w)\eta\left[\left(\frac{R_w}{r}\right)^2 + \frac{ln\frac{R_e}{r}}{ln\frac{R_e}{R_w}}\right] \quad (3.13)$$

$$\sigma_z = \sigma_z^o - \vartheta\left(2\left(\sigma_x^o - \sigma_y^o\right)\frac{R_w^2}{r^2}\cos 2\theta + 4\tau_{xy}^o\frac{R_w^2}{r^2}\sin 2\theta\right)$$
$$-(P_a - P_w)\eta\left[\frac{2ln\frac{R_e}{r} - \vartheta}{ln\frac{R_e}{R_w}}\right] \quad (3.14)$$

The above equations calculate the wellbore poro-elastic normal stresses; however, since formation pressure does not have any effect on shear stress components, the same elastic shear stress formulas as given in Equations (2.8)-(2.10) could be used in poro-elastic wellbore stress analysis.

The poro-elastic wellbore stress solution could be used when the borehole is not cased, and the wellbore fluid has enough communication with the surrounding formation. It could also be used for a cased wellbore where either wellbore is perforated adequately, or the cement sheath does not exist or is not sealing properly; therefore, the wellbore fluid could easily dissipate into the formation porous medium. However, since in a cased perforated wellbore, most fluid dissipation takes place through the perforations, it is essential to stablish the perforation poro-elastic stress analysis.

3.2.2 Poro-Elastic stress distribution around perforation

In a cased perforated wellbore, the main communication path between the wellbore and formation rock are the perforation holes. Therefore, when the wellbore and perforations are pressurized with the fracturing fluid, the pore pressure in vicinity of the perforation holes may increase. This pore pressure variation occurs when the rock permeability is not very low, and a low viscous fracturing fluid is used to slowly pressurize the well. As a result, the formation pressure will no longer remains constant and a varying pore pressure profile will be formed, affecting the stress distribution around the perforation. Thus, elastic perforation stress calculation may not be accurate any more, and poro-elastic equations should be derived to analyse the perforation stress distribution.

Since the perforation hole is considered to be a micro-cylinder (see Figure 2-3), similar to the wellbore poro-elastic stress equations, Darcy's law and superposition principle could be implemented to derive the perforation poro-elastic stress solutions. Therefore, the poro-elastic terms from Equations (3.9)-(3.11) should be included in the perforation elastic stress formulas (Equations (2.11)-(2.13)); however, P_w and R_w should be substituted by the perforation parameters P_p and R_p, respectively.

$$\begin{aligned}\sigma_{rp} = {} & \frac{\sigma_z + \sigma_\theta}{2}\left(1 - \frac{R_p^2}{r^2}\right) + \frac{\sigma_z - \sigma_\theta}{2}\left(1 + 3\frac{R_p^4}{r^4} - 4\frac{R_p^2}{r^2}\right)\cos 2\theta_p \\ & + \tau_{\theta z}\left(1 + 3\frac{R_p^4}{r^4} - 4\frac{R_p^2}{r^2}\right)\sin 2\theta_p + P_p\frac{R_p^2}{r^2} \\ & + (P_a - P_p)\eta\left[\left(\frac{R_p}{r}\right)^2 - \frac{ln\,\frac{R_e}{r}}{ln\,\frac{R_e}{R_p}}\right]\end{aligned} \tag{3.15}$$

$$\begin{aligned}\sigma_{\theta p} = {} & \frac{\sigma_z + \sigma_\theta}{2}\left(1 + \frac{R_p^2}{r^2}\right) - \frac{\sigma_z - \sigma_\theta}{2}\left(1 + 3\frac{R_p^4}{r^4}\right)\cos 2\theta_p \\ & - \tau_{\theta z}\left(1 + 3\frac{R_p^4}{r^4}\right)\sin 2\theta_p - P_p\frac{R_p^2}{r^2} \\ & - (P_a - P_p)\eta\left[\left(\frac{R_p}{r}\right)^2 + \frac{ln\,\frac{R_e}{r}}{ln\,\frac{R_e}{R_p}}\right]\end{aligned} \tag{3.16}$$

$$\sigma_{zp} = \sigma_r - \vartheta\left(2(\sigma_z - \sigma_\theta)\frac{R_p^2}{r^2}\cos 2\theta_p + 4\tau_{z\theta}\frac{R_w^2}{r^2}\sin 2\theta_p\right) - (P_a - P_P)\eta\left[\frac{2ln\frac{R_e}{r} - \vartheta}{ln\frac{R_e}{R_P}}\right] \quad (3.17)$$

Similar to the wellbore stress analysis, pore pressure variation does not have any effect on the perforation shear stress components. This is due to the fact that formation fluid cannot implement much shear force one surface of the formation grains, even when it is highly viscous and flowing at high flow rate. Generally, the shear stress that a flowing fluid could apply on underground rock is orders of magnitudes lower than the existing rock shear stress components. Accordingly, the perforation shear stress components could be obtained from the elastic analysis as given in Equations (2.14)-(2.16).

In order to analyse the fracture initiation mechanism in a perforation made in a permeable rock, poro-elastic stresses should be calculated on the surface of the perforation hole. This could be done by approaching r to R_p in Equations (3.15)-(3.17); consequently, the below formulas are obtained;

$$\sigma_{rp} = P_p \quad (3.18)$$

$$\sigma_{\theta p} = \sigma_z + \sigma_\theta - 2(\sigma_z - \sigma_\theta)\cos 2\theta p - 4\tau_{z\theta} sin2\theta p - P_p + 2\eta(P_p - P_a) \quad (3.19)$$

$$\sigma_{zp} = \sigma_r - \vartheta(2(\sigma_z - \sigma_\theta)\cos 2\theta p + 4\tau_{z\theta} sin2\theta p) + 2\eta(P_p - P_a) \quad (3.20)$$

In the above equations, P_p stands for perforation pressure. Since, in the first step of hydraulic fracturing, there is not much fluid flow from the wellbore into the perforation, P_p is equal to the wellbore pressure. Equations (3.18)-(3.20) could be used to calculate the poro-elastic normal stress components on the surface of the perforation, and the corresponding shear stresses could be obtained from Equation (2.21). Accordingly, the numerical method presented in Section 2.4.2 should be used to analyse the process of fracture initiation along a perforation hole. This would provide a poro-elastic fracture initiation analysis for arbitrarily oriented perforated wellbores.

However, as it is mentioned earlier, the fracturing fluid may cause temperature variations in the rock surrounding the perforations. Consequently, the perforation stress distribution is influenced by such temperature change; therefore, it is essential to expand the analytical model to implement the effect of varying formation temperature on the fracture initiation mechanism.

3.2.3 Thermo-Elastic stress distribution around perforation

When a fracturing fluid is introduced to a well, it will impose temperature variation, because the fracturing fluid is normally cooler than underground formations. The rate of this temperature variation is a function of rock/fluid conduction and convection processes, and its impacts depend on rock/fluid thermal expansion coefficients. When the formation temperature varies, the formation may expand or shrink, consequently the stresses will change. Therefore, it is of great interest to develop a thermo-elastic model for analysing the perforation stress distribution, and thereby simulating fracture initiation mechanism more accurately.

Fjar et al. (2008) introduced the correspondence between thermo-elasticity and poro-elasticity, and accordingly presented a set of thermo-elastic equations to calculate the stress components on the surface of a vertical wellbore in a formation with isotropic horizontal stresses;

$$\sigma_r = P_w$$

$$\sigma_\theta = 2\sigma_h - P_w + \frac{E}{1-\vartheta} \propto_T (T_w - T_f) \tag{3.21}$$

$$\sigma_z = \sigma_v + \frac{E}{1-\vartheta} \propto_T (T_w - T_f)$$

where T_w is the wellbore temperature (fracturing fluid temperature), T_f is the formation temperature, $\propto_T$ is the coefficient of linear thermal expansion and E is the Young's modulus of the formation. As it is seen in the above equations, the temperature variations affect the wellbore tangential and axial stresses, while the radial stress is just a function of the wellbore pressure.

Comparing Equation (3.21) with the elastic stress solutions for a vertical wellbore as presented in Equation (2.1), it is realized that an extra term is appeared in the above equations to account for the temperature effect. Therefore, based on superposition principle, thermo-elastic stress solutions for the stress analysis on the surface of a perforation could also be obtained by adding similar thermo-elastic

terms to the basic elastic solutions. Accordingly, Equation (2.21) is used to develop the following thermo-elastic stress solutions for the perforation surface;

$$\sigma_{rp} = P_p \tag{3.22}$$

$$\sigma_{\theta p} = \sigma_z + \sigma_\theta - 2(\sigma_z - \sigma_\theta)\cos 2\theta p - 4\tau_{z\theta} sin2\theta p - P_p + \frac{E}{1-\vartheta} \propto_T (T_w - T_f) \tag{3.23}$$

$$\sigma_{zp} = \sigma_r - \vartheta(2(\sigma_z - \sigma_\theta)\cos 2\theta p + 4\tau_{z\theta} sin2\theta p) + \frac{E}{1-\vartheta} \propto_T (T_w - T_f) \tag{3.24}$$

Having the thermo-elastic perforation stress distribution, the numerical method presented in Section 2.4.2 could be used to analyse the process of fracture initiation along a perforation hole.

3.3 Results and discussion

3.3.1 Introduction

After developing the required model in Section 3.2, in this section some results of the model are presented and discussed. Since the developed poro-elastic and thermo-elastic analytical models are uncoupled, the results of each model are presented separately, so that the effect of each governing parameter could be studied distinctly. Therefore, in this section, the results are presented in several sub-sections.

In the first section, the wellbore poro-elastic stress solutions are used to investigate the process of fracture initiation with pore pressure variations. This part contains some studies on the effects of stress regimes and borehole orientations. In addition, the influence of Poisson's ratio and Biot's constant on FIP is analysed.

After that, the perforation poro-elastic stress model is analysed, while the wellbore stress distribution is considered to be elastic. The poro-elastic and elastic results of the model are compared in this section. This section continues with some investigations to see how much the model is sensitive to pore pressure gradient, Poisson's ratio and Biot's constant.

In the next section, the thermo-elastic perforation stress model is studied, while the wellbore stress distribution is again considered to be elastic. The impact of different stress regimes, stress anisotropy and well trajectory is studied at various temperature variations. Then, wellbore poro-elastic stress solutions are applied along with the effect of thermo-elasticity on perforation stress distribution in order to study the both effects of formation temperature and pore pressure variations. In this way an uncoupled thermo-poro-elastic model is investigated, which can better simulate a real hydraulic fracture initiation process. In addition, some other results of this modelling are published in a paper previously (see Paper1).

In the following sections the FIP is calculated using the developed model for a perforated wellbore with a perforation hole oriented towards the x axis of the well (see Figure 2-2). Specific wellbore orientations and in-situ stress regimes are investigated, while some defined cement and rock properties are used. Table 3.1 summarises some common values for these properties, which are used in the numerical modelling as presented in Section 2.4.2. It is noteworthy that a tensile strength similar to the data obtained in Chapter 4 (see Figure 4-5) is used here, since the model developed in the current chapter is later used in Chapter 4 for modelling and analysing three field wellbores' fracturing.

Table 3.1 Modelling input parameters, their units and assigned magnitudes.

Parameter	**Unit**	**Magnitude**
Wellbore true vertical depth	ft	10000
Wellbore radius	in	3.5 - 4
Maximum principal stress	psi	9000
Intermediate stress gradient	psi	8000
Minimum stress gradient	psi	7000
Pore pressure	psi	4560
Cement thickness	in	1
Cement Biot's constant	-----	0.8
Cement Poisson's ratio	-----	0.25
Coeficent of linear thermal expansion	1/°F	5×10^{-6}
Formation elasticity modulus	psi	3×10^{6}
Formation rock Biot's constant	-----	0.8
Formation rock Poisson's ratio	-----	0.25
Formation rock tensile strength	psi	3000

3.3.2 Poro-Elastic wellbore stress distribution

The elastic stress solutions developed in Chapter 2 are the stress equations for non-porous rocks or for porous rocks with constant formation pressure. Based on the superposition principle, the pore pressure variation effects are added to the wellbore elastic stress equations in Section 3.2.1. In this way, the accuracy of the model is improved, since in reality most underground formations are porous and permeable and there is always some pore pressure change.

Applying the wellbore poro-elastic equations, which have been presented in Section 3.2.1 along with the elastic perforation stress equations, the following results are obtained.

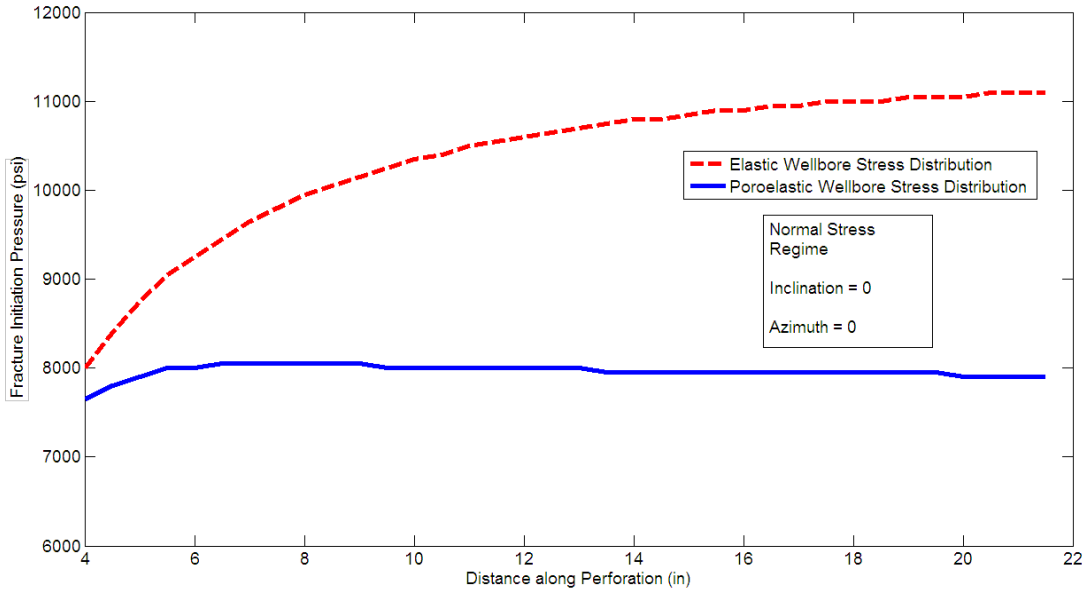

Figure 3-1 The effect of poro-elastic wellbore stress distribution on FIP.

Figure 3-1 compares the FIP along a perforation hole for two different wellbore stress modelling, poro-elastic and elastic modelling approaches. It is obvious from above graph that, when the wellbore stress profile is modelled by poro-elastic formulation, lower fracture initiation pressure is required.

Actually, in such a case when the fracturing fluid pressure increases, the local pore pressure around the well also increases. This rise in the formation pressure leads to a local reduction in the effective stresses around the wellbore. Consequently, the perforation effective stresses will also reduce, and this will in turn decrease the FIP. This is a way to reduce the FIP, which is a challenge in most of cased wellbores. In fact, one may increase the local pore pressure in order to have lower formation break down pressure. It is essential to examine this finding in different stress regimes, as presented in the following graph.

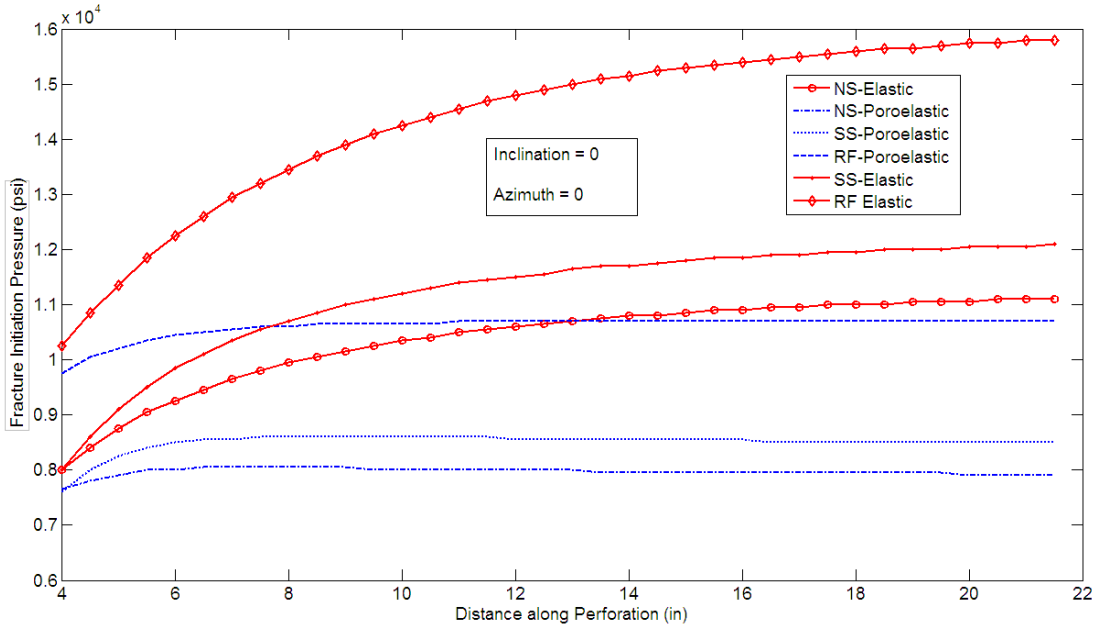

Figure 3-2 The effect of various stress regimes on FIP while the wellbore poro-elastic stress distribution is applied for a vertical wellbore in normal (NS), reverse (RF) and strike slip(SS) faulting stress regimes.

Figure 3-2 presents the influence of various stress regimes on the FIP, while the poro-elastic and elastic borehole stress distributions are considered. As it is seen from the above graph, in all three stress regimes, the fracture initiation pressure is lower for the case of poro-elastic modelling. This is again due to the fact that poro-elastic model considers the formation pressure increase, accordingly lower effective minimum principal stress is calculated; therefore, lower FIP is obtained.

The other important feature of Figure 3-2 is the comparison between various stress regimes. If an oilfield has a prevailing reverse fault stress regime, higher fracturing pressure is required with respect to a field with strike slip stress regime. In turn, a field with strike slip stress regime needs more fracturing pressure than a field with normal stress regime. This result is obtained for a vertical wellbore, with a specific perforation direction (x axis oriented), and could not be generalized to all other wellbore and perforation orientation. The effect of various wellbore orientations is examined in the next graph.

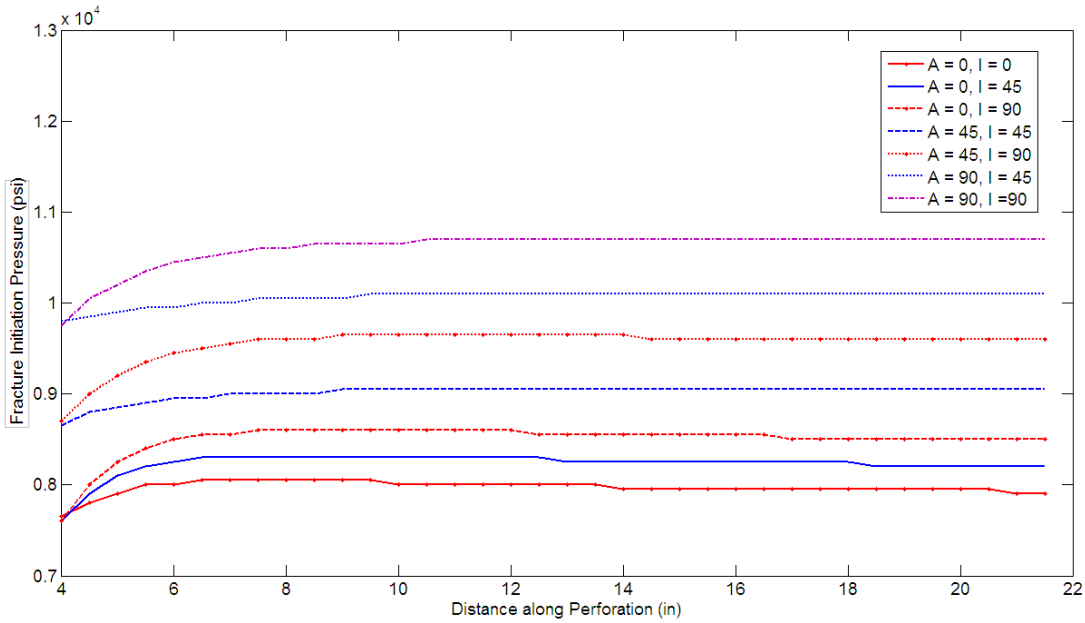

Figure 3-3 The effect of borehole orientation on FIP in a normal stress regime, while the wellbore poro-elastic stress distribution is applied.

What is observed from Figure 3-3 confirms the results which have been already achieved. Basically, in all these studies, the direction of the perforation is taken to be on the lowermost point of the well (x axis in Figure 2-2), so as the direction of the wellbore is changing, the perforation stress profile also changes, because the 3D geometrical position of the perforation is changing with respect to the in-situ stresses. Therefore, as Figure 3-3 shows, for more deviated wellbores higher pressure is required to start hydraulic fracturing operation. In addition, the azimuth of the well is also a very critical parameter, because as the well azimuth increases, more fracturing pressure is required. Such result is in good agreement with what has been concluded from the application of wellbore elastic stress analysis (see Section 2.5.4).

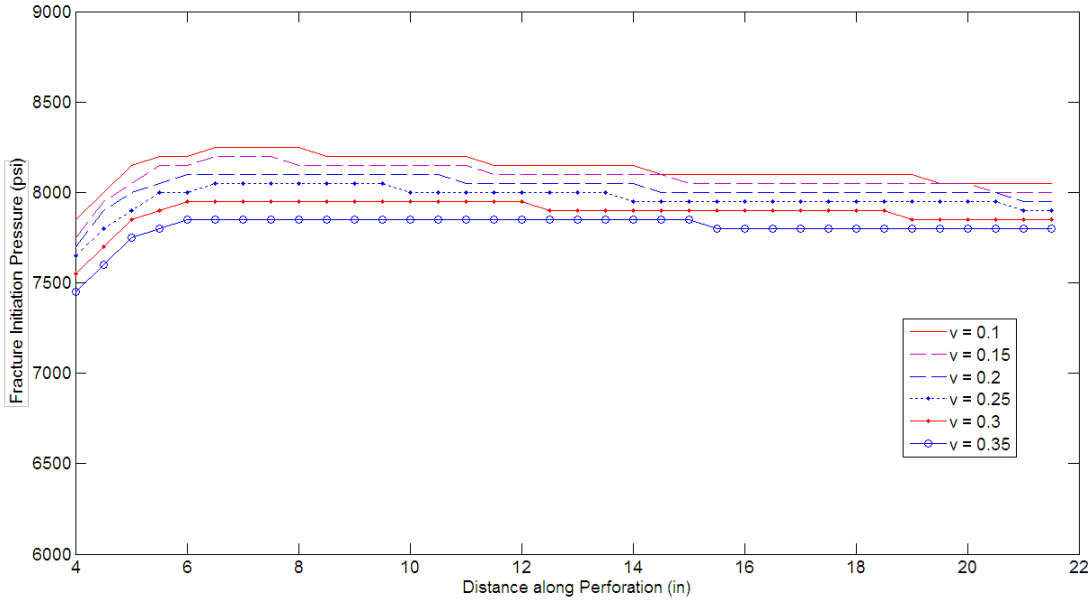

Figure 3-4 The effect of Poisson's ratio on FIP while the wellbore poro-elastic stress distribution is considered.

There are several important parameters which are used to develop the wellbore poro-elastic analytical model. Therefore, it is important to investigate the influence of these parameters on the results of the modelling. Here the effects of Poisson's ratio and Biot's constant are studied.

As Figure 3-4 demonstrates, the Poisson's ratio plays an important role on the perforation FIP in a vertical borehole. It is seen that, as this parameter increases, initiating a starter fracture occur at a lower pressure. That means formations with lower values of Poisson's ratios are harder to be hydraulically fractured. However, the effect of this parameter was found negligible on FIP, when the wellbore elastic stress solution was implemented (see Section 2.6.4). It is also noteworthy that Poisson's ratio affects the magnitudes of in situ stresses, since the horizontal stresses directly depend on this parameter. However, to produce the graph in Figure 3-4, the magnitudes of horizontal stresses were considered constants (as per Table 3.1) at various Poisson's ratios.

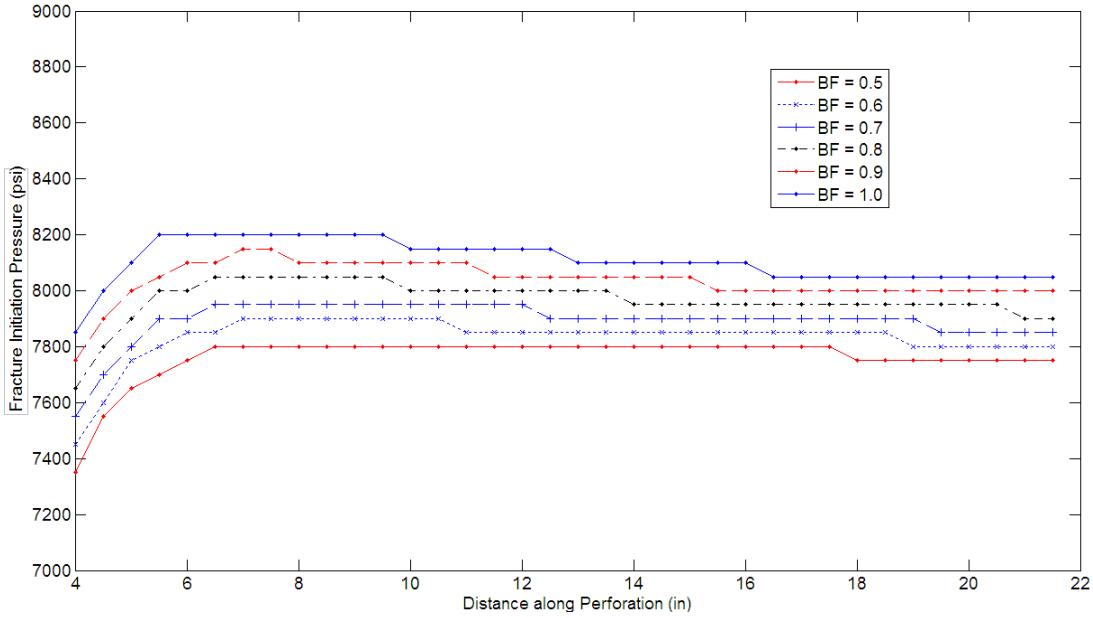

Figure 3-5 The effect of Biot's constant on FIP while the wellbore poro-elastic stress distribution is considered.

Figure 3-5 exhibits the effect of Biot's constant in a vertical perforated borehole while the wellbore poro-elastic stress solution is used. As it is shown in this graph, by increasing the Biot's constant, the FIP also increases. For example, when the Biot's constant changes from 0.5 to 1.0, the FIP rises for almost 500 psi. However, when the wellbore elastic solutions are applied, an increase in the Biot's constant will reduce the perforation FIP (see Section 2.6.1). This is due to the fact that Biot's constant has a direct effect on reduction of effective minimum principal stress in the elastic model. But the effect of this parameter is more complicated in the poro-elastic model, since it is involved in the poro-elastic stress coefficient η (see Equation (3.8)).

The poro-elasticity effect could also be included in the perforation stress analysis as presented in Section 3.2.2. Thus, in the next section, the perforation poro-elastic solutions are applied to study various aspects of fracture initiation.

3.3.3 Poro-Elastic perforation stress distribution

Since in a perforated wellbore, most fluid dissipation occurs through the perforations, the formation pore pressure around the perforations will change, and accordingly, the perforation stress distribution will alter. Therefore, in this section the perforation poro-elastic solutions derived in Section 3.2.2 are applied along with the wellbore elastic equations (as presented in Section 2.2.1) to investigate the effect of pore

pressure variation on fracture initiation. This is done using the numerical methos developed in Section 2.4.2.

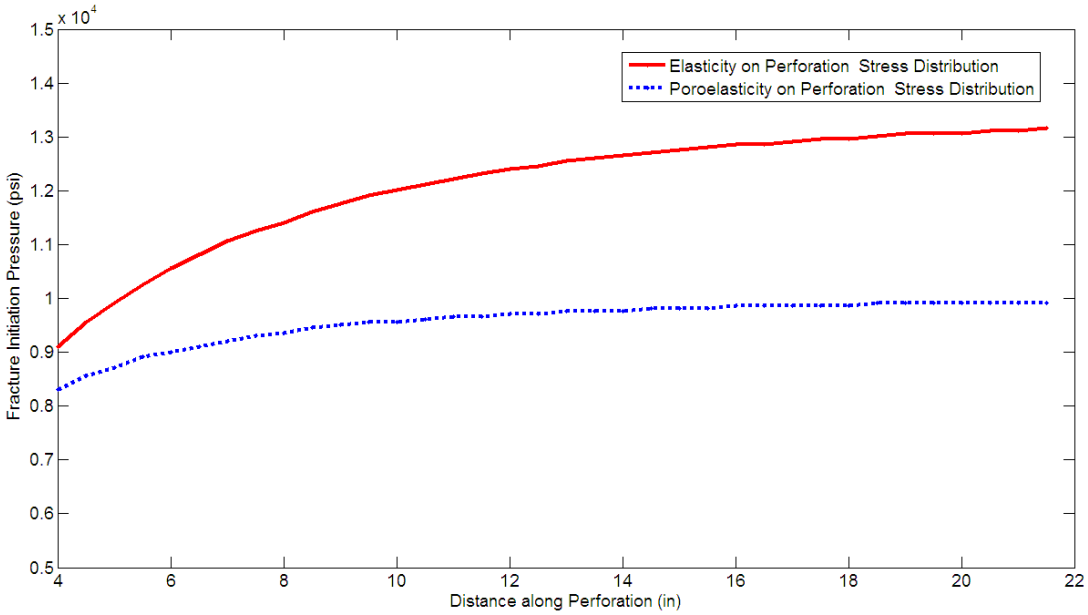

Figure 3-6 The effect of perforation poro-elastic stress distribution on FIP.

Figure 3-6 depicts the influence of perforation poro-elasticity on FIP in a vertical wellbore which is drilled in a normal stress regime. This graph shows a comparison between elastic and poro-elastic perforation stress distribution and its effect on the pressure of starter fracture initiation along a perforation hole. As it is demonstrated, when the perforation poro-elastic model is used, lower FIPs will be obtained all along the perforation hole. This result is very similar to the case when poro-elastic wellbore stress model was applied (see Section 3.3.2).

Generally, by increasing the local pore pressure around the perforations, the total stresses will locally increases. But the effective stresses reduce, and this is the reason of such FIP reduction. A poro-elastic model is, therefore, more precise than an elastic model, because formations' rocks are always porous and permeable. Consequently, there is always some pore pressure variation, because the fracturing fluid pressure is higher than the formation pore pressure.

Now that the pore pressure variation and perforation poro-elastic model is analysed in a vertical wellbore, it is motivating to apply this model for various wellbore orientation. This is done by varying the wellbore azimuth and inclination angles as presented in the next graph.

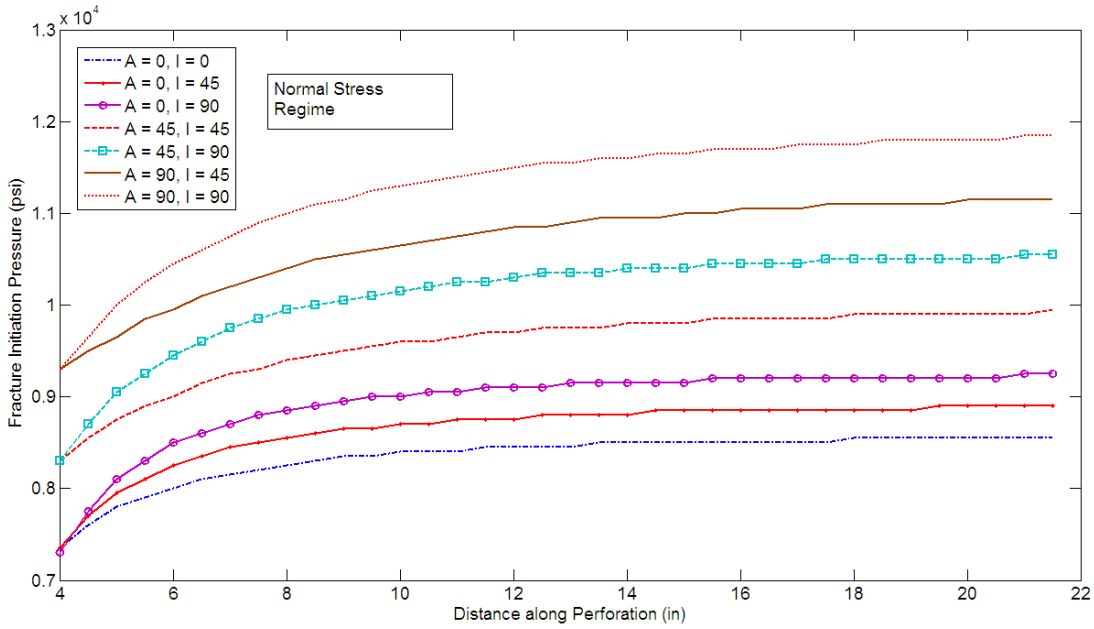

Figure 3-7 The effect of borehole orientation on FIP in a normal stress regime, while the perforation poro-elastic stress distribution is applied. The perforation is oriented towards the lowermost point of the well (x axis in Figure 2-2).

As it is demonstrated in Figure 3-7, more inclined boreholes require higher pressure for start of hydraulic fracturing, which means a horizontal borehole needs more initiation pressure than a vertical or inclined borehole. However, it should be noted that this conclusion is probably only valid for boreholes drilled in a normal stress regime field, while the perforations are oriented towards the x axis of the wellbore. Almost similar result was observed when the perforation elastic stress equations were used in Section2.5.4.

As an example, when the azimuth of the wellbore is 0° (i.e. wellbore is parallel to the maximum horizontal stress), as the inclination of the wellbore increases, the FIP along the perforation tunnel also increases. However, in this case, the minimum FIP occurs at the perforation and wellbore interface, and it is not a function of wellbore inclination angle. Such FIP behaviour is reasonable from the physical point of view, since in such specific wellbore and perforation orientation, the perforation hole is located in the PFP. Therefore, the minimum FIP does not change by the wellbore inclination. Basically, the fracturing fluid dissipation into the permeable formation rock will continue as long as there is some driving force (i.e. pressure differential), and it does not stop by the wellbore and perforation orientation. Therefore the inclination and azimuth angles of the wellbore do not impact the poro-elastic stress effect.

The other important feature of Figure 3-7 is the effect of well azimuth. One may say that as the well azimuth deviates from the direction of maximum horizontal stress towards the direction of minimum horizontal stress, the facture initiation pressure increases. This is due to the changes happening to wellbore and consequently perforation stress distribution.

There are some other important parameters that are involved in perforation poro-elastic model; therefore, it is important to study the influence of these parameters. In this part the sensitivity of the presented model to some parameters like pore pressure, Biot's constant and Poisson's ratio is investigated.

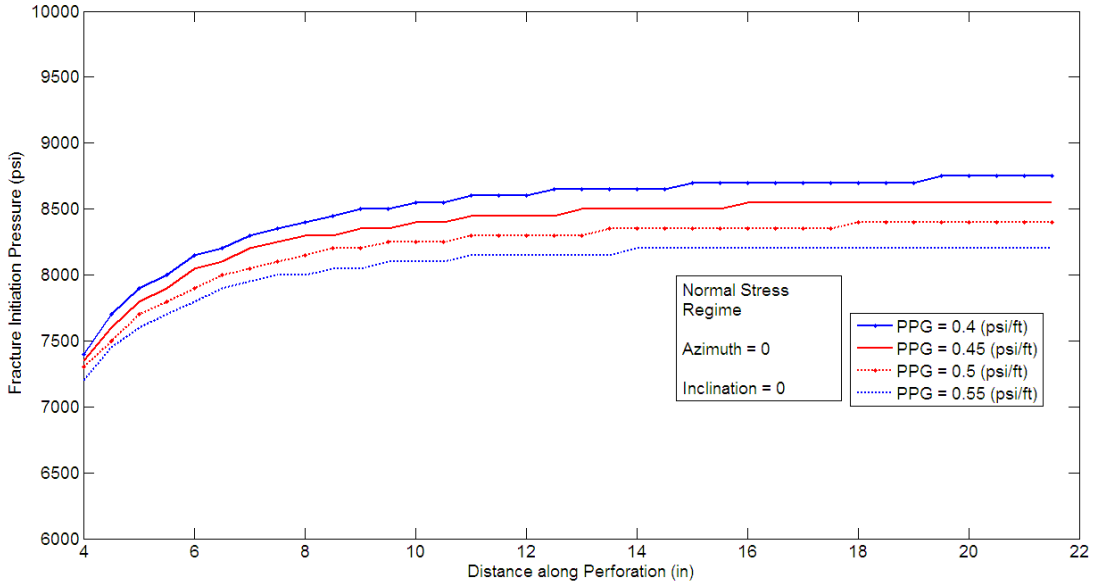

Figure 3-8 The effect of pore pressure gradient (PPG) on FIP in a normal stress regime, while the perforation poro-elastic stress distribution is applied. The perforation is oriented towards the lowermost point of the well (x axis in Figure 2-2).

Pore pressure or formation pressure is a fundamental property of any reservoir. The pressure of any underground formation might be normal, subnormal or abnormal. The hydrostatic gradient of underground saline water generates the normal pressure gradients; however, subnormal and abnormal pore pressures may exist when the formation pressure is less or more than the normal pressure, respectively.

Figure 3-8 studies the effect of formation pressure on FIP. Having a look on this figure, it is realized that a formation with a pore pressure gradient (PPG) of 0.55 psi/ft requires lower fracturing pressure in comparison to a formation having a PPG of 0.5 psi/ft. Therefore, as the pore pressure gradient increases, the pressure, which is required for initiating the fracture, reduces. This is due to the fact that, an increase in

the formation pore pressure can lead to lower effective stress, thereby reducing the fracture initiation pressure.

Considering above graph, one can conclude that, a reservoir with a higher pore pressure is easier to be hydraulically fractured. This result is in contrary to fluid injection processes, such as water flooding, where it requires more injection pressure when the formation pore pressure is higher.

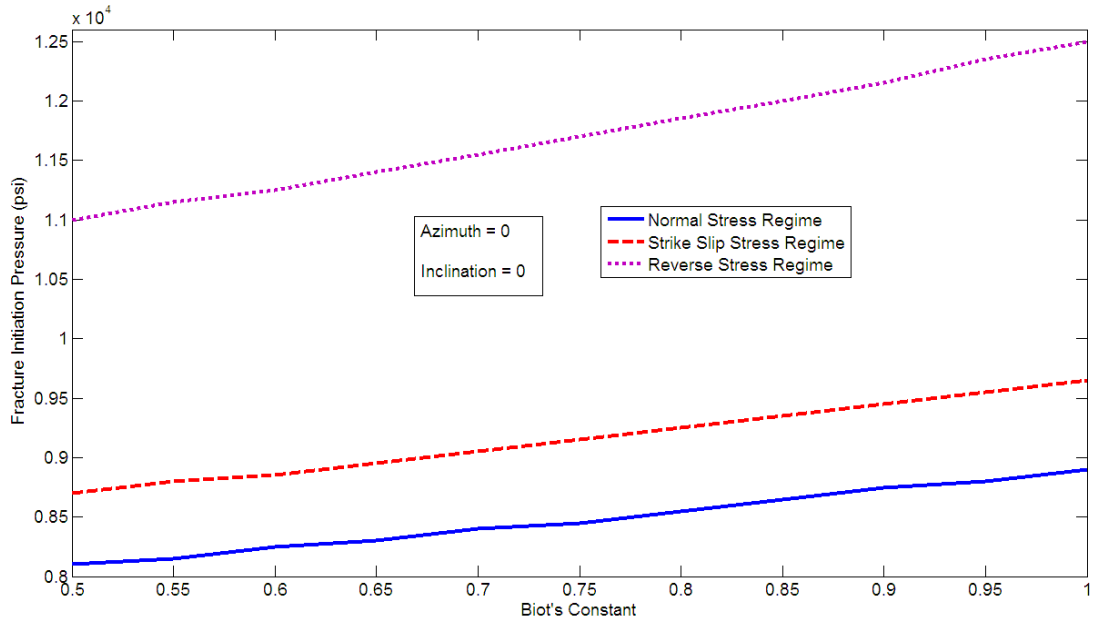

Figure 3-9 The effect of Biot's constant on FIP in different stress regimes, while the perforation poro-elastic stress distribution is applied.

Biot's constant is a poro-elastic rock parameter which generally indicates the effect of pore pressure on effective stress (see Equation (2.34)). As it is depicted in Figure 3-9, as the Biot's constant increases the fracture initiation pressure also increases. This effect could be better analysed by reviewing Equations (3.19) and (3.20); based on these equations, an increase in the Biot's constant will cause some increase in both the tangential and axial stresses of the perforation. This will in turn lead to a rise in the perforation principal stresses; therefore higher pressure will be required to initiate a fracture in such perforation.

The effect of field dominant stress regime is also demonstrated in Figure 3-9. Generally, a well which is drilled in a reverse stressed area needs higher pressure for starting the hydraulic fracturing process. Off course, as it mentioned earlier, this result is obtained for a specific case in which the perforation orientation is towards the x axis of the wellbore, and it has to be checked for other cases.

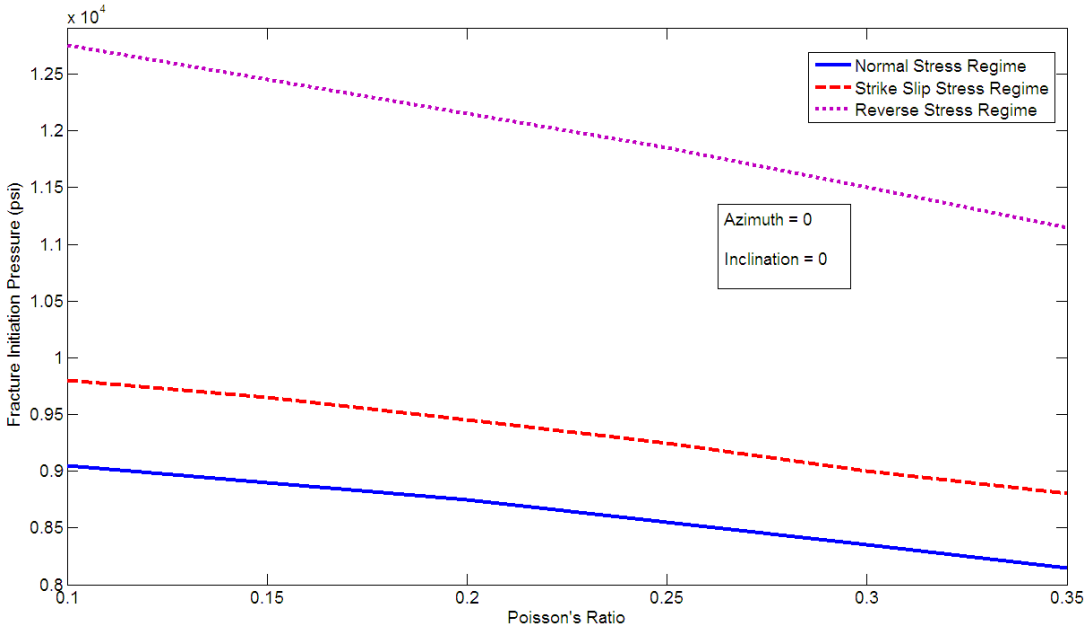

Figure 3-10 The effect of Poisson's ratio on FIP in different stress regimes, while the perforation poro-elastic stress distribution is applied.

Basically, when a rock is stressed in one direction and it has high value of Poisson's ratio, it will generate high stresses in other directions. Therefore, underground formations with higher Poisson's ratio possess higher horizontal stresses under similar vertical stress. However, horizontal stresses, as given in Table 3.1, were used at various Poisson's ratio to produce the gragh presented in Figure 3-10.

Based on Figure 3-10, similar to the case where wellbore poro-elastic model was studied, any increase in the value of Poisson's ratio will lead to a reduction in fracture initiation pressure. That means a rock with higher amount of Poisson's ratio requires lower amount of fracturing pressure to be hydraulically fractured through perforations. In addition, this influence is independent of the state of the stress regime. As it is depicted in Figure 3-10, regardless of the prevailing stress regime, lower FIP is expected when the Poisson's ratio increases.

However, similar to the result obtained from Figure 3-9, higher pressure is required to initiate a perforation fracture for a wellbore which is located in a reverse fault stress regime. Again, this result could not be generalized, since the trends in Figure 3-10 are obtained only for vertical boreholes, which are perforated along the x axis of the wellbore. Different results may be achieved for some other wellbore and perforation orientations.

3.3.4 Thermo-Elastic perforation stress distribution

In addition to pore pressure variation, formation temperature may also vary by the introduction of the fracturing fluid. This is due to the fact that the fracturing fluid is normally cooler than underground formations. As the formation temperature changes, the perforation stress distribution will alter, and as a result, the fracture initiation will be affected.

In this section, the perforation thermo-elastic stress solutions developed in Section 3.2.3 are used along with the wellbore elastic equations, as presented in Section 2.2.1, to investigate the effect of temperature variations on the perforation fracture initiation mechanism. To do so, the numerical method presented in Section 2.4.2 is applied.

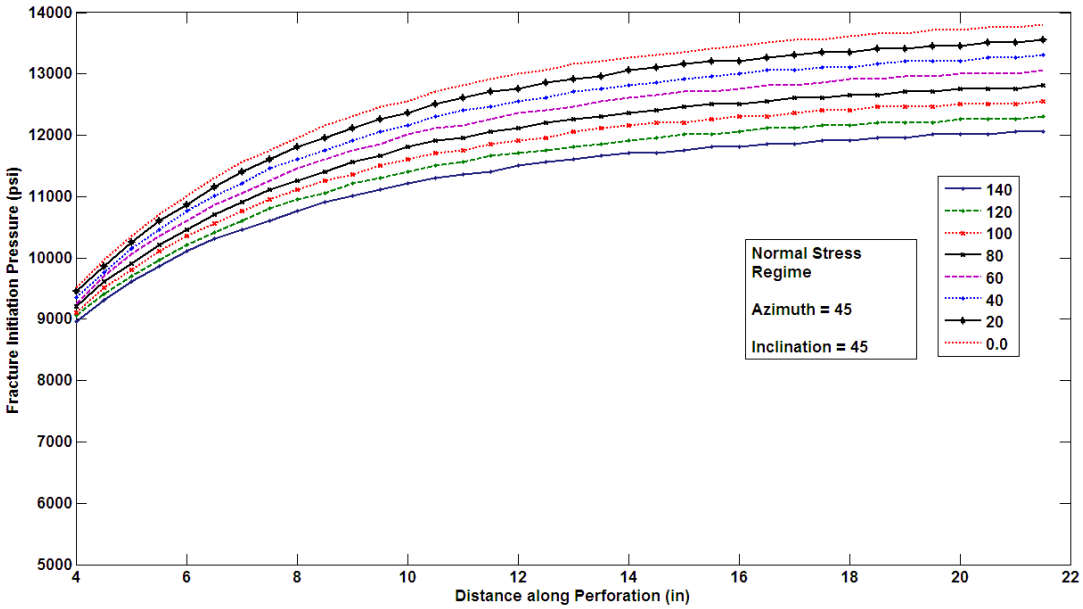

Figure 3-11 The effect of temperature variation on FIP in normal stress regime for an inclined wellbore.

Figure 3-11demonstrates the effect of temperature variation on fracture initiation pressure along the perforation tunnel. As it is shown, by increasing the temperature difference between fracturing fluid and formation rock (from $0^{\circ}F$ to $140^{\circ}F$), the fracture initiation pressure reduces. This is due to the fact that, a cooler fracturing fluid will decrease the local stresses around the perforation and that will consequently reduce the perforation minimum principal stress and in turn FIP. According to this result, it could be concluded that by applying a cooler pad fluid, the process of hydraulic fracturing would be much easier, since the perforation could be fractured at a lower wellbore pressure.

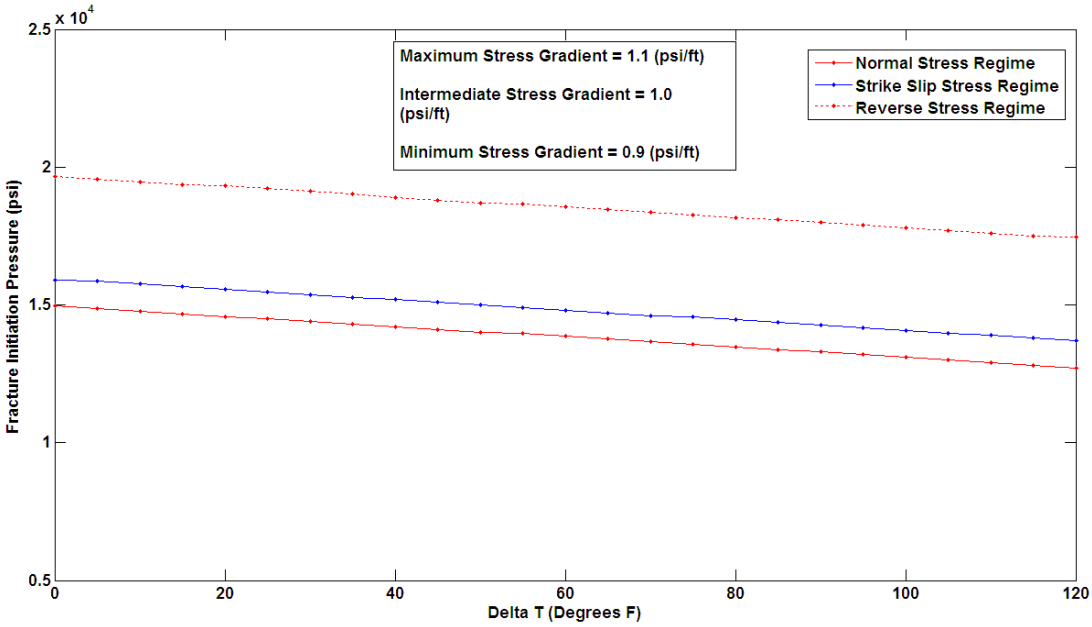

Figure 3-12 The effect of temperature variation on FIP in different stress regimes for a vertical wellbore.

Since there are three main in-situ stress regimes, it is important to study the effect of formation temperature variation in each stress regime. Figure 3-12 investigates the effect of temperature variation in various stress regimes. As it is seen in this graph, by increasing the temperature difference, the fracture initiation pressure generally decreases. However, in a constant temperature difference the value of this pressure is not similar in all three stress regimes.

This shows that, when a well is drilled in a reverse stress regime area, higher pressure is required to break down the formation than in an area with a strike slip stress regime. In addition, an oil/gas field which is normally stressed would require the lowest pressure for fracture initiation. Again, this result is only valid for a vertical wellbore with aforementioned perforation orientation. However, the effect of temperature variation in all three stress regimes is almost the same.

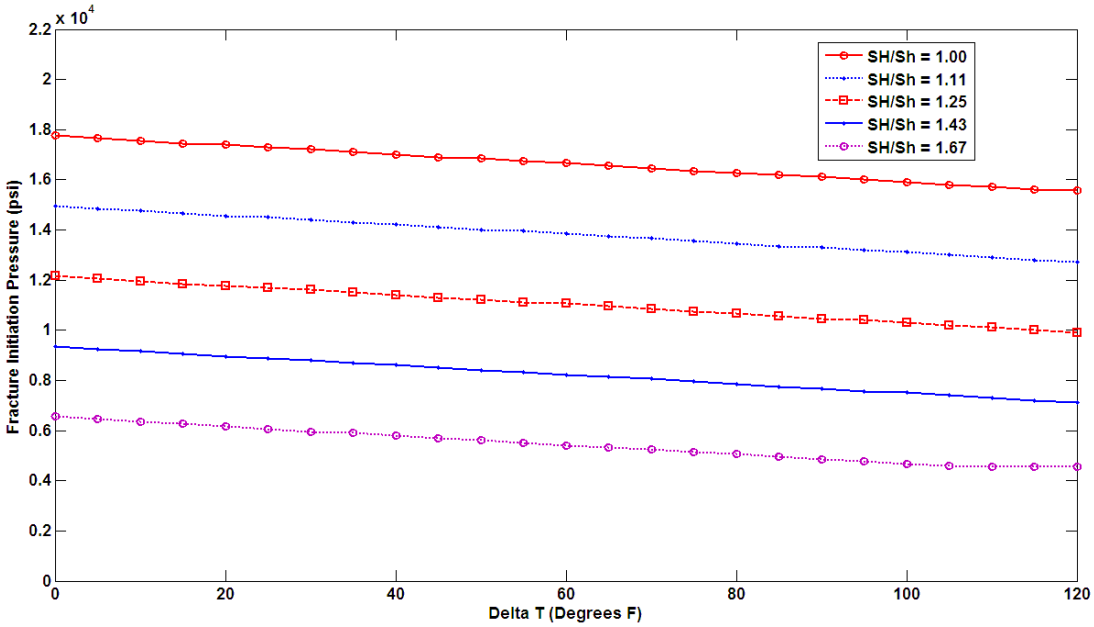

Figure 3-13 The effect of temperature variation on FIP in various stress anisotropies for a vertical wellbore.

A field with similar horizontal stresses is called an isotropic stressed field. This state is not normally the case in all oil/gas fields, and most of reservoirs have anisotropic stress state. What is seen in Figure 3-13 is the effect of temperature variation in various stress anisotropies. As it is shown, a warmer fracturing fluid needs more pressure to be able to initiate a fracture in the perforation, and the state of the stress anisotropy would not alter this conclusion.

Figure 3-13 demonstrates that, as the stress anisotropy increases, the fracture initiation pressure decreases. This means that for a vertical wellbore in a field, where there is a big difference between the horizontal stresses, it is easier to initiate a fracture. This is based on the state of the stress around the well and also around the perforation which influence the amount of FIP. Similar result was observed when the elastic wellbore and perforation stress solutions were applied, as presented in Section 2.5.4.

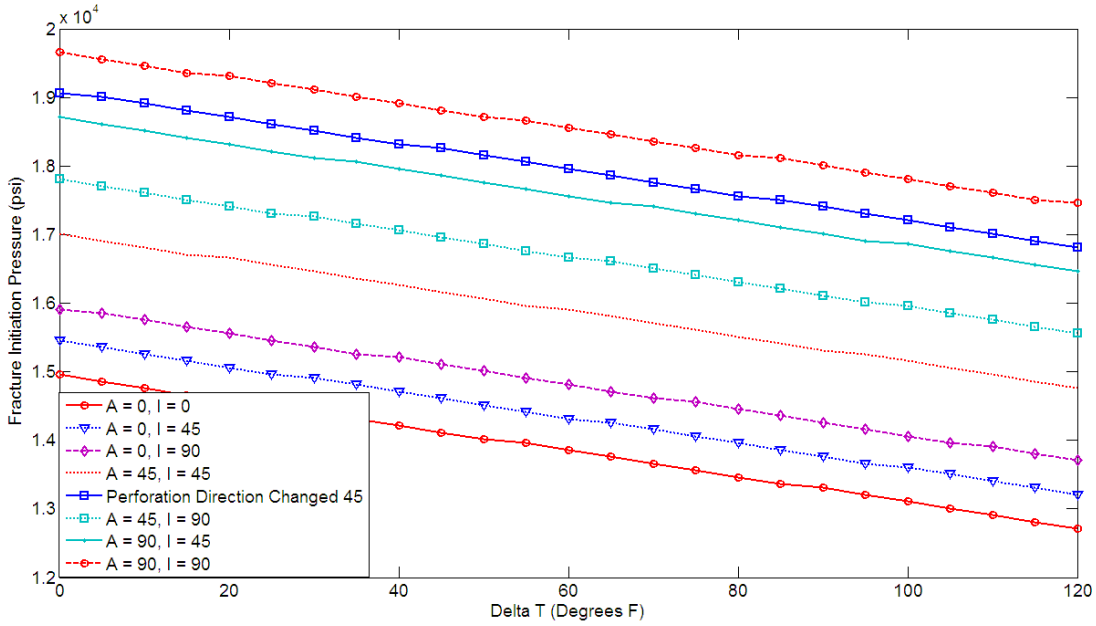

Figure 3-14 The effect of temperature variation on FIP in various wellbore inclination and azimuth angles.

With the new technologies in drilling industry, it is possible to drill a well in any direction with various inclinations and azimuths. Therefore, it is important to know the thermo-elastic effect on the fracture initiation in a deviated perforated borehole in order to properly design hydraulic fracturing treatment in such boreholes.

Figure 3-14 demonstrates the effect of temperature variation in various well trajectories. As it is seen in this graph, the influence of thermal stress is nearly the same in various well directions. For example, when the difference between the fracturing fluid and formation temperatures is 120 °F, the FIP reduces almost 2000 psi in various borehole orientations.

As it is shown in Figure 3-14, the well inclination and azimuth angles also greatly affects the FIP. Generally, as the well gets more inclined, higher pressure is required to initiate a fracture from the perforations. In addition, when the azimuth of the well gets further away from the maximum horizontal stress direction, more fracturing pressure is required. The other important feature of the above graph is the effect of perforation direction. As it is shown, by changing the orientation of the perforation by 45˚ away from the wellbore x axis, FIP significantly increases, because by this orientation change, the stress profile around the perforation redistributes.

3.3.5 Combining thermo-elastic and poro-elastic effects

So far the pore pressure and temperature variations effects have been analysed thoroughly; however, they have been studies separately. Nevertheless, in a real

hydraulic fracturing operation, both pore pressure and temperature of the formation may change when a fracturing fluid is pumped into a perforated wellbore. Therefore, it is of great interest to analyse these two effects simultaneously.

Since the effects of thermo-elasticity and poro-elasticity are developed in the stress solutions based on superposition principle, these effects are uncoupled (see Section 3.2). In this section, the wellbore poro-elastic stress equations are applied along with the thermo-elastic perforation stress solutions. In this way, the pore pressure variation around the wellbore is modelled while the formation temperature changes are also taken into account. Therefore, this approach is supposed to analyse the fracture initiation mechanism more accurately, since both pore pressure and temperature effects are included. In the following parts various results of this approach is presented and discussed.

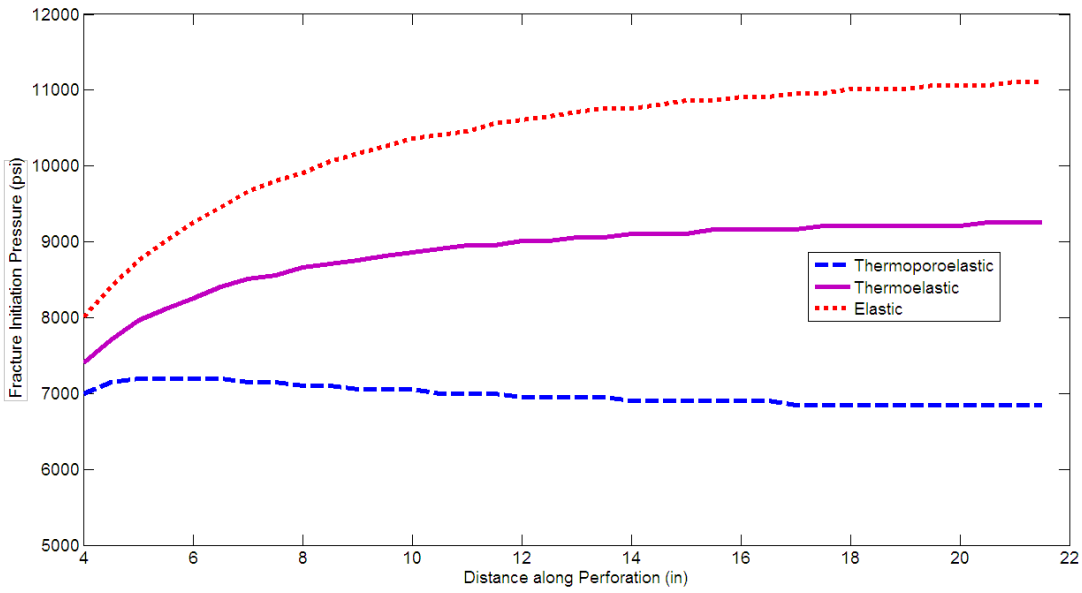

Figure 3-15 A comparison between three different modelling approaches, elastic, thermo-elastic and thermo-poro-elastic for a vertical wellbore in a normal stress regime.

Figure 3-15 demonstrates a very interesting result; it compares the outputs obtained from thermo-poro-elastic, thermo-elastic and elastic modelling. As it is seen from the above graph, the FIP has the highest value when the elastic modelling approach is used. This means, when the modelling does not apply the thermal and poro-elastic influences, a high value for the formation break down pressure would be obtained.

However, when the thermal effect is added to the elastic modelling, the FIP will reduce. This must be a better simulation of the actual fracture initiation. In addition,

when a thermo-poro-elastic methodology is applied, the lowest value of FIP is obtained. Generally both of these variations in formation properties (temperature reduction and pore pressure increase), help the process of hydraulic fracturing. Therefore, if a cool fracturing fluid is used to reduce the formation temperature, and if the well pressure is increased over a long period of time for pressurizing the formation pore pressure, a lower FIP will be expected. Consequently, by considering the poro-elastic and thermo-elastic effects, fracture will be initiated at a lower pressure and accordingly lower surface pressure would be required.

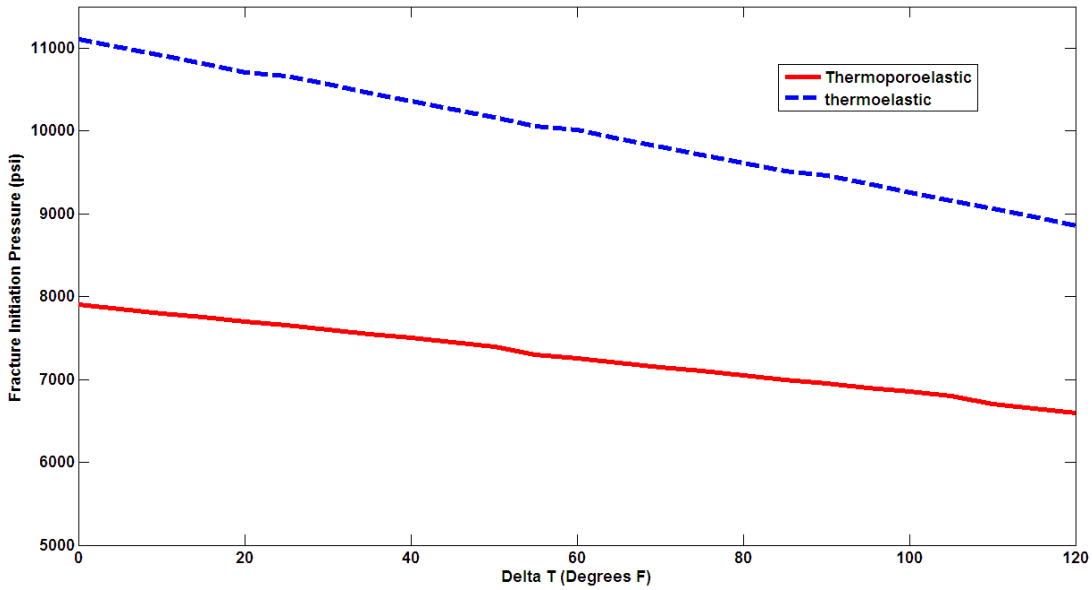

Figure 3-16 A comparison between thermo-poro-elasticity and thermo-elasticity while varying the temperature difference for a vertical wellbore in a normal stress regime.

Both thermo-poro-elasticity and thermo-elasticity modelling consider the thermal effect; therefore, it is motivating to compare these two approaches in various temperature differences. Figure 3-16 demonstrates this comparison. As it is obvious from this figure, for both modelling methodologies, by increasing the difference between the fracturing fluid and formation rock temperatures, the FIP reduces. This is due to the reduction in the amount of local stresses.

However, the amount of this reduction is more pronounced for the case of thermo-elastic approach. This is due to the fact that in the thermo-poro-elastic modelling the effect of pore pressure increase is also included; therefore, the FIP calculated from this method is lower than FIP of the other method at 0°F temperature difference. Accordingly, as the fracturing fluid temperature reduces, the thermal effect is more sensible in the thermo- elastic model, since its FIP at 0°F is quite higher. The thermal

and poro-elastic approaches may also be applied to analyse the properties of the cement sheath behind the casing.

The analytical model presented in this chapter was used to study various parameters of the cement sheath in order to avoid micro-annulus creation. The results of this study are presented in more details in Paper 1. The effect of various properties of cement, including Poisson's ratio, elasticity modulus, thermal expansion coefficient, Biot's constant and permeability were investigated on fracture initiation. In addition, in this paper, the effect of the casing on the wellbore stress distribution is modelled through a simple approach. It also presents some results of fracture initiation in perforated wellbores, while the effect of the steel casing is considered.

3.4 Summary

Since most underground formations are porous and permeable, fracturing fluid may dissipate into the formation porous space and increase the pore pressure. In addition, the local temperature of the formation may also decreases when it comes into contact with a low temperature fracturing fluid. Such variations in formation pore pressure and temperature will impact the wellbore and perforation stress distribution, thus, the FIP may change.

Consequently, in this chapter, the wellbore and perforation analytical elastic stress model, which was developed in Chapter 2, was further advanced to account for the formation pore pressure and temperature variations. Wellbore and perforation stress distribution equations were modified to adjust the stress analysis for poro-elasticity and thermo-elasticity effects. Darcy's law was used to model the pore pressure variation, and superposition principal was implemented to include the effect of this pressure variation in the elastic model. As a result, wellbore and perforation general poro-elastic stress analysis equations were derived, which could be used for various wellbore and perforation orientations.

Then the correspondence between thermo-elasticity and poro-elasticity was used to derive perforation stress equations which account for formation temperature variations. Next, the numerical method presented in Chapter 2 was applied to study perforation fracture initiation using the developed poro-elastic and thermo-elastic

models. Various aspects and results of the developed models were presented in the rest of this chapter.

It was found that by increasing the temperature difference between the fracturing fluid and formation rock, the FIP reduces. This is due to the fact that, a cooler fracturing fluid will decrease the local stresses around the perforation and that will accordingly reduce the FIP. Therefore, it is concluded that by applying a cooler pad fluid, the process of hydraulic fracturing would be easier. In addition, as the Poisson' ratio increases the thermal effect can reduce the stresses more significantly, and this will lead to lower FIP. Moreover, the effect of temperature difference is more noticeable when the rock has higher modulus of elasticity and linear thermal expansion.

Comparing the elastic and poro-elastic perforation stress distribution results, and their effects on the FIP, a noticeable decrease is observed in the amount of FIP; in all three stress regimes, the FIP is less for the case of poro-elastic modelling. And as the pore pressure gradient increases, the pressure, which is required for initiating the fracture, reduces. However, when the modelling does not apply the thermal and poro-elastic influences, a high value for the FIP would be obtained. But, when the thermal effect is added to the elastic modelling, the FIP will reduce. This must be a better simulation of the actual fracture initiation. In addition, when an uncoupled thermo-poro-elastic methodology is applied, the lowest value of FIP is calculated. Generally both of these variations in formation properties (temperature reduction and pore pressure increase), help the process of hydraulic fracturing.

4 Case study

4.1 Introduction

In this chapter the analytical models developed in Chapter 2 and Chapter 3 are applied to some field case studies. Required input parameters are obtained from several raw field data and then applied to the developed models to study the fracture initiation mechanism in three different cased and perforated wellbores (wells A, B and C). These cased perforated wells are selected from Ahwaz oil field. This field, which is one of the largest hydrocarbon-bearing structures in the world, is a huge northwest-southeast-trending anticline with a subsurface area of 80 by 10.5 km. Figure 4-1 shows the location of Ahwaz oil field;

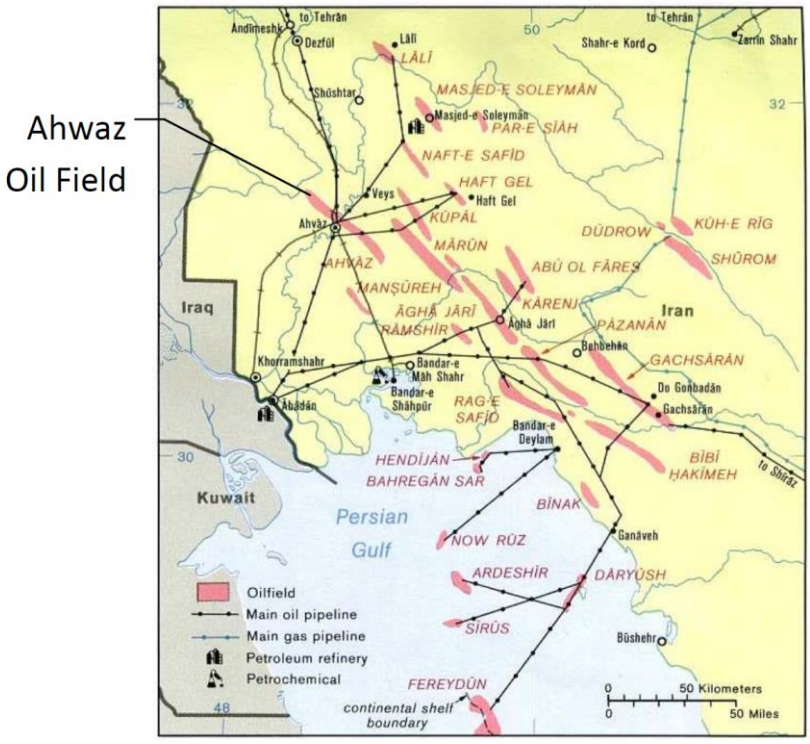

Figure 4-1 The location of Ahwaz oil field ("http://www.globalsecurity.org,").

The selected wells have been drilled to produce from Bangestan reservoir. While some of Bangestan carbonate layers are believed to be naturally fractured, most of them do not have a sufficient production rate with enough wellhead pressure including Ilam and Sarvak Layers. This weak production performance is mainly due

to very low matrix permeability and disconnected natural fractures. Therefore, these producing layers are good candidates to be hydraulically fractured, in order to connect the natural fractures to each other, and also to provide a proper well to reservoir connection. However, it is essential to perform proper fracturing design before any treatment is operated, especially because these three boreholes are cased and perforated.

In the following sections various raw field data is used to obtain required parameters to be applied in the model and the results of this modelling are presented and discussed in the subsequent sections.

4.2 Input data preparation

As it was discussed in Section 2.5.1, some input data is required to run the developed fracture initiation model. In-situ principal stresses, wellbore radius and orientation, cement sheath and rock properties are the main parameters required as inputs in this modelling. In this part, logging and also experimental rock data are used along with some correlations to obtain these required input parameters.

4.2.1 In-Situ principal stresses

There are always three principal stress components in every underground formation, typically a vertical and two horizontal components. In this section, these three principal stresses are calculated for Ahwaz oil field. To calculate the vertical stress, the density of overlying layers is required, because basically the vertical stress is the weight of the upper layers. Bulk density log is a vital tool for obtaining the density of formations, but unfortunately this log is not available for whole depth interval of the three considered wellbores.

One way of resolving this issue is to use some correlations to predict the formation densities from some other available log data. Gardner et al. (1974) performed a series of field and experimental studies on sedimentary saturated rocks. Accordingly, they established a correlation, as shown below, to calculate formation density from P-wave velocity; such approach has been used in seismic analysis for many years.

$$\rho = a \times V^b \tag{4.1}$$

where ρ is the bulk density in gr/cc, and V is P-wave velocity in ft/s. Constants a and b were also calculated for the sedimentary rock under study to be 0.23 and 0.25, respectively. These two correlation constants have to be established for every sedimentary setting to be used in Equation (4.1). Zare (2009) used the above equation and some logging data to estimate constants a and b for Ahwaz oil field, and he published the following equation;

$$\rho = 0.2577 \times V^{0.2376} \tag{4.2}$$

Equation (4.2) is used to predict the bulk density log for the whole depth of a well in Ahwaz oil field. Then, since the vertical stress is the weight of the overlaying sediments, the following equation is used to calculate this principal stress component.

$$\sigma_v = \int_0^h \rho g \, dh \tag{4.3}$$

where h is the depth of interest, ρ is the bulk density and g is the gravitational acceleration. This equation is then solved numerically by Simpson's rule, and finally it is found that the vertical stress gradient in Ahwaz oil field is 1.04 psi/ft for formations deeper than 10000 ft.

Another way of finding the vertical stress is to use the reported average densities of Ahwaz oil field's formations, which are listed in Table 4.1;

Table 4.1 Lithology, average density and thickness of each formation in Ahwaz oilfield (Safian, 2012).

Formation Name	Lithology	Density (gr/cc)	Average Thickness (m)
Aghajary	Sandstone	2.435	1700
Mishan	Marl	2.535	100
Gachsaran 7	Evaporite	2.617	100
Gachsaran 6	Anhydrite	2.617	110
Gachsaran 5	Dolomite	2.558	220
Gachsaran 4	Shale	2.587	200
Gachsaran 3	Anhydrite	2.517	90
Gachsaran 2	Salt	2.514	80
Gachsaran 1	Evaporite	2.475	50
Asmari	Sandstone	2.677	400
Pabdeh	shale	2.365	180
Gurpi	shale	2.365	300
Ilam	limestone	2.7	160

Using the data provided in above table, it is possible to find a thickness weighted average density by the following equation;

$$\rho_a = \frac{\sum(h \times \rho)}{\sum h} \tag{4.4}$$

where h is the formation thickness and ρ is formation density. In this way the average density is obtained to be 2.496 gr/cc which leads to a vertical stress of 1.08 psi/ft. This is very close to the value obtained through the previous method, therefore, an average value of 1.06 psi/ft is assumed in this modelling.

In the next step, horizontal stresses have to be found. Unfortunately, in Ahwaz oil field, no horizontal stress measurement has been done so far. Therefore, the world stress map (see Figure 4-2) is used to evaluate the prevailing stress regime. Figure 4-2 demonstrates a reverse fault stress regime in the Zagros area, including Ahwaz oil field, in which the direction of maximum horizontal stress is N30E (Yaghoubi & Zeinali, 2009). The prevailing reverse fault stress regime is mainly due to active tectonic plates in the area (Safian, 2012).

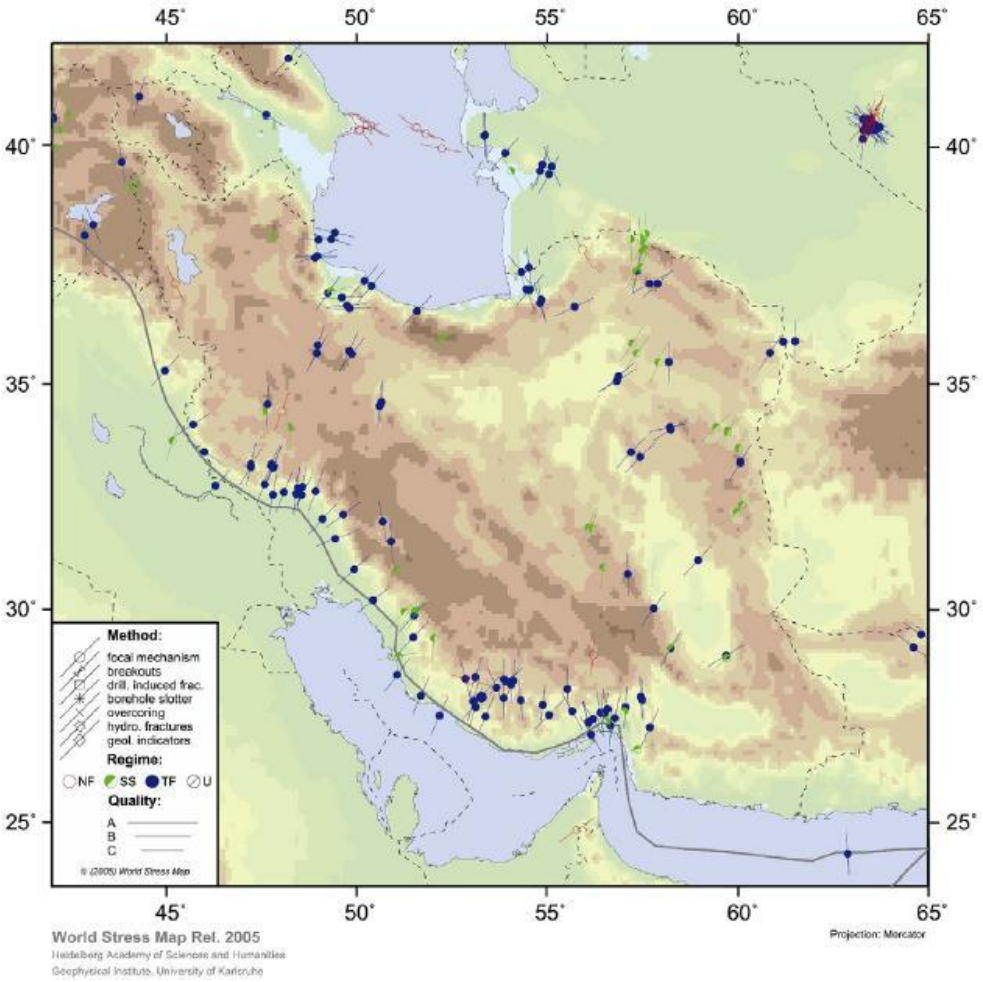

Figure 4-2 World stress map showing the direction of maximum horizontal stress (Yaghoubi & Zeinali, 2009).

In addition, wellbore stability analysis in this field confirms the direction of maximum stress. Zare (2009) studied the mechanical instability of several wellbores in this field and estimated a maximum horizontal stress (σ_H) of 1.2 psi/ft and a minimum horizontal stress (σ_h), of 1.1 psi/ft. In fact, he obtained a reasonable match between the modelling results and actual borehole instabilities, when the estimated horizontal stresses were applied. Therefore the same stress values will be used in this case study. In addition, a formation pore pressure gradient of 0.45 psi/ft has been obtained from repeated formation tests to (Safian, 2012).

4.2.2 Poisson's ratio

After estimating the in-situ stresses and pore pressure gradient of the field, it is now required to obtain some mechanical and elastic properties of the reservoir rock. Poisson's ratio is an elastic rock property which has wide application in every geomechanics study. Generally, Poisson effect refers to the tendency of a piece of

rock to expand in two directions when it is stressed in the other direction. And Poisson's ratio shows the degree of the Poisson effect of the rock. In this study the following equation is used to calculate the Poisson's ratio from sonic log (Fjar et al., 2008);

$$\vartheta = \frac{V_p^2 - 2V_s^2}{2\left(V_p^2 - V_s^2\right)} \tag{4.5}$$

where ϑ is Poisson's ratio, and V_p and V_s are compressional and shear sonic velocities respectively. Compressional sonic velocity data is available in the wells under study, but shear sonic velocity only exists in a nearby well. To estimate the shear sonic velocity in the other wells, one may find a correlation between the compressional and shear velocities, similar to those presented in literature. For example the following equation uses a straight line interpolation approach to obtain shear wave velocity (Castagna et al., 1985);

$$V_s = 0.8619 \times V_p - 1172\,, \qquad (\frac{ft}{s}) \tag{4.6}$$

The available data of V_p and V_s in the nearby well is applied to obtain a similar relationship to be used for Ahwaz geological environment. Figure 4-3 presents a plot of V_s verses V_p, and the best trend line that provides correlation between these two parameters.

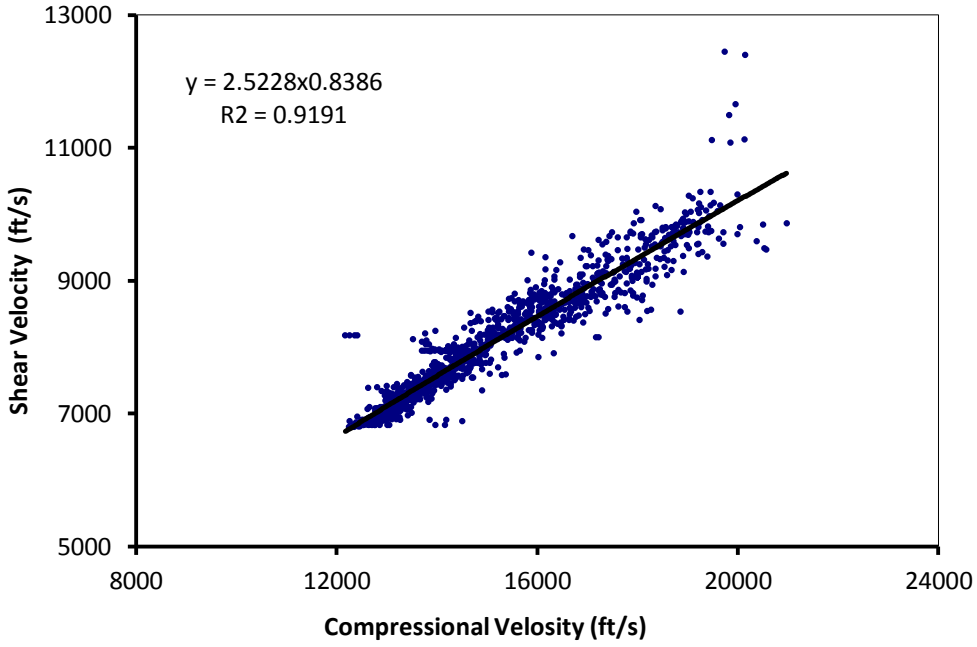

Figure 4-3 The power law relationship between compressional and shear velocities.

According to the trend line given in Figure 4-3, the following power law correlation is developed;

$$V_s = 2.5228 \times V_p{}^{0.8386} \tag{4.7}$$

Using the above equation, it is possible to estimate the shear sonic velocity to be used for Poisson's ratio calculation. Because the three wells under study are all producing from the same reservoir, Poisson's ratio calculations are just done for well A and the same results are used for the other two wells.

Figure 4-4 shows the calculated values of Poisson's ratio for the interested interval (i.e. Ilam and Sarvak Layers). Appendix B contains some tables presenting raw logging data and calculated Poisson's ratio.

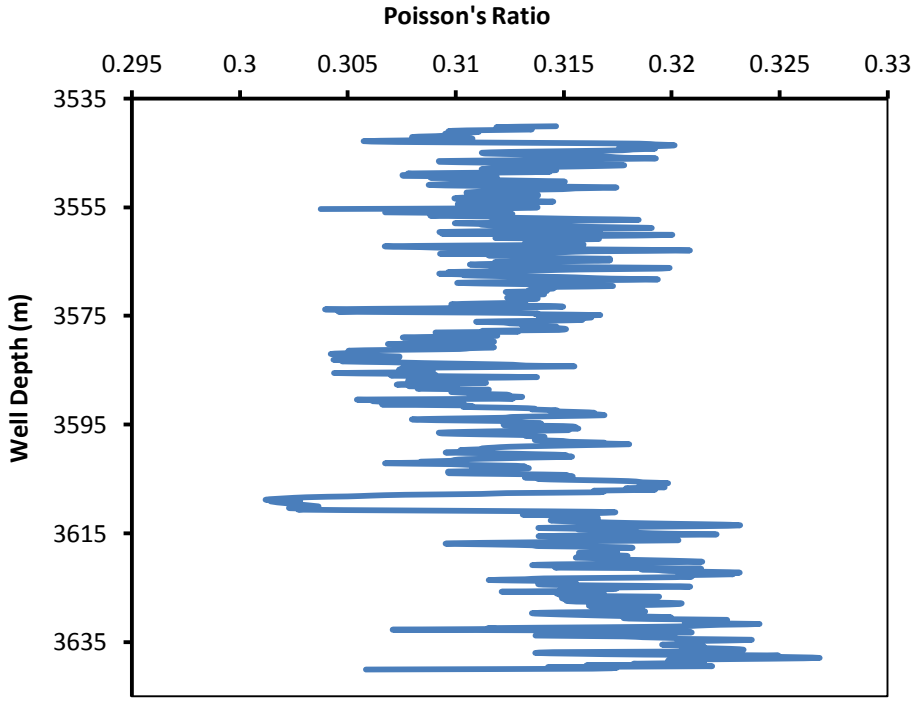

Figure 4-4 Poisson's ratio at interested interval.

As it is seen from Figure 4-4, a value of 0.31 could be used as a reasonable average value for Poisson's ratio.

4.2.3 Tensile strength

Tensile strength is a rock parameter which affects the tensile failure of the formation. It is directly related to Uni-axial Compressive Strength (UCS) of the formation. So, one has to calculate the UCS of the formation firstly and then use it to estimate the formation's tensile strength. Some correlations have been found in the literature for

calculating UCS by using logging data (Chang et al., 2006); among them the followings are applicable for limestone formations;

$$UCS = 7600 \times e^{-0.064\,\Delta t_c} \tag{4.8}$$

Where Δt_c is compressional sonic transit time in $\mu s/ft$, and UCS is in MPa. The next equation is;

$$UCS = 292.47 \times e^{-9.541\varphi} \tag{4.9}$$

in which φ is the neutron porosity in fraction and UCS is again in MPa. These two equations have been applied for UCS determination, and after that tensile strength has been calculated based on a general rule which states that the tensile strength is one tenth of UCS (Fjar et al., 2008). Figure 4-5 presents the calculated value of tensile strength for interested interval of the wellbore.

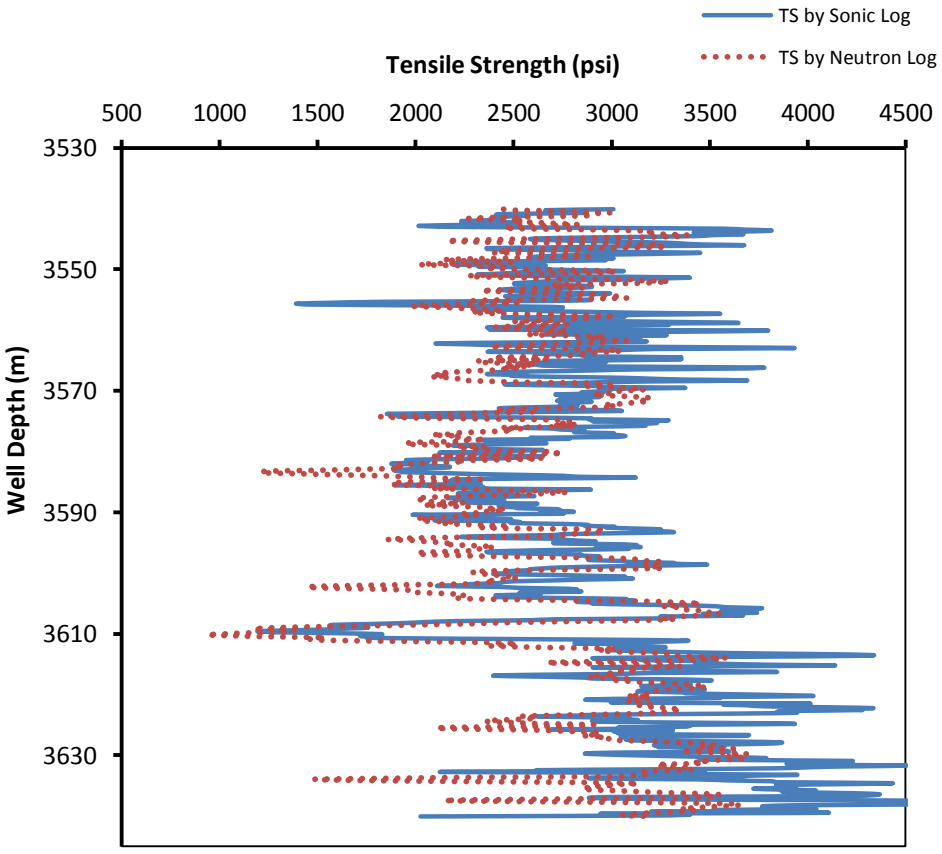

Figure 4-5 Tensile strength obtained from sonic and neutron logs.

Having a look on Figure 4-5, one may distinguish the small difference between two calculated tensile strength values, which is negligible. Totally, an average value between 2000 psi to 3000 psi can be used in the model for this depth interval.

4.2.4 Biot's constant

The next important parameter which can be calculated from available data is Biot's constant, which significantly influences the effective stress of the rock. It can be calculated by Equation (2.34). in this equation bulk modulus is the reverse of compressibility. Few experimental results are available for some rock samples in Ahwaz oilfield, including some samples from our depths of interest. The bulk formation modulus has been reported to be $4.6\times10^6\ psi$, and limestone bulk modulus, which is available in literature is $78\times10^9\ Pa$ (Safian, 2012). Converting the units and applying Equation (2.34), Biot's constant is found to be 0.6.

Unfortunately there is no data available about the cement. Therefore it is assumed that the cement sheath has similar value of Biot's constant as the formation rock. In addition the cement sheath Poisson's ratio is assumed to be 0.2, since cement rock typically has lower Poisson's effect. And the tensile strength of the cement is assumed to be 3000 psi; these are some common cement properties.

Table 4.2 Summary of input parameters required for case studies.

Input Parameter	Unit	Quantity
Vertical stress gradient	psi/ft	1.06
Max. horizontal stress gradient	psi/ft	1.2
Min. horizontal stress gradient	psi/ft	1.1
Formation pore pressure gradient	psi/ft	0.45
Formation Biot's constant	-----	0.6
Formation Poisson's ratio	-----	0.31
Formation tensile strength	psi	2500
Cement Biot's constant	-----	0.6
Cement Poisson's ratio	-----	0.2
Cement tensile strength	psi	3000

It is noteworthy that making these assumptions will not be detrimental to the modelling results, since as it is described in Section 2.6, the FIP is not very sensitive to these cement properties. Table 4.2 summarizes the calculated input parameters, which are used in the following section;

4.3 Results and discussion

In this section, the wellbore and formation parameters prepared in Section 4.2 are used to analyse the perforation FIP in the three aforementioned wellbores. Both elastic, and uncoupled thermo-poro-elastic models developed in Chapters 2 and 3 are used to study fracture initiation in these wellbores. Accordingly, the results are presented and discussed. It is noteworthy that well A, which is a vertical well, has experienced an unsuccessful hydraulic fracturing operation. While wells B and C, which are two deviated wellbores, are not fractured yet, but they have been considered as potential candidates for fracturing treatment (Safian, 2012).

4.3.1 Results of modelling well A

As it is mentioned previously, well A has been drilled to produce oil from Bangestan reservoir. As it is shown in the schematic of this wellbore (see Figure 4-6), the well firstly has been producing from an open hole of radius 3 in. After a period of production, the wellhead pressure has reduced to a level lower than required, therefore production engineers have decided to block the open hole, and produce from upper layers. They have done that by cementing the open hole section and perforating the upper reservoir strata. But after a short period of production, the rate has decreased and the wellhead pressure fell down (Safian, 2012).

Several acidizing operation have not improved the rate of production and the producing pressure. Finally production department has decided to hydraulically fracture the formation. They have allocated a big investment on this project by making a contract with a fracturing service company (Safian, 2012).

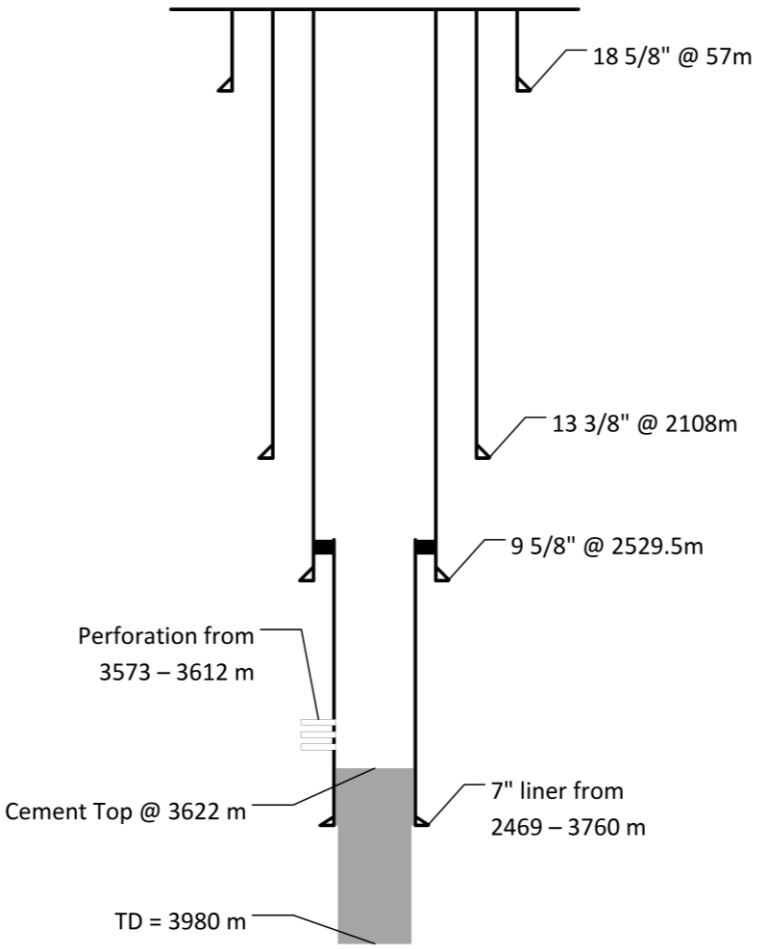

Figure 4-6 A Schematic of well A, showing well casings, setting depths and perforation interval (Safian, 2012).

Before executing the hydraulic fracturing operation, they have killed the well and replaced the production wellhead by a 10000 psi wellhead. After that, they have set up the pumps and made the connections. And then they started to inject the pad fluid for doing the mini-frac test. The wellhead pressure was increased to 10000 psi (the limit of the wellhead) and the fracture did not initiate, because the pressure did not fall down (Safian, 2012).

They couldn't increase the pressure anymore, because of wellhead restriction; therefore they have turned off the pumps and left the unsuccessful hydraulic fracturing operation. The pad fluid had an average density of 66 pcf, equivalent to 0.458 psi/ft (Safian, 2012); therefore, the maximum downhole pressure could be calculated by adding the wellhead pressure to the pressure of column of fluid in the wellbore. Considering the midpoint of the perforated interval (3592.5 m = 11786.2 ft), the downhole pressure is equal to 15400 psi, and the pressure gradient will be 1.307 psi/ft.

One may ask why such a huge downhole pressure did not lead to fracture initiation. To answer this question, it is required to model fracture initiation mechanism, while considering the perforation and wellbore stress distribution. This is done using the developed analytical models and the results are presented below.

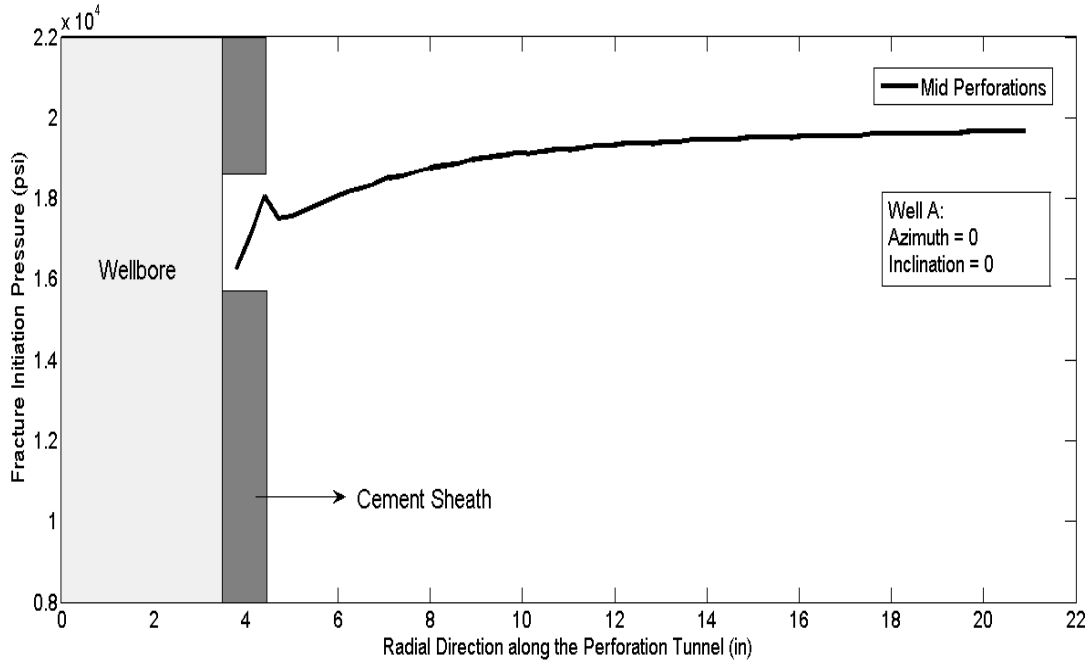

Figure 4-7 Elastic modelling of FIP in well A.

Figure 4-7 presents the FIP for well A, along a perforation hole, at mid-perforation interval. The elastic modelling approach (see Chapter 2) was used to generate this graph. As it is seen from the graph, the minimum required FIP is 16400 psi, which corresponds to fracturing the cement sheath. This is 1000 psi more than the actual downhole pressure (15400 psi). While the minimum FIP in the formation is almost 17500 psi; this indicates why the actual fracturing treatment was unsuccessful. Basically, higher downhole pressure was required to initiate starter fractures in the perforations.

It should also be noted that because the state of the stress in this field is a reverse fault stress regime (see Table 4.2), the PFP (Preferred Fracturing Plane) would be a horizontal plane. This is a unique stress regime in such a depth, because usually at deep wells, the PFP is a vertical plane, resulting from a normal or strike slip stress regime. So the initiated fracture from each perforation has to be linked to each other and turn towards a horizontal plane; this will result in a very tortuous near wellbore fracture plane. Therefore, even if enough pressure is applied to initiate the fractures in the perforations, high pressure drop and possibly premature screen out is expected,

The fracture initiation mechanism of this well is also simulated using the developed uncoupled thermo-poro-elastic model (see Chapter 3). In addition, the casing effect is investigated,

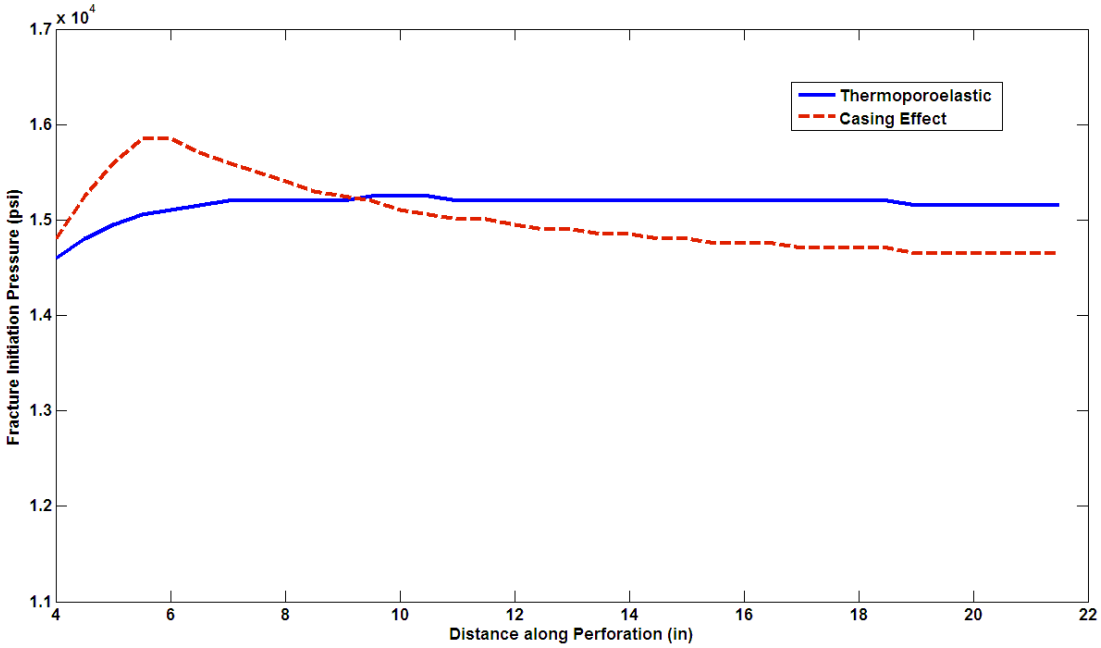

Figure 4-8 Uncoupled thermo-poro-elastic modelling of FIP in well A.

As it is seen from Figure 4-8, when the thermo-poro-elastic model is used, the fracture will initiate somewhere at the beginning of the perforation tunnel. As expected, the thermo-poro-elastic model estimates a lower FIP in comparison to the elastic model. But when the casing effect is also added to the modelling, the result is very different. In such a case, which is more close to reality, at first the fracture may initiate somewhere in the middle or end of the perforation. However, when the fracturing pressure increases to 15400 psi (i.e. the actual treatment maximum pressure), another fracture will initiate at the entrance of the perforation tunnel. This is called multiple fracturing.

After that some other fractures may develop in other points of the perforation. This will generally lead to unsuccessful fracturing operation, because the fracturing fluid is exposed to many small fractures in each perforation tunnel, and in this way the fracturing fluid is just lost and no significant fracture will be generated. This is possibly the reason of this unsuccessful hydraulic fracturing operation.

Studying this specific unsuccessful hydraulic fracturing operation demonstrates the importance of near wellbore parameters, and states the vital value of analysing the stress distribution around a perforation hole.

4.3.2 Results of modelling well B

After analysing a vertical well in the Ahwaz oilfield (Well A), it is worth to model the fracture initiation in some deviated wellbores. Wells B and C are two deviated boreholes with almost the same inclinations, but different azimuth angles. Table 4.3summarizes the specifications of these two wells.

Table 4.3 The specifications of wells B and C.

Well Name	B	C
Total Depth (m)	3500	3373
Inclination (degree)	35	30
Azimuth (degree)	60	20
Mid Perforation Depth (m)	3266	3184
Producing Layer	Ilam	Ilam

Because these two wells are producing from the same reservoir as well A, the same input parameters as presented in Table 4.2 are used for this modelling here. Actually no real hydraulic fracturing has been done for these wells; therefore this modelling can be used for designing future possible hydraulic fracturing.

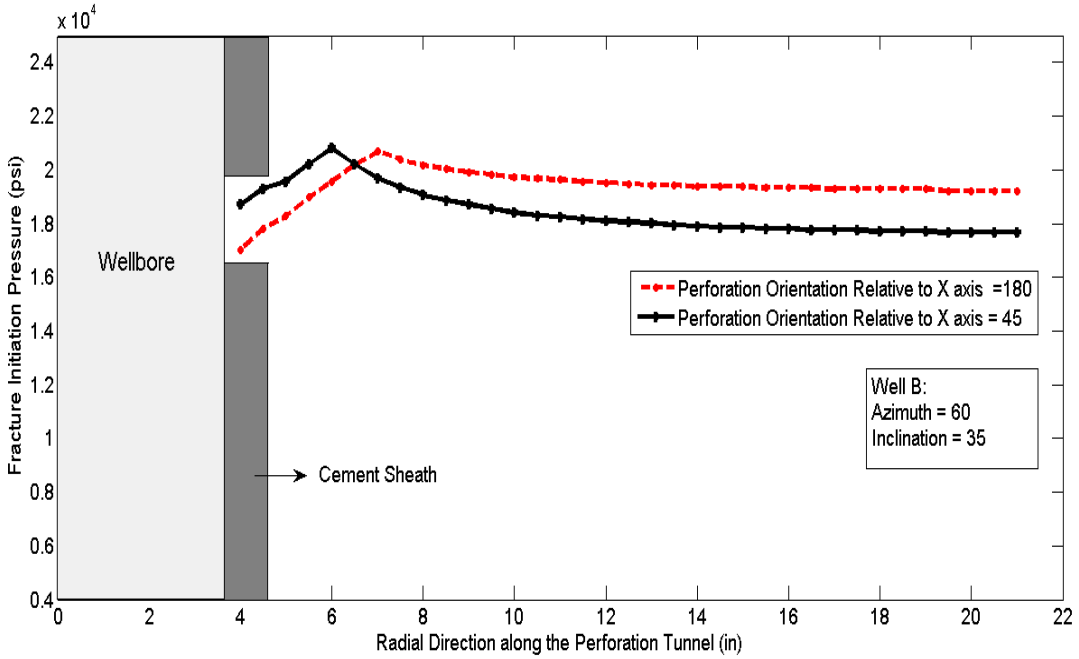

Figure 4-9 Elastic modelling of FIP in well B.

As Figure 4-9 shows, a minimum of about 17000 psi downhole pressure is required to initiate a fracture in well B. However, when the perforation orientation is 180° with respect to lowermost point of the well (x axis), an undesirable micro-annulus will be created. It is possible to avoid the micro-annulus by re-perforating the well before hydraulic fracturing. Perforations oriented to a direction 45° away from x axis require lower pressure to be broken down with respect. In addition, in the perforation orientation, the fracture will be initiated in the formation rock, rather than the cement sheath. Such perforation orientation could be compared with the wellbore tensile zone.

According to Figure 2-12, the tensile zone of this well is about 120° from x axis. Comparing above perforation orientation to the tensile zone location, it is clear that a perforation tunnel which is further away from tensile zone, will lead to a more desirable fracture initiation. This again emphasizes that, it is not a general rule to get better results when perforation orientations are close to tensile zone. This is due to perforation stress redistribution, which occurs by changing the perforation orientation.

The formation pore pressure and temperature variations may also influence the perforation stress distribution, and accordingly the FIP in this wellbore. Therefore, fracture initiation is also analysed using the uncoupled thermo-poro-elastic model.

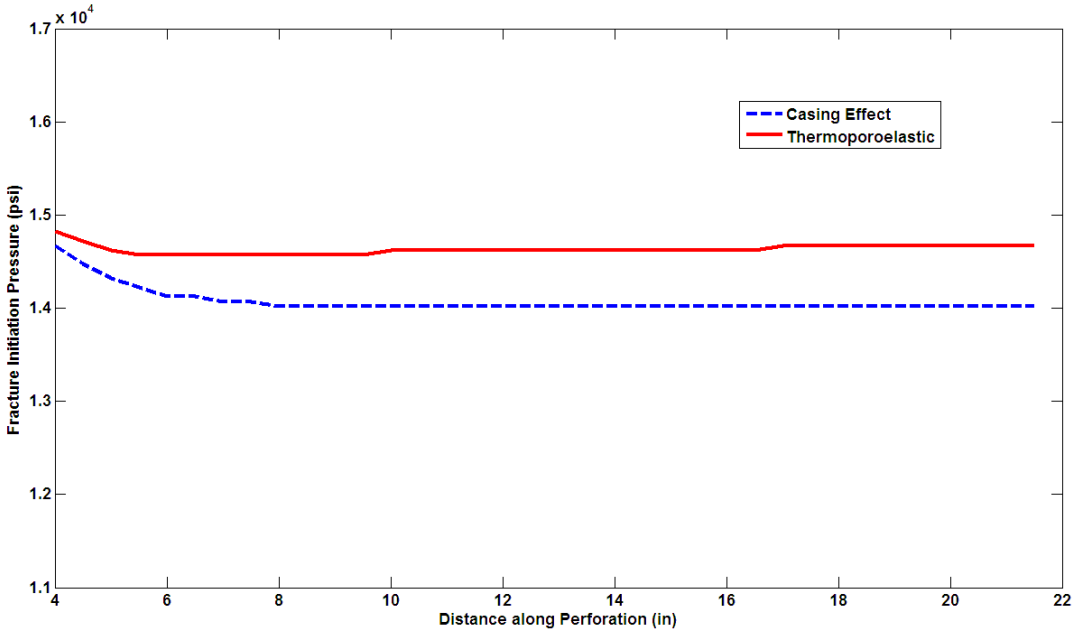

Figure 4-10 Uncoupled thermo-poro-elastic modelling of FIP in well B.

As Figure 4-10 demonstrates, when the thermo-poro-elastic approach is applied, a minimum of 14500 psi well pressure is required to initiate the fracture; and the

fracture will be initiated somewhere in the middle of the perforation tunnel. This is again lower than the FIP obtained from the elastic approach. Since in this analysis, the thermal and poro-elastic effects are both considered.

But when the casing effect is applied to the model, the fracture initiation pressure reduces. This is in contrast to what has been recognized for well A. The reason is the effect of well trajectory. As it is mentioned before, well B is a deviated well. Therefore, the perforation stress profile for such a well is not similar to a vertical well, so the fracture initiation pressure is not also the same.

4.3.3 Results of modelling well C

As it is mentioned earlier, well C has nearly similar inclination with respect to well B, while their azimuth angles are not alike. In this section, the FIP is simulated for this wellbore.

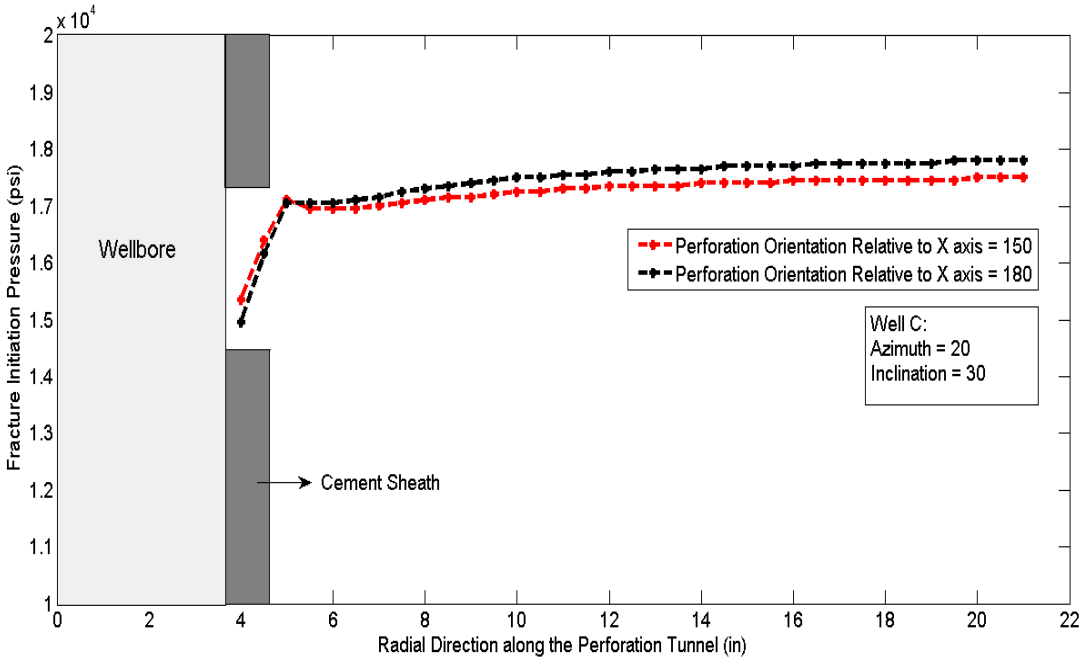

Figure 4-11 Elastic modelling of FIP in well C.

Figure 4-11 presents the FIP simulated using the elastic model for a perforation in well C. According to this figure, the minimum FIP occurs in the cement sheath of the perforation. Therefore, if the downhole pressure increases to 15000 psi a micro-annulus may be formed, which is not desirable. The other feature of Figure 4-11 is that, a perforation orientation of 150° requires less pressure with respect to that with an orientation of 180°; however, the difference is not too much. Knowing that the tensile zone of this well is 150° away from x axis (see Figure 2-12), one can say that, for the specific orientation of well C, the tensile zone rule satisfies. This means

getting further away from tensile zone will cause an increase in required fracturing pressure.

However, it has generally been observed that, the tensile zone rule is not always true (see Section 2.5.5). That means in some specific wellbore orientation and stress regime conditions, a perforation with an orientation further away from the tensile zone would require less FIP.

The fracture initiation for this wellbore is also analysed using the uncoupled thermo-poro-elastic model, which is presented in the following graph.

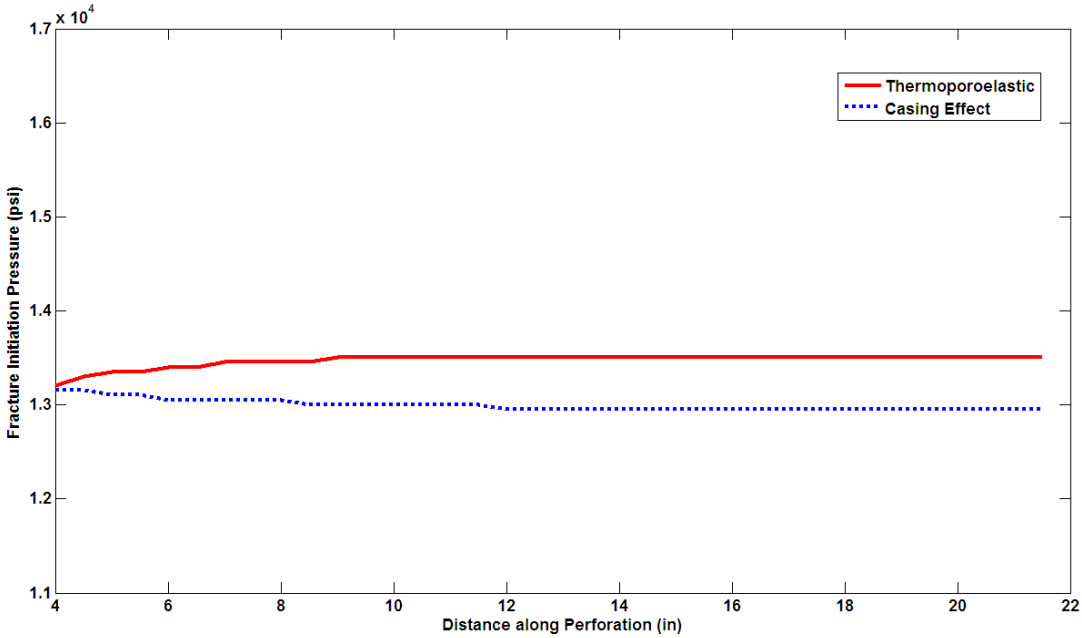

Figure 4-12 Uncoupled thermo-poro-elastic modelling of FIP in well C.

Comparing Figure 4-12 with Figure 4-10, it is generally observed that the FIP for well C is lower than that of well B. This is while both wells B and C are located in the same field with similar characteristics. The main reason of this difference is the effect of well azimuth. Actually the azimuth angel of well C is less than that of well B, and this has resulted in a difference between the wellbore and perforation stress distributions of the two wellbores; accordingly, the FIP is impacted.

In addition, Figure 4-12 demonstrates that, generally, uncoupled thermo-poro-elastic model predicts a lower FIP in comparison to an elastic model. This is because formation pore pressure increase and temperature reduction lead to fracturing pressure reduction. Also, when the casing effect is applied lower fracture initiation pressure is obtained. This is due to the fact that the whole wellbore radial stress is not transferred through the casing; therefore, the surrounding formation will experience

less radial stress. Therefore, depending on wellbore and perforation orientation, the minimum perforation principal stress may reduce, resulting in lower FIP.

In addition, it has to be taken into consideration that, again for this well, because of reverse fault stress regime, the PFP will be a horizontal plane. Therefore, a tortuous near wellbore fracture plane will be created around the wellbore. Consequently, even if a company re-perforates the well and provides the best perforation orientation for fracture initiation, the near wellbore fracture tortuosity has to be accurately analysed.

4.4 Summary

In this chapter the analytical models developed in Chapter 2 and Chapter 3 were applied to three different wellbores (wells A, B and C). These cased perforated wells were selected from Ahwaz oil field, which is located in south of Iran. These wellbores are producing from low permeability carbonate reservoirs; therefore, they are potential candidates for fracturing treatment, and well A has already experienced an unsuccessful fracturing operation. Accordingly, raw field data and experimental results were used to calculate the required parameters in order to simulate the fracture initiation in these wellbores, and to investigate the reasons of failed fracturing in well A.

Both elastic and uncoupled thermo-poro-elastic models were used to study the process of fracture initiation in these wellbores. As a result it was found that, according to elastic model, the cause of failed fracturing operation in well A was insufficient downhole pressure. In fact, high stress concentration around the wellbore and perforation had led to abnormally high FIP. In addition, the existence of a reverse fault stress regime would have resulted in a horizontal PFP. Therefore, despite the lower FIP simulated by the uncoupled thermo-poro-elastic model, it is believed that multiple fracturing and near wellbore fracture tortuosity resulted in failed fracturing operation in well A.

The fracture initiation is also studied in the other two wellbores using the developed analytical models. Accordingly, the results are presented and discussed in order to provide some insight to assist future possible fracturing treatments for these cased wellbores.

5 Experimental Study*

5.1 Introduction

Several laboratory fracturing studies have been performed in the past to investigate various features of fracturing in perforated wellbores (Abass et al., 1994; Behrmann & Elbel, 1991; Abbas Daneshy, 1973; El Rabaa, 1989; Hallam & Last, 1991); however, they have not carried out any dimensional analysis. Dimensional analysis makes the experimental results more reliable as it takes into account the relative dimensional aspects of a laboratory fracturing experiment with respect to the physical phenomenon occurring in field fracturing operations.

Therefore, in this study, the laboratory test parameters are scaled to enhance simulating the fracturing mechanism at field scale. Hydraulic fracturing tests are conducted on 100 and 150 mm synthetically manufactured mortar as well as tight sandstone samples. Synthetic cubic tight mortar samples with particular properties were made for the purpose of performing scaled experiments. The use of cube samples allows application of three independent stresses to mimic real far field stress conditions. Accordingly, a true tri-axial stress cell (TTSC) is used for this purpose.

Several series of fracturing tests were carried out. As a preliminary study, in the first series of experiments, two parallel notches were created in the borehole of each 100 mm sample to simulate the perforations. In these experiments, the effect of the relative orientation of the borehole notches, with respect to horizontal stresses, was investigated on fracture initiation and near wellbore propagation. The procedure and results of these tests are presented and discussed in Paper 2.

---

*Some of the contents given in this chapter are based on the material presented in:

Paper 2. An experimental study to investigate hydraulic fracture reorientation with respect to the principal stresses.

Paper 3. An investigation of hydraulic fracturing initiation and near-wellbore propagation from perforated boreholes in tight formations.

Paper 4. Challenges in hydraulic fracturing from perforated boreholes in unconventional reservoirs.

Paper 5. The Impacts of Fracturing Fluid Viscosity and Injection Rate on the Near Wellbore Hydraulic Fracture Propagation in Cased Perforated Wellbores.

In the second series of the fracturing experiments, the hole and perforations were made into the sample after casting and curing were completed. Various scenarios of vertical and horizontal wells and in situ stress regimes were modelled. These factors are believed to play a significant role in fracture initiation and near-wellbore propagation behaviour; however, they are not independent parameters, hence should be studied simultaneously. Paper 3 presents these experiments along with their results and corresponding discussions. It is noteworthy that some of the tests performed in the second set of the experiments were conducted for the purpose of validating the analytical model (see Section 2.5.2).

Furthermore, the initiation of hydraulic fracturing from a perforated tunnel was studied numerically using a finite element method. The numerical model was generated to represent a laboratory experimental test, which has been carried out on tight concrete cubic samples. A perforated wellbore in a linearly elastic tight formation was modelled using ABAQUS software through three-dimensional numerical analysis. Two different perforation orientations were considered to analyse the fracture initiation pressure (FIP) and the location and initial direction of the crack. Different far field stresses were considered to study the effect of in-situ stresses and perforation directions on the fracture initiation mechanism. The outcomes were then compared to laboratory and analytical outcomes; the corresponding results and discussions are presented in Paper 4.

In the last series of the experiments, three different fracturing fluids with viscosities ranging from 20 to 600 Pa.s were used to investigate the effects of varying fracturing fluid viscosities and fluid injection rates on fracturing mechanism in cased perforated wellbores. Hence, in these set of experiments, the borehole drilled in the centre of each sample was firstly cased, and then perforations were created in the cased borehole. In addition, in order to properly analyse the tests' results, a new methodology was developed for predicting the fracture propagation time from the pressure-time curves. Accordingly, the fracture initiation and break down pressures were analysed, based on the particular fluid viscosity and injection flow rate implemented for each test, and the results are discussed in Paper 5.

In the following sections, firstly the process of sample preparation is discussed. This process includes preparing appropriate cement and sand slurry mix, casting the slurry, and creating the borehole and perforations. The hydro-mechanical properties of the samples and fracturing fluids' characteristics are also presented. Then the

experimental set-up including the TTSC and fluid injection system are presented in details. Scaling analysis is the next topic which is covered in this chapter. And at the final section of this chapter, the results of different series of the experiments are presented briefly; more detailed discussions could be found in the attached papers to this thesis.

5.2 Sample preparation

In this section, the process of sample preparation is discussed. This process includes preparing appropriate cement and sand slurry mix and casting the slurry in cubic moulds. Then cased wellbore and perforations are created in the samples after casting and curing were completed. At the end of this section, the properties of the synthetic sample and fracturing fluid are presented.

5.2.1 Casting cement samples

To conduct scaled hydraulic fracturing tests, rock samples with particular hydro-mechanical properties are required. However, rock samples with desired properties are not readily available, as it is practically impossible to acquire a sufficiently large size intact sample from downhole. Additionally, the properties of rocks obtained from the outcrop (considering that they are a good representative of downhole rock samples) may not be homogeneous. Therefore, synthetic mortar samples were made to conduct these laboratory experiments, because it is possible to prepare these samples with reasonably homogenous properties (Perkins & Weingarten, 1988).

The components of synthetic samples are cement, sands and water. Mechanical and hydraulic properties of any synthetic sample are significantly affected by the percentage of each individual component used in the cement slurry preparation. During sample preparation, it has been observed that a slight variation in the ratio of the components of the cement slurry could significantly alter the characteristics of the final concrete block. This emphasizes the importance of systematic selection of the cement, water and sand ratios. In addition, the sand grain size distribution influences the sample properties. Figure 5-1 shows the grain size distribution used to prepare the samples.

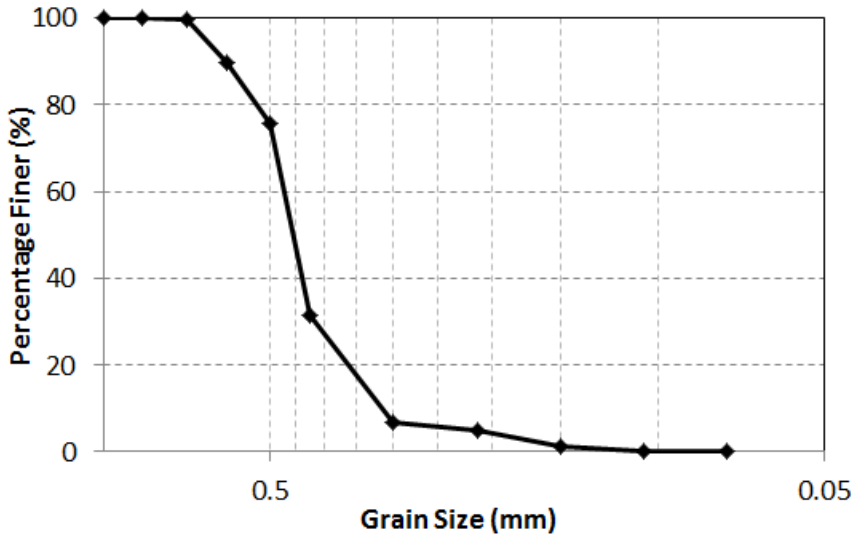

Figure 5-1 Grain size distribution for synthetic sample preparation.

Grain sizes were carefully chosen to be in the range of 200 to 850 μm in order to have a low permeable final mortar block. Low permeability will reduce fracturing fluid leak off, which is suitable for scaling analysis. This is explained in more details in section 5.4.

The synthetic samples prepared in this study were produced based on the procedure presented by Sarmadivaleh (2012). The proposed cement slurry mixture consisted of Portland cement-sand and water-cement weight ratios of 1 and 0.4, respectively. Initially dry sand and cement were adequately mixed and then water was added to the mixture. The cement, sand and water were gradually mixed together using a heavy duty mixing equipment in a way that it reduced the volume of the air bubbles entering the slurry whilst also producing a homogenous mixture. The optimum mixing time was found to be 15 minutes at which point a uniform grain distribution was achieved.

To simulate the real field in-situ stress conditions, the experiments were planned to be carried out on cube-shaped samples, where three independent stresses could be applied. Therefore, standard concrete cubic moulds were used to make 150 × 150 × 150 mm^3 and 100 × 100 × 100 mm^3 mortar blocks. The cement slurry was poured into the cubic moulds which were slightly overfilled to compensate for the slight shrinkage of the cement. After filling the moulds, the samples were placed on a vibration plate so that the air bubbles present within the slurry moved their way to the surface. It was found that the optimum vibration time was around 10 minutes. This was a sufficient time for air bubbles to graduate from the slurry with no

separation of particles within the mixture due to its relatively high viscosity. Finally, around an hour after the casting, in which time the cement samples had partially shrunk, the top side of the samples were flattened using a wet trowel. The samples were then allowed to set for a day after which time they were removed from their moulds and placed in a water bath for 28 days. This allowed the cement to cure and reach its ultimate compressive strength (Mindess et al., 2003).

5.2.2 Preparing cased perforated samples

As the next step, the wellbore had to be drilled into the sample with its entire length being cased. This is mainly because the existence of the casing could significantly affect the wellbore stress distribution, and consequently the fracturing pressure and near wellbore fracture geometry would be affected (S. Fallahzadeh & Rasouli, 2012). Open hole perforated samples were also prepared for some fracturing experiments; further details for these samples could be found in Paper 3.

Stainless steel tubing with an outer diameter of 12.7 mm, that could withstand a maximum internal pressure of 48.3 MPa, was selected to be used as the casing. A wellbore was drilled directly through the centre of each sample. The hole was drilled at 650 rpm through the entire length of the sample with a 14 mm masonry drill bit. The slow rate of penetration ensured maximum cutting efficiency. The hole was drilled as soon as the sample was removed from the water bath to reduce the risk of micro cracks forming around the wellbore.

The hole was then cleaned and a 400 mm long piece of the aforementioned tubing was cut to be glued in the wellbore; 150 mm length of the tubing was accommodated in the wellbore and the rest of the tubing was considered for connection purposes to the fracturing fluid chamber; this will be explained in more details in Section 5.3.2. As the OD of the tubing was 12.7 mm and the wellbore diameter was 14 mm, a narrow annulus of only 0.65 mm wide was considered for the placement of the adhesive. Such narrow annulus was designed to minimize the effect of the adhesive on casing and wellbore stress distribution, for the time when the cubic sample would be under stress. However, some difficulties arose, due to this narrow annulus, when gluing the tubing in the hole, because the adhesive material was quite viscous and it could not easily fill and seal the annulus between the casing and the wellbore. To resolve this problem, initially the tubing was plugged at one end by an 8 mm OD steel rod, and it was slightly roughened to provide a better bond between the casing,

glue and cement. Then one side of the wellbore was placed on a rubber sheet and enough adhesive was carefully poured into the wellbore from the other side. At this stage, the plugged end of the tubing was inserted in the wellbore and firmly pushed against the adhesive at the bottom of the hole. While enough force was applied and the rubber sheet was sealing the bottom side of the wellbore, the adhesive flowed upward in the annulus and filled the whole space. This upward flow of the adhesive ensured that no air bubble was left in the narrow annulus and consequently guaranteed the sealing of the dried adhesive.

It is noteworthy that the first tubing was glued in the wellbore using Selleys Liquid Nails adhesive; however, the rest of the samples were prepared using Super Strength Araldite adhesive. This was mainly because the former glue did not demonstrate enough strength and the fracturing fluid could break through it, when the fracturing test was in progress. The strength properties of these adhesives are presented in Table 5.1.

The wellbore glue was allowed to cure for three days at which point two perforations were drilled into each sample. Each one was drilled at the centre of the two parallel faces of the sample, perpendicular to the wellbore and orientated so that the perforations were facing directly opposite each other. The perforations were drilled through to the casing with a 4 mm masonry bit and a 4 mm general purpose drill bit through the steel casing. Each perforation was then cleaned and plugged with 35 mm of 3.75 mm steel rod using Araldite. The samples were allowed to cure for another 3 days after which they were cleaned up using a variety of files and sandpapers to guarantee that each surface of the sample was completely level and ensure a completely uniform stress distribution being applied to each face when under stress.

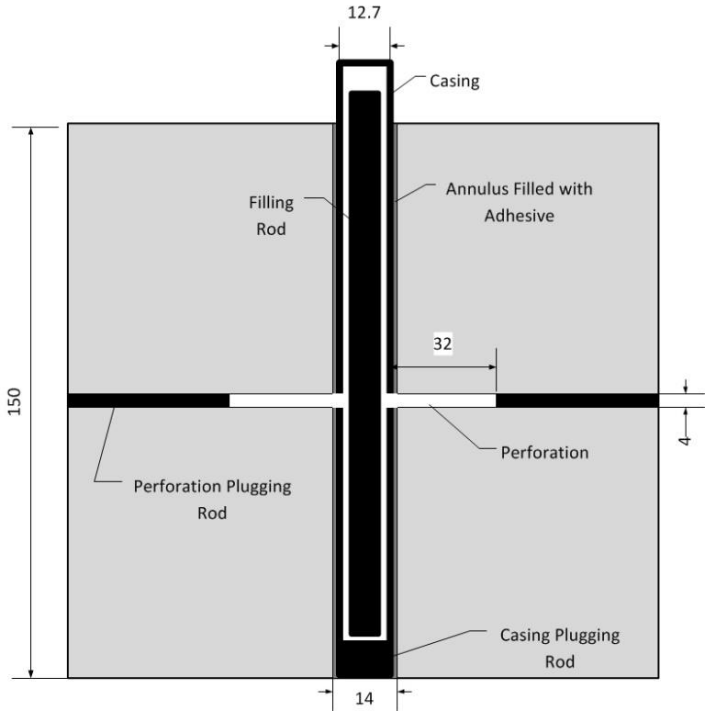

Figure 5-2 A schematic of 150 mm cubic sample with a cased wellbore at the centre and two 4 mm perforations that are perpendicular to the axis of the wellbore and at an angle of 180° from each other (all dimensions are in mm).

Before the sample was placed inside the TTSC a 380 mm length of 6.2 mm OD steel rod was placed inside the wellbore to minimize the volume of the wellbore and hence reduce the wellbore filling time once the test had commenced. The other benefit of having this rod was to reduce the dead volume of the fracturing fluid. As a result, when the fracturing test was in progress, less compressed fracturing fluid would be present inside the hole at the time of fracture break down; therefore the fracture propagation could be better controlled.

The completed samples were now representative of a cased and perforated wellbore, with the perforations being aligned perpendicular to the maximum horizontal stress in the TTSC in order to promote fracture initiation. Figure 5-2 shows a schematic of the cased perforated block.

5.2.3 Sample and fluid properties

To perform scaling analysis for hydraulic fracturing experiments, samples' physical and mechanical properties as well as fracturing fluids' viscosity are needed. Sarmadivaleh (2012) conducted conventional lab experiments including rock mechanics tests on core plugs to estimate some hydro-mechanical properties of the

samples. Table 5.1 presents a summary of the physical and mechanical properties of the samples as well as the adhesives' strength properties.

Table 5.1 Properties of the synthetic sample and the adhesives used for sample preparation.

Mechanical Properties		**Value**	**Unit**	**Testing Methodology**
UCS	Uni-axial compressive strength	79.5	MPa	Unconfined compression test*
T_o	Tensile strength	3.5	MPa	Brazilian tensile test*
K_{IC}	Fracture Toughness	0.78	MPa$\sqrt{m}$	Semi-Circular bend test*
Elastic Properties				
ν	Poisson's ratio	0.19	-	Unconfined compression test*
E	Young's Modulus	27.74	GPa	Unconfined compression test*
Adhesives Shear Strength				
τ_o	Selleys Liquid Nails	1.1	MPa	Sandblasted aluminum lap shear**
τ_o	Super Strength Araldite	26	MPa	Sandblasted aluminum lap shear**
Physical Properties				
ρb	Bulk density	2047	Kg/m^3	Density measurement test
ρg	Grain density	2500	Kg/m^3	Density measurement test
φ	Porosity	13.5	%	Two Boyle's cells
K	Permeability	0.019	mD	Transient gas flooding

*Presented by Sarmadivaleh (2012).

**Provided by manufacturer.

5.3 Experimental set-up

5.3.1 True tri-axial stress cell (TTSC)

For conducting the fracturing tests three independent stresses should be applied on each cubic mortar sample to simulate the underground in-situ stresses. To achieve this objective, a true tri-axial stress cell (TTSC) was implemented (Rasouli, 2012). The TTSC is capable of applying three independent orthogonal stresses in three directions on a sample. These stresses are applied to a sample using a series of hydraulic rams which are powered by three separate syringe pumps.

Each syringe pumps is capable of providing a maximum pressure of 9500 psi at a maximum injection rate of 107 mL/min. The TTSC is designed in such a way that it could accommodate cubic samples of up to 300 mm in size. However, with the aid of a number of aluminium spacer blocks the TTSC could also be employed for testing a variety of smaller cubic sized samples. For 150 mm samples, six 145 × 145 × 75 mm spacers were applied to properly accommodate the prepared samples at the centre of the TTSC. The face of each spacer, which comes into contact with the face of the sample, is 5 mm smaller on each side; this is to ensure that the adjacent spacers would not come into contact with each other when there is some displacement in the

sample. Figure 5-3 shows a top view of the TTSC and the syringe pumps, which were used for applying the stresses, and also a 150 mm sample accommodated in the cell using the spacer blocks.

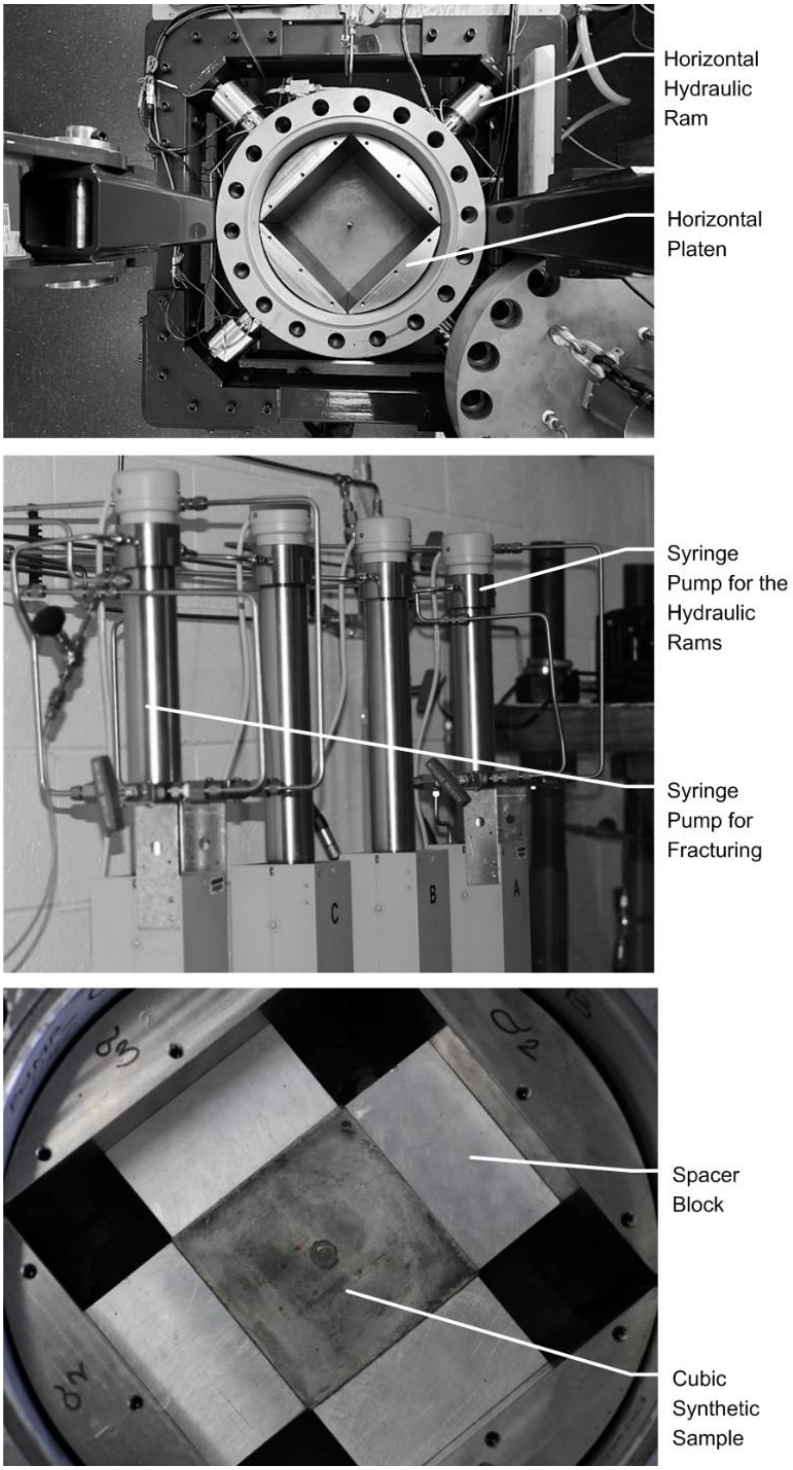

Figure 5-3 A view of the TTSC with the horizontal platen and the horizontal hydraulic rams (top), syringe pumps for the hydraulic rams and fracturing fluid injection (Middle), a synthetic sample accommodated in the TTSC using the spacer blocks (Bottom).

It is noteworthy that the principal stresses were applied in three stages. Initially, all three stresses were concurrently increased to the minimum principal stress

magnitude. At this point, the corresponding minimum stress syringe pump was set on a constant pressure mode to simulate the minimum in-situ stress. Then the other two stresses were increased to the intermediate principal stress, and at this stage the intermediate stress was kept constant. At the final stage, the maximum principal stress was increased to its required value and then its corresponding pump was set on constant pressure mode. This stress path was consistently applied to all samples tested in this study.

5.3.2 Fracturing fluid injection

Three high viscous fluids were used as the fracturing fluid to examine the effects of viscosity on fracturing pressures and propagation geometry. These fluids included honey, and two different silicon oils; the properties of which are listed in Table 5.2. The fracturing fluids were used to hydraulically fracture the synthetic samples, and for each sample a particular fluid was injected with a specific flow rate ranging from 0.05 to 5 cc/minute.

Table 5.2 Fracturing fluid physical properties.

Fracturing Fluid	Viscosity (Pa.s)	Specific Density	Compressibility (1/psi)
Honey	20	1.36**	1.00×10^{-4}**
Poly DMS-T51	97.7*	0.977	$< 9.43 \times 10^{-5}$
Poly DMS-T56	586.8*	0.978	$< 9.43 \times 10^{-5}$

* Viscosities reported at 34.5 MPa by producer

** Obtained from (Min et al., 2010).

A displacement chamber with a total volume of 120 cc was used along with a syringe pump to inject the high viscous fracturing fluid into the wellbore. The chamber was carefully cleaned and filled with the desired fracturing fluid before each set of tests. This process was strictly followed to make sure that no air bubbles could enter the fluid. Since air bubbles can easily get trapped in the high viscous fracturing fluids resulting in a detrimental effect on the fracturing experiment. This is due to the fact that air is much more compressible than the fracturing fluid. Therefore, when the wellbore is pressurizing with the fracturing fluid, the air bubbles shrink, while maintaining the same pressure as the wellbore. Once the fracture initiates in the sample, some new volume would be created and as a result some wellbore pressure reduction is expected. This variation in the wellbore pressure will be interpreted later to analyse the fracturing pressures and geometries. However, with

the presence of compressed air bubbles, they could easily expand and compensate for the new created volume; consequently the wellbore pressure would not reduce much and the fracturing process may be misinterpreted. In addition, the expansion of the air bubbles could provide sufficient pressure to propagate the fracture very quickly to the boundary of the sample (i.e. uncontrolled fracture propagation), which is not favourable.

As three different fracturing fluids were used for these experiments, testing required the fluid chamber to be filled with the three different fluids. The nature of these fluids, particularly their high viscosity made this filling process to become a cumbersome and time consuming task. An alternative and more efficient approach was to first fill a larger chamber with a capacity of 750cc, then allowing the viscous fluid to settle in the chamber, and finally pressurising the chamber and slowly releasing the pressure so that all the air bubbles were removed from the fluid. The fracturing fluid was then displaced into the smaller fluid chamber before testing took place.

In order to inject the fracturing fluid into the wellbore, the fluid chamber should have been connected to the tubing of the sample. As it is seen in Figure 5-3, there is a hole at the bottom of the cell which is designed for the sample's casing to pass through. The top side of the casing, (located underneath the cell), is at the point where the fracturing fluid chamber was connected. Once testing commenced, the fracturing fluid was injected into the borehole of the sample from beneath the TTSC and the pre and post choke injection pressures were measured and recorded using two pressure transducers. These transducers were installed as close to the sample as possible and separated by a partially opened needle valve which acted as a choke (flow restrictor).

The choke helped to restrict and regulate the flow of the fracturing fluid which enabled more precise controlling of fracture growth (Bunger, 2005). If we consider the moment at which the wellbore is pressurized enough so that a fracture initiates from the perforation(s); some new volume is expected to develop which leads to a reduction in wellbore pressure. Therefore, the pressurized fluid, which is in the fracturing fluid chamber, would naturally flows at a higher flow rate towards the wellbore to compensate for this pressure reduction. This would consequently provide higher pressure in the wellbore and the initiated fracture would propagate uncontrollably and quickly towards the boundary of the sample. Such fast fracture

growth in the laboratory-scale could not be reasonably compared with field-scale fracture propagation. Hence, the chock could control the flow of compressed fracturing fluid into a newly initiated fracture and accordingly would control the fracture propagation speed. Figure 5-4 shows a schematic of the fracturing fluid injection set-up. It should be noted that each synthetic sample was initially accommodated in the TTSC (Figure 5-3) and then it was connected to the fracturing fluid injection line.

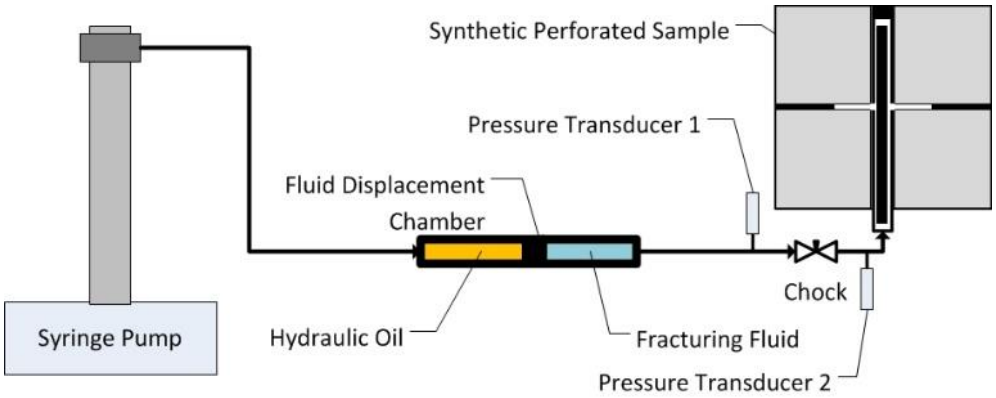

Figure 5-4 A schematic of fracturing fluid injection set-up.

5.4 Scaling analysis

In order to reasonably compare the results of laboratory scale hydraulic fracturing experiments to field scale operations, it is fundamentally important that scaling laws are applied. Scaling laws are simply the dimensional analysis involving the energy dissipation during fracture growth. Known information such as sample size, wellbore dimensions and the hydro-mechanical properties of the sample are normally used as the inputs into the scaling model. This enables the output variables such as fluid viscosity, injection rate and total fracture propagation time, to be properly calculated and aided in the design of the laboratory hydraulic fracturing test (De Pater et al., 1994).

At a laboratory scale, the majority of previous experimental works were conducted without the consideration of scaling laws (Weijers, 1995). As a consequence experimental parameters such as fluid viscosity and injection rates were based on the values used in real field operations. This resulted in very low fluid viscosities and highly exaggerated injection rates being used in the laboratory. However, in order to properly monitor and analyze the fracture initiation and propagation in a small sample at lab scale, fracturing fluids with significantly higher

viscosities are often required as well as drastically reduced injection rates. This ensures that the fracture is contained within the sample and allows fracture growth to be monitored without being affected by boundary conditions.

During hydraulic fracturing the time at which the wellbore pressurization rate reaches its maximum value is recognized as the fracture initiation point. Therefore, in this study, the fracture initiation time was considered as the reference point for scaled time. Conversely fracture breakdown is usually defined as the time at which the wellbore pressure reaches its maximum value, and fracture initiation typically occurs before this breakdown point (Lhomme, 2005). Therefore the scaling period of a laboratory experiment starts with fracture initiation and runs through to the final stage of the fracture propagation.

Over the course of a hydraulic fracturing operation in the field, the initiation and propagation of the real fracture is influenced by three essential boundaries of viscosity, toughness and leak-off dominated regimes (Bunger, 2005). In these tests, the permeability of the synthetic samples was around 0.019 mD and therefore the effect of leak off and the leak off regime could be regarded as negligible. During the majority of field fracturing operations, fracture growth is predominately toughness dominated throughout fracture initiation, however as the fracture develops it rapidly becomes viscous dominated (Mack & Warpinski, 2000). Furthermore for a radial fracture the regime becomes more toughness dominated during the final stage of the fracture growth (Detournay, 2004). In this study scaling laws developed by de Pater et al (De Pater et al., 1994) were applied whilst also validating our interpretations against more recent studies (Bunger, 2005; Detournay, 2004; Lhomme, 2005) to ensure that the majority of the fracture growth is viscous dominated similar to what happens in the field fracturing. In order to have viscous dominated fracture propagation the following equation should be satisfied (De Pater et al., 1994):

$$K_{IC} < 2P_n \sqrt{\frac{r_f}{\pi}} \tag{5.1}$$

Here, K_{IC} is the fracture toughness, P_n is net fracture pressure and r_f is fracture radius. Considering the hydro-mechanical properties and dimensions of the samples used in this study, and based on the study done by Sarmadivaleh (2012), the right hand side of Equation (5.1) is always larger than the synthetic sample's fracture toughness; this is valid for the range of injection rates and fluid viscosities

considered for this study. However, the injection time is different for each set of fracturing fluid viscosity and flow rate.

In order to have a viscous dominated propagation regime, the dimensionless toughness parameter of a Penny-Shaped fracture can be calculated using following equation (Detournay, 2004);

$$K = K' \left(\frac{t^2}{\mu'^5 Q_o'^3 E'^{13}} \right)^{1/18} \tag{5.2}$$

In this equation t is the time of the experiment and Q_o' is the flow rate. In theory, based on Equation (5.2), the fracture propagation will be viscous dominated if K is less than one, whereas if K is greater than four the propagation will be toughness dominated (Detournay, 2004). It must be noted that the dimensionless toughness number, K is time dependent; hence the fracture regime may change as time evolves. Other parameters are as follows:

$$K' = \left(\frac{32}{\pi} \right)^{0.5} K_{IC} \tag{5.3}$$

$$E' = \frac{E}{1 - \vartheta^2} \tag{5.4}$$

$$\mu' = 12\mu \tag{5.5}$$

where, μ is fracturing fluid viscosity, E is rock's Young's modulus, and ϑ is the Poisson's ratio. Using the samples' hydro-mechanical properties (Table 5.1), along with the fracturing fluid viscosities (Table 5.2) plus the range of the flow rates, which were used in this study, the dimensionless toughness numbers (K) were calculated and presented in Table 5.3. As it is seen in this table, all K values are less than one, confirming that the conducted experiments in this study are viscous dominated fracture propagation.

It is noteworthy that the time of the experiment is 1000 s, which was selected based on the previous experimental experiences. However, it was observed that in some of the experiments, the propagation time were less than 1000 s, which again would result in a K value smaller than one, as K is directly proportional to the propagation time.

Table 5.3 Dimensionless toughness number for each fracturing fluid flowing at a particular flow rate.

Fracturing Fluid	Viscosity (Pa.s)	Flow Rate (cc/min)	Dimensionless Toughness
Honey	20	1	0.65
Honey	20	2	0.58
Honey	20	5	0.49
Poly DMS-T51	97.7	0.05	0.69
Poly DMS-T51	97.7	0.1	0.61
Poly DMS-T51	97.7	1	0.42
Poly DMS-T56	586.8	0.1	0.37
Poly DMS-T56	586.8	1	0.25

5.5 Results and discussion

As it is mentioned in Section 5.1, several series of fracturing experiments were carried out in this study. In the first series of experiments, two parallel notches were created in the borehole of each sample to simulate the perforations; this was performed as a preliminary study. In the second series of experiments, various scenarios of vertical and horizontal wells and in situ stress regimes were modelled in perforated borehole. It is noteworthy that some of the tests performed in the second set were conducted for the purpose of validating the analytical model (see 2.5.2). Furthermore, the initiation of hydraulic fracturing from a perforated tunnel was studied numerically using a finite element method. The numerical model was generated to represent a laboratory experimental test, which has been carried out on tight concrete cubic samples. And, in the last series of the experiments, three different fracturing fluids were used to investigate the effects of varying fracturing fluid viscosities and fluid injection rates on fracturing mechanism in cased perforated wellbores.

Detailed procedures and result of these set of experiments as well as the numerical modelling are discussed in the attached papers (i.e. Papers 2, 3, 4, and 5). Yet, they are briefly presented in the following sections.

5.5.1 Preliminary fracturing tests

This study investigated the initiation and near wellbore propagation of hydraulic fracture from notched open boreholes. Two parallel notches were created in the borehole of each sample to simulate the perforations. The TTSC was used to apply three independent stresses of vertical, maximum horizontal and minimum horizontal to 100 mm cubic tight sandstone and mortar samples. In Figure 5-5 a view of the TTSC and the process of loading a 100mm cube sample is shown. Six 95 × 95 × 100 mm spacers were applied to properly accommodate the prepared samples at the centre of the TTSC.

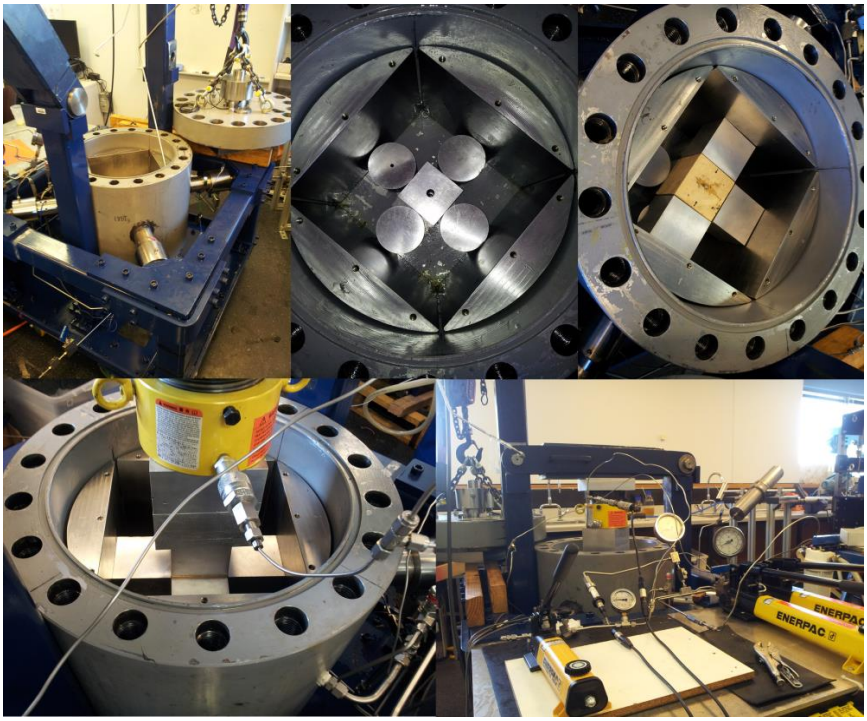

Figure 5-5 The TTSC shown from unloaded through to sample loading and pressure lines connected and ready for hydraulic fracturing testing to start.

Large stress anisotropy was applied in order to help the fracture to initiate more easily. Injection of the fracturing fluid was possible through a hole drilled at the centre of the sample which was plugged in top and bottom sections to give an openhole length of approximately 40 mm in the sample centre. The hydraulic fracturing tests were conducted on four different samples with different orientations for the notch to investigate how the fracture would propagate from different starting angles. In fact, the effect of the relative orientation of the borehole notches, with respect to horizontal stresses, was investigated on fracture initiation and near wellbore propagation.

Four samples were tested in this study; the experimental parameters of these four samples are summarized in Table 1 in the Paper 2. As an example, in sample one, two notches were created on opposite sides in the drilled hole along the planned direction of maximum lateral stress (horizontal stress). Notches were created to assist the fracture to initiate around the borehole. Therefore, in this test it was expected that both fracture wings would open in the direction of maximum lateral stress.

Figure 5-6 View of sample one after HF test; one fracture wing (on the left) was not propagated along the maximum stress direction.

As shown in Figure 5-6, one fracture wing did open in the expected direction while the other wing unexpectedly opened on an angle approximately 45° to the direction of maximum lateral stress. There could have been a variety of reasons for this occurring but it was most likely due to an inhomogeneity along the wellbore in that particular area of the sample which made fracturing in that direction more favourable. It is known that the fracture will be influenced by rock inhomogeneities in low stress anisotropy which is what appears to have been the case in this test. It can be seen from the results that towards the boundary of the sample, the fracture began to turn towards the direction of maximum stress as the fracture passed the possible inhomogeneity. The causes of inhomogeneity in the samples were either due to drilling the borehole and creating the notches, or were due to the existence of the possible air bubbles eventually trapped in the sample. This is while they were all vibrated, when casting, to remove all the air bubbles.

Comprehensive results of these tests are presented and discussed in Paper 2. The results of these experiments have shown that a hydraulic fracture will generally initiate from the borehole notches. Then it tends to propagate and reorient in a direction which is perpendicular to minimum stress after overcoming effects from inhomogeneities both at the wellbore wall and throughout the formation. The

complexity of hydraulic fracturing operations was apparent in these tests as even in a highly controlled laboratory environment, some fractures unexpectedly opened and propagated in directions different to that of the maximum lateral stress direction.

The results have also indicated that on a small scale, a fracture will deviate due to the effects of natural fractures that are either pre-existing in the formation or have been created from drilling and completions operations. On a larger scale and for field applications, it can be seen that the fracture would twist and reorient to propagate towards the direction of maximum horizontal stress after the effects of inhomogeneities have caused a change in propagation direction.

5.5.2 Effects of wellbore/perforation orientations and stress regime

In the second series of the fracturing experiments, the hole and perforations were made into the sample after casting and curing were completed. In these experiments, hydraulic fracturing tests were conducted on 100 and 150 mm synthetic cubic tight mortar samples. The TTSC was used to apply three independent stresses on the samples, while Poly DMS-T51 fracturing fluid with a viscosity of 97.7 Pa.s was injected at very low flow rate (0.05–0.1 cc/min) through the borehole and perforations located at the centre of the sample. As a result, fracture initiation and near-wellbore propagation were analysed by precisely interpreting the pressure-time curves. In addition, the geometry of the fractures near the wellbore including fracture turning and twisting and also multiple fracturing are investigated.

Various scenarios of vertical and horizontal wells and in situ stress regimes were modelled. These factors are believed to play a significant role in fracture initiation and near-wellbore propagation behaviour; however, they are not independent parameters, hence should be studied simultaneously. Paper 3 presents details of these experiments along with their results and corresponding discussions. It is noteworthy that some of the tests performed, in this set of the experiments, were conducted for the purpose of validating the analytical model (see Section2.5.2).

Eight mortar samples were tested of which five samples of 100 mm and three samples of 150 mm cubic blocks. One of the 100 mm samples had no perforation; an open hole without any perforation was tested as a base case. Each of the other 100 mm samples had one perforation, either in the direction of intermediate or minimum stress. Each 150 mm sample had four perforations in two rows, being 180˚ apart from each other. Table 5.4 summarizes the experimental parameters including

applied stresses on each sample. It is noteworthy that, as mentioned in Paper 3, the sample in test 1-3 had some pre-existing fractures; however, sample 1-4 had no fracture initially. Also, test 2-1 was conducted with an injection rate of 0.05 cc/min, while the injection rate in test 2-2 was 0.1 cc/min.

Table 5.4 Experimental parameters and results.

Test No.	σ_1 (MPa)	σ_2 (MPa)	σ_3 (MPa)	No. of Perforations / Orientation	Injection Rate (cc/min)	Initiation Pressure (MPa)	Break down Pressure (MPa)
1-1	20.68	13.79	6.89	0 / -	0.05	10.68	12.41
1-2	20.68	13.79	6.89	1 / Intermediate Stress	0.05	12.75	14.27
1-3	20.68	13.79	6.89	1 / Minimum Stress	0.05	6.27	6.89
1-4	20.68	13.79	6.89	1 / Minimum Stress	0.05	19.30	21.16
1-5	20.68	13.79	6.89	1 / Intermediate Stress	0.05	6.82	7.58
2-1	20.68	10.34	6.89	4 / Minimum Stress	0.05	-----	----
2-2	20.68	10.34	6.89	4 / Minimum Stress	0.1	12.41	14.47
2-3	20.68	10.34	6.89	4 / Intermediate Stress	0.1	6.89	7.62

As it is mentioned in Section 5.3.2, two pressures were recorded while the fracturing fluid was injected into the wellbore. The first pressure was measured before the chock and the second one was measured after the chock, just at the entrance of the wellbore (see Figure 5-4). As the length of the wellbore is quite short, there would be very little frictional pressure drop along its length, considering the very low injection flow rate which was applied; therefore, the pressure recorded after the chock could be considered the fracturing pressure.

The pressure reading before the chock was used as a guide for estimating the initiation and break down pressures. Basically, when the wellbore is pressurized, both pressures are increasing; however, when the fracture initiates, some small fissures are created and, therefore, the rate of increase in wellbore pressure reduces. In this situation, due to the existence of the chock, the pressure record before the chock does not sense this reduction and increases more than the pressure recorded after the chock. Therefore, the point at which the two pressures begin to deviate from each other is the fracture initiation point. Figure 5-7 shows a pressure-time curve which was recorded during test 1-2.

The corresponding injection flow rate curve is also shown in the same figure. The fracture initiation point is clearly visible in this figure and that is where the two pressure recordings deviate from each other. In this figure the break down point is shown as the maximum wellbore pressure. In addition, fracture propagation interval

is also indicated. Some pressure fluctuations are seen in Figure 5-7, which is believed to be due to the presence of some possible air bubbles in the fracturing fluid.

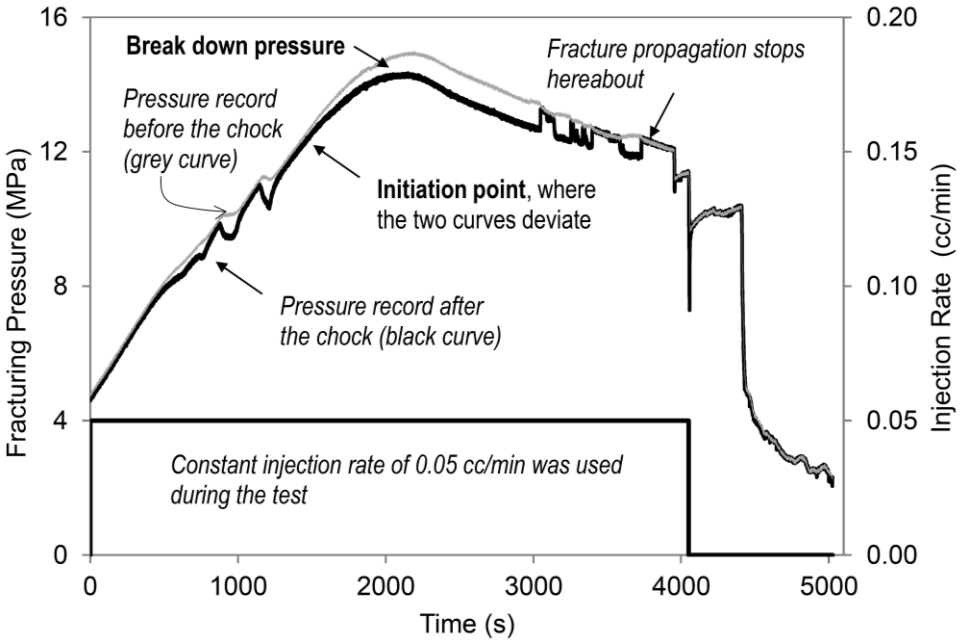

Figure 5-7 Pressure-time curve for test 1-2, showing various pressures during fracturing test.

Three independent normal stresses were applied on each sample. The direction of maximum stress was selected to be always parallel to the axis of the borehole; so that deferent in situ stress regimes and wellbore directions (vertical or horizontal) could be analysed. Each test may represent three real field scenarios.

Table 5.5 Various wellbore directions and stress regimes for tests 1-2 and 1-3.

Test No.	**Wellbore Direction**	**Stress Regime**	**Perforation Direction**
1-2	Horizontal	Reverse	Min. Horizontal
		Strike Slip	Vertical Stress
	Vertical	Normal	Max. Horizontal
1-3	Horizontal	Reverse	Vertical Stress
		Strike Slip	Min. Horizontal
	Vertical	Normal	Min. Horizontal

For instance, in test 1-2, the direction of perforation was parallel to the intermediate stress, and the maximum stress was applied along the wellbore direction; therefore, this single test could be compared to (a) a vertical wellbore in a

normal stress regime area, where the perforations are in the direction of maximum horizontal stress, (b) a horizontal wellbore in a reverse fault stress regime area, where the perforations are oriented to the direction of minimum horizontal stress, and (c) a horizontal wellbore in a strike slip stressed region, where the perforations are aligned with the direction of vertical stress. Table 5.5 presents various wellbore directions and stress regimes that can be considered for two different tests 1-2 and 1-3.

As another example, test 1-4 represents a vertical wellbore in a normal faulting stress regime, where its perforation is along the direction of minimum horizontal stress. A comparison between this test and test 1-5, which represents a horizontal wellbore in a reverse faulting stress regime with a perforation along the direction of minimum horizontal stress, shows that, while in both scenarios the perforations are in the same direction, the fracture initiation and breakdown pressures in test 1-4 are almost three times larger than that of test 1-5. Additionally, in terms of near-wellbore fracture geometry, test 1-4 shows multiple fracturing and fracture tortuosity, while it is seen that the fracture created in test 1-5 is almost planar. Figure 5-8 shows the view of the sample with the location of induced fracture planes in these two tests.

The main cause of such differences between the fracturing results in these two samples is related to the relative orientation of perforation and applied stresses. In test 1-4 the perforation was aligned with the direction of minimum stress; therefore, two other stresses were perpendicular to the axis of perforation tunnel. This caused a very high-stress concentration around the perforation and, therefore, the fracturing pressures increased significantly. However, in test 1-5, where the perforation was run along the intermediate stress direction, the minimum and maximum stresses were perpendicular to the axis of perforation. So the fracture was initiated and propagated at much lower pressures.

In addition, the difference between FIP and break down pressure (BDP) in test 1-5 is less pronounced than that of test 1-4, which resulted in observing less multi-fractures created in various sections of the perforation tunnel. Instead, more planar fracture has been formed along the perforation tunnel (Figure 5-8). As a conclusion, it appears that the lower the differences between FIP and BDP, the less the chance for having multi-fracturing.

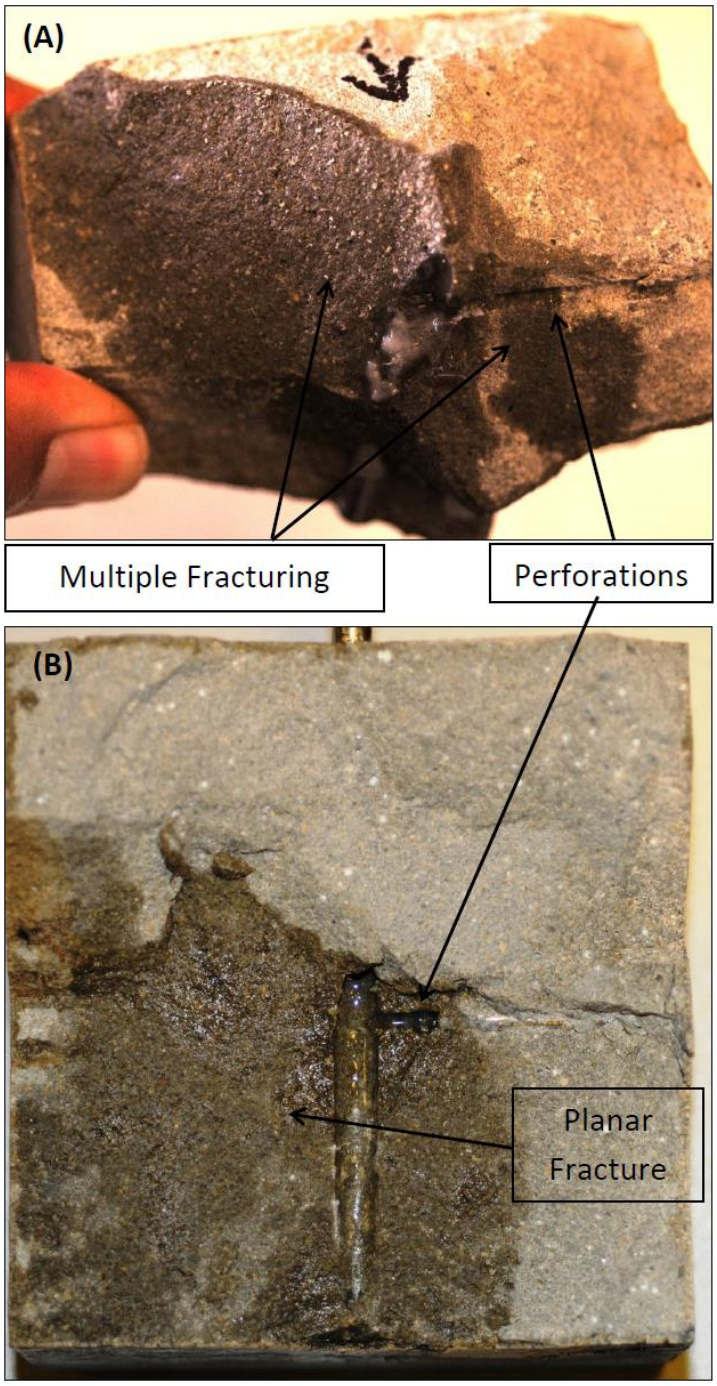

Figure 5-8 (A) Multiple fracture planes and fracture turning in test 1-4 and (B) development of a planar fracture in test 1-5.

The results of this study showed that a lower initiation pressure is observed when the minimum stress component is perpendicular to the axis of the perforations. It was also seen that, even when the cement sheath behind the casing fails, the orientation of the perforations may affect the initiation of the induced fracture noticeably. Furthermore, it was found that stress anisotropy influences the fracturing mechanism in a perforated borehole, and affects the geometry of the initiated near-wellbore fracture. Further discussions and conclusions on the results of the other tests including the effects of various stress regimes and wellbore directions, stress anisotropy, and perforation orientations are presented in Paper 3.

5.5.3 Numerical simulation

Several analytical solutions have been derived to formulate the stresses around a borehole in plane-strain (2D) conditions. In this case, the axial dimension of the borehole is assumed to be infinite and the out of plane stress has no effect on in-plane stress components. It should be mentioned that in this case the out of plane stress is a function of in-plane stresses (Sadd, 2009). The analytical solutions can be used, to some extent, to simulate the experimental results; however, because these solutions are constrained to some specific assumptions, they cannot be used for complicated boundary conditions and constitutive models. The numerical simulations should, therefore, be performed.

The hydraulic fracturing laboratory experiments, which were conducted in TTSC, were simulated using ABAQUS software. Because of the presence of perforations in the tested blocks, the axis of the borehole could not be considered infinite with respect to the lateral perforation dimension. Therefore, 2D numerical models could not be used. Instead, 3D numerical models were generated to simulate the cubic mortar samples, which were subjected to true tri-axial stress conditions, that is, where three independent principal stresses are applied to the samples.

The initiation of a hydraulic fracture from a perforated tunnel was studied numerically using a finite element method. The numerical model was generated to represent a laboratory experimental test, which has been carried out on tight concrete cubic samples. A perforated wellbore in a linearly elastic tight formation was modelled using ABAQUS software through three-dimensional numerical analysis. Two different perforation orientations were considered to analyse the FIP and the location and initial direction of the crack. Different far field stresses were considered

to study the effect of in-situ stresses and perforation directions on the fracture initiation mechanism. The outcomes were then compared with laboratory and analytical results; the corresponding results and discussions are presented in Paper 4.

Some details on this numerical modelling are presented in this section; further details can be found in the attached Paper 4. The geometry and boundary conditions of the numerical models were defined based on the sample dimensions and experiment setup. Due to the symmetrical nature of the problem only a quarter of the sample was modelled. As a result, smaller numbers of elements were required for the model and, therefore, less time was needed for the simulation to converge. The rotation components and normal displacement of the two symmetric faces were fixed in the model. These two symmetric faces with fixed displacements eliminated the rigid body motion.

The boundary conditions, which were defined for the numerical model, were the same as those applied to the real sample in the laboratory experiments. Three independent stresses were applied to the boundary of the model, and a uniform wellbore pressure was applied to both wellbore and perforation surfaces. Figure 5-9 shows the geometry and boundary conditions of a model, which is generated to simulate a 100 mm sample. The sizes of the modelled block and it's wellbore and perforation are identical to the real 100 mm sample.

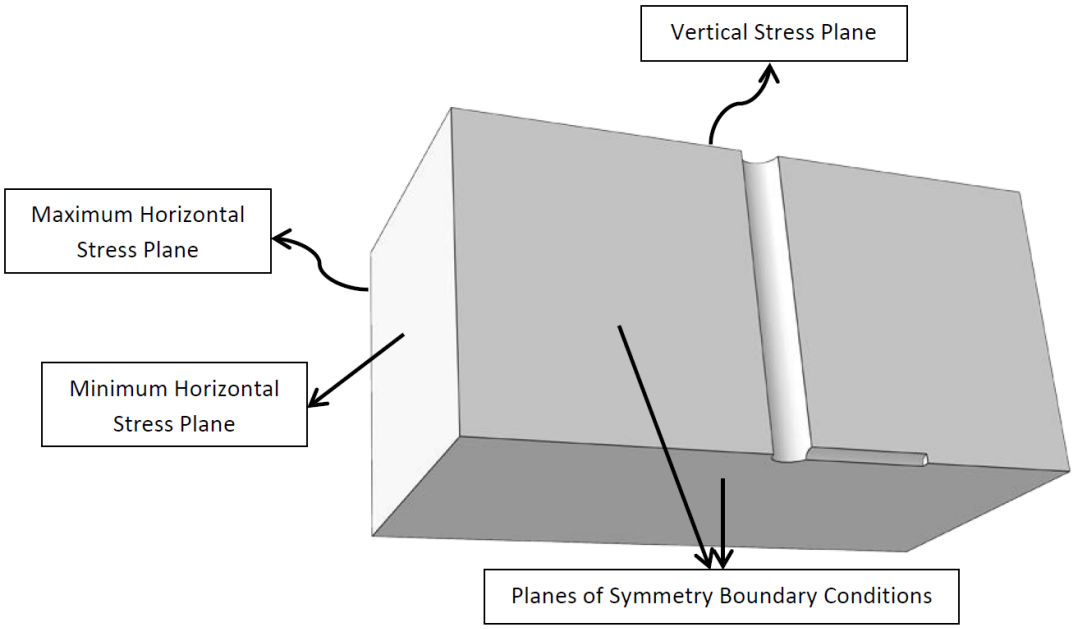

Figure 5-9 3D numerical model geometry and boundary conditions for a 10 cm cubic sample.

The wellbore and perforation pressures are simultaneously increased until the first crack, which is a tensile failure, is formed on the surface of the perforation tunnel.

The minimum wellbore pressure, which could create the first crack, is the FIP. In addition, the location and angle of the crack with respect to the perforation axis gives an indication of the near wellbore fracture geometry; if the initiated fracture is along the direction of PFP, less fracture tortuosity will be expected.

A mesh sensitivity analysis was also performed; five different mesh densities were used in the model and the changes in the values of stress components on the wellbore wall were monitored. A linear elastic material with the properties given in Table 5.1 was generated for this analysis. The model was loaded by uniform lateral and vertical stresses of 5 MPa and the wellbore pressure was zero. The results of each of the five mesh densities are shown in Table 2. As seen in this table, the results of the very coarse, coarse and moderate mesh densities are very different, especially for tangential stress component; however, the results of the fine and very fine mesh densities are almost the same.

Table 5.6 Results of mesh sensitivity analysis.

Mesh	**Number of Elements**	**Relative (to "very coarse" results) Stress Components at Wellbore Wall**	
		Radial Stress	Tangential Stress
Very Coarse	3637	1.00	1.00
Coarse	11417	1.00	1.50
Moderate	101532	1.06	2.60
Fine	519666	1.11	3.37
Very Fine	2128115	1.14	3.58

The convergence of the results is plotted in Figure 5-10. As shown in this figure, when the number of elements is more than 1.5 million, the accuracy of the results do not change significantly. For a larger number of elements, however, a significant amount of memory and solution time would be required for the model to converge. 1.5 million elements, therefore, were applied to all the models in this study.

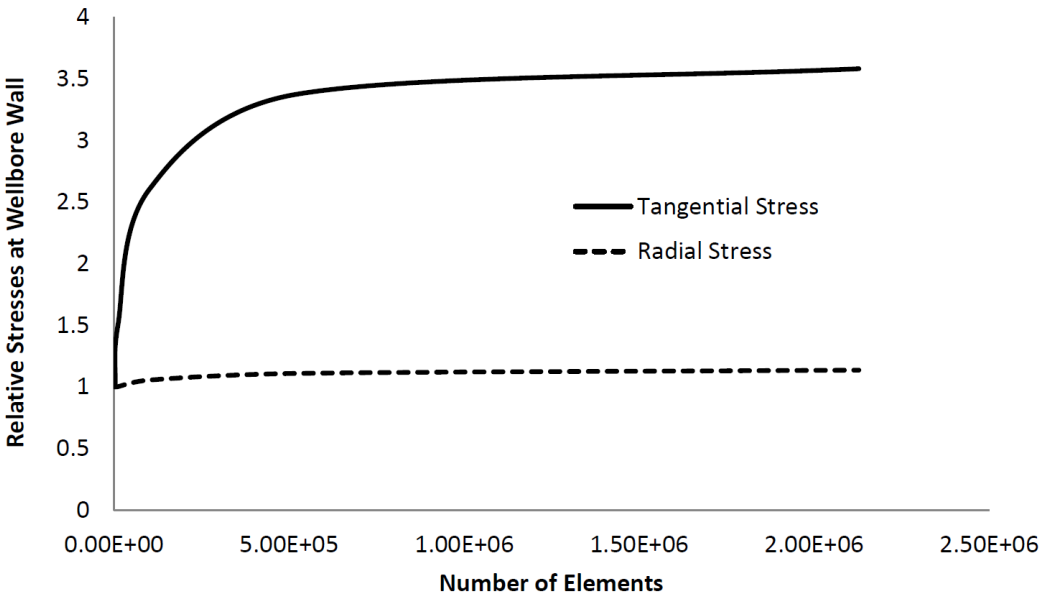

Figure 5-10 Convergence of the results in a mesh refinement analysis.

In order to validate the generated numerical model, wellbore analytical stress solutions (as presented in Chapter 2) are used. Elastic analytical solutions are widely used to calculate the stress distribution around a borehole in a plane which is subjected to lateral stresses. These analytical formulations are generally based on plane-strain concepts, in which the axial strain is assumed to be zero. For the validation of the generated 3D numerical model, therefore, a special case of zero axial strain was considered. As the axial load is applied through displacement, it is possible to generate a plane-strain model by putting axial displacement equal to zero.

A maximum horizontal stress of 7 MPa and a minimum horizontal stress of 5 MPa are applied to the lateral boundaries of the model, and a wellbore pressure of 5 MPa is loaded on the wellbore surface. The model is run and radial and tangential stress components are obtained in the direction of maximum horizontal stress. The same components of stress are also calculated using analytical solutions (Fjar et al., 2008). The results are compared in Figure 5-11. As it is seen from this figure, there is a good agreement between the numerical simulation results and analytical calculations. This shows that the numerical model is a good representation of the real laboratory samples; therefore, the model can be used in various boundary conditions to simulate the experiments.

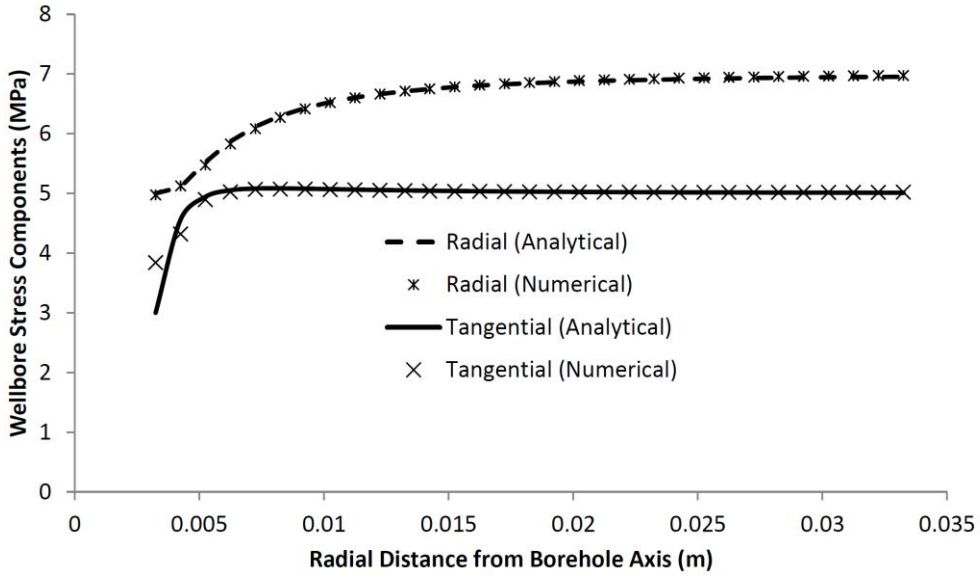

Figure 5-11 Comparison of numerical simulation results with analytical solution.

After validating the numerical model against the analytical solutions, the model was used to analyse fracture initiation. The results of the numerical modelling are presented, and they are compared with the results of experimental and analytical studies. Table 5.7 presents the experimental and numerical parameters of four different samples along with their fracturing pressures.

Table 5.7 Experimental and numerical parameters and results.

Sample No.	σ_1 (MPa)	σ_2 (MPa)	σ_3 (MPa)	σ_2 to σ_3 Stress Ratio	Perforations Orientation	Experimental Results		Numerical Results
						Initiation Pressure (MPa)	Break down Pressure (MPa)	Initiation Pressure (MPa)
1-4	20.68	13.79	6.89	2	Minimum Stress	19.30	21.16	20
1-5	20.68	13.79	6.89	2	Intermediate Stress	6.82	7.58	6.2
2-2	20.68	10.34	6.89	1.5	Minimum Stress	12.41	14.47	12.1
2-3	20.68	10.34	6.89	1.5	Intermediate Stress	6.89	7.62	7

A comparison between the experimental and numerical initiation pressures shows that the experimental results closely matches with numerical results. For example, sample 1-4 has experienced a fracture initiation pressure of 19.3 MPa at the

laboratory to break down, and the numerical model of this sample has predicted a 20 MPa initiation pressure. Similar correspondence can be seen when comparing the other three samples. This shows that the numerical model is capable of predicting the fracture initiation pressures accurately. Further discussions, results and conclusions of the numerical modelling are provided in Paper 4.

5.5.4 Effects of fracturing fluid viscosity and injection rate

In the last series of the experiments, three different fracturing fluids with viscosities ranging from 20 to 600 Pa.s were used to investigate the effects of varying fracturing fluid viscosities and fluid injection rates (0.05 to 5 mL/min) on fracturing mechanism in cased perforated wellbores. Hence, in these set of experiments, the borehole drilled in the centre of each sample was firstly cased, and then perforations were created in the cased borehole. In addition, in order to properly analyse the tests' results, a new methodology was developed for predicting the fracture propagation time from the pressure-time curves. Accordingly, the fracture initiation and break down pressures were analysed, based on the particular fluid viscosity and injection flow rate implemented for each test, and the results are discussed in Paper 5.

As it was mentioned earlier, the main goal of this study was to investigate the effects of the fracturing fluid viscosity and flow rate on the fracture initiation and near wellbore propagation geometry; therefore, a particular stress regime was considered to be applied on all samples in this study. Consequently, a maximum principal stress (σ_1) of 13.8 MPa (2000 psi), an intermediate principal stress (σ_2) of 10.3MPa (1500 psi), and a minimum principal stress (σ_3) of 6.9 MPa (1000 psi) were applied on each sample. Such stress components would represent a normal in-situ stress regime where $\sigma_1 > \sigma_2 > \sigma_3$.

In ideal circumstances it is expected that a hydraulic fracture initiate and propagate in a plane known as preferred fracture plane (PFP), which is perpendicular to the minimum principal stress direction. Therefore, all testing samples were placed in the cell in such a way that the perforations were along the direction of the intermediate principal stress, and the maximum principal stress was set along the wellbore axis. This would facilitate and ease the fracture to be developed in PFP.

The mortar samples were prepared with significant levels of caution and care to ensure that the stress distribution being applied to each face of the sample was uniform. Further to this, the internal structure of the sample (i.e. the wellbore and

perforations) were prepared with repeatability to make sure that the stress distribution applied by the high pressure fracturing fluid would be near identical in each sample. This allowed control of the majority of the variables present in the experiment, and the accurate monitoring and study of the effects of varying the fracturing fluid viscosity and fluid injection rate.

Table 5.8 presents the fracturing tests' parameters and the fracture initiation and break down pressures for each test.

Table 5.8 Fracturing tests' parameters and main results.

Test No.	Fluid Viscosity (cP)	Injection Rate (cc/min)	Initiation Pressure (MPa)	Breakdown Pressure (MPa)	Propagation Time (s)
H-1	20000	1.00	8.96	9.10	----
H-2	20000	1-2.0	12.82	14.19	320
H-3	20000	2.00	10.69	11.41	669
H-4	20000	5.00	15.24	18.68	636
SL-1	97700	1.00	18.40	19.96	340
SL-2	97700	0.10	17.44	18.19	936
SL-3	97700	0.05	7.98-14.37	8.16-14.65	499
SH-1	586800	1.00	32.75	35.65	364
SH-2	586800	0.10	28.27	32.72	460

Figure 5-12 shows a pressure-time curve corresponding to test number, SL-1. In this figure, the pre and post chock pressures, P1 and P2, (see Figure 5-4) are shown as well as the wellbore pressurization rate. In addition, the difference between P1 and P2 is calculated and displayed as a function of time. This would greatly help in predicting the moment of fracture initiation as well as predicting the fracture propagation time.

As it is seen in Figure 5-12, over the first 550 seconds of the injection time, the pressure did not increase much, because the fracturing fluid was just filling the wellbore and the perforations. After the wellbore was completely filled, the two pressures started to build up and as a result the wellbore was pressurized.

The initiation pressure could be estimated as the point where the pre and post choke pressure readings begin to deviate from each other, whereas the breakdown pressure is taken as the maximum wellbore pressure. In essence as the wellbore is being pressurized, both the pre and post choke pressures would be increasing, however when the fracture initiates, micro fractures are created and hence the rate of increase of the wellbore pressure reduces. This is due to the fact that the pressurized

fracturing fluid in the wellbore expands to fill the volume of the newly initiated flaws and consequently the wellbore pressure decreases. However, because of the presence of the chock, the pre choke transducer does not sense this reduction in pressure and increases more than that of post choke pressure, therefore the point at which the difference between the two pressures increases indicates the fracture initiation (see Figure 5-12).

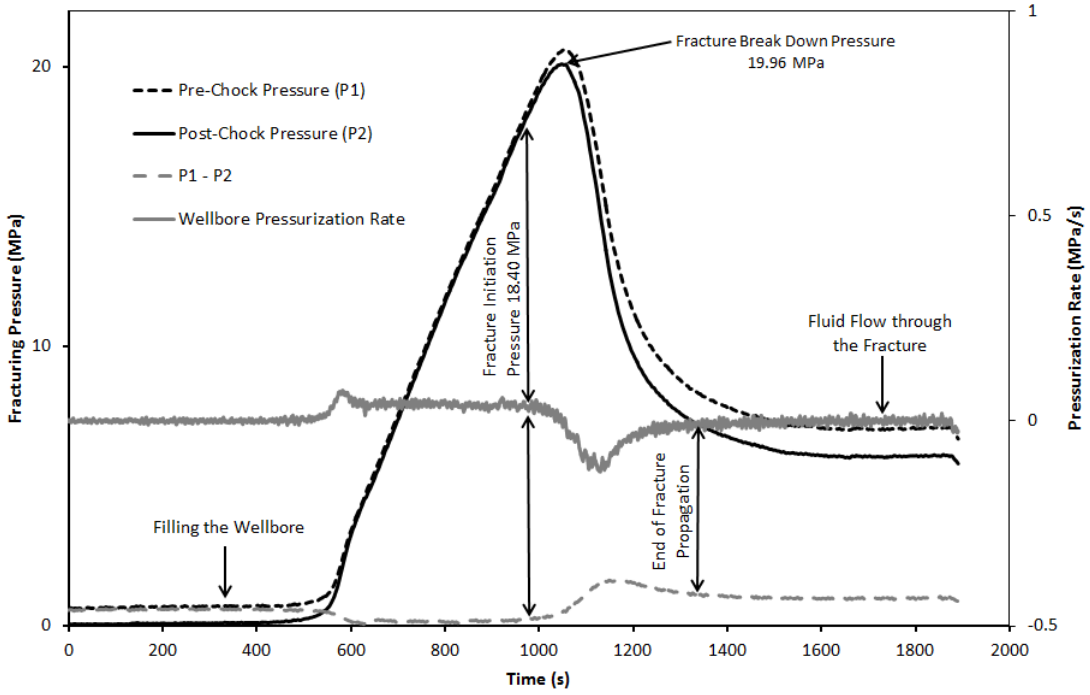

Figure 5-12 Fracturing pressures recording and wellbore pressurization rate for test number SL-1.

The other evidence to mark the fracture initiation point is the reduction in the wellbore pressurization rate. This is basically due to the fact that as a fracture initiates, the wellbore pressure reduces and consequently the pressurization rate would decrease. This reduction in the pressurization rate along with the increase in the difference between the pre and post chock pressures were implemented in all these tests to precisely specify the moment of fracture initiation.

Because every test had a specific flow rate and viscosity, the product of flow rate and viscosity ($Q \times \mu$) is considered in order to ease the tests' results comparison and simplify the analysis. Considering the unit of flow rate (m^3/s) and the unit of viscosity ($N.s/m^2$), it is realized that the unit of the product of flow rate and viscosity will be $N.m$. This means that this product is representing the energy which is supplied for hydraulic fracturing. Such fracturing energy concept is later used to better interpret the tests' results.

Analysing the fracture initiation and break down pressures presented in Table 5.8 along with their corresponding fracturing fluid viscosities and flow rates would reveal that as the product of flow rate and viscosity increases, generally higher pressures are experienced.

For instance, test number, SL-3, was performed using silicon oil as the fracturing fluid with a viscosity of 97700 cp, and the injection flow rate was 0.05 cc/min. This sample exhibited multiple fracturing and the first fracture was initiated at a pressure of 7.98 MPa and its break down pressure was 8.16 MPa. This first fracture did not propagate much and the wellbore pressure increased again and the second fracture was initiated at a wellbore pressure of 14.37 MPa and at this time the break down pressure was recorded to be 14.65 MP. Comparing this test with test SH-1, in which silicon oil viscosity was 586800 cp and the injection flow rate was 1 cc/min, it is observed that the latter test demonstrated a much larger fracturing pressures; where the initiation and break down pressures were 32.75 MPa and 35.65 MPa, respectively.

Similarly, comparing tests SH-1 and SH-2 would lead to the same result. These two tests were both conducted using silicon oil with a viscosity of 586800 cp; however, the injection flow rate in test SH-2 was one tenth of the flow rate in test SH-1. Consequently, in test SH-2, the fracture was initiated at a pressure of 28.27 MPa, while it was 32.75 MPa in test SH-1. The break down pressures also showed a difference of almost 3 MPa between the two tests. These comparisons highlight that a larger product of injection flow rate and viscosity would lead to higher fracturing pressures.

This is mainly because as a viscous fracturing fluid is injected at a higher flow rate, more energy is supplied to the wellbore. Consequently, the wellbore pressurization rate increases, this makes the fracturing process more dynamic, and as a result larger fracture initiation and break down pressures would be required to create a fracture. Physically, when a rock or concrete sample is loaded dynamically, it would exhibit larger strength parameters (Fjar et al., 2008); the same concept appears to be valid for a hydraulic fracturing test.

A description of fracture geometries for every sample is presented in Paper 5. Analysis of these fracture geometries along with the experimental parameters, shown in table Table 5.8, demonstrate how the injection flow rate and fluid viscosity may influence the near wellbore fracture geometry. Generally, because every sample had

two perforations parallel to the direction of intermediate principal stress (maximum horizontal stress), it was expected that a two-wing fracture plane would be initiated from the top and bottom side of each perforation, and propagated vertically, perpendicular to the direction of minimum principal stress. However, most of these fractures were initiated in an angle with respect to the vertical plane (herein preferred fracture plane). These fractures propagated in a curved path away from the wellbore, and eventually the tip of the fractures grew towards the vertical plane.

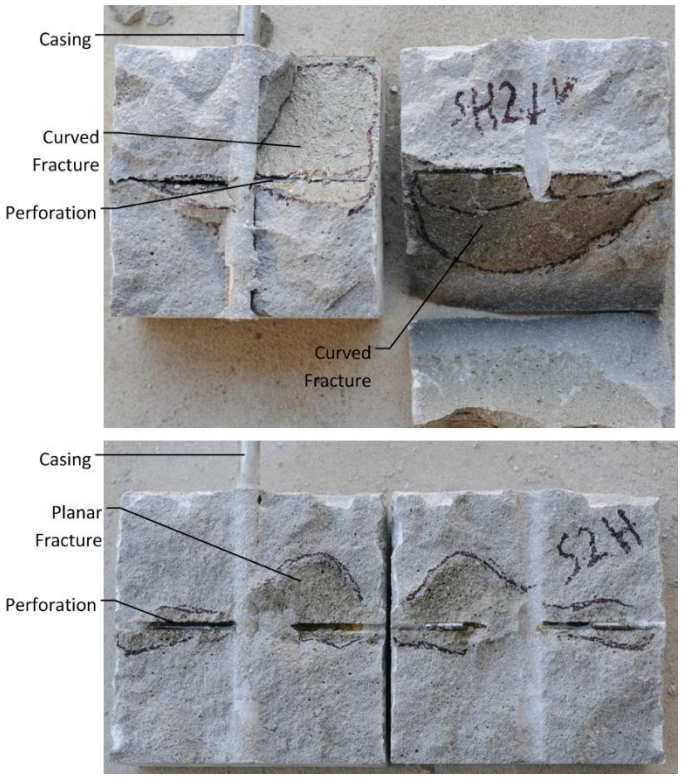

Figure 5-13 Test H-3 (top) and H-2 (Bottom) fracture geometries.

Figure 5-13 shows the fracture geometries of the samples fractured in tests number H-2 and H-3. As it is seen in this figure, in test H-2 almost a vertical fracture (along PFP) was developed; however, test H-3 resulted in a curved fracture plane, where the fracture was initiated from the perforations in an angle with respect to PFP, but each wing of fracture propagated in a curved path towards the PFP. Tests H-4, SL-1, SL-3, and SH-1 also experienced curved fracture planes; however, the angles (with respect to PFP) at which the fractures were initiated from the perforations, as well as the curvature of the fracture planes were not the same in all these tests. For instance, as it is shown in Figure 5-14 for test H-4, two-wing fractures were initiated from each perforation. However, the bottom fracture was initiated at a larger initiation angle than the top fracture. Moreover, the bottom

fracture propagated almost in the horizontal plane, which is perpendicular to the vertical stress, while the top wing grew in a curved path and tends to align with the PFP.

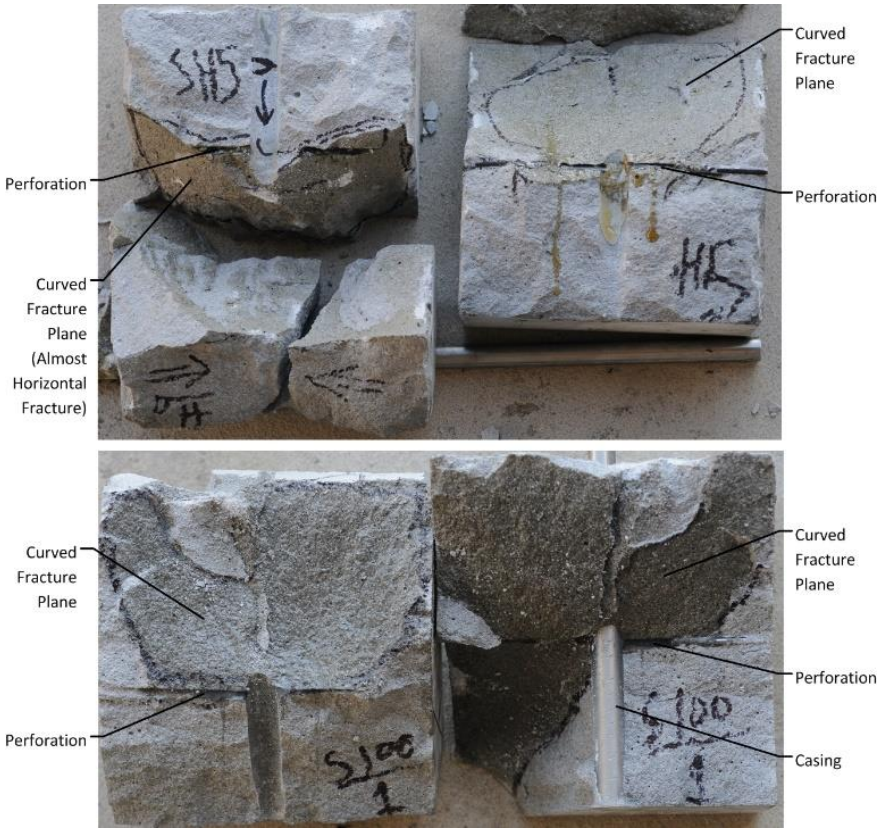

Figure 5-14 Fracture geometries of tests H-4 (top) and SL-1 (Bottom).

Test SL-1 also resulted in two-wing fractures; however, the fracture initiation angle for this test is less than that of test H-4. Additionally, the curvature of top and bottom fractures in test SL-1 is relatively less compared to the curvature of propagated fractures in test H-4.

In order to recognize the relationship between direction of fracture initiation (i.e intiatione angle) and propagation geometry with the injection flow rate and viscosity, it is helpful to recall the product of these two parameters ($Q \times \mu$). The product of injection flow rate and viscosity is calculated for each test and presented in Table 5.9. As it is mentioned earlier, although by increasing the product value, higher initiation and break down pressures were recorded, it appears that some of the tests have the same product values, while their fractures' geometries are different. For instance, tests H-4 and SL-1 have almost the same product value (see Table 5.9); however, their fracture geometries are not the same.

Table 5.9 Fracturing tests' energy, pressurization time, power, and fracture geometry characteristics.

Test No.	Injection Rate (m^3/s)×10^{-8}	Fluid Viscosity (Pa.s)	Q × μ (Fracturing Energy) (N.m) ×10^{-10}	Pressurization Time (s)	Fracturing Power (N.m/s) ×10^{-10}	Fracture Initiation Angle (°)	Fracture Propagation geometry
H-2	1.67	20.0	3763	3100	1.2	5	Planar
H-3	3.33	20.0	6667	900	7.4	35	Curved
H-4	8.33	20.0	16667	70	238.1	80	Curved
SL-1	1.67	97.7	16283	500	32.6	65	Curved
SL-2	0.17	97.7	1628	3200	0.5	3	Planar
SL-3	0.08	97.7	814	14000	0.06	0 - 70	Curved
SH-1	1.67	586.8	97800	700	139.7	75	Curved
SH-2	0.17	586.8	9780	4400	2.2	25	Almost Planar

To clarify this controversy, it is worthwhile to remember that the product of injection flow rate and viscosity represents the amount of energy applied to pressurize the wellbores and create the fractures. However, because every test had a particular injection rate and fluid viscosity, the wellbore pressurization time was not the same for all tests. For example, sample H-4 was pressurized with a flow rate of 5 cc/min using honey with a viscosity of 20 Pa.s, while sample SL-1 was tested using silicon oil with a viscosity of 97.7 Pa.s and a flow rate of 1 cc/min. Hence, sample H-4 was pressurized much faster than sample SL-1, as much less viscous fluid was injected into its wellbore at a higher flow rate. This is while both samples had almost the same level of fracturing energy (Q × μ), but sample H-4 had received this energy at a faster rate. Therefore, it would be significantly helpful to divide the fracturing energy by the time interval at which this energy was supplied to each sample. Energy divided by time would introduce a new parameter which is considered to be the fracturing power as given below:

$$P_{fracturing} = \frac{Q \times \mu}{t} \tag{5.6}$$

The time interval t is considered to be the wellbore pressurization time in each test. This time interval starts with the moment when the wellbore begins to pressurize and ends when the fracture breaks down.

Table 5.9 summarizes the fracturing energy, pressurization time, and fracturing power as well as the characteristics of fracture geometry for each test, excluding test H-1 in which no fracture was developed in the sample. Each fracture geometry is characterized by an initiation angle, which is the angle at which the fracture was initiated from the perforation with respect to the PFP. Additionally, the fracture propagation plane is also generally characterized as either planar or curved.

Comparing the fracturing powers of tests H-4 and SL-1 indicates why the fracture geometry in test H-4 had a larger initiation angle and a more curved fracture plane (see Figure 5-14), although they have almost equal fracturing energy of about 16×10^{-7} N.m. The same result is concluded when comparing the fracturing power and geometries in the other tests. For example, test SH-1experienced a fracturing power of almost 140×10^{-10} N.m/s, and as a result a curved fracture with an initiation angle of 75 degrees was created in this test.

In contrary, tests H-2, SL-2 and SH-2 had very low fracturing powers, and subsequently an almost planar fracture was initiated from their perforations and propagated in the vertical direction, along PFP. Thus, generally, it is concluded that the fracturing energy could not be directly related to the fracture initiation and propagation geometry. Nevertheless, the fracturing power could be associated with the fracture geometry very well.

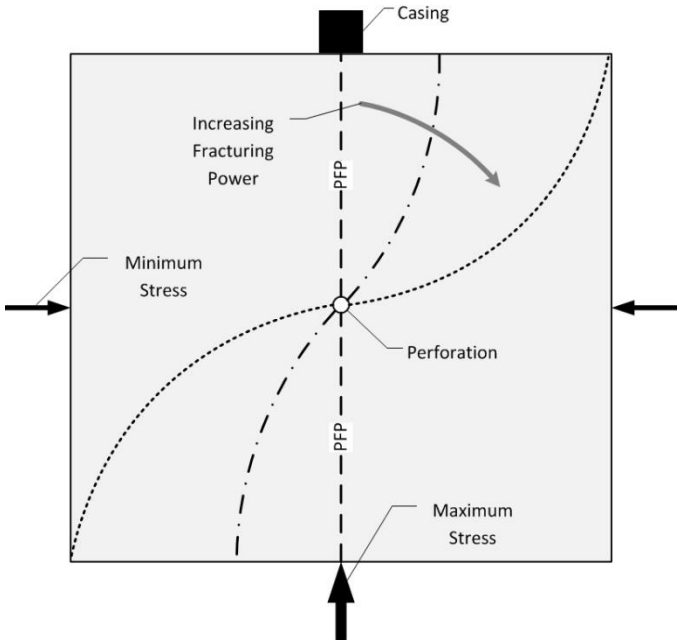

Figure 5-15 A schematic of the fracture initiation angle and propagation geometry in response to variation in the fracturing power.

Basically, as it is demonstrated in Figure 5-15, by increasing the fracturing power supplied to the sample, the wellbore pressurization rate increases, and consequently the fracture initiation angle increases. This means that at higher fracturing power, fractures could be initiated from the perforations in a direction which is perpendicular to higher stress components (herein vertical stress), and accordingly the fracture propagation would have a longer curved path so that it could get aligned with the PFP (the plane to which the minimum stress is perpendicular). In other words, eexcessive energy may forcefully initiate a fracture in the direction of non-PFP; however, as it propagates, it would tend to align to the direction of PFP, where it would require to spend less energy.

Further discussions, results and conclusions of this series of experimental tests could be found in Paper 5.

5.6 Summary

Dimensional analysis makes the experimental results more reliable as it takes into account the relative dimensional aspects of a laboratory fracturing experiment with respect to the physical phenomenon occurring in field fracturing operations. Therefore, in this study, the laboratory test parameters were scaled to enhance simulating the fracturing mechanism at field scale. Hydraulic fracturing tests were

conducted on 100 and 150 mm synthetically manufactured mortar as well as tight sandstone samples. Synthetic cubic tight mortar samples with particular properties were made for the purpose of performing scaled experiments. The use of cube samples allows application of three independent stresses to mimic real far field stress conditions. Accordingly, a true tri-axial stress cell (TTSC) was used for this purpose.

Several series of fracturing experiments were carried out in this study. In the first series of experiments, two parallel notches were created in the borehole of each sample to simulate the perforations; this was performed as a preliminary study. In the second series of experiments, various scenarios of vertical and horizontal wells and in situ stress regimes were modelled in perforated borehole. In addition, some of the tests performed in the second set were conducted for the purpose of validating the analytical model (see 2.5.2).

Furthermore, the initiation of hydraulic fracturing from a perforated tunnel was studied numerically using a finite element method. The numerical model was generated to represent a laboratory experimental test, which has been carried out on tight concrete cubic samples. And, in the last series of the experiments, three different fracturing fluids were used to investigate the effects of varying fracturing fluid viscosities and fluid injection rates on fracturing mechanism in cased perforated wellbores.

In order to analyse the fracturing pressure-time curves a new methodology was introduced in this study to predict the fracture propagation time directly from the pressure-time curves. This has helped to indicate the time at which the fracture tip reached the boundary of the sample, and accordingly the rest of the pressure data after this time would be considered as representing the flow of the fracturing fluid through the propagated fracture. Therefore, this methodology improved the results' interpretations.

Detailed procedures and results of these set of experiments as well as the numerical modelling are discussed in the attached papers (i.e. Papers 2, 3, 4, and 5). However, the main conclusions are briefly summarized here.

It was observed that the stress anisotropy generated from the stress components in the directions perpendicular to the perforation axis influenced the FIP, i.e., the stress magnitude along the perforation tunnel was neutralized; the larger this stress anisotropy ratio, the greater the initiation pressure. In addition, it was found that the effect of the direction of a wellbore on fracturing mechanism in a perforated wellbore

should be analysed simultaneously with the prevailing stress regime, since these two parameters collaboratively affect the fracture initiation. Furthermore, it was found that the direction of the perforation can affect the angle between the initiated fracture and the perforation axis.

The experimental results for a perforated wellbore with no cement sheath indicated that the existence and orientation of the perforation tunnel play a noticeable role in FIP. For example, the results showed that a perforated wellbore, in which the perforations are aligned with the direction of minimum stress, though the cement sheath is failed, will experience larger fracturing pressures in comparison to an open bore hole.

Experimental results also demonstrated that as the product of viscosity and injection flow rate increases, higher fracture initiation and break down pressures would be recorded. This product value has the same dimension as energy; therefore, it is considered to represent an energy term, named as fracturing energy. Hence, as the fracturing energy increases the fracturing pressures would increase accordingly.

Nevertheless, it was observed that the fracture initiation angle and near wellbore propagation geometry may not be directly related to fracturing energy. Therefore, a new parameter was introduced by dividing the fracturing energy by the wellbore pressurization time, named as fracturing power. It was observed that as the fracturing power rises, the fracture initiation angle increases and a more curved fracture plane would be propagated.

It was also observed that casing has a significant effect on the wellbore and perforation stress distribution. As a result, larger fracture initiation and break down pressures would be expected in a cased perforated completion, in comparison to a perforated open hole wellbore. Additionally, casing would cause a vertical fracture to deviate from the wellbore and propagate in a curved path toward the PFP.

Moreover, the strength properties of the cement sheath play an important role in the hydraulic fracturing mechanism in a cased perforated wellbore. Low shear strength cement sheath may result in creation of micro-annulus. Accordingly, the hydraulic fracture would propagate in the annulus between the casing and the wellbore wall, and as a result the wellbore pressure would decrease and consequently there would be no or little chance of the creation of hydraulic fracture in the formation.

6 Conclusions and recommendations

Regarding the results obtained throughout this study; in this chapter the main conclusions are presented. Since both analytical and experimental investigations were conducted in this study, the conclusions are summarized in two sections. Some recommendations are also made for further researches to better understand the mechanism of fracture initiation in perforated wellbore, and to simulate the near wellbore fracture propagation and geometry.

6.1 Analytical modelling

As it was reviewed in Chapter 1, a few researchers have tried to analytically analyse the perforation stress concentration. However, they have developed some equations, merely analysing the perforation tangential stress that could only predict a fracture, which initiates right at the wellbore and perforation edge, and is opening perpendicular to the perforation tangential stress. Nevertheless, since a fracture may initiate anywhere along the perforation tunnel and at any direction, there is significant limitations using the previous models. Therefore, in this study, a new analytical model was developed to calculate the stress distribution for arbitrarily oriented perforated wellbore, evaluating perforation's tangential, radial and axial stresses all along the perforation tunnel; which is used to accurately study the mechanism of fracture initiation.

A new methodology is introduced to calculate the stress distribution on the surface of a perforation, while the effect of the wellbore stress concentration is superimposed on the perforation stress modelling. Since it is not possible to analytically derive solutions to predict the FIP and the angle of the initial fracture for every wellbore and perforation orientation; therefore, a numerical method is applied to resolve the problem and calculate the desired parameters. In addition, for validation of the analytical model, the results of scaled fracturing experiments were compared with the results obtained from the analytical model. The comparison demonstrated good agreement between the results, and confirmed the accuracy of the

developed analytical model. Based on this model, the following conclusions are drawn:

- The location of the tensile zone on the circumference of a wellbore depends on the wellbore orientation as well as the prevailing in-situ stress regime.
- In cased holes, the relative direction of the perforation orientation and the wellbore tensile zone, is a main factor influencing both the FIP and near wellbore fracture propagation.
- In contradiction to what is supposed in literature, this study demonstrated that, it is not a general rule to have lower FIP when the perforations are aligned with the tensile zone of the well. Meaning that, in some specific well and stress conditions, by locating the perforation away from the tensile zone, lower FIP would be required.
- FIP considerably depends on the well orientation, and also the state of the in situ stresses. Besides, the impact of each of these parameters is not independent from the others.
- When the regional stress regime is normal, the fracture initiation pressure increases as the well gets more inclined. However generally, the situation is vice versa in a reverse stress regime area, where FIP mostly reduces with well inclination increase.
- The impact of well azimuth on FIP is also significant, when the prevailing stress regime is strike slip, though it does not greatly affect the fracturing pressure for wells which are drilled in other stress regime areas.
- Stress anisotropy is the next important factor, influencing the fracture initiation pressure. Generally more anisotropic stress state will lead to lower fracture initiation pressure. This effect does not depend on the prevailing stress regime and on the well direction.
- The effects of cement tensile strength, Biot's constant and Poisson's ratio are included in the developed model, so that the possibility of micro-annulus creation can be specifically inspected. An increase in the formation Biot's constant will result in less pressure required for fracture initiation. Also, any increase in pore pressure implies similar effect.

- The fracture initiation angle (β) is obtained using the perforation stress model, which gives an estimation of near wellbore fracture tortuosity while comparing with PFP, wellbore and perforation orientations.
- Poro-elastic and thermo-elastic analytical solutions are developed to model the wellbore and perforation stress distributions more accurately. As a result the effects of formation pore pressure and temperature variations are included in the analytical fracture initiation model for perforated wellbores.
- By increasing the temperature difference between the fracturing fluid and formation rock, the FIP reduces. This is due to the fact that, a cooler fracturing fluid will decrease the local stresses around the perforation and that will accordingly reduce the FIP. Therefore, it is concluded that by applying a cooler pad fluid, the process of hydraulic fracturing would be easier.
- Independent of the thermo-poro-elastic concept, when the azimuth of the well gets farther away the maximum horizontal stress, more fracturing pressure is needed.
- As the Poisson' ratio increases the thermal effect can reduce the stresses more significantly, and this will lead to lower FIP.
- The effect of temperature difference is more noticeable when the rock has higher modulus of elasticity, and linear thermal expansion.
- Comparing the elastic and poro-elastic perforation stress distribution results, and their effects on the FIP, a noticeable decrease is observed in the amount of FIP; in all three stress regimes, the FIP is less for the case of poro-elastic modelling.
- As the pore pressure gradient increases, the pressure, which is required for initiating the fracture, reduces.
- When the modelling does not apply the thermal and poro-elastic influences, a high value for the FIP would be obtained. However, when the thermal effect is added to the elastic modelling, the FIP will reduce. This must be a better simulation of the actual fracture initiation. In addition, when an uncoupled thermo-poro-elastic methodology is applied, the lowest value of FIP is calculated. Generally both of these variations in formation properties (temperature reduction and pore pressure increase), help the process of hydraulic fracturing.

- When the ratio between the formation elastic modulus and casing elastic modulus reduces, generally the FIP increases. This is because by increasing the casing elastic modulus, some part of the wellbore pressure would not be transferred to the formation. So, higher wellbore (fracturing) pressure is needed to fracture the rock. In addition, as the casing elastic modulus increases, the initial fracture will be initiated further away the wellbore wall through the perforation hole.
- The main reason of the unsuccessful hydraulic fracturing, which has been experienced in well A of Ahwaz oilfield, is related to fracture initiation and some near wellbore parameters. Actually, not taking into account the effects of perforation stress profile resulted in an incorrect (underestimated) prediction of FIP.
- Based on the reverse stress regime that exists in Ahwaz oilfield, horizontal PFP is expected to be created deep into the formation. Therefore high tortuous near wellbore fracture geometry will be formed if a company hydraulically fractures a vertical or low inclined well in this area.

6.2 Experimental study

Based on this experimental study, the following conclusions are drawn:

- The stress anisotropy generated from the stress components in the directions perpendicular to the perforation axis will influence the FIP, i.e., the stress magnitude along the perforation tunnel is neutralized. The larger this anisotropy ratio the greater the initiation pressure will be.
- The effect of the direction of a wellbore on fracturing mechanism in a perforated wellbore should be analysed simultaneously with the prevailing stress regime, since these two parameters collaboratively affect the fracture initiation.
- It was observed that a vertical wellbore in a normally stressed formation with perforations along the direction of minimum horizontal stress required larger initiation pressures (both FIP and BDP) compared to when a perforation was oriented in the direction of minimum horizontal stress in a horizontally drilled wellbore in a reverse fault regime area. It is

important to note that in both cases the perforations were in the same direction.

- When the perforations were oriented in a direction such that the intermediate and maximum stresses were perpendicular to the axis of perforations, larger fracture initiation and breakdown pressures were required compared to any other orientations chosen for the perforations. This in turn resulted in a higher chance for development of multiple fracturing planes around the perforation tunnel. Also, it was found that the lower the difference between FIP and BDP, the lesser the chance for having multiple fracturing.
- Additionally, it was observed that the direction of the perforation can affect the angle between the initiated fracture and the perforation axis.
- The experimental results for a perforated wellbore with no cement sheath indicated that the existence and orientation of the perforation tunnel play a noticeable role in FIP. For example, the results showed that a perforated wellbore, in which the perforations are aligned with the direction of minimum stress, though the cement sheath is failed, will experience larger fracturing pressures in comparison to an open bore hole.
- A numerical model for analysing the mechanisms of fracture initiation and near wellbore fracture geometry was developed. This model was established in a way to simulate the FIP in perforation tunnels of a borehole that is drilled in tight formations. The results of the numerical modelling were compared with some experimental fracturing tests and good agreement was observed.
- In order to analyse the fracturing pressure-time curves a new methodology was introduced in this study to predict the fracture propagation time directly from the pressure-time curves. This has helped to indicate the time at which the fracture tip reached the boundary of the sample, and accordingly the rest of the pressure data after this time would be considered as representing the flow of the fracturing fluid through the propagated fracture. Therefore, this methodology improved the results' interpretations.

- Experimental results demonstrated that as the product of viscosity and injection flow rate increases, higher fracture initiation and break down pressures would be recorded. This product value has the same dimension as energy; therefore, it is considered to represent an energy term, named as fracturing energy. Hence, as the fracturing energy increases the fracturing pressures would increase accordingly.
- Nevertheless, it was observed that the fracture initiation angle and near wellbore propagation geometry may not be directly related to fracturing energy. Therefore, a new parameter was introduced by dividing the fracturing energy by the wellbore pressurization time, named as fracturing power. It was observed that as the fracturing power rises, the fracture initiation angle increases and a more curved fracture plane would be propagated.
- It was also observed that casing has a significant effect on the wellbore and perforation stress distribution. As a result, larger fracture initiation and break down pressures would be expected in a cased perforated completion, in comparison to a perforated open hole wellbore. Additionally, casing would cause a vertical fracture to deviate from the wellbore and propagate in a curved path toward the PFP.
- Moreover, the strength properties of the cement sheath play an important role in the hydraulic fracturing mechanism in a cased perforated wellbore. Low shear strength cement sheath may result in creation of micro-annulus. Accordingly, the hydraulic fracture would propagate in the annulus between the casing and the wellbore wall, and as a result the wellbore pressure would decrease and consequently there would be no or little chance of the creation of hydraulic fracture in the formation.

6.3 Recommendations for future studies

- The results of this study were according to the assumption of linear elasticity, in which the elastic moduli of the rocks are considered independent of the stress state. However, normally elastic moduli of rocks are, to some extent, stress dependent. In addition, there is always high stress concentration around the wellbore and perforations. Thus, it is reasonable to assume that the elastic

moduli close to the wellbore and perforation will differ from those of the virgin formation, due to the stress alteration in the vicinity of the borehole and perforations. Therefore, it is worth to modify the presented model by assuming stress dependent elastic moduli.

- During the life of a well, it may be under several loading conditions. Alternative pressurization by drilling, completion and various work over operations are together with unloading periods of production. These loading variations impose a so called stress history on the formation. Therefore the formation mechanical properties change due to this stress history, and consequently it behaves more plastically. So it is important to model the rock as an elasto-plastic material rather than a pure elastic substance, and use this model for studying the fracturing process.
- The next influencing item is the steel casing, which has different elastic moduli from its surrounding cement and rock. So it can affect the wellbore and consequently the perforation stress distribution. In this study only radial casing displacement was considered. Taking into consideration the effects of various displacement components of the casing can make the results of this study more accurate.
- The mechanism of formation break down from a cased perforated hole is modelled in this study. After the fracture initiates from a perforation, it will develop and link to other small fractures to make a bigger fracture and to propagate in the direction of PFP. So the next step is to improve the presented model, so that it can simulate the propagation of the fracture and the proppant passage in the near wellbore tortuous path.
- Knowledge of the mechanical properties and the in situ stresses of the subsurface formations are essential in connection with wellbore stability problems, fracturing operations, subsidence problems and sand production evaluation. Unfortunately these data are not commonly available is Ahwaz oilfield. Therefore it is strongly suggested to perform some experimental measurements on core samples to obtain rock mechanical properties, so that logging results can be validated with experimental results. In addition, it is critically important to execute some field tests like, leak off, mini frac and

micro frac tests to obtain reliable magnitudes of horizontal stresses in this huge oil filed.

- Based on world stress map, the state of the stresses in Ahwaz oilfield is a reverse fault regime, therefore the PFP is a horizontal plane in this area. As a result, it would be improving to hydraulically fracture the horizontal wells or the wells with high inclination angles. In this way, the created fracture would be more or less, along the axis of the well, resulting in less tortuous near wellbore fracture plane, and consequently improving the well/reservoir connection.
- In this study the effects of the temperature variations and pore pressure variations have been included in the modelling for wellbore and perforation stress distributions. It is recommended to build a model for coupling these two important parameters, so that the effect of each one on the other one can be calculated and applied.
- In this study only vertical and horizontal perforated wellbores were experimentally studied. It is worth to perform experiments on samples deviated perforated wellbores and study the effect of the inclination and azimuth angles experimentally. In addition, it would be great to study various perforation arrangements.
- It is also recommended to carry out some experimental fracturing tests on cased perforated samples, while different casing's elastic moduli are applied. Furthermore, various cement sheath properties could be studied through laboratory tests.

References

Aadnoy, B. S. (1989). Stresses around horizontal boreholes drilled in sedimentary rocks. *Journal of Petroleum Science and Engineering, 2*(4), 349-360.

Abass, H., Brumley, J., & Venditto, J. (1994). *Oriented perforations-a rock mechanics view.* Paper presented at the SPE Annual Technical Conference and Exhibition.

Adachi, J., Siebrits, E., Peirce, A., & Desroches, J. (2007). Computer simulation of hydraulic fractures. *International Journal of Rock Mechanics and Mining Sciences, 44*(5), 739-757.

Alekseenko, O., Potapenko, D., Cherny, S., Esipov, D., Kuranakov, D., & Lapin, V. (2012). 3D Modeling of Fracture Initiation From Perforated Noncemented Wellbore. *SPE Journal, 18*(03), 589-600.

Atkinson, C., & Eftaxiopoulos, D. (2002). Numerical and analytical solutions for the problem of hydraulic fracturing from a cased and cemented wellbore. *International journal of solids and structures, 39*(6), 1621-1650.

Aud, W., Wright, T., Cipolla, C., & Harkrider, J. (1994). *The effect of viscosity on near-wellbore tortuosity and premature screenouts.* Paper presented at the SPE Annual Technical Conference and Exhibition.

Behrmann, L., & Elbel, J. (1991). Effect of perforations on fracture initiation. *Journal of Petroleum Technology, 43*(5), 608-615.

Behrmann, L., & Nolte, K. (1999). Perforating requirements for fracture stimulations. *SPE Drilling & Completion, 14*(4), 228-234.

Berumen, S., Tiab, D., & Rodriguez, F. (2000). Constant rate solutions for a fractured well with an asymmetric fracture. *Journal of Petroleum Science and Engineering, 25*(1), 49-58.

Bradley, W. (1979). Mathematical concept-Stress Cloud-can predict borehole failure. *Oil Gas J.;(United States), 77*(8).

Britt, L. K., Smith, M. B., Haddad, Z. A., Lawrence, J. P., Chipperfield, S. T., & Hellman, T. J. (2006). *Waterfracs: We do need proppant after all.* Paper presented at the SPE Annual Technical Conference and Exhibition.

Bunger, A. P. (2005). *Near-surface hydraulic fracture.* University of Minnesota, 2005. Major: Geological engineering.

Castagna, J. P., Batzle, M. L., & Eastwood, R. L. (1985). Relationships between compressional-wave and shear-wave velocities in clastic silicate rocks. *Geophysics, 50*(4), 571-581.

Chang, C., Zoback, M. D., & Khaksar, A. (2006). Empirical relations between rock strength and physical properties in sedimentary rocks. *Journal of Petroleum Science and Engineering, 51*(3), 223-237.

Chen, Z., & Economides, M. (1995). *Fracturing pressures and near-well fracture geometry of arbitrarily oriented and horizontal wells.* Paper presented at the SPE Annual Technical Conference and Exhibition.

Cherny, S. G., Lapin, V. N., Chirkov, D. V., Alekseenko, O., & Medvedev, O. O. (2009). *2D Modeling of Hydraulic Fracture Initiating at a Wellbore with or without Microannulus.* Paper presented at the SPE Hydraulic Fracturing Technology Conference.

Cipolla, C. L., Warpinski, N. R., Mayerhofer, M. J., Lolon, E., & Vincent, M. C. (2008). *The relationship between fracture complexity, reservoir properties, and fracture treatment design.* Paper presented at the SPE Annual Technical Conference and Exhibition.

Cleary, M., Johnson, D., Kogsb? ll, H., Owens, K., Perry, K., Pater, C., . . . Mauro, T. (1993). *Field implementation of proppant slugs to avoid premature screen-out of hydraulic fractures with adequate proppant concentration.* Paper presented at the Low Permeability Reservoirs Symposium.

Crook, A. J., Yu, J.-G., & Willson, S. M. (2002). *Development of an orthotropic 3D elastoplastic material model for shale.* Paper presented at the SPE/ISRM Rock Mechanics Conference.

Crump, J., & Conway, M. (1988). Effects of perforation-entry friction on bottomhole treating analysis. *Journal of Petroleum Technology, 40*(08), 1,041-041,048.

Daneshy, A. (1973). Experimental investigation of hydraulic fracturing through perforations. *Journal of Petroleum Technology, 25*(10), 1201-1206.

Daneshy, A. (2004). *Analysis of off-balance fracture extension and fall-off pressures.* Paper presented at the SPE International Symposium and Exhibition on Formation Damage Control.

Daneshy, A. A. (2011). *Hydraulic fracturing of horizontal wells: Issues and insights.* Paper presented at the SPE Hydraulic Fracturing Technology Conference.

Davidson, B., Saunders, B., Robinson, B., & Holditch, S. (1993). *Analysis of abnormally high fracture treating pressures caused by complex fracture growth.* Paper presented at the SPE Gas Technology Symposium.

De Pater, C., Weijers, L., Cleary, M., Quinn, T., Barr, D., & Johnson, D. (1994). Experimental verification of dimensional analysis for hydraulic fracturing. *SPE Production and Facilities (Society of Petroleum Engineers);(United States), 9*(4).

Detournay, E. (2004). Propagation regimes of fluid-driven fractures in impermeable rocks. *International Journal of Geomechanics, 4*(1), 35-45.

Economides, M. J. (2000). *Reservoir stimulation* (Vol. 18).

Economides, M. J., Watters, L. T., & Dunn-Norman, S. (1998). *Petroleum well construction*: John Wiley Sons.

El Rabaa, W. (1989). *Experimental study of hydraulic fracture geometry initiated from horizontal wells.* Paper presented at the SPE Annual Technical Conference and Exhibition.

Fallahzadeh, S., James Cornwell, A., Rasouli, V., & Hossain, M. (2015). *The Impacts of Fracturing Fluid Viscosity and Injection Rate on the Near Wellbore Hydraulic Fracture Propagation in Cased Perforated Wellbores.* Paper presented at the 49th US Rock Mechanics/Geomechanics Symposium.

Fallahzadeh, S., & Rasouli, V. (2012). *The impact of cement sheath mechanical properties on near wellbore hydraulic fracture initiation.* Paper presented at the ISRM International Symposium-EUROCK 2012.

Fallahzadeh, S. H., Rasouli, V., & Sarmadivaleh, M. (2013). *Experimental Investigation of Hydraulic Fracturing in Vertical and Horizontal Perforated Boreholes.* Paper presented at the 47th US Rock Mechanics/Geomechanics Symposium.

Fisher, M., Heinze, J., Harris, C., Davidson, B., Wright, C., & Dunn, K. (2004). *Optimizing horizontal completion techniques in the Barnett shale using microseismic fracture mapping.* Paper presented at the SPE Annual Technical Conference and Exhibition.

Fjar, E., Holt, R. M., Raaen, A., Risnes, R., & Horsrud, P. (2008). *Petroleum related rock mechanics* (Vol. 53): Elsevier.

Freund, L. B. (1998). *Dynamic fracture mechanics*: Cambridge university press.

Gardner, G., Gardner, L., & Gregory, A. (1974). Formation velocity and density-the diagnostic basics for stratigraphic traps. *Geophysics, 39*(6), 770-780.

Gidley, J. L. (1989). Recent advances in hydraulic fracturing.

Guangqing, Z., & Mian, C. (2009). Complex fracture shapes in hydraulic fracturing with orientated perforations. *Petroleum Exploration and Development, 36*(1), 103-107.

Gulrajani, S. N., & Romero, J. (1996). *Evaluation and modification of fracture treatments showing near-wellbore effects.* Paper presented at the European Petroleum Conference.

Haimson, B., & Fairhurst, C. (1967). Initiation and extension of hydraulic fractures in rocks. *Society of Petroleum Engineers Journal, 7*(03), 310-318.

Haimson, B., & Fairhurst, C. (1969). Hydraulic fracturing in porous-permeable materials. *Journal of Petroleum Technology, 21*(07), 811-817.

Hainey, B., Keck, R., Smith, M., Lynch, K., & Barth, J. (1999). On-site fracturing disposal of oilfield-waste solids in Wilmington Field, California. *SPE production & facilities, 14*(02), 83-87.

Hallam, S., & Last, N. (1991). Geometry of hydraulic fractures from modestly deviated wellbores. *Journal of Petroleum Technology, 43*(06), 742-748.

Hayashi, K., & Haimson, B. C. (1991). Characteristics of shut-in curves in hydraulic fracturing stress measurements and determination of in situ minimum compressive stress. *Journal of Geophysical Research: Solid Earth (1978–2012), 96*(B11), 18311-18321.

Hossain, M., Rahman, M., & Rahman, S. (2000). Hydraulic fracture initiation and propagation: roles of wellbore trajectory, perforation and stress regimes. *Journal of Petroleum Science and Engineering, 27*(3), 129-149.

Howard, G. C., & Fast, C. R. (1970). Hydraulic fracturing. *NEW YORK, SOCIETY OF PETROLEUM ENGINEERS OF AIME, 1970. 210 P.*

http://www.globalsecurity.org. 2014

Jaeger, J. C., Cook, N. G., & Zimmerman, R. (2009). *Fundamentals of rock mechanics*: John Wiley & Sons.

King, G. (1989). Perforating the horizontal well. *Journal of Petroleum Technology, 41*(07), 671-672.

Kirsch, G. (1898). *Die theorie der elastizität und die bedürfnisse der festigkeitslehre*: Springer.

Lehman, L., & Brumley, J. (1997). *Etiology of multiple fractures.* Paper presented at the SPE Production Operations Symposium.

Lhomme, T. P. Y. (2005). *Initiation of hydraulic fractures in natural sandstones.* (PhD), Delft University of Technology.

Li, Y. (1991). *On initiation and propagation of fractures from deviated wellbores*.

Mack, M. G., & Warpinski, N. (2000). Mechanics of hydraulic fracturing *Reservoir Stimulation* (pp. 6-1).

McDaniel, B., McMechan, D., & Stegent, N. (2001). *Proper use of proppant slugs and viscous gel slugs can improve proppant placement during hydraulic fracturing applications.* Paper presented at the SPE Annual Technical Conference and Exhibition.

Medlin, W., & Masse, L. (1979). Laboratory investigation of fracture initiation pressure and orientation. *Society of Petroleum Engineers Journal, 19*(02), 129-144.

Min, S., Sastry, S., & Balasubramaniam, V. (2010). Compressibility and density of select liquid and solid foods under pressures up to 700MPa. *Journal of food engineering, 96*(4), 568-574.

Mindess, S., Young, J. F., & Darwin, D. (2003). *Concrete*.

Mitchell, R., Goodman, M., & Wood, E. (1987). *Borehole stresses: plasticity and the drilled hole effect.* Paper presented at the SPE/IADC Drilling Conference.

Murdoch, L. C., & Slack, W. W. (2002). Forms of hydraulic fractures in shallow fine-grained formations. *Journal of Geotechnical and Geoenvironmental Engineering, 128*(6), 479-487.

Murphy, H. D., & Fehler, M. (1986). *Hydraulic fracturing of jointed formations.* Paper presented at the International Meeting on Petroleum Engineering.

Narendran, V. M. (1983). *Analysis of growth and interaction of multiple hydraulic fractures.* Paper presented at the SPE Reservoir Simulation Symposium.

Nolte, K. (1988). Application of fracture design based on pressure analysis. *SPE Production Engineering, 3*(01), 31-42.

Pearson, C., Bond, A., Eck, M., & Schmidt, J. (1992). Results of stress-oriented and aligned perforating in fracturing deviated wells. *Journal of Petroleum Technology, 44*(01), 10-18.

Perkins, T., & Weingarten, J. (1988). *Stability and Failure of Spherical Cavities in Unconsolidated Sand and Weakly Consolidated Rock.* Paper presented at the SPE Annual Technical Conference and Exhibition.

Raaen, A., Skomedal, E., Kjørholt, H., Markestad, P., & Økland, D. (2001). Stress determination from hydraulic fracturing tests: the system stiffness approach. *International Journal of Rock Mechanics and Mining Sciences, 38*(4), 529-541.

Rasouli, V. (2012). A true triaxial stress cell (TTSC) used for simulations of real field operations in the lab. *True triaxial testing of rocks, 4*, 311.

Risnes, R., Bratli, R. K., & Horsrud, P. (1982). Sand stresses around a wellbore. *Society of Petroleum Engineers Journal, 22*(06), 883-898.

Romero, J., Mack, M., & Elbel, J. (1995). *Theoretical model and numerical investigation of near-wellbore effects in hydraulic fracturing.* Paper presented at the SPE Annual Technical Conference and Exhibition.

Romero, J., Mack, M., & Elbel, J. (2000). Theoretical model and numerical investigation of near-wellbore effects in hydraulic fracturing. *SPE production & facilities, 15*(02), 76-82.

Roshan, H., & Rahman, S. (2011). A fully coupled chemo-poroelastic analysis of pore pressure and stress distribution around a wellbore in water active rocks. *Rock Mechanics and Rock Engineering, 44*(2), 199-210.

Sadd, M. H. (2009). *Elasticity: theory, applications, and numerics*: Access Online via Elsevier.

Safian, G. (2012). *National Iranian South Oil Company Archive*.

Sarmadivaleh. (2012). *Experimental and Numerical Study of Interaction of a Pre Existing Natural Interface and an Induced Hydraulic Fracture.* (PhD), Curtin University.

Sarmadivaleh, M., & Rasouli, V. (2010). Studying the controlling parameters in Hydraulic Fracturing and fracture containment in tight formations. *APPEA J, 50*, 581-591.

Schmidt, D., & Zoback, M. (1989). *Poroelasticity Effect in the Determination of Minimum Horizontal Principal Stress in Hydraulic Fracture Test-A Proposed Breakdown Equation Employing a Modified Effective Stress Relation for Tensile Failure.* Paper presented at the International journal of rock Mechanics, Mining Science & Geomechanic Abstracts.

Soliman, M. (1990). *Interpretation of pressure behavior of fractured, deviated, and horizontal wells.* Paper presented at the SPE Latin America Petroleum Engineering Conference.

Stadulis, J. M. (1995). *Development of a completion design to control screenouts caused by multiple near-wellbore fractures.* Paper presented at the Low Permeability Reservoirs Symposium.

Valk, P., & Economides, M. J. (1995). *Hydraulic fracture mechanics*: Wiley, New York.

Van Ketterij, R., & De Pater, C. (1999). Impact of perforations on hydraulic fracture tortuosity. *SPE production & facilities, 14*(02), 117-130.

Van Poollen, H. (1957). *Theories of hydraulic fracturing.* Paper presented at the The 2nd US Symposium on Rock Mechanics (USRMS).

Veatch Jr, R. W., Moschovidis, Z. A., & Fast, C. R. (1989). An overview of hydraulic fracturing. *Recent Advances in Hydraulic Fracturing, Edited by JL Gidley, SA Holditch, DE Nierode, and RW Veatch Jr. Society of Petroleum Engineers, Henry L Doherty Series Monograph, 12*.

Venditto, J., McMechan, D., Simpson, G., Hyde, P., Friend, L., & Schindler, R. (1993). Study determines better well completion practices. *Oil and Gas Journal;(United States), 91*(4).

Waters, G. A., Dean, B. K., Downie, R. C., Kerrihard, K. J., Austbo, L., & McPherson, B. (2009). *Simultaneous hydraulic fracturing of adjacent horizontal wells in the Woodford Shale.* Paper presented at the SPE hydraulic fracturing technology conference.

Watson, D. R., Durst, D. G., Harris, J. T., & Contreras, J. D. (2008). *One-trip multistage completion technology for unconventional gas formations.* Paper presented at the CIPC/SPE Gas Technology Symposium 2008 Joint Conference.

Weijers, L. (1995). The near-wellbore geometry of hydraulic fractures initiated from horizontal and deviated wells.

Weng, X. (1993). *Fracture initiation and propagation from deviated wellbores.* Paper presented at the SPE Annual Technical Conference and Exhibition.

Westergaard, H. M. (1940). Plastic state of stress around a deep well.

Wiley, C., Barree, B., Eberhard, M., & Lantz, T. (2004). *Improved Horizontal Well Stimulations in the Bakken Formation, Williston Basin, Montana.* Paper presented at the SPE Annual Technical Conference and Exhibition.

Wong, G., Fors, R., Casassa, J., Hite, R., & Shlyapobersky, J. (1993). *Design, execution, and evaluation of Frac and Pack (F&P) treatments in unconsolidated sand formations in the Gulf of Mexico.* Paper presented at the SPE Annual Technical Conference and Exhibition.

Yaghoubi, A. A., & Zeinali, M. (2009). Determination of magnitude and orientation of the in-situ stress from borehole breakout and effect of pore pressure on borehole stability—Case study in Cheshmeh Khush oil field of Iran. *Journal of Petroleum Science and Engineering, 67*(3), 116-126.

Yew, C., & Li, Y. (1988). Fracturing of a deviated well. *SPE Production Engineering, 3*(04), 429-437.

Yew, C., Mear, M., Chang, C., & Zhang, X. (1993). *On perforating and fracturing of deviated cased wellbores.* Paper presented at the SPE Annual Technical Conference and Exhibition.
Yew, C., Schmidt, J., & Li, Y. (1989). *On fracture design of deviated wells.* Paper presented at the SPE Annual Technical Conference and Exhibition.
Yew, C. H., & Weng, X. (2014). *Mechanics of hydraulic fracturing*: Gulf Professional Publishing.
Zare, M. (2009). *Mechanical Stability Analysis of Deviated Wells: a Case Study in Ahwaz Oilfield.* (Master of Science), Petroleum University of Technology.

"Every reasonable effort has been made to acknowledge the owners of copyright material. I would be pleased to hear from any copyright owner who has been omitted or incorrectly acknowledged."

Appendix A Matlab program to numerically calculate FIP in perforation hole

A part of the generated Matlab program is presented in this section.

```
clc
clear

rw  = input('Well Radius(in)=');
h   = input('Well Depth(ft)=');
Az  = input('Well Azimuth(degree)=');
CT  = input('Cement Thickness(in)=');
T   = input('Tensile zone Location(degree)=');

TS  = input('Formation Tensile Strength(psi)=');
TSc = input('Cement Tensile Strength(psi)=');
vf  = input('Formation Poisson Ratio=');
vc  = input('Cement Poisson Ratio=');
BFf = input('Formation Biot Factor=');
BFc = input('Cement Biot Factor=');

Svg = input('Vertical Stress Gradient(psi/ft)=');
SHg = input('Maximum Horizontal Stress
Gradient(psi/ft)=');
Shg = input('Minimum Horizontal Stress
Gradient(psi/ft)=');
Pog = input('Formation Pore Pressure Gradient(psi/ft)=');

  Pi = input('Pressure Interval(psi)=');
  Ri = input('Radius Interval(in)=');

  Sv  = Svg*h;
  SH  = SHg*h;
  Sh  = Shg*h;
  Pup = Sv*3;
  Po  = Pog*h;
  a   = (Az*pi)/180;
  t   = (T*pi)/180;
  m   = (5*rw)/Ri;

  for in = 1:10

  i = ((in-1)*10*pi)/180;

  Lxx = cos(a)*cos(i);
```

```
Lxy = sin(a)*cos(i)
Lxz = -sin(i);
Lyx = -sin(a);
Lyy = cos(a);
Lyz = 0;
Lzx = cos(a)*sin(i);
Lzy = sin(a)*sin(i);
Lzz = cos(i);

Sx  = lxx^2*SH+lxy^2*Sh+lxz^2*Sv;
Sy  = lyx^2*SH+lyy^2*Sh+lyz^2*Sv;
Sz  = lzx^2*SH+lzy^2*Sh+lzz^2*Sv;
xy  = lxx*lyx*SH+lxy*lyy*Sh+lxz*lyz*Sv;
Tyz = lyx*lzx*SH+lyy*lzy*Sh+lyz*lzz*Sv;
Tzx = lzx*lxx*SH+lzy*lxy*Sh+lzz*lxz*Sv;

for j  = 1:m

r  = rw+(j)*Ri;
rt =(rw/r)^2;
rf =(rw/r)^4;
Pp = round(Po/Pi);
Pmax = round(Pup/Pi);
n = Pmax-Pp;

for k = 1:n
    Pw(k) = Po+(k-1)*Pi;

    Sr(j,k) = ((Sx+Sy)/2)*(1-rt)+((Sx-Sy)/2)*
   (1+3*rf-4*rt)*cos(2*t)+Txy*(1+3*rf-
   4*rt)*sin(2*t)+Pw(k)*rt;

    St(j,k) = ((Sx+Sy)/2)*(1+rt)-
    ((Sx-Sy)/2)*(1+3*rf)*cos(2*t)-
    Txy*(1+3*rf)*sin(2*t)-Pw(k)*rt;

    if r<=(rw+CT)
       v = vc;
    else v = vf;
    end

    Szt(j,k) = Sz-v*(2*(Sx -Sy)*rt*cos(2*t)+
    4*Txy*rt*sin(2*t));


    Trt(j,k) = ((Sx-Sy)/2)*(1-3*rf+2*rt)*sin(2*t)+
    Txy*(1-3*rf+2*rt)*cos(2*t);

    Ttz(j,k) = (-Tzx*sin(t)+Tyz*cos(t))*(1+rt);

    Trz(j,k) = (Tzx*cos(t)+Tyz*sin(t))*(1-rt);
```

```
      Srp(j,k) = Pw(k);


      for tp1 = 1:180
          tp = (tp1*pi)/180;

          Stp(j,k,tp1) = Szt(j,k)+St(j,k)-2*(Szt(j,k)
St(j,k))*cos(2*tp)-4*Ttz(j,k)*sin(2*tp)-Pw(k);

          Sztp(j,k,tp1) = Sr(j,k)-v*(2*(Szt(j,k)-
St(j,k))*cos(2*tp)+4*Ttz(j,k)*sin(2*tp));

          Trtp(j,k,tp1) = 0;
          Ttzp(j,k,tp1) = 2*(Trt(j,k)*cos(tp)-
Trz(j,k)*sin(tp));
          Trzp(j,k,tp1) = 0;


          S3(j,k,tp1) =
0.5*((Stp(j,k,tp1)+Sztp(j,k,tp1))-    sqrt((Stp(j,k,tp1)-
Sztp(j,k,tp1))^2+4*Ttzp(j,k,tp1)^2));

      end


      S3min = min(min(S3(j,k,tp1)));


      if r<=(rw+CT)
         BF = BFc;
         TS = TSc;
      else BF = BFf;
           TS = TSf;
      end


      if S3min-BF*Po<-TS
         tpmin = find(S3(j,k,:)==S3min);

         Gama(j)= (0.5*atan((2*Ttzp(j,k,tpmin))/
  (Stp(j,k,tpmin)-Sztp(j,k,tpmin))))*(180/pi);

         FIP(j)= Pw(k);
      break

      end

    end

  end
  FFIP = min(FIP);
```

```
jF(in) = min(find(FIP(:)==FFIP));
GamaFrac(in) = -Gama(jF(in));

End

rr = (rw+Ri):Ri:(6*rw);
plot(rr,FIP,'r*');
hold on
```

Appendix B Raw logging data

Some raw logging data (Safian, 2012) along with some calculated parameters are presented in this appendix. In the following tables TS stands for tensile strength, NPHI is the neutron porosity, V_p and V_s are compressional and shear sonic velocities, respectively.

Table B.1: Logging and calculated parameters for a depth interval of 3573-3576 (m).

Depth (m)	V_p **(ft/s)**	V_s **(ft/s)**	ϑ	**TS (psi) (sonic log)**	$NPHI$ **(%)**	**TS(psi) (NPHI)**
3573.78	15676	8317.8	0.304	1865.2	6.6	2266.8
3573.93	15899	8416.9	0.305	1975.1	7.1	2161.1
3574.08	15972.4	8449.5	0.306	2012	7.6	2058.9
3574.24	15784.6	8366.1	0.305	1918.4	8.9	1821.7
3574.39	16983.2	8895.7	0.311	2553.9	8.5	1893.9
3574.54	17574.4	9154.6	0.314	2899	7.2	2145.2
3574.69	17550.2	9144	0.314	2884.6	5.4	2544.8
3574.85	18208	9430.6	0.317	3290.7	4.6	2744.8
3575	17579.9	9157	0.314	2902.3	4.5	2771.1
3575.15	18083.5	9376.5	0.316	3212.1	4.4	2797.2
3575.3	18114.7	9390	0.316	3231.7	4.5	2770.3
3575.46	17984.9	9333.6	0.316	3150.3	4.7	2719.6
3575.61	17922.1	9306.3	0.315	3111.3	4.3	2822.8
3575.76	18013.5	9346.1	0.316	3168.2	4.8	2693.6
3575.91	17538.1	9138.7	0.314	2877.3	4.4	2793.7
3576.07	16980.5	8894.5	0.311	2552.4	5.8	2448.6
3576.22	17242	9009.2	0.312	2702.5	5.4	2542.1
3576.37	17303	9035.9	0.313	2738.1	5.7	2471.3
3576.52	17512.2	9127.4	0.314	2861.8	5.6	2494.1
3576.68	17421.6	9087.8	0.313	2807.9	5.9	2423
3576.83	17425.1	9089.3	0.313	2810	6.5	2288.6

Table B.2: Logging and calculated parameters for a depth interval of 3580-3584 (m).

Depth (m)	V_p **(ft/s)**	V_s **(ft/s)**	ϑ	**TS (psi) (sonic log)**	$NPHI$ **(%)**	**TS(psi) (NPHI)**
3580.03	16744.6	8790.7	0.31	2420.4	4.9	2667.1
3580.18	16186.2	8544.2	0.307	2121.4	4.9	2667.9
3580.33	16666.7	8756.4	0.309	2377.5	4.6	2741.2
3580.49	16668	8757	0.309	2378.2	6	2399.3
3580.64	16810.1	8819.5	0.31	2456.7	6.9	2202.5
3580.79	17150.2	8968.9	0.312	2649.3	7.5	2084.5
3580.94	16919.6	8867.7	0.311	2518	5.9	2426.6
3581.1	16829.5	8828.1	0.31	2467.5	5	2641.3
3581.25	16256	8575.1	0.307	2157.7	5.2	2589.7
3581.4	15850.2	8395.2	0.305	1950.8	6.1	2376.7
3581.55	16076.1	8495.4	0.306	2064.7	6.9	2204
3581.7	15973.3	8449.8	0.306	2012.4	6.8	2223.6
3581.86	15846.4	8393.5	0.305	1948.9	7.5	2080.6
3582.01	15701.7	8329.2	0.304	1877.7	7.8	2021.1
3582.16	16025.9	8473.2	0.306	2039.1	8.5	1891.8
3582.31	16053.5	8485.4	0.306	2053.2	8.5	1892.3
3582.47	16286.6	8588.6	0.307	2173.7	8.2	1946.3
3582.62	16283.8	8587.4	0.307	2172.2	8.4	1910.1
3582.77	15998.7	8461.1	0.306	2025.3	8.3	1926.1
3582.92	15871.4	8404.6	0.305	1961.4	9.4	1734
3583.08	15724.4	8339.3	0.304	1888.8	10.6	1545.3
3583.23	15847.4	8394	0.305	1949.4	12.8	1254.7
3583.38	15802	8373.8	0.305	1926.9	13.2	1208.4
3583.53	16210.5	8555	0.307	2134	13	1233.3
3583.69	16505.7	8685.4	0.309	2290.1	11.5	1422.3

Table B.3: Logging and calculated parameters for a depth interval of 3590-3594 (m).

Depth (m)	V_p **(ft/s)**	V_s **(ft/s)**	ϑ	**TS (psi) (sonic log)**	$NPHI$ **(%)**	**TS(psi) (NPHI)**
3590.1	17125.5	8958.1	0.312	2635.1	6.3	2332.7
3590.2	17314.3	9040.9	0.313	2744.7	6.7	2246.7
3590.4	15952.2	8440.5	0.306	2001.8	6.5	2289.7
3590.5	16284.3	8587.6	0.307	2172.5	6.4	2310.6
3590.7	16053.5	8485.4	0.306	2053.2	6.8	2223.8
3590.8	16263.2	8578.3	0.307	2161.5	7.3	2120
3591	16559.1	8709	0.309	2318.9	7.9	2003.8
3591.2	16855.8	8839.7	0.31	2482.2	7.6	2061.4
3591.3	16136.1	8522	0.307	2095.5	7.6	2061.2
3591.5	16836.2	8831	0.31	2471.2	7.7	2043.3
3591.6	16948.3	8880.3	0.311	2534.2	7	2182.5
3591.8	16867.9	8845	0.31	2488.9	7.2	2141.8
3591.9	17333.1	9049.1	0.313	2755.7	7.1	2163.6
3592.1	17543.6	9141.1	0.314	2880.6	6.4	2312.9
3592.2	17515.7	9129	0.314	2863.9	5.8	2447.4
3592.4	17761.4	9236.2	0.315	3012.3	5.9	2423.5
3592.5	17701.6	9210.1	0.314	2975.9	6.3	2335.4
3592.7	17955.4	9320.7	0.316	3131.9	5.5	2522.8
3592.8	18146.4	9403.8	0.316	3251.7	3.9	2934.4
3593	17923.5	9306.9	0.315	3112.2	3.8	2962
3593.1	18182.5	9419.5	0.317	3274.5	3.9	2934.1
3593.3	18243.3	9445.9	0.317	3313.2	3.9	2933.8
3593.4	17788.6	9248.1	0.315	3029	4	2905.1
3593.6	17330.2	9047.8	0.313	2754	4.4	2797.2
3593.7	17236.1	9006.6	0.312	2699.1	4.5	2770.3

Table B.4: Logging and calculated parameters for a depth interval of 3605-3609 (m).

Depth (m)	V_p **(ft/s)**	V_s **(ft/s)**	ϑ	**TS (psi) (sonic log)**	$NPHI$ **(%)**	**TS(psi) (NPHI)**
3605	17577.7	9156.1	0.314	2901	2.2	3450.5
3605.2	17893.5	9293.8	0.315	3093.6	2.3	3417.4
3605.3	18351.1	9492.7	0.317	3382.2	2.5	3352.4
3605.5	18588.1	9595.4	0.318	3536	2.8	3259.5
3605.6	18659.5	9626.3	0.319	3582.8	2.6	3321.9
3605.8	18937.6	9746.5	0.32	3768	2.5	3353.4
3605.9	18761.4	9670.4	0.319	3650.2	2.5	3353.7
3606.1	18725.5	9654.9	0.319	3626.4	2.4	3386.2
3606.2	18622.3	9610.2	0.319	3558.4	2.2	3450.8
3606.4	18659.1	9626.1	0.319	3582.6	2.2	3451.4
3606.5	18899.1	9729.9	0.32	3742.1	2	3517.6
3606.7	18484.7	9550.6	0.318	3468.5	1.9	3550.6
3606.9	18521.1	9566.4	0.318	3492.2	2	3517
3607	18790.4	9682.9	0.319	3669.5	2.1	3482.6
3607.2	18149.8	9405.3	0.316	3253.8	2.5	3353.1
3607.3	18247.8	9447.9	0.317	3316.1	2.6	3320.9
3607.5	18203.9	9428.8	0.317	3288.1	2.8	3259.5
3607.6	17268.8	9020.9	0.312	2718.1	2.6	3320.6
3607.8	17028.6	8915.6	0.311	2579.7	2.9	3225.1
3607.9	16336.8	8610.8	0.308	2200.1	3.8	2958.7
3608.1	16049.2	8483.5	0.306	2051	5	2639.4
3608.2	15844.4	8392.6	0.305	1947.9	5.9	2423
3608.4	15499.4	8239.1	0.303	1780.4	6.5	2287.2
3608.8	15177	8095.2	0.301	1630.9	10.5	1560.8
3609	15453.6	8218.7	0.303	1758.8	12.2	1327.9

Paper 1: *The impact of cement sheath mechanical properties on near wellbore hydraulic fracture initiation.*

Rock Engineering and Technology for Sustainable Underground Construction
Eurock 2012 – the 2012 ISRM International Symposium, 28-30 May 2012, Stockholm, Sweden.

The impact of cement sheath mechanical properties on near wellbore hydraulic fracture initiation

S. H. Fallahzadeh
Curtin University, Perth, Australia
Vamegh Rasouli
Curtin University, Perth, Australia

Abstract: Hydraulic fracturing is a stimulation technique which is used, in particular in unconventional reservoirs such as shale gas and tight sandstones, in order to enhance production of hydrocarbon. Hydraulic fracturing is usually operated through the perforations in cased-hole wellbores. The perforation tunnels cut the casing and cement sheath filled the annulus space between the casing and the wellbore wall to communicate the formation to the wellbore. The near wellbore condition is significantly important as the hydraulic fracture crosses this zone after its initiation from the wellbore wall. The presence of casing is considerably important in terms of stress distribution around the wellbore. Also, the quality of the cement sheath may affect the initiation of an induced fracture and the geometry of propagated fracture plane around the wellbore wall.

In this study a generic model was developed to analyze the wellbore stress distribution, considering the effects of casing and cement sheath. The effect of various properties of cement, including Poisson's ratio, elasticity modulus, thermal expansion coeficent, Biot's constant and permeability, on fracture initiation were investigated. In this model analytical equations were applied and numerical simulations were performed to estimate the stress profile around a cased cemented borehole with arbitrary inclination and azimuth. This model allows studying the fracture initiation in a cased perforated wellbore. The model was applied to the data from a real wellbore and good results were obtained.

Theme: Material Models.

Keywords: Hydraulic fracturing, cement sheath, casing, stress distribution, near wellbore.

1 INTRODUCTION

The most important goal of any hydraulic fracturing operation is to increase the rate of production by improving the connection between the wellbore and the reservoir. This connection is controlled by some factors called near-wellbore parameters, which also have great effects on the performance of a hydraulic fracturing process. In cased holes, perforations provide the connection of the wellbore to the surrounding formation. Economides & Nolte (2000) stated that ideal perforation for fracture initiation would have a minimum injection pressure drop, initiate only a single bi-wing fracture, and generate a fracture with minimum tortuosity (turning smoothly from the plane containing the perforation axes into the Preferred hydraulic Fracture Plane, PFP) at an achievable fracture initiation pressure. To achieve such an ideal situation, one has to understand the mechanism of fracture initiation in the near wellbore region, considering all influencing parameters, so that better fracturing design can be developed.

Many researchers have tried to study this concept. Pinching effect (Fracture width reduction) is the most serious near-wellbore phenomenon, which can greatly increase the pumping pressure and consequently may lead to screen out. Pinching can be caused by a number of factors. Fracture width reduction may occur due to incorrect perforation phasing (Romero et al., 2000). Berhmann & Elbel (1991) found that when the perforation phasing is deviated more than 10º from the Preferred Fracture Plane (PFP); the fracture may not start at the perforation tunnel. Based on experimental investigations, they also identified three major factors affecting fracture initiation from perforated completions: pore-pressure, pressurization of the annulus, and perforation orientation with respect to the plane perpendicular to the minimum horizontal stress.

When perforation is not oriented in the direction of PFP, a channel behind the casing will be created to transfer the fracturing fluid into the PFP (Behrmann & Nolte 1998). This channel is called micro-annulus. Romero et al. (2000) and cherny et al. (2009) attempted to model the formation of either an encircling (open hole) or a partial micro-annulus.

Another potential source of fracture pinching is the phenomenon of fracture tortuosity. Because the wellbore and perforation orientations are not always in the plane perpendicular to minimum in-situ stress, an initiated fracture has to turn and/or twist to get aligned with PFP (Gulrajani & Romero 1996; Atkinson & Eftaxiopoulos 2002).

For deviated open-hole Yew et al. (1989) derived equations which allow estimating the location and direction of initial fracture and fracturing pressure. It is shown that with high treating pressures, the fracture tends to turn towards PFP more slowly. However, this is happens in a different way in cased holes, where the presence of casing, cement sheath, and perforation redistribute the stress concentration. In addition, Weng (1993) used software to numerically investigate the fracture initiation and propagation behavior from deviated wells. Similar to the results obtained from experimental researches by Abass et al. (1994), numerical modeling demonstrates that fracture turning occurs within a few wellbore diameters distance away from the wellbore.

Several methods of mitigating pinching effects were suggested by Gulrajani & Romero (1996) to practically prevent or mitigate problems related to the near-wellbore fracture tortuosity. They have discussed that when there is a risk of multiple fracture development, high concentration slugs of small size proppant can be used to plug small fractures. Also, low concentration slugs may be applied to erode the perforation channels and initial fracture and thus remove pinching. Based on step-rate or constant-rate test they also discussed how to assess the presence of near-wellbore (NWB) problems (tortuosity or bad perforation), and their results were compared with the treatment decline analysis and theoretical estimations.

Based on McDaniel et al. (2001) study casing-hole entry problems, perforation tunnel entry problems, fracture plane twisting, and multiple fractures accepting fluid

are among the main NWB issues in hydraulic fracturing initiation. They tried to understand various practical methods for reducing the risks associated with NWB problems. Based on the field case analysis, they mentioned that the method most frequently used to mitigate NWB issues (proppant slug and gel slug) does not always give expected results. The best method is first to recognize the type of NWB problem, and then applying proppant and/or gel slugs or basically modifying the completion of the wellbore by re-perforating the well in order to mitigate the NWB problems.

Fallahzadeh et al. (2010) developed a new approach for investigating the fracture initiation in cased holes. They modeled the perforation stress profile in order to understand the mechanism of formation break down in a perforation tunnel. They considered that the perforation tunnel is a micro-hole perpendicular to the wellbore. Studying Fracture initiation pressure, fracture tortuosity and selecting the best perforation orientation are among the main outputs of their research.

Based on the above literature review, it is noticed that some issues are not well addressed. Generally, the micro-annulus creation is one of the most challenging problem in fracturing a cased wellbore. Basically a NWB tortuous fracture plane can be prevented from causing a premature screen-out by increasing the treating pressure. But if the pumping pressure increases while a micro-annulus is created down-hole, the chance of premature screen-out will increase. This is due to Poisson' effect of the rock. It causes the micro-annulus to narrow and will cause pressure increase and proppant bridging. Therefore, it is critically important to avoid having the occurrence of a channel behind the casing.

This study is aimed at investigating the effects of various parameters of the cement sheath as well as the influence of the steel casing on fracture initiation mechanism. Poisson' ratio, Young's modulus of elasticity, linear thermal expansion coefficient and Biot's constant are among the main important factors which are considered in this modeling. The wellbore and perforation stress profiles are modified in a way to consider the effects of pore pressure variation and temperature disturbance, which are normally induced by high pressure and low temperature fracturing fluids.

2 MODELING AND BACKGROUNDS

The stress profiles around the wellbore and perforation are applied to investigate the mechanism of fracture initiation and to study the effects of different parameters. While the rock formations are porous materials, the general elastic solution of wellbore stress distribution (Fjaer et al., 2008) is used in this modeling, which can be applied for boreholes with arbitrary inclination and azimuth. Basically, in a hydraulic fracturing initiation process, the formation pore pressure around the wellbore does not vary significantly, and that is why the elastic solutions are used here.

Here, a method is described to apply the wellbore stress profile for simulating the stress distribution on the surface of the perforation. In addition, for studying the effects of pore pressure and temperature variations in the formation adjacent to the perforation, the concepts of poroelasticity and thermoelasticity are then applied to this model development.

The other important parameter which is developed in this study is the effect of the steel casing. The influence of steel casing is implied on the wellbore stress distribution, which can in turn affect the perforation stress profile, and consequently the fracture initiation occurrence. After simulating the borehole and perforation stress profiles, the mechanism of fracture initiation from a perforated well is applied. Then, an iterative method is introduced for analyzing the fracture initiation mechanism and pressure.

2.1 Perforation stress distribution

To model stress profiles, the perforation is assumed as a cylindrical micro-hole perpendicular to the borehole axis. At distances close to the wellbore, it is reasonable to assume that the shape of a perforation tunnel is cylindrical. Therefore, the wellbore stress distribution is applied to estimate the stress distribution on the perforation wall, as shown in the following set of equations;

$$\begin{aligned}
&\sigma_{rp} = P_w \\
&\sigma_{\theta p} = \sigma_{zz} + \sigma_\theta - 2(\sigma_{zz} - \sigma_\theta)\cos 2\theta_p - 4\tau_{z\theta}\sin 2\theta_p - P_w \\
&\sigma_{zp} = \sigma_r - \upsilon\,(\,2(\sigma_{zz} - \sigma_\theta)\cos 2\theta_p + 4\tau_{z\theta}\sin 2\theta_p\,) \\
&\tau_{r\theta p} = \tau_{rzp} = 0 \\
&\tau_{\theta zp} = 2(-\tau_{rz}\sin\theta_p + \tau_{r\theta}\cos\theta_p)
\end{aligned} \tag{1}$$

In above equations, θp is the circular angle around the perforation. The subscript p indicates that the terms correspond to perforation. As it is seen in these formulas, wellbore pressure P_w is the perforation pressure. In the first step of hydraulic fracturing operation, when the well pressure is increased to initiate the fracture, the perforation pressure is simultaneously increased.

The principal stresses can be calculated using the Mohr circle. Having the stress profile on the surface of the perforation, the tensile failure criterion, which is the governing failure mode in a hydraulic fracturing treatment, is applied in order to simulate the process of fracture initiation along the perforation tunnel.

Each perforation is a tunnel passing through the casing, cement sheath and formation. To analyze the occurrence of the fracture initiation in the cement sheath, different properties of the cement is applied in the vicinity of the perforation tunnel. In this way, one can analyze which cement sheath properties must be controlled in order to minimize the chance of micro-annulus creation.

2.1.1 Thermoelasticity effect on stress distribution around perforation

When a fracturing fluid is introduced to a well, it will impose temperature variation, because the fracturing fluid is normally cooler than underground formations. The rate of this temperature variation is a function of rock/fluid conduction and convection processes, and its impacts depend on rock/fluid thermal expansion coefficients.

When the temperature changes, the formation expands or shrinks and the stresses will change. In this part the effect of this temperature variation is applied on the perforation stress distribution. This is done through the following formulation;

$$\begin{aligned}
&\sigma_{rp} = P_w \\
&\sigma_{\theta p} = \sigma_{zz} + \sigma_\theta - 2(\sigma_{zz} - \sigma_\theta)\cos 2\theta_p - 4\tau_{z\theta}\sin 2\theta_p - P_w + \frac{E}{1-\upsilon}\alpha_T(T_W - T_O) \\
&\sigma_{zp} = \sigma_r - \upsilon\,(\,2(\sigma_{zz} - \sigma_\theta)\cos 2\theta_p + 4\tau_{z\theta}\sin 2\theta_p\,) + \frac{E}{1-\upsilon}\alpha_T(T_W - T_O) \\
&\tau_{r\theta p} = \tau_{rzp} = 0 \\
&\tau_{\theta zp} = 2(-\tau_{rz}\sin\theta_p + \tau_{r\theta}\cos\theta_p)
\end{aligned} \tag{2}$$

In above equations T_w is the temperature in the well (fracturing fluid temperature), T_o is the reservoir temperature,α_T is the coefficient of linear thermal expansion, E is the Young's modulus and v is the Poisson's ratio of the rock (or cement, for the cement

section of the perforation). In these expressions, the final terms of the second and third formulas account for the temperature variations.

2.1.2 Poroelasticity effect on perforation stress distribution

In hydraulic fracturing, where the well pressure is higher than the reservoir fluid pressure, fluids are injected and the pore fluid pressure is increased around the perforations. This will give a tendency for the material to expand and the stresses increase. This effect is considerable when the rock permeability is reasonably not very low, and a low viscous fracturing fluid is used to slowly pressurize the well. As a result the formation pressure will no longer remains constant and a varying pore pressure profile will be formed, affecting the stress distribution around the wellbore and perforation. So it would be beneficial if someone takes into account this stresses change for analyzing the fracture break down mechanism. The following set of equations is derived to apply the effect of poroelasticity in perforation stress profile:

$$\begin{aligned}
&\sigma_{rp} = P_w \\
&\sigma_{\theta p} = \sigma_{zz} + \sigma_\theta - 2\left(\sigma_{zz} - \sigma_\theta\right)\cos 2\theta_p - 4\tau_{z\theta}\sin 2\theta_p - P_w + 2\eta\left(P_W - P_O\right) \\
&\sigma_{zp} = \sigma_r - \upsilon\left(\, 2\left(\sigma_{zz} - \sigma_\theta\right)\cos 2\theta_p + 4\tau_{z\theta}\sin 2\theta_p \,\right) + 2\eta\left(P_W - P_O\right) \\
&\tau_{r\theta p} = \tau_{rzp} = 0 \\
&\tau_{\theta zp} = 2\left(-\tau_{rz}\sin\theta_p + \tau_{r\theta}\cos\theta_p\right)
\end{aligned} \tag{3}$$

In above equations η, the poroelastic coefficient of rock or cement is defined as:

$$\eta = \frac{1-2\upsilon}{2(1-\upsilon)}\alpha \tag{4}$$

where, P_w is well pressure, P_o is pore pressure and α is the formation or cement Biot's constant. Generally, the final terms in the second and third formulas apply the effect of pore pressure variation on the perforation stress distribution.

2.2 The effect of casing on wellbore stress distribution

The next influencing parameter is the steel casing, which has different elastic moduli with respect to its surrounding cement and rock. So it can affect the wellbore and accordingly the perforation stress distribution. Consequently, the fracture initiation pressure would be affected by casing. The steel casing thus has a dominant effect on the stress distribution around the hole. In the following analysis, the in-situ stresses are assumed to be transmitted to the casing by rock creeping, and also the casing and its surrounding rock medium are in a state of static equilibrium. Taking into consideration the effects of casing can make the results of this study more accurate. Based on the linear elasticity concept, the following relations exist:

$$\begin{aligned}
&E_c = \frac{\sigma_c}{\varepsilon_c} \\
&E_f = \frac{\sigma_f}{\varepsilon_f}
\end{aligned} \tag{5}$$

in which E_c, σ_c and ε_c are respectively the elasticity moduli, radial stress and radial strain of the casing, and E_f, σ_f and ε_f are the elasticity moduli, radial stress and radial strain of the formation, respectively.

One can consider the same value of radial strain for both casing and the surrounding formation. Knowing that the radial stress inside the casing is the well pressure

(fracturing fluid pressure), the following equation can be obtained for the formation radial stress:

$$\varepsilon_c = \varepsilon_f$$
$$\sigma_f = \varepsilon_f \times E_f = \sigma_c \times \frac{E_f}{E_c} = P_W \times \frac{E_f}{E_c} \quad (6)$$

3 RESULTS AND DISCUSSIONS

After developing the required model in the previous section, in this part some applications of the model are presented and discussed. The aim of this paper is mostly to understand the effects of various cement properties and also the effect of the casing, so that decreasing the chance of fracture initiation in the cement sheath, and thereby reducing the occurrence of pre-mature screen-out in initial part of a hydraulic fracturing operation.

These analyses are performed at specific wellbore and in-situ stress situations, and also defined cement sheath and rock properties. Some common values for these properties are summarized in Table1.

Table 1. Wellbore, in-situ stresses, cement sheath and rock properties.

Parameter	*Unit*	*Quantity*
Wellbore TVD	ft	10000
Wellbore Radius	in	3.5 - 4
Maximum Stress Gradient	Psi/ft	0.9
Intermediate Stress Gradient	Psi/ft	0.8
Minimum Stress Gradient	Psi/ft	0.7
Pore Pressure Gradient	Psi/ft	0.4 - 0.55
Cement Sheath Thickness	in	1
Biot's Constant	-----	0.5 - 1.0
Poisson's Ratio	-----	0.15 – 0.35
Coeficent of Linear Thermal Expansion	1/°F	(4 – 6)×10^-6
Elasticity Modulus	psi	(2 – 4.5) ×10^6
Tensile Strength	Psi	3000

3.1 Casing effect

The steel casing has not the same mechanical properties as the formation rock, which is surrounding the casing; therefore it will affect the stress distribution around the wellbore. In this section, the results of applying the casing effect are presented.

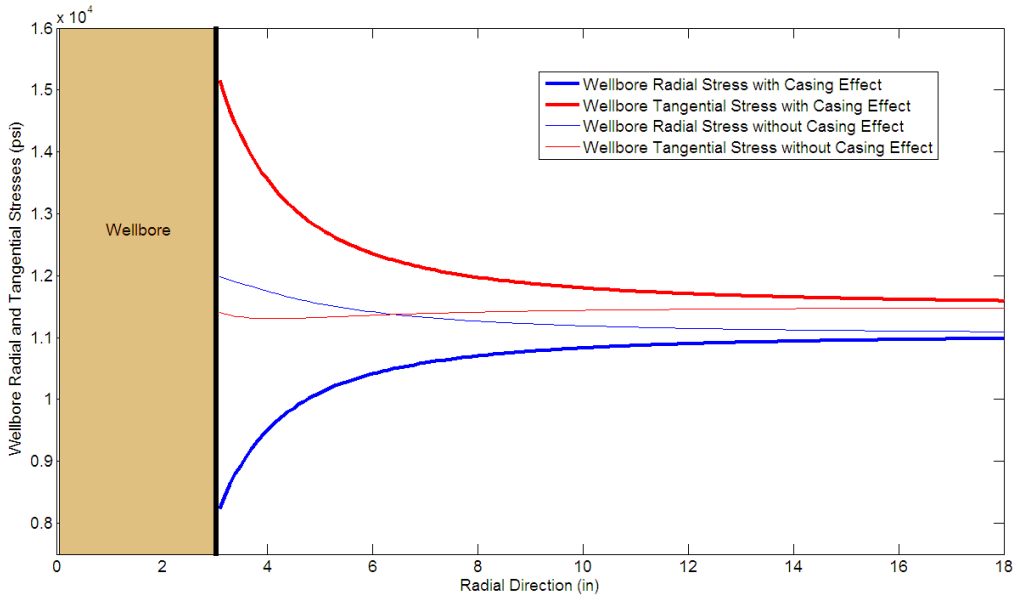

Figure 1. The effect of casing on wellbore radial and tangential stresses.

As it is seen from Figure 1, casing has a great impact on the wellbore stress profiles, especially in the region close to the wellbore. The presence of casing greatly reduces the radial wellbore stress and simultaneously significantly increases the tangential wellbore stress. This result is obtained when the well is under a hydraulic fracturing operation, where the wellbore pressure is much greater than that of formation pore pressure. From a physical point of view, when the casing exists, it does not allow the whole wellbore radial stress to be transferred to the formation, therefore the radial stress reduces and consequently the tangential stress increases.

These variations in the NWB stress profiles will definitely affect the perforation stress distribution. Therefore, the fracture initiation pressure and its location along the perforation tunnel will change accordingly.

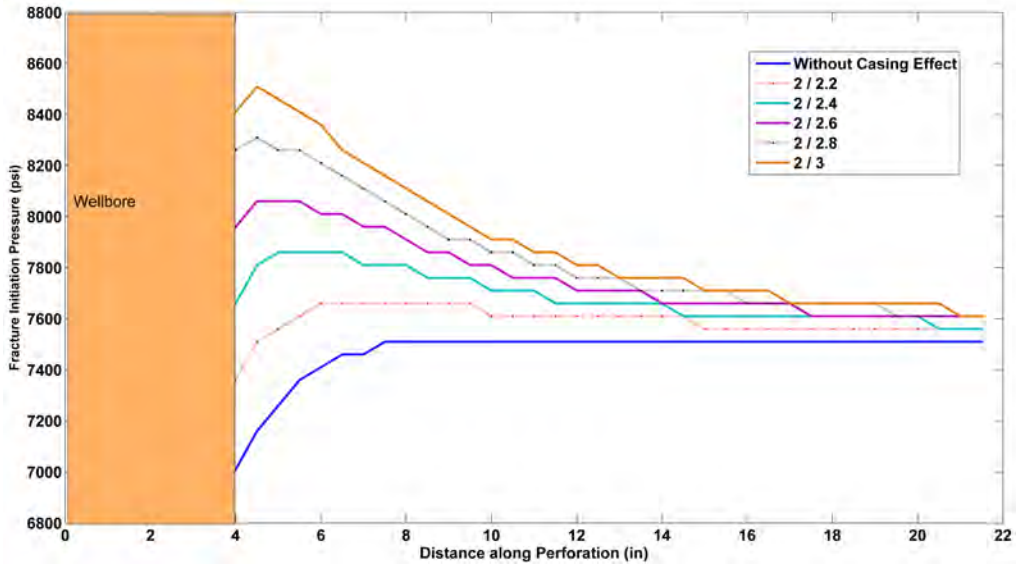

Figure 2. The effect of casing on fracture initiation pressure.

Figure 2 demonstrates the influence of the casing on the fracture initiation pressure along the perforation tunnel. As this graph shows, when the elastic moduli of the steel casing and formation rock are the same, the required pressure for fracturing the formation is low. In such a case, the influence of the casing is similar to that of the for-

mation itself (without casing effect). However, when the ratio between the formation and casing elastic moduli reduces, generally the fracture initiation pressure increases. The reason of this fact is that, by increasing the casing elastic modulus some part of the total wellbore pressure would not be conveyed to the formation. So, higher wellbore (fracturing) pressure is needed to break down the rock.

The other important and interesting feature of Figure 2 is the change in the position of fracture initiation along the perforation. As the casing elastic modulus is rising, the position of the fracture starting point is moved inside the perforation. This will reduce the chance of fracture initiation in the cement sheath, which is next to the casing, and consequently the micro-annulus problem will be mitigated.

3.2 Perforation phasing effect

Based on the well inclination and azimuth as well as the governing stress regime, the location of a perforation around the well can greatly influence the stress distribution around the perforation. Therefore, the best perforation orientation must be selected for each specific case to optimize the fracture initiation pressure and also to mitigate the NWB problems. Generally, a perforation strategy can be obtained to avoid fracturing the cement sheath and accordingly avoiding the micro-annulus creation.

Figure 3 demonstrates the application of this model for a well in one of Iranian southern oil reservoirs. It is a deviated cased wellbore with a depth of 3500 m. The neighboring well has experienced an unsuccessful hydraulic fraction operation which was due to great NWB issues.

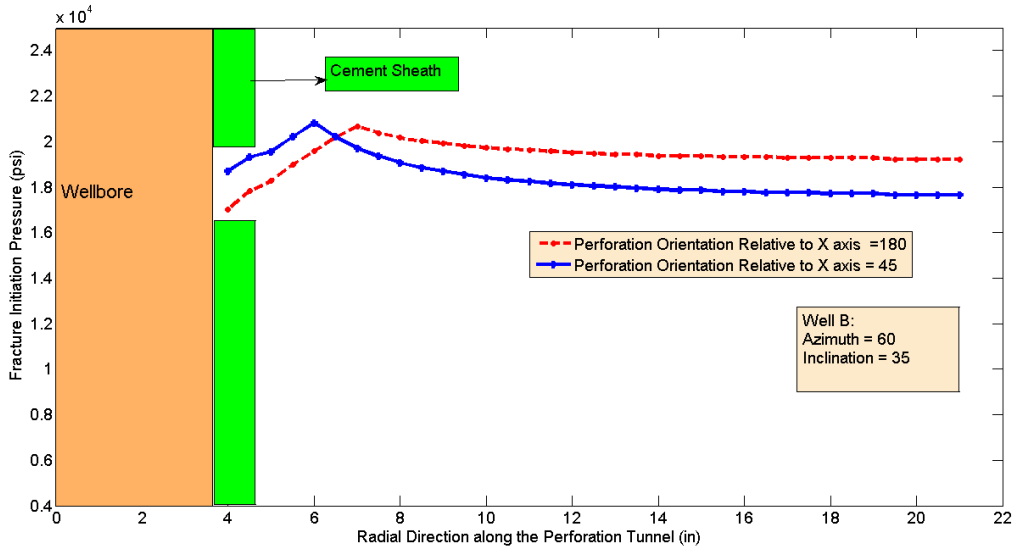

Figure 3. Avoiding the creation of micro-annulus by changing the perforation orientation.

As Figure 3 shows, a minimum of about 17000 psi well pressure is required to initiate the fracture. When the perforation orientation is 180° with respect to lowermost point of the well (x axis), an undesirable micro-annulus will be created. It is possible to avoid the micro-annulus by re-perforating the well before hydraulic fracturing. When the perforation direction is 45° away from the lowermost point of the well, the fracture will be initiated somewhere in the middle of the perforation tunnel, therefore the micro-annulus will not be occurred in the cement sheath. This happens because the perforation stress distribution changes due to this direction change.

3.3 The effects of temperature, Poisson's ratio and elasticity modulus

Usually formations underground are hotter than hydraulic fracturing fluids; therefore it is important to analyze the effect of various parameters of cement in such a temperature changing condition. In this section the thermoelastic stress distribution is applied to see how cement Poisson's ratio, elasticity modulus and linear thermal expansion coefficient affect the fracture initiation pressure.

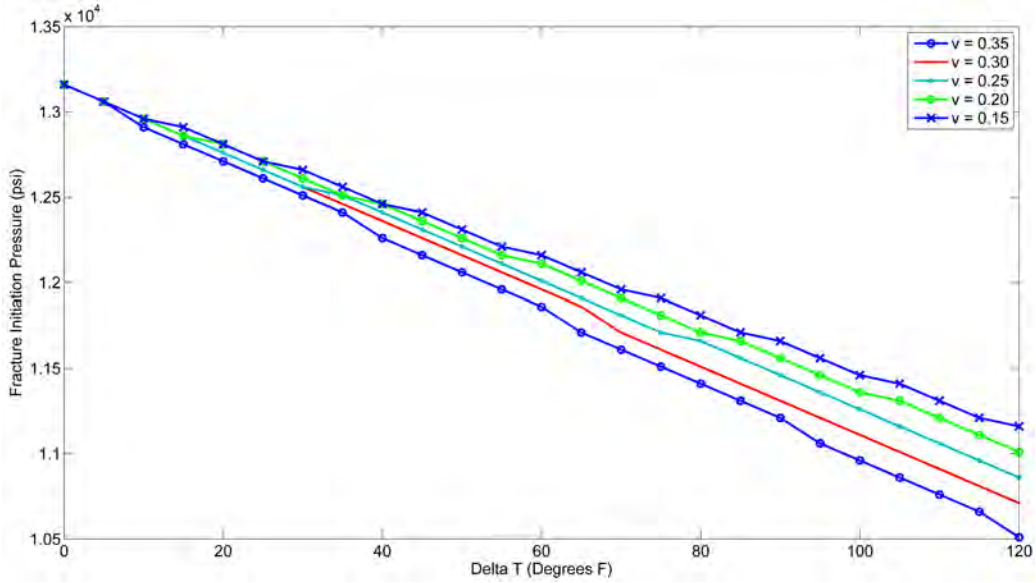

Figure 4. The effect of cement Poisson's ratio on fracture initiation pressure.

Figure 4 demonstrates the influence of the cement Poisson's ratio on fracture initiation pressure. As it is seen from this figure, when the fracturing fluid is cooler than the cement sheath, by increasing the Poisson's ratio, it is easier to break down the cement and initiate a fracture. The effect is more pronounced when the difference between the fracturing fluid temperature and formation temperature in higher. So, one may conclude that as the Poisson' ratio increases the thermal effect can reduce the stresses more and this will lead to lower fracture initiation pressure. Therefore, when it is intended to fracture a cased wellbore using a cool fracturing fluid, it is important to design the cement slurry composition in such a way that the final cement rock will have lower Poisson's ratio. In this way the possibility of micro-annulus creation will decrease for this specific scenario.

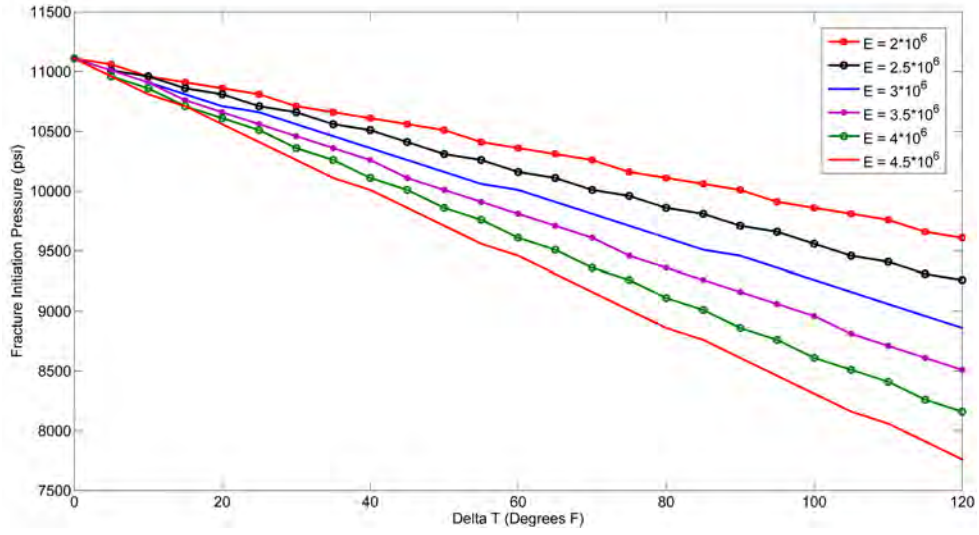

Figure 5. The effect of cement elasticity modulus on fracture initiation pressure.

Most materials have an ability to resist and recover from deformations produced by forces. This ability is called elasticity. It is the foundation for all aspects of rock mechanics. Elasticity modulus is a very important parameter of rock which indicates the relation between stress and strain.

As Figure 5 displays, the effect of temperature difference is more noticeable when the cement sheath has bigger value of elasticity modulus. Basically, when this parameter increases, less fracturing pressure is required. To physically understand this behavior, one may explain that, when the fracturing fluid temperature is lower than the formation temperature, the formation will shrink. Actually in this situation there will be a negative strain. This strain will consequently reduce the local cement stress based on the value of elasticity modulus. Essentially, as the elasticity modulus increases, there would be a bigger decrease in the amount of local stress, and consequently it would be easier to break down the cement rock. Therefore, a cement composition, which will lead to lower cement rock elasticity modulus, is more desirable for the wellbores that will be hydraulically fractured with low temperature fluids.

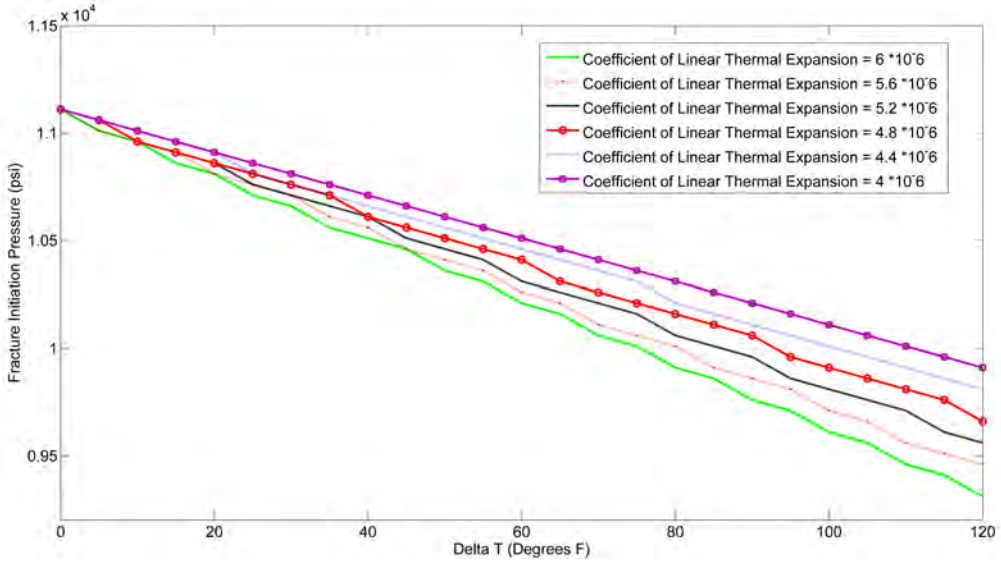

Figure 6. The effect of cement linear thermal expansion coefficient on fracture initiation pressure.

It is well known that (most) materials expand or contract under a temperature change. In order to take thermal effects into consideration, the stress strain relations are modified in this modeling to take the thermal stress and strain into account. The Coefficient of thermal expansion is a fundamental parameter in this study.

Figure 6 shows that how much this modeling is sensitive to this important factor. As it is seen from this figure, by increasing the coefficient of linear thermal expansion the fracture initiation pressure reduces. This influence is more remarkable when the difference between fracturing fluid and formation temperatures is higher. Actually, when the coefficient of linear thermal expansion is big enough, the thermal effect is more critical. Physically, in a cement sheath with high factor of thermal expansion, the fracturing fluid can easily shrink the cement rock; therefore there would be higher reduction in local stresses. Consequently, lower pressure is needed to initiate the fracture in the cement sheath. Therefore, if it is possible, the cement slurry has to be designed in such a way to have lower value of thermal expansion, so that the occurrence of micro-annulus will be avoided.

3.4 The effects cement's pore pressure and Biot constant

In this section the poroelastic stress profile equations are applied to investigate the effects of cement's pore pressure and Biot constant.

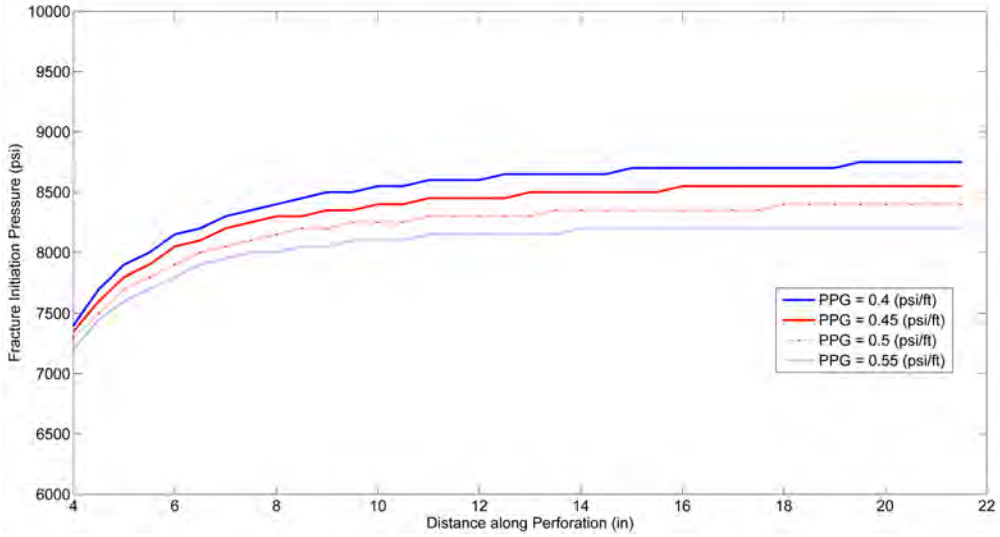

Figure 7. The effect of pore pressure variation on fracture initiation pressure.

Figure 7 shows the effect of formation pressure on fracture initiation pressure. From this figure, it is clear that a cement rock with a pore pressure gradient (PPG) of 0.55 psi/ft needs lower fracturing pressure in comparison to a cement rock having a PPG of 0.5 psi/ft. Therefore, as the pore pressure gradient increases, the pressure, which is required for initiating the fracture, reduces. This is due to the fact that, an increase in the cement pore pressure can lead to lower effective stress, thereby reducing the fracture initiation pressure.

Considering the results of Figure 7, one can conclude that a cement sheath which has a very low permeability is more desirable for a hydraulic fracturing operation. Because in such a cement sheath, the high pressure fracturing fluid cannot diffuse significantly, therefore the cement pore pressure will not increase. So it is important to design cement slurry which generates a cement rock with very low permeability.

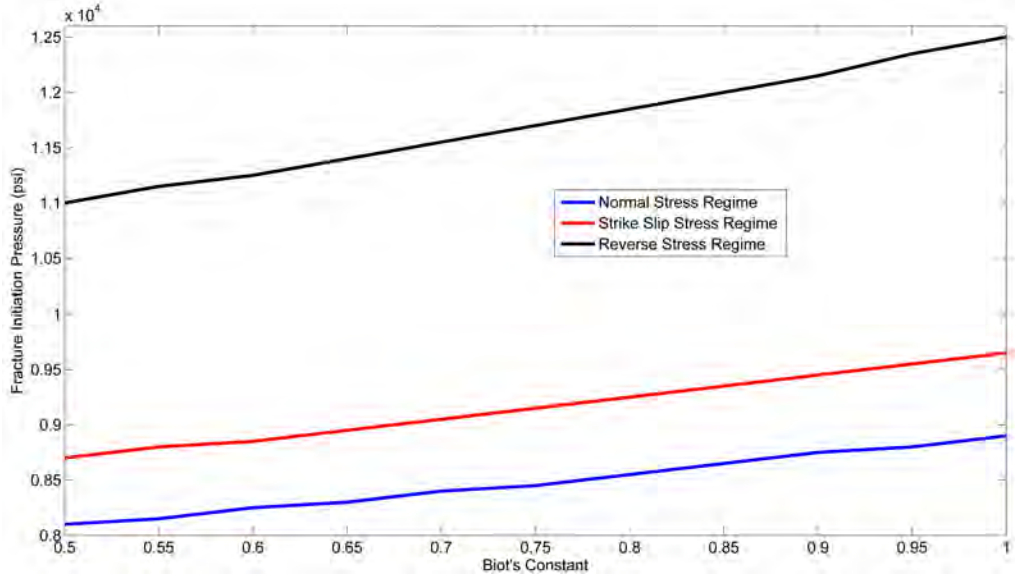

Figure 8. The effect of cement's Biot's constant on fracture initiation pressure.

Biot's constant is a poroelastic rock parameter which generally indicates the effect of pore pressure on effective stress. It is a constant ranging from 0 to 1, with the greater bound approached for compliant cement rocks and less occurring for a stiff, low porosity cement. From Figure 8, it is seen that as the Biot's constant increases the fracture initiation pressure also increases. Based on equations presented previously, an increase in the Biot's constant will cause some increase in both the tangential and axial stresses of the perforation. This will in turn lead to a rise in the perforation principal stresses; therefore the cement sheath break down stress will grow as well.

The effect of field dominant stress regime is also demonstrated in Figure 8. Generally, a well which is drilled in a reverse stressed area needs higher pressure for starting the hydraulic fracturing process. Of course this result is limited to the specific case of a vertical well with specific perforation orientation, and it has to be checked for other cases.

4 CONCLUSIONS

In this paper a new methodology was developed for modeling the thermal and poroelastic effects of the fracturing fluid for a cased perforated borehole. This model was applied to investigate the effects of various parameters for avoiding the occurrence of a micro-annulus in a hydraulic fracturing operation. The effect of steel casing was modeled and it was noticed that the presence of casing greatly influences the wellbore stress profiles. As the elastic modulus of casing increases, the fracture initiation pressure also increases. In addition, the chance of fracturing the cement sheath decreases when the casing Young modulus rises.

It was shown that the orientation of the perforation has a great impact on perforation stress profile. It was seen that as the perforation direction changes, the fracture initiation pressure along the perforation changes as well. Additionally, there is an optimum perforation orientation for any specific case, which results in avoiding creation of micro-annulus in the cement sheath.

It was also seen that when the fracturing fluid is cooler than the formation, as the cement Poisson's ratio, elasticity modulus and thermal expansion coefficient decrease, the perforation stresses change in such way that it is less possible for the fracturing fluid to break down the cement sheath. In addition, as the permeability and consequently the pore pressure of the cement rock decreases, its effective stresses increases, therefore it would be harder for the fracturing fluid to break it down.

5 NOMENCLATURE

PPG	Pore pressure gradient, psi/ft
PFP	Preferred fracture plane
w	Fracture width, in
σ_v	Principle vertical stress, psi
σ_r, σ_θ, σ_{zz}	Wellbore radial, tangential and axial stresses, respectively, psi
P_w	Wellbore pressure, psi
R_w	Wellbore radius, in
θ_p	Angular position around wellbore circumference, degrees
η	Poroelastic rock coefficient, dimensionless
υ	Poisson's ratio, dimensionless
$\tau_{r\theta}$, τ_{rz}, $\tau_{\theta z}$	Cylindrical wellbore shear stresses, psi
σ_{rp}, $\sigma_{\theta p}$, σ_{zp}	Perforation radial, tangential and axial stresses, respectively, psi
$\tau_{r\theta p}$, τ_{rzp}, $\tau_{\theta zp}$	Cylindrical perforation shear stresses, psi
P_p	Formation pore pressure, psi
α	Biot's constant, dimensionless

α_T	Coefficient of linear thermal expansion, 1/°F
T_w	Wellbore temperature, °F
T_o	Reservoi temperature, °F
E_f	Formation elasticity modulus, psi
E_c	Casing elasticity modulus, psi
σ_c	Casing radial stress, psi
σ_f	Formation radial stress, psi
ε_c	Casing radial strain, dimensionless
ε_f	Formation radial strain, dimensionless

6 REFERENCES

Economides, M.J., Nolte, K.G. (third ed.) 2000. *Reservoir Stimulation*. Wiley.

Romero, J., Mack, M.G. and Elbel, J.L. 2000. Theoretical Model and Numerical Investigation of Near-Wellbore Effects in Hydraulic Fracturing. *SPEPF 15* (2): 76-82. SPE-63009-PA.

Berhmann, L.A. and Elbel, J.L. 1991. Effect of Perforations on Fracture Initiation. *JPT* 43 (5): 608-615. SPE-20661-PA.

Behrmann, L.A. and Nolte, K.D. 1998. Perforating Requirements for Fracture Stimulations. Paper SPE 39453 presented at SPE Formation Damage Control Conference, Lafayette, Louisiana, 18-19 February.

Gulrajani, S.N. and Romero, J. 1996. Evaluation and Modification of Fracture Treatments Showing Near-Wellbore Effects. Paper SPE 36901 presented at European Petroleum Conference, Milan, Italy, 22-24 October.

Atkinson, C. and Eftaxiopoulos, D.A. 2002. Numerical and Analytical Solutions for the Problem of Hydraulic Fracturing from a Cased and Cemented Wellbore. *International Journal of Solids and Structures* 39: 1621-1650.

Yew, C.H., Schmidt, J.H. and Li, Y. 1989. On Fracture Design of Deviated Wells. Paper SPE 19722 presented at SPE Annual Technical Conference and Exhibition, San Antonio, Texas, 8-11 October.

Weng, X. 1993. Fracture Initiation and Propagation from Deviated Wellbores. Paper SPE 26597 presented at SPE Annual Technical Conference and Exhibition, Houston, Texas, 3-6 October.

Abass, H.H., Meadows, D.L., Brumley, J.B., Hedayati, S. and Venditto, J.J. 1994. Oriented Perforations - A Rock Mechanics View. Paper SPE 28555 presented at SPE Annual Technical Conference and Exhibition, New Orleans, Louisiana, 25-28 September.

Gulrajani, S.N. and Romero, J. 1996. Evaluation and Modification of Fracture Treatments Showing Near-Wellbore Effects. Paper SPE 36901 presented at European Petroleum Conference, Milan, Italy, 22-24 October.

McDaniel, B.W., McMechan, D.E. and Stegent, N.A. 2001. Proper Use of Proppant Slugs and Viscous Gel Slugs Can Improve Proppant Placement During Hydraulic Fracturing Applications. Paper SPE 71661 presented at SPE Annual Technical Conference and Exhibition, New Orleans, Louisiana, 30 September-3 October.

Fallahzadeh, S.H., Shadizadeh, S.R., Pourafshary, P., Zare M.R. 2010. Modeling the Perforation Stress Profile for Analyzing Hydraulic Fracture Initiation in a Cased Hole. SPE 136990, SPE International Conference and Exhibition, Nigeria, 31 July-7August.

Fjaer, E., Holt, R.M., Horsrud, P., Raaen, A.M., Risnes, R. (2nd edition) 2008. *Petroleum Related Rock Mechanics*, PP.145-147, Elsevier Publications.

Paper 2: *An experimental study to investigate hydraulic fracture reorientation with respect to the principal stresses.*

I, Seyed Hassan Fallahzadeh Abarghooei, co-author of the following paper, contributed in this paper by preparing rock samples for the experiments, laboratory preparation, running fracturing experiments, interpretation of the results and preparation of the following paper:

Gotti, A., S. H. Fallahzadeh, and V. Rasouli. "An experimental study to investigate hydraulic fracture reorientation with respect to the principal stresses." Petroleum and Mineral Resources 81 (2012): 197.

Signature: S. H. Fallahzadeh

Date: 10/12/2015

I, the first author of the paper, endorse that this level of contribution by the candidate indicated above is appropriate.

Name: ANDREW GOTTI

Signature: A. Gotti

Date: 10/12/2015

I, the co-author of the paper, endorse that this level of contribution by the candidate indicated above is appropriate.

Name: Vamegh Rasouli

Signature:

Date: 12/12/2015

An experimental study to investigate hydraulic fracture reorientation with respect to the principal stresses

A. Gotti, S.H. Fallahzadeh, V. Rasouli
Curtin University, Western Australia

Abstract

This study investigated the propagation of an induced hydraulic fracture experimentally. A true triaxial stress cell (TTSC) was used to apply three independent stresses of vertical, maximum horizontal and minimum horizontal to a cube of tight sandstone 100mm in size. A large stress anisotropy was applied in order to help the fracture to initiate more easily. Injection of the fracturing fluid was possible through a hole drilled at the centre of the sample which was plugged in top and bottom sections to give an openhole length of approximately 40mm in the sample centre. A pronounced notch was created in the direction of minimum horizontal stress, i.e. different than the direction at which the fracture intends to open naturally. The hydraulic fracturing tests were conducted on four different samples with different locations for the notch to investigate how the fracture would propagate from different starting angles.

The results indicated that while the fracture initiates along the direction of the notch, it tends to rotate towards the maximum stress direction as it moves away from the wellbore wall. As a fracture is propagating through rock, it passes through inhomogeneities which cause a deviation in the propagation direction. The results showed that a fracture will still reorient to the direction of maximum stress after passing inhomogeneities not just at the wellbore wall, but throughout the rock. The complexity of hydraulic fracturing became apparent in this experiment as even in a highly controlled laboratory environment, some fractures propagated in directions that were unexpected. The presented results demonstrate the need for having a good understanding about the state of stresses when designing a hydraulic fracturing job for the field.

Keywords: true triaxial stress cell, hydraulic fracturing, fracture propagation direction, in-situ stresses, fracture reorientation.

WIT Transactions on Engineering Sciences, Vol 81, © 2012 WIT Press
www.witpress.com, ISSN 1743-3533 (on-line)
doi:10.2495/PMR120181

1 Introduction

Hydraulic fracturing is a stimulation technique which is widely used to enhance production, in particular from unconventional reservoirs such as shale gas, tight formations and coalbed methane. As explained by Valko and Economides [1], the technique of hydraulic fracturing has allowed for low permeability reservoirs which would otherwise not be viable, to become economically producible. In a hydraulic fracturing design several parameters are involved; such as formation mechanical properties, e.g. elastic and strength properties, injecting fluid rheology and the state of principal stresses in the field. Initiation pressure required to open the formation in the vicinity of the wellbore wall is a function of stress anisotropy. Once the fracture initiated its propagation pressure is not only a function of in-situ stresses but also is influenced by the friction along the drill pipes, perforation tunnels and the pressure to keep the fracture open. The propagation direction of the induced fracture is dominantly along the direction of maximum stress, i.e. perpendicular to the least resistance force as shown by Hossain et al [2].

The results of past studies have indicated that the propagation of a fracture plane may deviate from the maximum stress direction when the ratio of stress anisotropy is low [3]. Theoretically, there is no preferred fracture direction when the induced stresses around the wellbore are isotropic [4]. In low stress anisotropy, the propagation direction of a fracture is more influenced by the rock inhomogeneity as shown by Rasouli et al [5]. A fracture around a wellbore tends to initiate from any weak point within the formation at the wellbore wall but will deviate towards the maximum stress direction as it becomes farther away from the wellbore and senses the in-situ stresses. This is the reason for having deviated fracture geometries at field scales when the fracture plane propagates tens of meters long.

In order for a fracture to open unnaturally and in the direction of minimum stress, a notch or inhomogeneity must be in place to assist the opening of the fracture. If no notch or inhomogeneity exists, the fracture will always open in a direction perpendicular to the minimum stress. Commonly used equations are used to theoretically calculate the fluid pressure that is required to fracture a sample at different angles around the wellbore that is under stress shown by Hudson and Harrison [6]. To initiate the fracture at the wellbore wall, the pressure required must be high enough to overcome the tensile strength of the rock plus the minimum effective stress.

Using the identical values for the tensile strength of the rock (TS), the pore pressure (P_p) and the maximum and minimum stresses (σ_H and σ_h), it can be shown that the solved value of σ_θ will always be lower in the direction of maximum stress. This is why a fracture will always naturally open in the maximum stress direction since a lower initiation pressure is required.

Evans and Rasouli [7] have shown the applications of the true triaxial stress cell to allow for laboratory simulations of hydraulic fractures and for monitoring propagation. This study explores the use of the true triaxial stress cell to investigate how a hydraulic fracture will reorient from its initiation direction

WIT Transactions on Engineering Sciences, Vol 81, © 2012 WIT Press
www.witpress.com, ISSN 1743-3533 (on-line)
doi:10.2495/PMR120181

with respect to the principal stresses. The following sections will explain the process of sample preparation, set up of the sample into the true triaxial stress cell (TTSC) which was used for the experiments and the results of the experiments.

2 Sample preparation

Four samples were tested in this study. Sample one was prepared by firstly cutting a section of sandstone to a cube 100mm in size. The sandstone used was well consolidated and had a very low permeability of approximately 3mD. A low permeability rock sample is critical for the experiment to ensure that there is minimal fracture fluid loss into the pores of the rock (i.e. leak-off) during fracturing. A 6mm drill bit was then used to drill a hole through the centre of the sample. Once drilled, two notches were created on opposite sides in the drilled hole along the planned direction of maximum stress. Notches were created to assist the fracture to initiate around the borehole.

Sample one was created as a base case to ensure the fracture would open in the direction of the notches. Once the notches were created, a 30mm long solid metal rod of 5mm in diameter was cut and used as a plug for the bottom of the sample. High strength adhesive glue was used to coat the metal rod and seal it at the bottom of the drilled hole in the sample. This glued rod acts as a packer to ensure injected fluid does not escape through the sample. Once in place, a metal pipe 5mm in diameter and 300mm long was glued 30mm in from the top of the sample. This metal rod provided a connection for the injection fluid to flow through to the 40mm of remaining open hole in the sample.

A small open hole section is left in the centre of the sample as having a small open hole section allows for a larger distance before the nearest boundary is met, at which point the fracture will stop propagating. The sample was then left to rest for 2 days to ensure the glue had set completely before being loaded into the TTSC. Figure 1 shows the 100mm cube sample (left) and the drilled hole at its centre (middle) and the connection pipe in place (right).

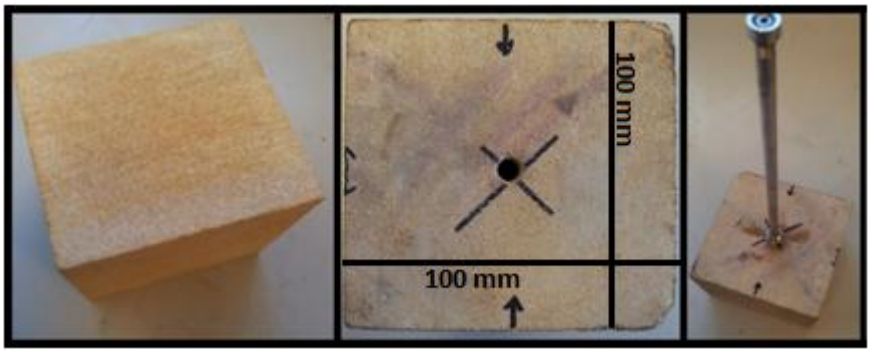

Figure 1: A 100mm sample (left) with a drilled hole at its centre (middle) and the connection pipe for fluid injection (right) was used for hydraulic fracturing experiment.

WIT Transactions on Engineering Sciences, Vol 81, © 2012 WIT Press
www.witpress.com, ISSN 1743-3533 (on-line)
doi:10.2495/PMR120181

Sample two was prepared in a similar way to sample one but the minimum stress in the TTSC, as will be explained in the next section was applied along the direction of the notches: this was to observe the tendency of the fracture to reorient to the maximum stress direction after propagating some distance apart from the wellbore wall. The largest deviation from the direction of maximum stress was chosen to provide results of a case where it would be most difficult for the fracture to curve back to the direction of maximum stress. This sample was completed in the same way as sample one, with a 40mm open hole section left in the centre of the sample between the two metal rods which seal the open hole section.

The third sample used for the experiment in this study was the already fractured sample two. The idea was to apply a large maximum stress perpendicular to the opened fracture plane and repeat the hydraulic fracturing test. High strength adhesive and impermeable glue was used to re-seal the opened fracture, but leaving a 10mm unglued section on both fracture wings around the wellbore open hole section. The result was two fracture wings 10mm x 40mm in area on each side of the wellbore, with the rest of the fracture being completely sealed by the glue. This in turn created a large notch or crevice to assist the fracture to open in the direction of minimum stress with the idea of observing any reorientation for the fracture once initiated around the borehole. The sample was put under a small amount of stress for three hours after the adhesive was applied to ensure the fracture was forced closed and so the glue would seal it consistently. Once the adhesive had set, a quick injection test was done to ensure that there were no leaks and so the sample would be ready for another fracture test.

Sample four was prepared differently after learning from the results of the first three samples. A different material was also chosen for the fourth test to compare results with how the fracture propagated though the sandstone. This sample was prepared in to a 100mm cube to keep constant with the other samples. Rather than drill through the entire sample and then require a plug at the bottom, this sample was only drilled 70mm down, leaving 30mm of the sample undrilled. It was also learned from previous tests that the fracture appears to reach the top of the sample before the bottom of the sample so the open hole area was adjusted in this sample to be slightly closer to the bottom of the sample to allow more time for a fracture to propagate before reaching the first boundary. A greater focus was placed on the creation of the notches with this sample as it was identified from previous tests that the notch size needed to be increased. To create the notch to be deeper, a much smaller drill bit was used to shave the sides of the wellbore from inside the hole which was more effective than using metal rods and other tools to manually scratch the wellbore wall to create a notch or crevice. Once the notches had been made at an angle of 45 degrees to the direction of maximum stress, the rod that then connects to the hydraulic fracturing fluid chamber was inserted and glued.


WIT Transactions on Engineering Sciences, Vol 81, © 2012 WIT Press
www.witpress.com, ISSN 1743-3533 (on-line)
doi:10.2495/PMR120181

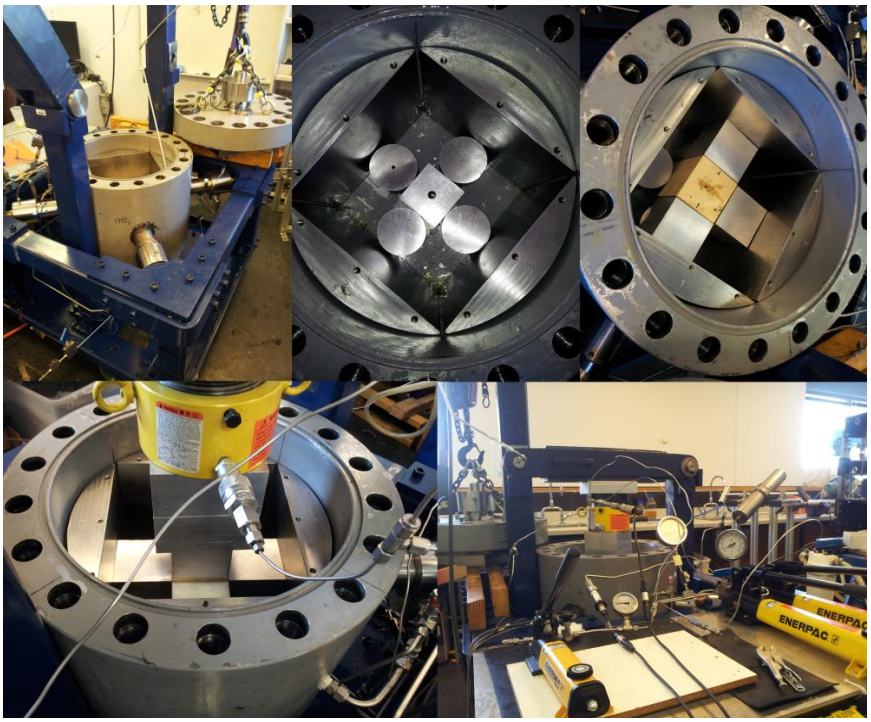

Figure 2: The TTSC shown from unloaded through to sample loading and pressure lines connected and ready for hydraulic fracturing testing to start.

3 Sample set up in TTSC

There are two main components to the TTSC for hydraulic fracturing tests which include the cell itself and the hydraulic fracturing fluid chamber which is a separate piece of equipment that is not directly connected to the TTSC. The TTSC is capable of supporting cube samples of up to 300mm, by using different sized surrounding aluminium blocks to bridge the gap depending on the sample size. The stress through each of the rams is powered by a piston which compresses the rams against the blocks surrounding the sample as oil is injected until the desired pressure has been reached. A very thin layer of lubricant was used between the ram and the blocks to ensure that the only stresses being applied were the principal stresses and that the blocks were not applying any shear stress to the sample which would negatively impact the results.

In Figure 2 a view of the TTSC and the process of loading a 100mm cube sample is shown. The stresses applied in the vertical and in both horizontal directions can be controlled individually and changed real-time while performing a fracturing test. The longer of the metal rods sealed in to the sample is connected to the hydraulic fracturing fluid chamber below the TTSC. This

chamber is loaded with a fracturing fluid with a viscosity of 100,000 cP which is then pressurised to flow in to the open hole area of the sample and begin the fracturing process. Such large fluid viscosity is necessary to be used for a small size sample at the lab scale to propagate the fracture very slowly, hence provide adequate time for recording pressure-time data. The required viscosity to simulate field operation hydraulic fracturing is obtained through the scaling analysis [8].

4 Test procedure

With the sample loaded into the TTSC, pressures are then set in each direction individually. Applying large stress anisotropy is desired to help the fracture to initiate more easily. Stresses in each direction are simultaneously built up until the minimum horizontal stress is reached. The vertical and maximum horizontal stresses are then increased together until the desired stress levels are reached. The area of the piston that pressure was applied to by the pumps was smaller than the area of the sample which meant that the pressure on the sample was not equal to the pressure on the piston. The actual pressure applied to the pistons therefore needed to be calculated based on the desired pressure on the sample.

While the stress is being applied in one direction, it also increases the stress in the other directions due to the Poisson's effect, so it was important to relieve pressure on the minimum horizontal stress plane as the others were being increased. Manual PDP hand pumps were used to apply pressure for the principal stresses while an automatic high pressure syringe pump was used to control the pressure of the fracturing fluid. Pressure transducers were used to enable recording and monitoring of the pressures on the three stress directions as well as for the hydraulic fracturing injection fluid.

With the principal stresses set, the fracturing fluid was then injected at a high flow rate up to a constant pressure of 1200 psi. At this pressure, the flow rate was set to a low 7cc/hour until the sample fractured. It was important to maintain a low injection rate with a high viscosity fluid to allow for the fracture to open and propagate slowly towards the sample boundary. Slower propagation was desired in this experiment in particular to allow time for the fracture to reorient towards the direction of maximum stress once it had been initiated in the direction of minimum stress. When the test had concluded and a fracture had successfully propagated through the sample, all pressures were reduced back to atmospheric pressure, relieving stresses on the sample so it could be unloaded from the TTSC.

5 Results and Discussions

Table 1 shows the magnitude of the three independent stresses applied to each sample and the pressure at which the hydraulic fracture initiated at the borehole wall. In the following sub-sections the produced results in each tested sample are presented and interpreted.


WIT Transactions on Engineering Sciences, Vol 81, © 2012 WIT Press
www.witpress.com, ISSN 1743-3533 (on-line)
doi:10.2495/PMR120181

Table 1: Principal stresses and fracture initiation pressure for each sample.

Test Number	σ_V (psi)	σ_H (psi)	σ_h (psi)	Fracture Initiation P (psi)
1	2600	2000	1000	1900
2	1600	1000	500	1720
3	2400	2000	500	2310
4	5000	3650	500	2450

5.1 Sample One

In this sample it was expected that both fracture wings would open in the direction of maximum stress. As shown in Figure 3, one fracture wing did open in the expected direction while the other wing unexpectedly opened on an angle approximately 45° to the direction of maximum stress. There could have been a variety of reasons for this occurring but it was most likely due to an inhomogeneity along the wellbore in that particular area of the sample which made fracturing in that direction more favourable. It is known from previous studies that the fracture will be influenced by inhomogeneities in low stress anisotropy which is what appears to have been the case in this test.

It can be seen from the results that towards the boundary of the sample, the fracture began to turn towards the direction of maximum stress as was expected for a fracture initially in different direction. Although this was not the planned or expected result, it provided good evidence that a fracture will begin to curve towards the direction of maximum stress even if it is initiated in a different direction at the wellbore. In this case, a larger sample size would have been ideal to allow the fracture more time to curve back to the direction of maximum stress.

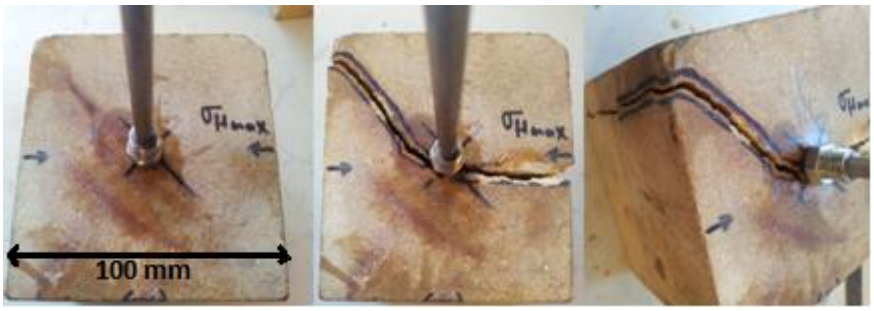

Figure 3: View of sample one after HF test: one fracture wing was not along the maximum stress direction.

WIT Transactions on Engineering Sciences, Vol 81, © 2012 WIT Press
www.witpress.com, ISSN 1743-3533 (on-line)
doi:10.2495/PMR120181

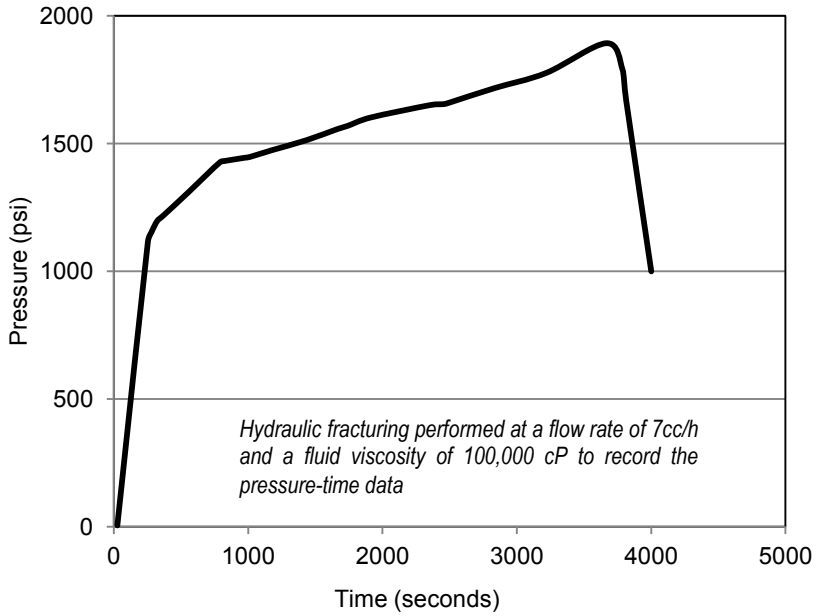

Figure 4: Pressure-Time curve showing the pressure build up of the fracturing fluid before the fracture initiation pressure.

The pressure-time curve plotted in Figure 4 shows the build up of pressure in the open hole area of the sample. The flow rate had been decreased when the expected fracture initiation pressure was being approached which is why the build up gradient decreased at approximately 1200 psi and again at 1450psi. Once the pressure reached 1900 psi, the pressure quickly declined which is a sign that the fracture had propagated to the boundary of the sample and testing had been completed.

5.2 Sample Two

For sample two, the expectation was that fractures would initiate where the notches were created at the direction of minimum stress, and then curve back to the direction of maximum stress. As can be seen from the sample results displayed in Figure 4, the fracture failed to open in the direction of minimum stress and was instead opened in the direction of maximum stress. This is likely due to the notches created not being deep enough so the fracturing fluid pressure required to overcome the tangential stress at the notches was greater than the stress required to fracture the rock along the direction of maximum stress, hence the fracture propagated in this direction. The resulting fracture was very clean and did not deviate from the direction of maximum stress. This sample showing a regular fracture in the direction of maximum stress can be used as a base case for comparison with other samples of different fracture direction.

WIT Transactions on Engineering Sciences, Vol 81, © 2012 WIT Press
www.witpress.com, ISSN 1743-3533 (on-line)
doi:10.2495/PMR120181

Figure 5: Figure 5: View of sample two after HF test: the fracture opened along the maximum stress direction.

5.3 Sample Three

This was in fact sample two which was used for a second hydraulic fracturing test as per preparation explained in the previous section. In this test the open fracture plane at 90° to the direction of maximum stress was partially used as a notch for this sample. The resulting new fracture, as pictured in Figure 5, shows that the new fracture opened in the direction of minimum stress as desired, but did not curve back towards the direction of maximum stress. The fracture crossed over and in some sections joined up with the glued previous fracture and re-opened it. This was due to the glued section acting as an inhomogeneity which therefore affected the propagation direction of the fracture throughout the sample.

The results observed demonstrated the importance of an existing natural fracture in the results of a hydraulic fracturing test. It was again noted that for future testing a larger sample size would be idea to allow the fracture more time and space to be able to curve back to the maximum stress direction. The rock sample is brittle and so once the fracture initiates, it quickly travels to a boundary which limits the time for the fracture to react to the principal stresses and curve to the direction of maximum stress.

WIT Transactions on Engineering Sciences, Vol 81, © 2012 WIT Press
www.witpress.com, ISSN 1743-3533 (on-line)
doi:10.2495/PMR120181

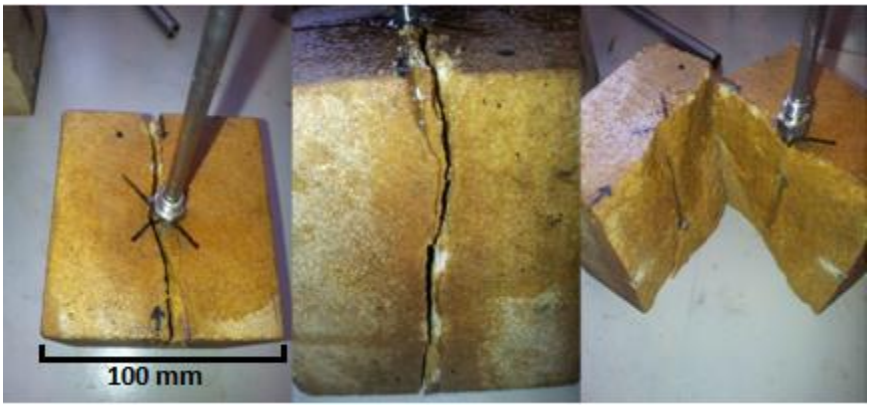

Figure 6: View of sample three after HF test: a new fracture created alongside the previously opened fracture from sample two.

5.4 Sample Four

In this sample, where a deep notch was made at 45° to the direction of maximum stress, a large stress anisotropy was set in order to reduce the effect of any inhomogeneity in the sample on the fracture propagation. It was expected that the fractures would open at an angle of 45° to the direction of maximum stress where notches were created and then curve back to align with the direction of maximum stress. As can be seen from the images of the fractured sample in Figure 4, the fracture wings initiate from the location a notch but in both cases they quickly curve back to the direction of maximum stress towards the boundary of the sample.

The results from this test help prove that if a fracture is being affected by an inhomogeneity in the formation, once propagated away from the wellbore wall and senses the far field stresses it will eventually reorient itself towards the direction of maximum stress regardless of the local effects around the borehole due to sample inhomogeneity or existence of natural fractures. It can also be seen that the fractures tend to deviate in the rock in areas away from the wellbore which is due to inhomogeneities. After passing through these inhomogeneities, the fracture will respond to the principal stresses and rotate back to the direction of maximum stress.

WIT Transactions on Engineering Sciences, Vol 81, © 2012 WIT Press
www.witpress.com, ISSN 1743-3533 (on-line)
doi:10.2495/PMR120181

Figure 7: View of sample four after HF test: two deviated fracture wings that curve back to the direction of maximum stress.

6 Conclusions

This paper examined the outcomes of hydraulic fracture tests on three 100mm tightly consolidated sandstone cube samples and one 100mm cement cube sample. The results of these experiments have shown that a hydraulic fracture will tend to propagate and reorient in a direction which is perpendicular to minimum stress after overcoming effects from inhomogeneities both at the wellbore wall and throughout the formation. The complexity of hydraulic fracturing operations was apparent in these tests as even in a highly controlled laboratory environment, some fractures unexpectedly opened and propagated in directions different to that of the maximum stress direction.

The results have also indicated that on a small scale, a fracture will deviate due to the effects of inhomogeneities or natural fractures that are either pre-existing in the formation or have been created from drilling and completions operations. On a larger scale and for field applications, it can be seen the fracture would curve and reorient towards the direction of maximum stress after the effects of inhomogeneities have caused a change in propagation direction.

References

[1] Valko, P. & Economides, M.J., *Hydraulic Fracture Mechanics*, Chichester: John Wiley & Sons, 1995.
[2] Hossain, M.M., Rahman, M.K. & Rahman, S.S., Hydraulic fracture initiation and propagation: roles of wellbore trajectory, perforation and stress regimes. *Journal of Petroleum Science and Engineering 27*, pp. 129-149, 2000.
[3] Nabipour, A., Evans, B. & Sarmadivaleh, M., Active Monitoring of a Hydraulic Fracture Propagation: Experimental and Numerical Study. *APPEA Journal 2011*, pp. 479-486, 2011.

WIT Transactions on Engineering Sciences, Vol 81, © 2012 WIT Press
www.witpress.com, ISSN 1743-3533 (on-line)
doi:10.2495/PMR120181

[4] Yew, C., *Mechanics of Hydraulic Fracturing*, Houston: Gulf Publishing Company, 1997.
[5] Rasouli, V., Sarmadivaleh, M. & Nabipour, A., Some Challenges in Hydraulic Fracturing of Tight Gas Reservoirs: An Experimental Study. *APPEA Journal 2011*, pp. 499-506, 2011.
[6] Hudson, J. & Harrison, J., *Engineering Rock Mechanics - An Introduction to the Principles*, Oxford: Elsevier Ltd, 1997.
[7] Evans, B & Rasouli, V., A True Triaxial Stress Cell to Simulate Deep Downhole Drilling Conditions. *APPEA Journal 2010*, pp. 61-70, 2010.
[8] Sarmadivaleh, M. Experimental and Numerical Study of Interaction of a Pre-Existing Natural Interface and an Induced Hydraulic Fracture, *PhD thesis*, Curtin University, 2012.

WIT Transactions on Engineering Sciences, Vol 81, © 2012 WIT Press
www.witpress.com, ISSN 1743-3533 (on-line)
doi:10.2495/PMR120181

Paper 3: *An investigation of hydraulic fracturing initiation and near-wellbore propagation from perforated boreholes in tight formations.*

Rock Mech Rock Eng
DOI 10.1007/s00603-014-0595-8

ORIGINAL PAPER

An Investigation of Hydraulic Fracturing Initiation and Near-Wellbore Propagation from Perforated Boreholes in Tight Formations

S. H. Fallahzadeh · V. Rasouli · M. Sarmadivaleh

Received: 25 September 2013 / Accepted: 19 April 2014

Abstract In this study, hydraulic fracturing tests were conducted on 10 and 15 cm synthetically manufactured cubic tight mortar samples. The use of cube samples allowed application of three independent stresses to mimic real far field stress conditions. A true triaxial stress cell was used for this purpose. The lab test parameters were scaled to simulate the operations at field scale. The hole and perforations were made into the sample after casting and curing were completed. Various scenarios of vertical and horizontal wells and in situ stress regimes were modeled. These factors are believed to play a significant role in fracture initiation and near-wellbore propagation behavior; however, they are not independent parameters, hence should be analyzed simultaneously. In addition to experimental studies, analytical solutions were developed to simulate the mechanism of fracture initiation in perforated boreholes in tight formations. Good agreements were observed between the experimental and analytical results. The results of this study showed that a lower initiation pressure is observed when the minimum stress component is perpendicular to the axis of the perforations. It was also seen that, even when the cement sheath behind the casing fails, the orientation of the perforations may affect the initiation of the induced fracture noticeably. Furthermore, it was found that stress anisotropy influences the fracturing mechanism in a perforated borehole, and affects the geometry of the initiated near-wellbore fracture.

Keywords Hydraulic fracturing · Tight formations · Perforated borehole · Initiation pressure · Near-wellbore geometry

S. H. Fallahzadeh (✉) · V. Rasouli · M. Sarmadivaleh
Curtin University, Perth, WA, Australia
e-mail: s.fallahza@postgrad.curtin.edu.au

1 Introduction

The applications of hydraulic fracturing in unconventional reservoirs have increased during the last decade because of the evolution of low permeability reservoirs such as gas shales and tight sandstones. The use of this stimulation technique in perforated boreholes is still a challenging subject due to the complexity of parameters involved in this operation. Problems like high near-wellbore friction and premature screen-out may be observed during hydraulic fracturing operation from a perforation tunnel (Aud et al. 1994; Cleary et al. 1993). In addition, abnormally high operating pressures (Davidson et al. 1993) and development of multiple fracture planes are other operational consideration during hydraulic fracturing (Lehman and Brumley 1997). These are more challenging in perforated boreholes, where presence of perforations causes a complex mechanism of fracture initiation and near-wellbore propagation (Abass et al. 1994; Behrmann and Elbel 1991). This could potentially lead to weak hydraulic fracturing treatment, and consequently a substantial reduction in production rate.

Many researchers have studied different aspects of hydraulic fracturing in a perforated wellbore and its near-wellbore effects. Behrmann and Nolte (1999) conducted an experimental study and found that when the perforation gun orientation is not properly selected and/or when the directions of the in situ stresses are not accurately known, the width of the fracture near the wellbore would be mostly less than that of the main body of the fracture. This is because the magnitudes of induced stresses are larger near the wellbore compared to in situ stresses. Almost the same results were obtained through a theoretical and numerical investigation conducted by Romero et al. (1995). In another experimental study done by Behrmann and Elbel

Published online: 22 May 2014

(1991), they recognized that for cased holes, formation pore-pressure, pressurization of the annulus, and perforation orientation with respect to preferred fracture plane (PFP) (the minimum in situ stress is perpendicular to this plane) are three major influencing factors on the fracturing mechanism in a cased hole. In their experiments, they observed that when the perforation phasing was deviated more than 10° away from the direction of the PFP, the fracture plane may not initiate from the perforations and the fracturing fluid would break down the cement sheath behind the casing, which in turn results in forming a pinch point.

Atkinson and Eftaxiopoulos (2002) applied analytical and numerical methods to study the fracture propagation in a cased cemented wellbore. They developed a 2D plane model and concluded that when the cement sheath bonding to the casing and rock has failed, no fracture turning would occur and higher pressure is required. Weng (1993) also investigated the fracture initiation and propagation using a numerical modeling analysis and found that the initiated fracture plane from the wellbore has a tortuous path in a distance close to the wellbore. This distance is not more than a few wellbore radii. Similar results have also been reported by Abass et al. (1994) based on their experimental studies. In an analytical study carried out by Fallahzadeh et al. (2010), they estimated the wellbore and perforation stress distributions for a porous homogenous elastic formation. In this study, it was shown that by altering the orientation of the perforation with respect to the tensile zone developed around the wellbore, the fracture initiation pressure (FIP) greatly increases.

Reviewing the previous experimental investigations (Abass et al. 1994; Behrmann and Elbel 1991; Daneshy 1973), it is found that none of them applied scaling laws in their experiments. The drawback of non-scaled hydraulic fracturing experiments is that they cannot represent field scale operations which makes it difficult to compare the results with real observations. Pater (1999) applied the scaling laws in their fracturing tests; nevertheless, they only analyzed a deviated wellbore with an azimuth of 60° from the preferred fracture plane and a deviation of 49°. They applied dimensionless numbers developed based on rock and fracturing fluid properties to scale the test parameters in the lab. The parameters which are scaled for a design of hydraulic fracturing lab experiment include the flow rate and viscosity of the fracturing fluid.

The results of the previous studies show that perforation parameters, wellbore trajectory, casing and cement sheath properties, and the state of the in situ stresses are the basic governing parameters in fracture initiation from a cased hole. However, the influence of each parameter and the interactions between these parameters are not yet well established. In addition, inconsistencies are observed in the output results of different studies.

This study is one of the very first attempts to investigate the process of hydraulic fracture initiation and near-wellbore propagation in tight formations. In this study, a recently developed analytical model (Fallahzadeh and Shadizadeh 2013; Fallahzadeh et al. 2010) was further expanded and improved to analyze the process of fracture initiation in elastic homogenous tight formations. This model determines the stress distribution around the wellbore and uses these data to compute the stress distribution along the perforation cavity. The model predicts the FIP, the location of the first crack developed in the perforation tunnel, and the angle of the initiated fracture with respect to perforation axis. The results obtained from this analytical solution were compared with series of scaled hydraulic fracturing tests performed in perforated boreholes on very low permeable mortar samples. Also, the effects of perforation orientation, wellbore trajectory (vertical and horizontal), state of in situ stresses and stress anisotropy were investigated. A true triaxial stress cell (TTSC) was used to apply three independent stresses on 10 and 15 cm cubic mortar samples, while a specific fluid with a viscosity of 97,700 cp was injected at very low flow rate (0.05–0.1 cc/min) through the borehole and perforations located at the center of the sample. As a result, fracture initiation and near-wellbore propagation were analyzed by precisely interpreting the pressure-time curves. In addition, the geometry of the fractures near to the wellbore including fracture turning and twisting and also multiple fracturing are investigated. In the following sections, the details of experimental set-up and experiments are presented and the results are compared with analytical solutions.

2 Experimental Setup

In this section, the sample preparation procedure is explained briefly. The hydro-mechanical properties of the samples used in this study are presented, and a brief overview of the stress cell that was used for the experiments is given.

2.1 Sample Preparation

Cubic mortar samples of 10 and 15 cm were prepared based on the procedure explained by Sarmadivaleh (2012). Firstly, a cement slurry composed of a cement to sand mass ratio of one and a water to cement weight percentage of 40 % was prepared. The slurry was mixed for 15 min in order to homogenize the mix. The mix was poured into cubic and cylindrical moulds and a vibrator plate was used to help remove air bubbles. However, excessive vibration

was avoided for preventing the sand particles from being precipitated into the mortar sample. The mortar cubes were carefully taken out of the moulds after 12 h and preserved for 28 days in a 25 °C water bath. This was adopted from Mindess et al. (2003) who stated that the cement samples should obtain their final strength (i.e., more than 90 %) after 28 days.

In 10 cm cube samples, a 6.5 mm hole was drilled at the center. Then a 3 cm long stainless steel rod of 6 mm diameter was used to block the bottom of the hole. High-strength adhesive glue was used to coat the metal rod and seal it at the bottom of the drilled hole in the sample. After that, a metal tube 6 mm in diameter and 30 cm long was inserted and glued 3 cm inside the opposite side of the hole. This metal tube acts as a casing and later the fracturing fluid was injected through this conduit to the 4 cm of remaining open hole interval inside the sample. Then a 3 mm hole was drilled perpendicular to the larger hole and the bottom of the hole was blocked by a 2.8 mm metal rod glued in from the end of the small size hole. The rod was 2.7 cm long and a section of 2 cm of the hole was left open to act as a perforation tunnel.

For 15 cm samples, a 14 mm diameter hole was drilled at the center of the cube. Here, the samples were only drilled 11 cm, leaving 4 cm of the sample undrilled. Then a 12.7 mm OD section of metal tube, which was 30 cm long, was glued in from the top of the hole. The tube represents the casing and a 7 cm long open hole was left at the center of the sample. Later, two 6 mm diameter holes were drilled perpendicular to the larger hole such that they crossed the main hole and continued on the other side. These two holes were drilled in parallel and 3 cm apart from each other. Finally, the ends of smaller holes were blocked using two 2.8 mm long metal rods, with diameter of 5.8 mm, glued inside the holes. Figure 1 shows a schematic of the 15 cm cubic sample view before fracturing tests.

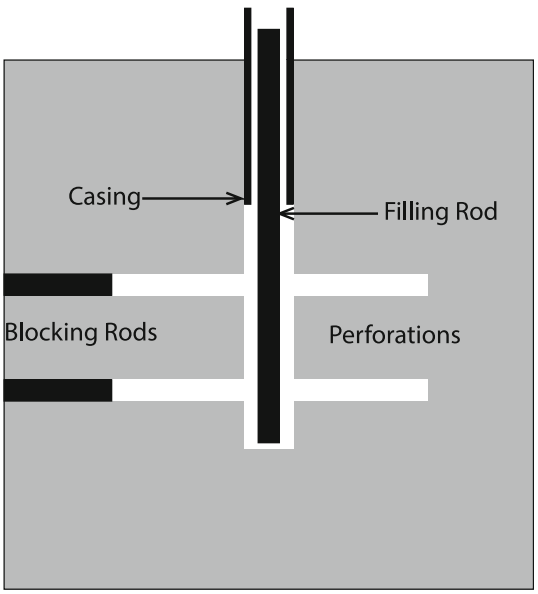

Fig. 1 A schematic of 15 cm cubic sample showing a 7 cm open hole with four perforations on the sides of the hole 180° apart from each other

A section of metal rod, 37 cm long and 6 mm in diameter was placed inside the hole to reduce the dead volume of the system. As a result, when the fracturing test was in progress, less fracturing fluid was compressed inside the hole at the time of fracture break down; therefore, propagation of the fracture plane was better controlled.

When a casing is cemented in a borehole, on many occasions the bonding between the casing and cement sheath or the cement sheath and the formation is weak. This could be due to the presence of residual mud cake which prevents proper cement bonding and/or shrinkage of the cement after it sets, which develops some fissures in the cement sheath (Nelson 1990; Thiercelin et al. 1997). In addition, the variation of downhole conditions over the life of the wellbore can cause crack development in the cement sheath (Thiercelin et al. 1997). Also, when the wellbore is pressurized during fracturing operation, a micro-annulus may be created, especially if the perforations are not aligned in proper orientation (Romero et al. 1995). Therefore, these sets of experiments were carried out in open hole perforated samples in order to simulate the fracturing mechanism in a cased perforated borehole, where commonly a micro-annulus is created in the cement.

2.2 Hydro-Mechanical Properties

Hydro-mechanical properties of the samples are needed to conduct the scaling analysis. Sarmadivaleh (2012) used cylindrical samples for doing a range of tests to measure these properties. A summary of the hydro-mechanical properties of the samples used in this study is presented in Table 1. As it is seen from this table, the permeability of the samples is 0.018 mD, which is a very low value, corresponding to tight formations.

Table 1 Hydro-mechanical properties of samples used in this study (Sarmadivaleh 2012)

Property	Value
Uniaxial compressive strength (UCS) (MPa)	79.5
Poisson's ratio	0.19
Young's modulus (E) (GPa)	27.74
Tensile strength (T_0) (MPa)	3.5
Fracture toughness (K_{IC}), (MPa m)	0.78
Porosity (f), %	14.7
Permeability, K (mD)	0.018

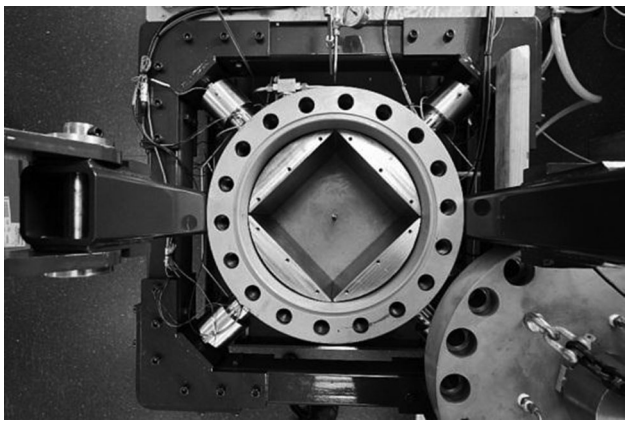

Fig. 2 A *top* view of the TTSC

2.3 True Triaxial Stress Cell

For conducting the fracturing tests a TTSC was used (Rasouli 2012). Figure 2 shows a top view of the TTSC. The TTSC is capable of receiving cube samples of 30 cm or any smaller sizes when aluminum or steel spacers are used to fill the gaps between the sample and the rams. The sizes of the blocks are 2.5 % smaller than the sample sizes so that they do not come into contact when large displacements are expected for the sample.

The stress through each of the rams is powered by a piston which compresses the rams against the sample as oil is injected until the desired stress is reached. The fracturing tests were done using a fracturing fluid, which is a silicon oil having a viscosity of 97,700 cp at a pressure of 5,000 psi and a temperature of 28 °C. The fluid is contained in a small displacement chamber with a total volume of 120 cc which is connected to the casing of the mortar sample.

A specific pump with a flow rate of 0.05–0.1 cc/min was used for injecting the fracturing fluid into the wellbore. Two pressure transducers were also installed at the closest possible point to the casing to record the injection pressure, and there was a chock (flow restrictor) in between these two devices. The function of the chock was to control the flow of compressed fracturing fluid into a newly initiated fracture for having a stable fracture growth, especially during the initiation phase (Bunger 2005).

3 Scaling Analysis

In order to have a reasonable correspondence between the results of lab experiments to field scale operations, dimensional analyses are performed which are known as scaling laws. The scaling laws discuss various fracture propagation regimes, which consist of the main fracturing mechanisms. The energy of fracturing dissipates through different mechanisms. At each specified time, the main dissipating mechanism is the fracturing propagation regime. In fact, an infinite number of mechanisms may be considered for each fracturing case; however, the main dissipation mechanism is considered for the propagation mechanism (Bunger 2005). For designing a laboratory hydraulic fracturing experiment, the injection rate, fluid viscosity, and the total fracture propagation time must be obtained from the scaling analysis. By knowing the sizes of the sample and the wellbore, and also sample hydro-mechanical properties, one would be able to calculate the required viscosity, flow rate, and injection time for running a hydraulic fracturing test.

The time at which the wellbore pressurization rate reaches a maximum value is considered the fracture initiation point; the moment of fracture initiation is the reference point for scaling the time of the experiment. Fracture breakdown is usually defined as the time at which the wellbore pressure reaches its maximum value. Fracture initiation typically occurs before breakdown point (Lhomme 2005). Therefore, the scaled time of a test starts with the time of fracture initiation and will last up to the final stage of injection.

Basically the initiation and propagation of a real fracture in the field can be generally considered under the influence of three extreme boundaries of viscosity-, toughness-, and leak-off-dominated propagation regimes (Bunger 2005). In field fracturing operations, during the initiation phase the fracture development is toughness-dominated; however, it becomes viscous-dominated quickly (Mack and Warpinski 2000), and for a radial fracture, it becomes once more toughness dominated at the final stage of fracture extension (Detournay 2004).

The permeability of the samples in this study was 0.018 mD (see Table 1), which was very low; therefore, the effect of the leak-off is considered to be negligible. In order to have a viscous-dominated propagation regime, the dimensionless toughness parameter of a penny-shaped fracture can be calculated using the following equation (Detournay 2004):

$$k = K'\left(\frac{t^2}{\mu'^5 Q_0'^3 E'^{13}}\right)^{1/18}. \quad (1)$$

In this equation t is the time of the experiment and $Q_0'^3$ is the flow rate. Other parameters are as follows:

$$K' = \left(\frac{32}{\pi}\right)^{1/2} K_{IC} \quad (2)$$

$$E' = \frac{E}{1-\nu^2} \quad (3)$$

$$\mu' = 12\mu \tag{4}$$

where μ is fracturing fluid viscosity, E is rock's Young's modulus, v is the Poisson's ratio, and K_{IC} is fracture toughness. According to the study done by Detournay (2004), when the dimensionless toughness number $k \leq 1$, the propagation regime can be approximated by a limit solution which is obtained with an assumption of zero toughness. Therefore, when $k \leq 1$, the regime is considered to be viscosity dominated. And when $k \geq 4$, the propagation regime can be approximated by a limit solution which is obtained with an assumption of zero viscosity; therefore, it is considered toughness dominated.

Applying the hydro-mechanical properties of the samples, a fracturing fluid with a viscosity of 97,700 cp, and flow rates of 0.05 and 0.1 cc/min, the dimensionless toughness numbers are calculated to be 0.82 and 0.73, respectively. These two numbers are both <1, confirming that the conducted experiments in this study were at viscous-dominated fracture propagation mode. The value of experiment time in Eq. 1 is considered to be 5,000 s; therefore, for any experiment time <5,000 s, the fracture propagation would be viscous dominated.

4 Analytical Modeling

This section describes an analytical solution which has been developed earlier by Fallahzadeh and Shadizadeh (2013) to analyze fracture initiation from a perforation tunnel. In this paper, the analytical model is modified to simulate fracture initiation in elastic homogenous tight formations.

4.1 Wellbore and Perforation Stress Distribution

Generally there are three principal stresses in any underground formation, which are caused by the weight of overlying layers. On most occasions, two of these stress components are in the horizontal direction with the third one being vertical. Elastic wellbore stress distribution formulations have been presented in the literature in order to obtain the cylindrical stress profile around the wellbore using the three in situ principal stresses. A series of these equations can be found in different references (e.g., Fjar et al. 2008; Fallahzadeh and Shadizadeh 2013).

When the wellbore stress profile is calculated, it can be used to compute the distribution of stresses along the perforation tunnel (Fallahzadeh and Shadizadeh 2013). The perforation tunnel is assumed to be a cylinder which is normal to the wellbore. Then normal and shear components of the wellbore stresses are used as the input parameters to calculate the stress distribution at the surface of the perforation tunnel. This is applied along the perforation tunnel (equivalent to the radial direction away from the wellbore). For each point along the perforation tunnel, the wellbore stress components at that radial distance from the center of the wellbore are applied. As a result, the cylindrical stress concentration on the surface of the perforation is obtained:

$$\begin{aligned}
\sigma_{rp} &= P_w \\
\sigma_{\theta p} &= \sigma_{zz} + \sigma_\theta - 2(\sigma_{zz} - \sigma_\theta)\cos 2\theta_p - 4\tau_{z\theta}\sin 2\theta_p \\
&\quad - P_w \\
\sigma_{zp} &= \sigma_r - \upsilon\left(2(\sigma_{zz} - \sigma_\theta)\cos 2\theta_p + 4\tau_{z\theta}\sin 2\theta_p\right) \\
\tau_{r\theta p} &= \tau_{rzp} = 0 \\
\tau_{\theta zp} &= 2\left(-\tau_{rz}\sin\theta_p + \tau_{r\theta}\cos\theta_p\right)
\end{aligned} \tag{5}$$

where σ_{rp}, $\sigma_{\theta p}$, and σ_{zp} are the normal radial, tangential and axial stresses at the surface of the perforation tunnel, respectively. Corresponding perforation shear stresses ($\tau_{r\theta p}$, $\tau_{\theta zp}$, and τ_{rzp}) are also formulated in the above equations. One should note that σ_r, σ_θ, and σ_{zz} are normal radial, tangential, and axial components of the wellbore stress along the orientation of the perforation tunnel. Also, corresponding shear wellbore stress components (τ_{rz}, $\tau_{z\theta}$, and $\tau_{r\theta}$) are used in the above equations. θ_p is the radial angle around the perforation circumference.

4.2 Fracture Initiation Mechanism

After simulating the stress profile along the perforation, one can analyze the fracture initiation mechanism and pressure. To do so, principal stresses need to be calculated along the perforation tunnel, and then tensile failure criterion is applied. Based on tensile failure criterion (Eq. 6) the fracturing fluid will fracture the rock in a plane perpendicular to the minimum effective principal stress.

$$\sigma_3 - \alpha P_p < -\mathrm{TS}. \tag{6}$$

In the above equation, σ_3 is the minimum principal stress, α is the Biot's factor, P_p is the formation pore pressure, and TS is the tensile strength of the rock. Because the mortar samples were tested dry, the term related to pore pressure is ignored in above equation. This would ensure that the results of analytical simulation can better match the results of experimental study.

As is seen from Eq. 5, two of the three shear stresses are zero at the surface of the perforation. This means that the normal stresses are not principal stresses. Because $\tau_{r\theta p} = \tau_{rzp} = 0$, σ_{rp} is one of the principal stresses, however, it is not the minimum principal stress. By applying the Mohr circle concept the two other principal stresses can be calculated. One of the principal stresses is the radial stress and two others are located on a plane tangent to the surface

Table 2 Experimental parameters

Test no.	σ_1 (MPa)	σ_2 (MPa)	σ_3 (MPa)	No. of perforations/ orientation	Injection rate (cc/min)	Initiation pressure (MPa)	Break down pressure (MPa)
1-1	20.68	13.79	6.89	0/–	0.05	10.68	12.41
1-2	20.68	13.79	6.89	1/intermediate stress	0.05	12.75	14.27
1-3	20.68	13.79	6.89	1/minimum stress	0.05	6.27	6.89
1-4	20.68	13.79	6.89	1/minimum stress	0.05	19.30	21.16
1-5	20.68	13.79	6.89	1/intermediate stress	0.05	6.82	7.58
2-1	20.68	10.34	6.89	4/minimum stress	0.05	–	–
2-2	20.68	10.34	6.89	4/minimum stress	0.1	12.41	14.47
2-3	20.68	10.34	6.89	4/intermediate stress	0.1	6.89	7.62

of the perforation. Therefore, the fracture will be initiated on this suface.

The fracture initiation plane is always normal to minimum principal stress around the perforation tunnel; however, the plane of fracture initiation is not necessarily along the perforation axis but in general makes an angle β with this direction. It is possible to use the Mohr circle method to calculate this angle through the following equation:

$$\beta = 0.5 \tan^{-1}\left(\frac{2\tau_{z\theta(\mathrm{cr})p}}{\sigma_{\theta(\mathrm{cr})p} - \sigma_{z(\mathrm{cr})p}}\right) \quad (7)$$

Here, subscript (cr) denotes a critical point θ_{cr} on the circumference of the perforation tunnel, where the minimum principal stress exists; therefore, the fracture will initiate at this point. The near-wellbore fracture geometry can be established considering angle β together with well, perforation, and PFP directions. Therefore, this angle can be used to select the best perforation orientation in order to lessen the near-wellbore fracture tortuosity, and consequently decrease the chance of screen out.

Generally, the analytical model divides the perforation length into some increments and calculates the stress distribution at the surface of each section all around the perforation circumference. After that, it calculates the FIP at each increment, and also evaluates the location and angle of the initiated fracture. The minimum possible FIP along the perforation tunnel will be considered as the FIP of the fracturing operation.

5 Results and Discussion

In this study eight mortar samples were tested, five 10 cm and three 15 cm cubic blocks. One of the 10 cm samples had no perforation; an open hole without any perforation was tested as a base case. Each of the other 10 cm samples had one perforation, either in the direction of intermediate or minimum stress. Each 15 cm sample had four perforations in two rows, being 180° apart from each other. Table 2 summarizes the experimental parameters including applied stresses to the samples.

As is mentioned in previous section, two pressures were recorded while the fracturing fluid was injected into the wellbore. The first pressure was measured before the chock and the second one was measured after the chock, just at the entrance of the wellbore. As the length of the wellbore is quite short, there would be very little frictional pressure drop along its length, considering the very low injection flow rate which was applied; therefore, the pressure recorded after the chock could be considered the fracturing pressure.

The pressure reading before the chock was used as a guide for estimating the initiation and break down pressures. Basically, when the wellbore is pressurized, both pressures are increasing; however, when the fracture initiates, some small fissures are created and, therefore, the rate of increase in wellbore pressure reduces.

In this situation, due to the existence of the chock, the pressure record before the chock does not sense this reduction and increases more than the pressure recorded after the chock. Therefore, the point at which the two pressures begin to deviate from each other is the fracture initiation point (Sarmadivaleh 2012). Figure 3 shows a pressure-time curve which was recorded during test 1-2. The corresponding injection flow rate curve is also shown in the same figure. The fracture initiation point is clearly visible in this figure and that is where the two pressure recordings deviate from each other. In this figure the break down point is shown as the maximum wellbore pressure.

In Fig. 3 the fracture propagation interval is also shown. Some pressure fluctuations are seen in this figure, which is believed to be due to the failure of some sections of the glue around the casing, or the presence of some possible air bubbles in the fracturing fluid.

After conclusion of each test, the sample was taken out of the TTSC and was carefully broken apart along the

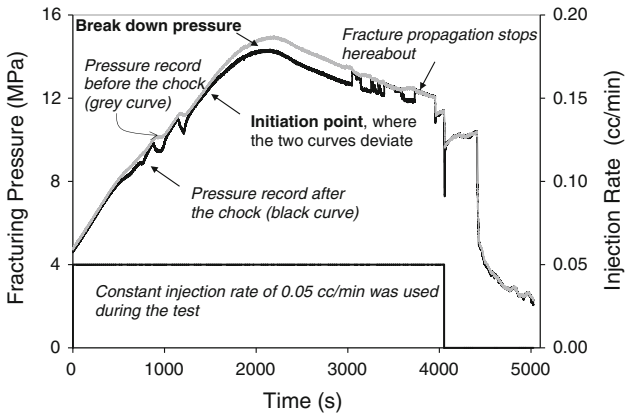

Fig. 3 Pressure-time curve for test 1-2, showing various pressures during fracturing test

Table 3 Various wellbore directions and stress regimes for tests 1-2 and 1-3

Test no.	Wellbore direction	Stress regime	Perforation direction
1-2	Horizontal	Reverse	Min. horizontal
		Strike slip	Vertical stress
	Vertical	Normal	Max. Horizontal
1-3	Horizontal	Reverse	Vertical stress
		Strike slip	Min. horizontal
	Vertical	Normal	Min. horizontal

induced fracture plane, and then the fracture planes were photographed and the geometries of the fractures were analyzed. Table 4 presents a brief description of the fracture geometries.

5.1 Stress Regime and Wellbore Direction

Three independent normal stresses were applied on each sample. The direction of maximum stress was selected to be always parallel to the axis of the borehole; so that various in situ stress regimes and wellbore directions (vertical or horizontal) could be analyzed. Each test may represent three real field scenarios.

For instance, in test 1-2, the direction of perforation was parallel to the intermediate stress, and the maximum stress was applied along the wellbore direction; therefore, this single test could be compared to (a) a vertical wellbore in a normal stress regime area, where the perforations are in the direction of maximum horizontal stress, (b) a horizontal wellbore in a reverse fault stress regime area, where the perforations are oriented to the direction of minimum horizontal stress, and (c) a horizontal wellbore in a strike slip stressed region, where the perforations are aligned with the direction of vertical stress. Table 3 presents various

Table 4 Description of induced fracture geometries in different tests

1-1	Multiple fractures were initiated and propagated mostly perpendicular to the direction of minimum stress. The fractures are propagated on both sides of the wellbore; however, they are typically located in the bottom section of the block
1-2	A fracture plane was developed from the beginning of the perforation, but it is not aligned with the axis of the perforation. It is also developed on the other side of the wellbore. Both fracture wings are not perpendicular to the direction of minimum stress close to the wellbore wall; however, as they propagate away from the wellbore, they turn towards PFP
1-3	The sample had some interior natural fractures before doing the test; therefore, the fracturing fluid just opened the natural fractures and flowed through them
1-4	Multiple fractures and fracture turning and twisting are the main feature of this sample. Fractures were opened against the intermediate stress and then propagated towards PFP
1-5	A planar fracture was created along the axis of the perforation on both sides of the wellbore in PFP; however, the wing of the fracture, which is developed in perforation, is stopped from being propagated to the boundary of the sample
2-1	After 9,000 s of injection, the initiated fractures did not reach the boundary of the sample so a higher injection rate was required; therefore, the sample was left for another fracturing test
2-2	A single fracture plane was developed against the maximum stress, initiating from one of the perforations at the bottom of the sample, and then it changed its direction towards the other two stress directions
2-3	Along the axis of each perforation, one fracture was initiated, which were later joined each other and formed an almost a planar fracture in PFP

wellbore directions and stress regimes that can be considered for two different tests 1-2 and 1-3.

Test 1-4 represents a vertical wellbore in a normally stressed formation, where its perforation is along the direction of minimum horizontal stress. A comparison between this test and test 1-5, which represents a horizontal wellbore in a reverse fault stressed layer with a perforation along the direction of minimum horizontal stress, shows that, while in both scenarios the perforations are in the same direction, the fracture initiation and breakdown pressures in test 1-4 are almost three times larger than that of test 1-5. Additionally, in terms of near-wellbore fracture geometry, test 1-4 shows multiple fracturing and fracture tortuosity, while it is seen that the fracture created in test 1-5 is almost planar. Figure 5 shows the view of the sample with the location of induced fracture planes in these two tests, and Table 4 presents a description of fracture geometries for each test.

For comparison purposes, analytical models were developed in Matlab® to study the stress profiles and determine the location of fracture initiation point along the perforation tunnel. The mortar sample properties (Table 1) and the amount of applied stresses were the input data into

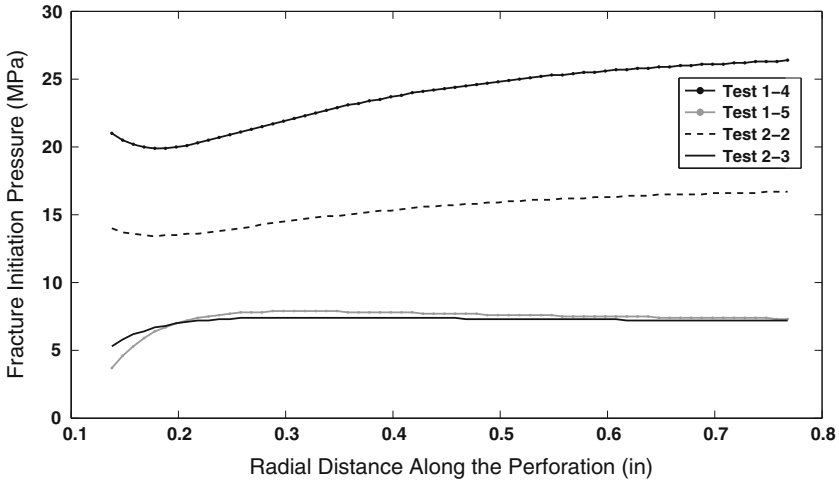

Fig. 4 FIP along the perforation tunnel for four different tests

the analytical simulator. Figure 4 presents the changes in FIP along the perforation tunnel length for four different tests. As is seen in this figure, the minimum pressure for initiating a fracture in test 1-4 is 20 MPa which is very close to the FIP that was measured in the lab (i.e., 19.3 MPa). This close agreement shows the benefits of using analytical models as a starting point when studying hydraulic fracturing from a perforated wellbore. Also it should be mentioned that, the curve corresponding to test 1-4 in Fig. 4 shows that the fracture has not been initiated at the intersection point of the perforation and wellbore, but at a distance away inside the perforation hole.

The breakdown pressure (BDP) in test 1-4 was 21.16 MPa. According to the results of Fig. 4, when the wellbore pressure reaches the BDP, it appears that some additional fracture planes have been initiated along the perforation tunnel: this is because the BDP is larger than the FIPs at some other sections of the perforation hole. This has resulted in multiple fracturing, which was observed in this test. From Fig. 4 the FIP for test 1-5 is 5.3 MPa which is close to the experimental result (i.e., 6.82 MPa). In addition, the results of this figure shows that the fracture was initiated at the intersection of the perforation hole and wellbore wall.

The difference between FIP and BDP in test 1-5 is less pronounced than that of test 1-4, which resulted in observing less multi-fractures created in various sections of the perforation tunnel. Instead, more planar fracture has been formed along the perforation tunnel. As a conclusion, from the above findings it appears that the lower the differences between FIP and BDP, the less the chance for having multi-fracturing.

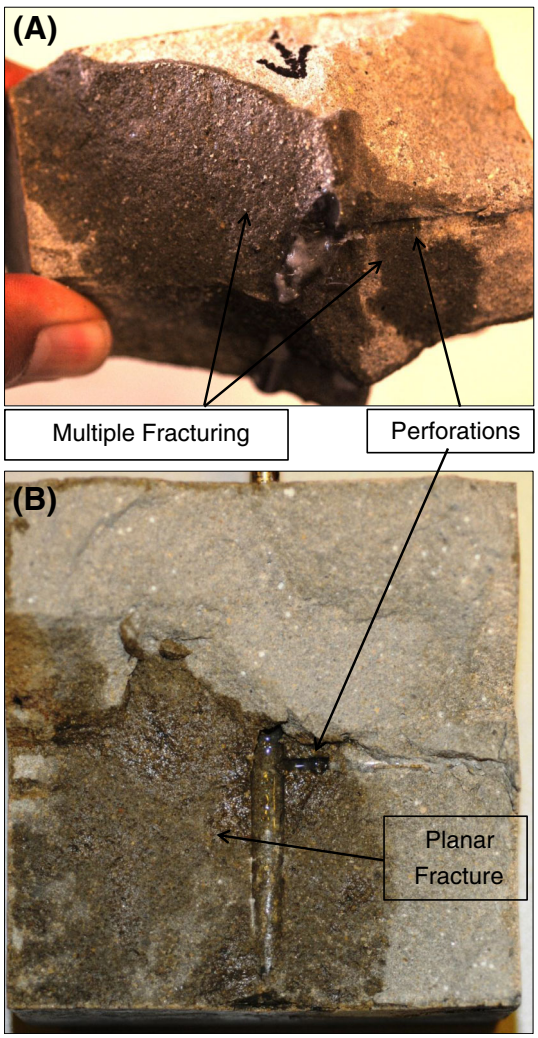

Fig. 5 **a** Multiple fracture planes and fracture turning in test 1-4 and **b** development of a planar fracture in test 1-5

5.2 Stress Anisotropy

The effect of stress anisotropy in the experiments performed in this study was noticeable. It was observed generally that when stress anisotropy increases, larger initiation and breakdown pressures are expected. Tests 1-4 and 2-2 have the same perforation orientation with respect

to the applied stresses. A comparison between the fracturing pressures of these two tests shows that test 2-2 has experienced a lower fracturing pressure because of lower stress contrast. Comparing the results of test 1-2 and 2-3 will lead to the same conclusion.

Very similar results are obtained from the analytical calculations. Figure 4 shows a pressure of 13 MPa as the FIP in test 2-2, which is in good agreement with the experimental result (i.e., 12.41 MPa). As is seen in Fig. 5, in comparison to test 1-4, test 2-2 has lower FIP along the perforation tunnel; however, tests 2-3 and 1-5 have almost the same FIPs. Similar results were obtained from the experiments. Comparing the fracturing pressures of tests 1-5 and 2-3 in Table 2, which have similar perforation orientation and fracture geometries (both have planar fractures), it is seen that they have very similar pressures because their planar fractures are opened against the minimum stress direction, and the value of this stress is the same in both tests.

As an outcome of the results obtained above, it is seen that, when the perforations are aligned with the intermediate stress direction, the stress anisotropy does not have a pronounced influence on fracturing pressures; however, when it is in the direction of minimum stress, stress anisotropy will have a great influence on fracturing pressures. In other words, depending on the perforation direction, if the stress anisotropy is associated with the values of those stress components which are perpendicular to the axis of the perforation, the perforation stress distribution will be affected to some extent; therefore, the fracturing pressure will also be influenced. Pater (1999) found that an increase in stress anisotropy reduces the probability of the link-up of the initiated fractures from various perforations; however, he did not mentioned anything about the effect of stress anisotropy on fracturing pressure.

5.3 Perforation Orientation

Based on the presented results, it is observed that the orientation of the perforation around the wellbore can greatly affect the fracture initiation and near-wellbore propagation pressures. This is basically as a result of stress redistribution due to the existence of a perforation tunnel. The wellbore stress distribution has a great impact on perforation stress profile, and because the wellbore stress distribution is a function of the angle around the wellbore, the direction of the perforation tunnel will affect the perforation stress profile.

In test 1-4 the perforation was aligned with the direction of minimum stress; therefore, two other stresses were perpendicular to the axis of perforation tunnel. This caused a very high-stress concentration around the perforation and, therefore, the fracturing pressures increased significantly. In test 1-5, where the perforation was run along the intermediate stress direction, the minimum and maximum stresses were perpendicular to the axis of perforation. So the fracture was initiated and propagated at much lower pressures. The same results are obtained from the analytical simulation (Fig. 4).

An evaluation of the results of tests 2-2 and 2-3 yields similar conclusions. The FIP in test 2-2, where the perforations are oriented towards the minimum stress direction, is 12.41 MPa, whereas it is 6.89 MPa for test 2-3, in which the perforations are in the direction of intermediate stress.

Using the analytical model, FIPs have been developed for various perforation orientations (PO). The PO is measured from the direction of intermediate stress; this could be the maximum horizontal stress for a vertical wellbore that is drilled in a normal stress regime field. As it is demonstrated in Fig. 6, as the angle between the perforation orientation and the intermediate stress increases, FIP rises along the perforation tunnel. In addition, the location of fracture initiation moves from the wellbore and perforation intersection point (for PO = 0) towards the interior of the perforation tunnel (for PO = 90).

In addition, the near-wellbore geometry of the fracture is affected by orientation of perforations. Multiple fracturing and fracture tortuosity are the consequences of an improper perforation orientation. This is clearly visible in Fig. 5 where the fracture planes corresponding to tests 1-4 and 1-5 are shown. Multiple fracturing and fracture turning are observed in test 1-4, whereas the sample in test 1-5 experienced development of a planar fracture.

The effect of multiple fracturing can also be monitored on pressure-time curves. Figure 7 shows the pressure-time curve corresponding to test 1-4, which has several multiple fractures. The sequence of fracture development is clearly seen in this figure. One of the fractures was opened approximately against the maximum stress direction, which is detected by the maximum pressure reading on the plot.

Another example of a perforation misalignment which caused severe near-wellbore fracture tortuosity was seen in test 2-2. In this test, a 15 cm block with four perforations penetrated in the direction of minimum stress was tested. In this experiment, a fracture was initiated from one of the perforations at the bottom of the sample. Figure 8a shows a view of the developed fracture plane in this test. The fracture plane was firstly opened horizontally in a plane perpendicular to the maximum stress direction; therefore, a large fracture break down pressure was recorded (14.47 MPa). Then the fracture turned towards the vertical plane, to which the intermediate and minimum stresses are applied. Near the boundary of the sample, the fracture was almost in the PFP direction.

Figure 8b shows the fracture plane corresponding to test 2-3. As is seen in this figure, a planar fracture is developed.

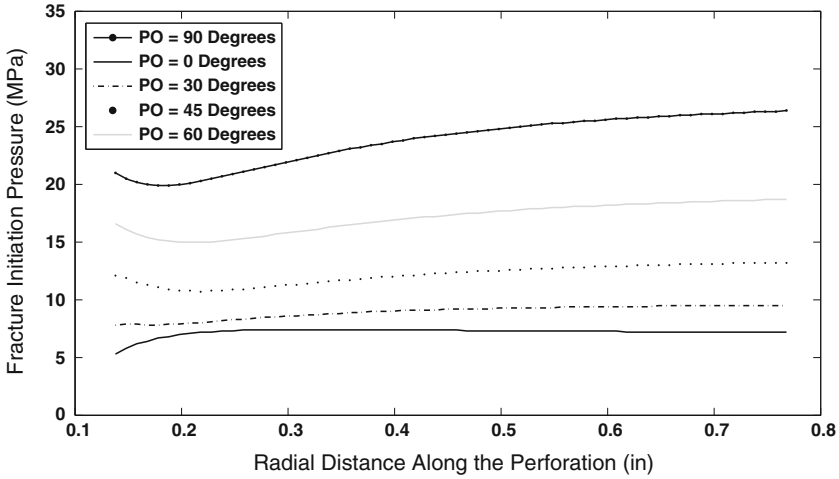

Fig. 6 FIP along the perforation tunnel for various perforation orientations (PO) with respect to intermediate stress direction

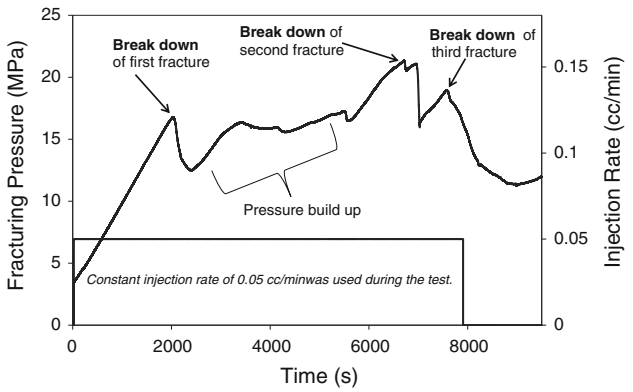

Fig. 7 Multiple fracturing observed in test 1-4 is tracked on its pressure-time curve

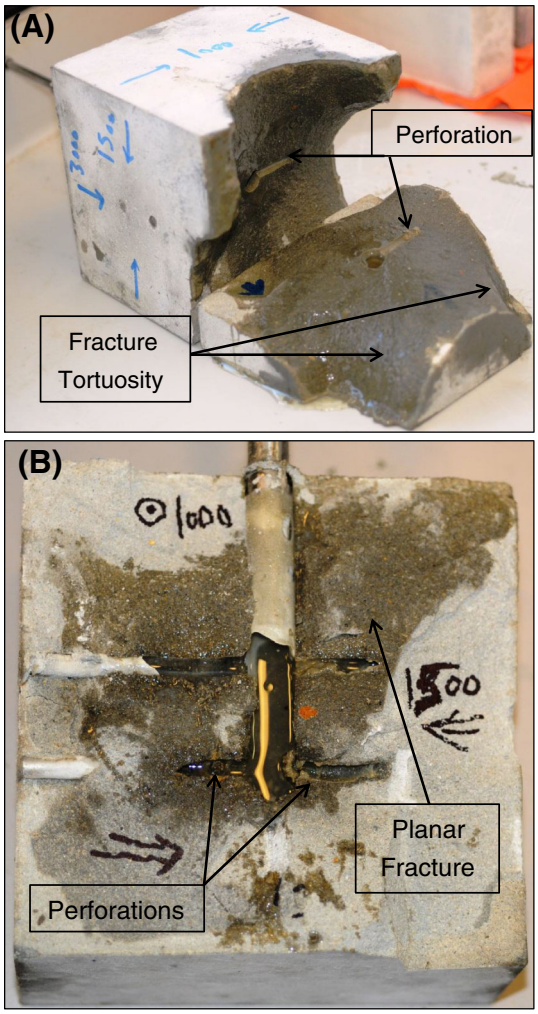

Fig. 8 **a** Fracture turning observed in test 2-2, due to perforation misalignment and **b** planar fracture developed in test 2-3

Initially, fractures are initiated from each perforation, and then they are linked up to each other in order to form the main fracture plane.

Based on the analytical model, which was presented in Sect. 4, the initiated fracture from a perforation hole could have an angle β with the axis of the perforation. This angle can be estimated for any fracture plane initiating along the perforation tunnel, which may help in determining the potential for having tortuous fracture plane growth around the wellbore wall. Figure 9 shows the fracture initiation angle for various perforation orientations. As it is seen from this figure, angle β would be zero for any fracture initiated at a perforation that makes an angle 0° or 90° with respect to intermediate stress. This means that all the initiated fractures in these specific perforation orientations would be aligned with the axis of the perforation. This is also the observation from Fig. 5, where the initiated fractures corresponding to tests 1-4 and 1-5 are shown. The perforation tunnel in test 1-4 has an angle of 90° to the direction of intermediate stress, whereas this angle for test 1-5 is 0°. For both of these tests, the initiated fracture is aligned with the axis of the perforation tunnel. Figure 9 also demonstrates that for PO other than 0° and 90°, angle β gets larger as the initiated fracture departs farther from

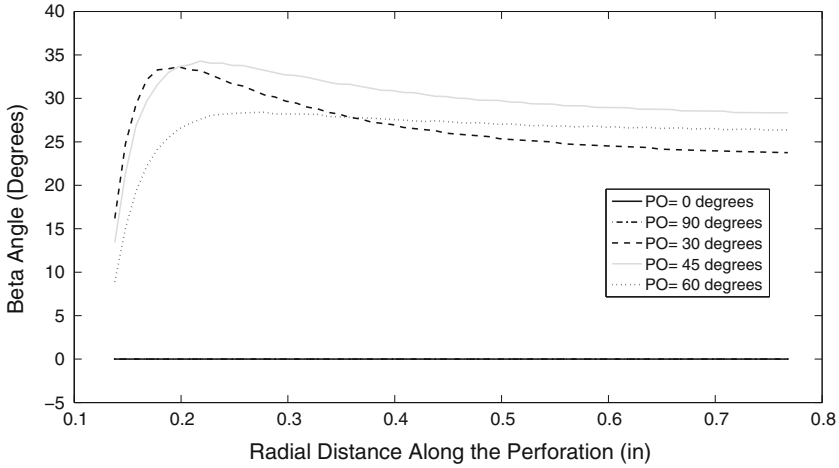

Fig. 9 Fracture angle (β) with respect to perforation axis for various perforation orientations (PO)

the wellbore wall, and this could result in tortuous fracture propagation near-wellbore.

It is also interesting to note that the sample used in test 1-1 has no perforation, and a FIP of 10.68 MPa was recorded in this test. In comparison, in test 1-4 with having one perforation in the direction of minimum stress, an initiation pressure of 19.3 was observed. This shows that, although both tests were conducted in open holes, representing a situation where the cement sheath has failed, the presence of perforation in an improper direction can significantly increase the fracturing pressure.

Additionally, if one compares the fracturing pressures of test 1-1 with that of test 1-5, it is seen that the existence of perforation in test 1-5, which was aligned with the direction of intermediate stress, caused a reduction in initiation pressure: this is a reduction from 10.68 MPa in test 1-1 to 6.82 MPa in test 1-5. This means that, even in an open hole, the existence of a perforation in an appropriate direction can greatly reduce the fracturing pressures.

6 Conclusions

The results of experimental and analytical investigations presented in this study showed that in a perforated wellbore, which is drilled in a tight formation, an increase in the stress anisotropy will affect the fracturing pressures. The stress anisotropy generated from the stress components in the directions perpendicular to the perforation axis will influence the FIP, i.e., the stress magnitude along the perforation tunnel is neutralized. The larger this anisotropy ratio the greater the initiation pressure will be.

The results of this study also indicated that the effect of the direction of a wellbore on fracturing mechanism in a perforated wellbore should be analyzed while the prevailing stress regime is considered. A vertical wellbore in a normally stressed formation with perforations along the direction of minimum horizontal stress requires larger initiation pressures (both FIP and BDP) compared to when a perforation penetrates in the direction of minimum horizontal stress in a horizontally drilled wellbore in a reverse fault regime area. It is important to note that in both cases the perforations are in the same direction.

From the lab test and analytical results it was observed that when the perforations are oriented in a direction such that the intermediate and maximum stresses are perpendicular to the axis of perforations, larger fracture initiation and breakdown pressures will be required compared to any other orientations chosen for the perforations. This in turn results in a higher chance for development of multiple fracturing planes around the perforation tunnel. Also, it was found that the lower the difference between FIP and BDP, the less the chance for having multiple fracturing. Additionally, it was observed that the direction of the perforation can affect the angle between the initiated fracture and the perforation axis (β).

Simulations of perforation in open hole condition was considered to mimic the situation where the cement sheath has lost its integrity in cased hole perforation. The results of simulations in this case indicated that the existence and orientation of the perforation tunnel play a noticeable role in fracture initiation pressure. For example, the results showed that a perforated wellbore, in which the perforations are aligned with the direction of minimum stress, though the cement sheath failed, will experience larger fracturing pressures in comparison to an open bore hole.

References

Abass H, Brumley J, Venditto J (1994) Oriented perforations—a rock mechanics view. In: SPE annual technical conference and exhibition

Atkinson C, Eftaxiopoulos D (2002) Numerical and analytical solutions for the problem of hydraulic fracturing from a cased and cemented wellbore. Int J Solids Struct 39(6):1621–1650

Aud W, Wright T, Cipolla C, Harkrider J (1994) The effect of viscosity on near-wellbore tortuosity and premature screenouts. In: SPE annual technical conference and exhibition

Behrmann L, Elbel J (1991) Effect of perforations on fracture initiation. J Petrol Technol 43(5):608–615

Behrmann L, Nolte K (1999) Perforating requirements for fracture stimulations. SPE Drill Complet 14(4):228–234

Bunger AP (2005) Near-surface hydraulic fracture. In: Major: geological engineering, University of Minnesota

Cleary M, Johnson D, Kogsbøll H, Owens K, Perry K, Pater C, Alfred S, Holger S, Mauro T (1993) Field implementation of proppant slugs to avoid premature screen-out of hydraulic fractures with adequate proppant concentration. In: Low permeability reservoirs symposium

Daneshy A (1973) Experimental investigation of hydraulic fracturing through perforations. J Petrol Technol 25(10):1201–1206

Davidson B, Saunders B, Robinson B, Holditch S (1993) Analysis of abnormally high fracture treating pressures caused by complex fracture growth. In: SPE gas technology symposium

Detournay E (2004) Propagation regimes of fluid-driven fractures in impermeable rocks. Int J Geomech 4(1):35–45

Fallahzadeh SH, Shadizadeh SR (2013) A new model for analyzing hydraulic fracture initiation in perforation tunnels. Energy Sources Part A Recover Utili Environ Eff 35(1):9–21

Fallahzadeh SH, Shadizadeh SR, Pourafshary P (2010) Dealing with the challenges of hydraulic fracture initiation in deviated-cased perforated boreholes. In: Trinidad and Tobago energy resources conference

Fjar E, Holt RM, Raaen A, Risnes R, Horsrud P (2008) Petroleum related rock mechanics, vol 53. Elsevier

Lehman L, Brumley J (1997) Etiology of multiple fractures. In: SPE production operations symposium

Lhomme TPY (2005) Initiation of hydraulic fractures in natural sandstones. In: Delft University of Technology

Mack MG, Warpinski N (2000) Mechanics of hydraulic fracturing. In: Reservoir stimulation, pp 6–1

Mindess S, Young JF, Darwin D (2003) Concrete

Nelson EB (1990) Well cementing. Elsevier

Pater C (1999) Impact of perforations on hydraulic fracture tortuosity. Old Prod Facil 14(2):117–130

Rasouli V (2012) A true triaxial stress cell (TTSC) used for simulations of real field operations in the lab. True Triaxial Test Rocks 4:311

Romero J, Mack M, Elbel J (1995) Theoretical model and numerical investigation of near-wellbore effects in hydraulic fracturing. In: SPE annual technical conference and exhibition

Sarmadivaleh M (2012) Experimental and numerical study of interaction of a pre existing natural interface and an induced hydraulic fracture. Curtin University

Thiercelin M, Dargaud B, Baret J, Rodriguez W (1997) Cement design based on cement mechanical response. In: SPE annual technical conference and exhibition

Weng X (1993) Fracture initiation and propagation from deviated wellbores. In: SPE annual technical conference and exhibition

Paper 4: *Challenges in hydraulic fracturing from perforated boreholes in unconventional reservoirs.*

Challenges in hydraulic fracturing from perforated boreholes in unconventional reservoirs

Lead author
Seyed H. Fallahzadeh

S.H. Fallahzadeh and V. Rasouli
Department of Petroleum Engineering
Curtin University of Technology
613 (Rear), Level 6, ARRC
26 Dick Perry Ave, Kensington
Perth WA 6151
s.hasan.fallah@gmail.com

ABSTRACT

In recent years, with the evolution of unconventional reservoirs, hydraulic fracturing has been applied to tight sandstone and shale formations to improve the hydrocarbon production. The application of hydraulic fracturing in cased boreholes is always associated with many difficulties because the fracture has to be initiated from the perforations. There have been many cases of improper fracture initiation in tight formations, which have then resulted in premature screen out, and have not improved reservoir production.

In this study, initiation of hydraulic fracturing from a perforated tunnel was studied numerically using a finite element method. The numerical model was generated to represent a laboratory experimental test, which has been carried out on tight concrete cubic samples. A perforated wellbore in a linearly elastic tight formation was modelled using Abaqus software through three-dimensional numerical analysis. Two different perforation orientations were considered to analyse the fracture initiation pressure (FIP) and the location and initial direction of the crack. Different far field stresses were considered to study the effect of in-situ stresses and perforation directions on the fracture initiation mechanism. The results were then compared to laboratory and analytical outcomes, and good agreement was observed. The results provide a better understanding on how the stress regime, stress anisotropy, and perforation orientation could affect the pressure and geometry of fracture initiation in tight formations. Based on the outcomes of this study, better strategies can be decided for perforating a cased wellbore in a tight formation so that lower FIP is experienced and a better near wellbore fracture is created.

KEYWORDS

Fracture initiation pressure, perforation tunnel, near wellbore geometry, tight formation.

INTRODUCTION

The application of hydraulic fracturing in unconventional reservoirs has increased throughout the last decade due to its use in low permeability reservoirs, such as gas shales and tight sandstones. The use of such a stimulation technique in perforated boreholes is still a challenging subject due to the complexity of parameters involved. Problems like high near wellbore friction and premature screen-out may be observed from a perforation tunnel during hydraulic fracturing. (Cleary et al, 1993; Aud et al, 1994). In addition, abnormally high operating pressures (Davidson et al, 1993) and development of multiple fracture planes are other operational concerns during hydraulic fracturing (Lehman and Brumley, 1997). These are more challenging in perforated boreholes, where the presence of perforations causes a complex mechanism of fracture initiation and near wellbore propagation (Behrmann and Elbel, 1991; Abass et al, 1994). This could potentially lead to weak hydraulic fracturing treatment and consequently a substantial reduction in production rate.

Many researchers have studied different aspects of hydraulic fracturing in a perforated wellbore and its near wellbore effects. Behrmann and Nolte (1999) conducted an experimental study and found that when the perforation gun orientation is not properly selected and/or when the directions of the in-situ stresses are not accurately known, the width of the fracture near the wellbore would be mostly less than that of the main body of the fracture. This is due to the fact that the magnitudes of induced stresses are larger near the wellbore compared to in-situ stresses. Almost the same results were obtained through a theoretical and numerical investigation conducted by Romero et al (1995). In another experimental study done by Behrmann and Elbel (1991), they recognised that there are three major factors influencing the fracturing mechanism in cased holes; formation pore-pressure, pressurisation of the annulus, and perforation orientation in relation to the preferred fracture plane (PFP) (the minimum in-situ stress is perpendicular to this plane). In their experiments, they observed that when the perforation phasing was deviated more than 10° away from the direction of the PFP, the fracture plane may not initiate from the perforations and the fracturing fluid would break down the cement sheath behind the casing, which in turn results in the formation of a pinch point.

Atkinson and Eftaxiopoulos (2002) applied analytical and numerical methods to study fracture propagation in a cased cemented wellbore. Using a two-dimensional plane model they concluded that when the cement sheath bonding to the casing and rock has failed, no fracture turning would occur and higher pressure is required. Weng (1993) also investigated fracture initiation and propagation using numerical modelling analysis and found that the initiated fracture plane has a tortuous path in a distance, not more than few wellbore radii, close to the wellbore. Similar results have also been reported by Abass et al (1994). In an analytical study carried out by Fallahzadeh et al (2010), they estimated the wellbore and perforation stress distributions for a porous homogenous elastic formation. They showed that by altering the orientation of the perforation relating to the tensile zone developed around the wellbore, the fracture initiation pressure greatly increases.

In this study a three-dimensional numerical model is developed using the finite element method. Abaqus software is used to generate and analyse a perforated wellbore in an elastic tight formation. The main approach of the study is to construct some models which could be used to simulate a series of scaled hydraulic fracturing tests performed in perforated boreholes on very low permeablity mortar samples.

A true triaxial stress cell (TTSC) was used to apply three independent stresses on 10 cm and 15 cm cubic mortar samples, while a fluid with a viscosity of 97,700 cp was injected at very low flow rate (0.05–0.1 cc/min) through the borehole and perforations located at the centre of the sample. Fracture initiation and near wellbore propagation were analysed by precisely interpreting the pressure-time curves.

This study is one of the very first attempts to investigate the process of hydraulic fracture initiation and near wellbore propagation in tight formations. The results of the numerical modelling are also compared with a recently developed analytical model (Fallahzadeh et al, 2010; Fallahzadeh and Shadizadeh, 2013), which was further expanded and improved to analyse the process of fracture initiation in elastic homogenous tight formations. This model determines the stress distribution around the wellbore and uses this data to compute the stress distribution along the perforation cavity. The numerical model predicts the fracture initiation pressure (FIP), the location of the first crack developed in the perforation tunnel and the angle of the initiated fracture relating to the perforation axis. Two different perforation orientations are considered, and various in-situ stress regimes and stress anisotropies are assumed to perform the analysis. In the following sections, the numerical modelling and experimental set-up are presented and the results are compared with analytical solutions.

EXPERIMENTAL SET-UP

In this section the hydro-mechanical properties of the samples used in this study are presented. The paper then defines the material model used in numerical modelling. In addition, a brief description of scaling analysis is given.

Sample properties

Sample properties define the material model to be used in the numerical modelling. The experiments were conducted on synthetic samples whose mechanical properties are similar to typical tight formations. A consistent sample preparation procedure was established for the objectives of this study, which is explained in another paper (Fallahzadeh et al, 2013). 10 and 15 cm cubic samples were prepared to be fractured hydraulically; Figure 1 shows a schematic of the 15 cm cubic sample before fracturing tests. Hydro-mechanical properties of the samples are needed to conduct the scaling analysis. Sarmadivaleh (2012) used cylindrical samples for doing a range of tests using a triaxial machine and porosity-permeability apparatus to measure these properties. A summary of the hydro-mechanical properties of the samples used in this study is presented in Table 1. As seen from this table, the permeability of the samples is 0.018 mD, which is a very low value, corresponding to tight formations.

When casing is cemented in a borehole, on many occasions the bonding between the casing and cement sheath, or the cement sheath and the formation, is weak. This may be due to the presence of residual mud cake which prevents proper cement bonding and/or shrinkage of the cement after it sets, thus developing some fissures in the cement sheath (Nelson, 1990; Thiercelin et al, 1997). In addition, the variation of downhole conditions throughout the life of the wellbore can cause crack development in the cement sheath (Thiercelin et al, 1997). Also, when the wellbore is pressurised during fracturing operation, some micro-annulus may be created, especially if the perforations are not aligned in proper orientation (Romero et al, 1995). These sets of experiments, therefore, were carried out on open hole perforated samples to simulate the fracturing mechanism in a cased perforated borehole, where commonly a micro-annulus is created in the cement.

True triaxial stress cell (TTSC)

A true triaxial stress cell (TTSC) was used for conducting the fracturing tests (Rasouli, 2012). Figure 2 shows a top view of the TTSC. The TTSC is capable of receiving cubic samples of 30 cm or smaller. Aluminium or steel spacers are used to fill the gaps between the sample and the rams for the smaller sizes. The sides of the blocks are 2.5% smaller than the sample sizes so that they do not come into contact when large displacements are expected for the sample.

A specific pump with a flow rate of 0.05–0.1 cc/min was used for injecting the fracturing fluid into the wellbore. Two pressure transducers were also installed at the closest possible point to the casing to record the injection pressure, and there was a choke (flow restrictor) in between these two devices.

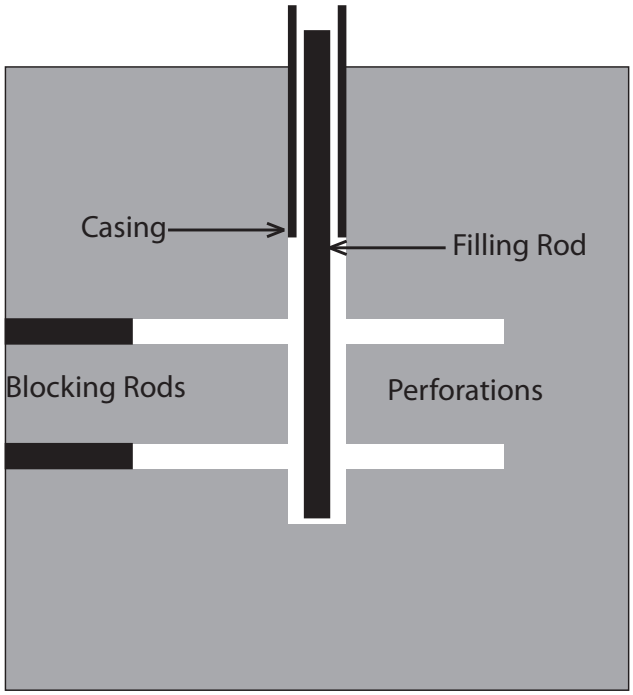

Figure 1. A schematic of 15 cm cubic sample showing a 7 cm open hole with four perforations on the sides of the hole 180°apart from each other.

Table 1. Hydro-mechanical properties of samples used in this study (Sarmadivaleh, 2012).

Property	Value
Uni-axial compressive strength (UCS) (MPa)	79.5
Poisson's ratio	0.19
Young's modulus, E, (GPa)	27.74
Tensile Strength, T_o, (MPa)	3.5
Fracture Toughness, K_{IC}, (MPa$\sqrt{m}$)	0.78
Porosity, Φ, %	14.7
Permeability, K, mD	0.018

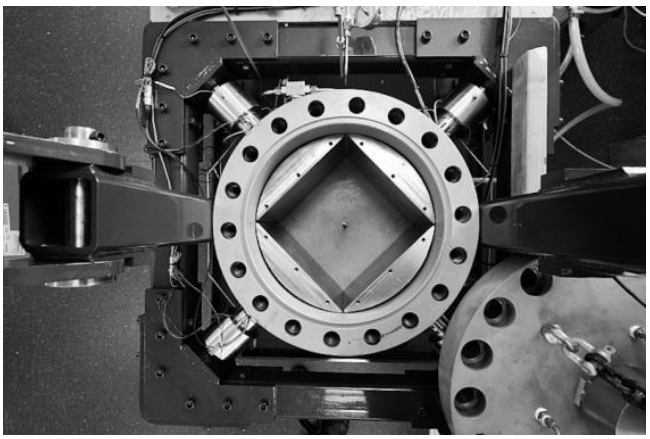

Figure 2. A top view of the TTSC.

The function of the choke was to control the flow of compressed fracturing fluid into a newly initiated fracture allowing a stable fracture growth, especially during the initiation phase (Bunger, 2005).

Scaling analysis

To have a reasonable correspondence between the results of laboratory experiments to field scale operations, dimensional analysis was performed. This is known as scaling laws. The concept of energy dissipation during fracture growth is the fundamental principle of scaling laws (Sarmadivaleh, 2012). In designing a laboratory hydraulic fracturing experiment, the injection rate, fluid viscosity and the total fracture propagation time must be obtained from the scaling analysis. By knowing the sample's hydro-mechanical properties, the required viscosity, flow rate and injection time for running a hydraulic fracturing test can be calculated.

The time at which the wellbore pressurisation rate reaches its maximum value is considered as the fracture initiation point; the moment of fracture initiation is the reference point for scaling the time of the experiment. Fracture breakdown is usually defined as the time at which the wellbore pressure reaches its maximum value. Fracture initiation typically occurs before the breakdown point (Lhomme, 2005). Therefore, the scaled time of a test starts with the time of fracture initiation and will last up to the final stage of injection. In these series of tests a fracturing fluid with a viscosity of 97,700 cp, and flow rates of 0.05 and 0.1 cc/min, were used, and the value of experiment time was constrained to be 5,000 seconds to make sure that the laboratory results are in correspondence with the field operations. The details of scaling analysis are discussed by Fallahzadeh et al (2013).

ANALYTICAL MODELLING

This section briefly explains analytical solutions that have been developed to analyse fracture initiation from a perforation tunnel in elastic homogenous tight formations. Generally, there are three principal stresses in any underground formation, which are due to the weight of overlying layers. In most occasions two of these stress components are in the horizontal direction with the third one being vertical. Elastic wellbore stress distribution formulations have been presented in literature to obtain the cylindrical stress profile around the wellbore. A series of these equations can be found in Fjar et al (2008) and Fallahzadeh and Shadizadeh (2013).

The wellbore stress profile can be used to calculate the distribution of stresses along the perforation tunnel. The steps of such a technique are explained by Fallahzadeh and Shadizadeh (2013). After simulating the stress profile along the perforation, the fracture initiation mechanism and pressure can be analysed. To do so, principal stresses are calculated along the perforation tunnel, and then tensile failure criterion is applied. Because the mortar samples were tested dry, the term related to pore pressure should be ignored (i.e. a zero pore pressure is assumed). This would ensure that the results of analytical simulation can better match the results of experimental study.

Generally, the analytical model divides the perforation length into some increments, and calculates the stress distribution at the surface of each section all around the perforation circumference. After that, it calculates the fracture initiation pressure at each increment, and also evaluates the location and angle of the initiated fracture. The minimum possible FIP along the perforation tunnel will be considered as the FIP of the fracturing operation.

NUMERICAL MODELLING

Compared to 3D, performing 2D numerical simulations could be more time and cost effective; however, less accurate results may be obtained. Several analytical solutions have been derived to formulate the stresses around a borehole in plane-strain (2D) conditions. In this case, the axial dimension of the borehole is assumed to be infinite and the out of plane stress has no effect on in-plane stress components. It should be mentioned that in this case the out of plane stress is a function of in-plane stresses (Sadd, 2009). The analytical solutions can be used, to some extent, to simulate the experimental results; however, because these solutions are constrained to some specific assumptions, they cannot be used for complicated boundary conditions and constitutive models. The numerical simulations should, therefore, be performed.

The hydraulic fracturing laboratory experiments, which were conducted in TTSC, were simulated using Abaqus software. Because of the presence of perforations in the tested blocks, the axis of the borehole could not be considered infinite with respect to the lateral perforation dimension. Therefore, 2D numerical models could not be used. Instead, 3D numerical models were generated to simulate the cubic mortar samples, which were subjected to true triaxial stress conditions, that is, where three independent principal stresses are applied to the samples.

Geometry and boundary conditions

The geometry and boundary conditions of the numerical models were defined based on the sample dimensions and experiment setup. Due to the symmetrical nature of the problem (Fig. 1) only a quarter of the sample was modelled. As a result, smaller numbers of elements were required for the model and, therefore, less time was needed for the simulation to converge. The rotation components and normal displacement of the two symmetric faces were fixed in the model. These two symmetric faces with fixed displacements eliminated the rigid body motion.

The boundary conditions, which were defined for the numerical model, were the same as those applied to the real sample in the laboratory experiments. Three independent stresses were applied to the boundary of the model, and a uniform wellbore pressure was applied to both wellbore and perforation surfaces. Figure 3 shows the geometry and boundary conditions of a model, which is generated to simulate a 10 cm sample. The sizes of the modelled block and its wellbore and perforation are identical to the real 10 cm sample.

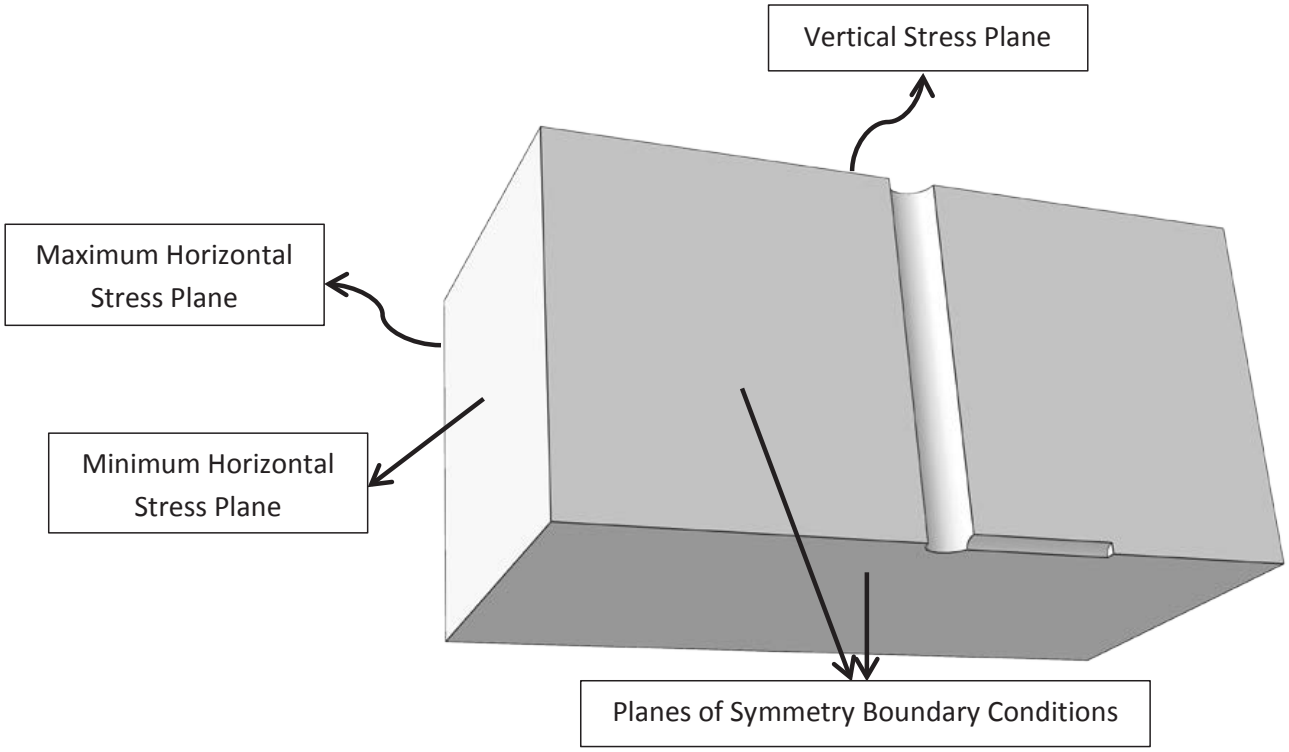

Figure 3. 3D numerical model geometry and boundary conditions for a 10 cm cubic sample.

The wellbore and perforation pressures are simultaneously increased until the first crack, which is a tensile failure, is formed on the surface of the perforation tunnel. The minimum wellbore pressure, which could create the first crack, is the FIP. In addition, the location and angle of the crack with respect to the perforation axis gives an indication of the near wellbore fracture geometry; if the initiated fracture is along the direction of PFP, less fracture tortuosity will be expected.

Elements and mesh

A mesh sensitivity analysis was performed; five different mesh densities were used in the model and the changes in the values of stress components on the wellbore wall were monitored. A linear elastic material with the properties given in Table 1 was generated for this analysis. The model was loaded by uniform lateral and vertical stresses of 5 MPa and the wellbore pressure was zero. The results of each of the five mesh densities are shown in Table 2. As seen in this table, the results of the very coarse, coarse and moderate mesh densities are very different, especially for tangential stress component; however, the results of the fine and very fine mesh densities are almost the same. The convergence of the results is plotted in Figure 4. As shown in this figure, when the number of elements is more than 1.5 million, the accuracy of the results do not change significantly. For a larger number of elements, however, a significant amount of memory and solution time would be required for the model to converge. 1.5 million elements, therefore, were applied to all the models in this study.

Model validation

Elastic analytical solutions are widely used to calculate the stress distribution around a borehole in a plane which is subjected to lateral stresses. These analytical formulations are generally based on plane-strain concepts, in which the axial strain is assumed to be zero. For the validation of the generated 3D numerical model, therefore, a special case of zero axial strain was considered. As the axial load is applied through displacement, it is possible to generate a plane-strain model by putting axial displacement equal to zero. A maximum horizontal stress of 7 MPa and a minimum horizontal stress of 5 MPa are applied to the lateral boundaries of the model, and a wellbore pressure of 5 MPa is loaded on the wellbore surface. The model is run and radial and tangential stress components are obtained in the direction of maximum horizontal stress. The same components of stress are also calculated using analytical solutions (Fjar et al, 2008). The results are compared in Figure 5.

As seen in Figure 5, there is a good agreement between the numerical simulation results and analytical calculations. This shows that the numerical model is a good representation of the real laboratory samples; therefore, the model can be used in various boundary conditions to simulate the experiments.

RESULTS AND DISCUSSION

In this section the results of the numerical modelling are presented, and they are compared with the results of experimental and analytical studies. Table 3 presents the experimental and numerical parameters of four different samples along with their fracturing pressures. As seen in this table, samples 1-4 and 2-2 have perforations along the direction of the minimum stress component; however, sample 1-4 is subjected to higher stress anisotropy. Samples 1-5 and 2-3 also have similar perforation orientation, that is, along the direction of intermediate stress component, but sample 1-5 is under higher stress anisotropy.

When the fracturing experiments were in progress, two pressures were recorded while the fracturing fluid was injected into the wellbore. The first pressure was measured before the choke and the second one was measured after the choke, just at the entrance of the wellbore. As the length of the wellbore is quite short, there would be very little frictional pressure drop along its length, considering the very low injection flow rate which was applied; therefore, the pressure recorded after choke could be considered as the fracturing pressure. The pressure reading before choke was used as a guide for estimating the initiation and break down pressures.

Table 2. Results of mesh sensitivity analysis.

Mesh	Number of elements	Relative (to very coarse results) stress components at wellbore wall	
		Radial stress	Tangential stress
Very coarse	3,637	1.00E+00	1.00E+00
Coarse	11,417	1.00E+00	1.50E+00
Moderate	101,532	1.06E+00	2.60E+00
Fine	519,666	1.11E+00	3.37E+00
Very fine	2,128,115	1.14E+00	3.58E+00

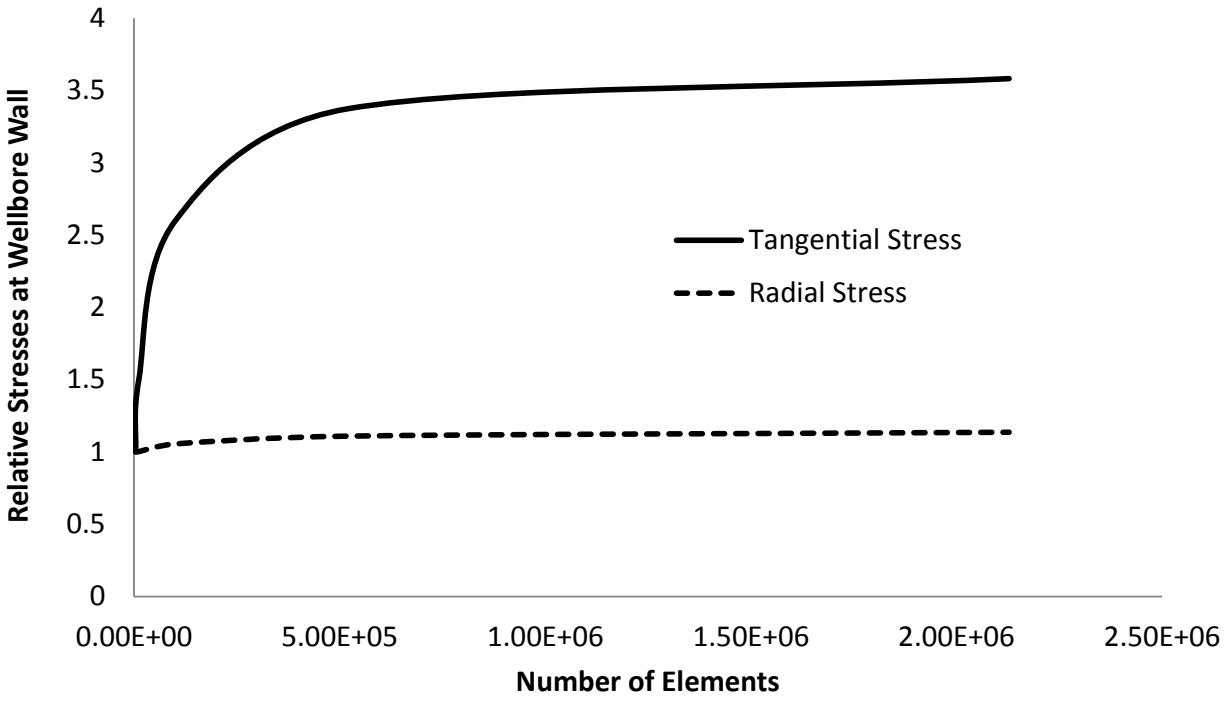

Figure 4. Convergence of the results in a mesh refinement analysis.

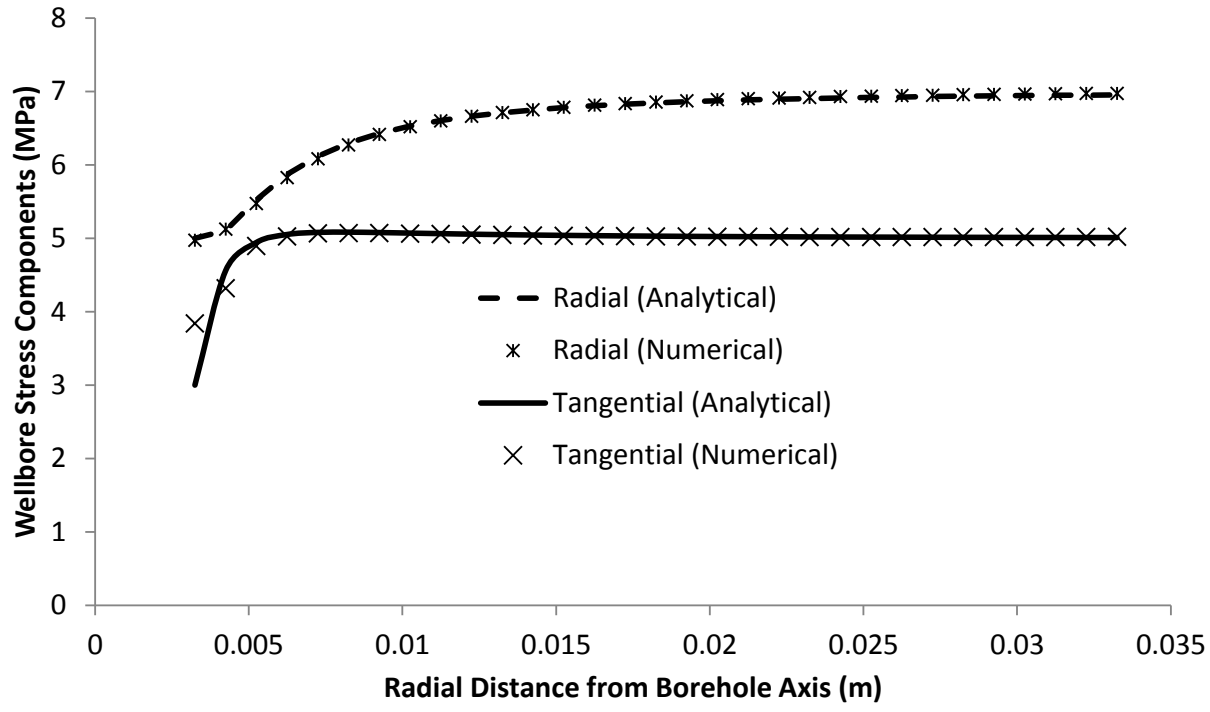

Figure 5. Comparison of numerical simulation results with analytical solution.

Table 3. Experimental and numerical parameters and results.

σ1(MPa)	σ2(MPa)	σ3(MPa)	σ2 to σ3 stress ratio	Perforations orientation	Experimental results		Numerical results
					Initiation pressure (MPa)	Break down pressure (MPa)	Initiation pressure (MPa)
20.68	13.79	6.89	2	Minimum stress	19.30	21.16	20
20.68	13.79	6.89	2	Intermediate stress	6.82	7.58	6.2
20.68	10.34	6.89	1.5	Minimum stress	12.41	14.47	12.1
20.68	10.34	6.89	1.5	Intermediate stress	6.89	7.62	7

Basically, when the wellbore is pressurised, both pressures are increasing; however, when the fracture initiates, some small fissures are created and, therefore, the rate of increase in wellbore pressure reduces. In this situation, due to the existence of the choke, the pressure recorded before the choke does not sense this reduction, and increases more than the pressure recorded after the choke. The point at which the two pressures begin to deviate from each other, therefore, is the fracture initiation point. Figure 6 shows a fracturing pressure-time curve. The corresponding injection flow rate curve is also shown in the same figure. The fracture initiation point is clearly visible in this figure, and is where the two pressure recordings deviate from each other. In this figure the break down point is shown as the maximum wellbore pressure.

In Figure 6 the fracture propagation interval is also shown. Some pressure fluctuations are seen in this figure, which is believed to be due to the failure of some sections of the glue around the casing, or the presence of some possible air bubbles in the fracturing fluid.

The fracture initiation pressures obtained from the numerical modelling are presented in Table 3. A comparison between the experimental and numerical initiation pressures shows that there is a good agreement between the results. For example, sample 1-4 has experienced a fracture initiation pressure of 19.3 MPa at the laboratory to break down, and the numerical model of this sample has predicted a 20 MPa initiation pressure. Similar correspondence can be seen when comparing the other three samples. This shows that the numerical model is capable of predicting the fracture initiation pressures accurately.

During the laboratory experiments, three independent normal stresses were applied to each sample. The direction of maximum stress was selected to always be parallel to the axis of the borehole, so that various in-situ stress regimes and wellbore directions (vertical or horizontal) could be analysed. Each test may represent three different real field scenarios. For example, sample 1-4 represents a vertical wellbore in a normally stressed formation, where its perforation is along the direction of minimum horizontal stress. A comparison between this test and sample 1-5, which represents a horizontal wellbore in a reverse fault stressed layer with a perforation along the direction of minimum horizontal stress, shows that, while in both scenarios the perforations are in the same direction, the fracture initiation and break down pressures in sample 1-4 are almost three times larger than that of sample 1-5. Additionally, using near wellbore fracture geometry, sample 1-4 shows multiple fracturing and fracture tortuosity, while it is seen that the fracture created in sample 1-5 is almost planar. Figure 7 shows a view of the sample with the location of induced fracture planes in these two tests.

From the numerical modelling, for sample 1-4, it was observed that at the initiation pressure, some cracks were created at the top and bottom sides of the perforation. A crack was also opened at the very end of the perforation tunnel, which was perpendicular to the perforation axis; this could cause multiple fracturing and fracture tortuosity. Such near wellbore fracturing pattern was also observed in the laboratory test for this sample (Fig. 7). In comparison, the numerical model of sample 1-5 shows that a fracture was initiated on the top and bottom sides of the perforation, and was along the perforation axis, which would lead to a planar fracture, because the initiated fracture was in the PFP direction. Such a result corresponds to what was seen in the laboratory for sample 1-5, where a planar fracture was created.

For comparison purposes, analytical models were developed in Matlab® to study the stress profiles and determine the location of the fracture initiation point along the perforation tunnel. The mortar sample properties (Table 1) and the amount of applied stresses were the input data into the analytical simulator. Figure 8 presents the changes in FIP along the perforation tunnel for four different samples. As seen in this figure, the minimum pressure for initiating a fracture in sample 1-4 is 20 MPa, which is very close to the FIP that was measured in the lab (i.e. 19.3 MPa). In addition, such initiation pressure is similar to the value obtained from numerical modelling (Table 3). This close agreement shows the benefits of using numerical models as a starting point when studying hydraulic fracturing from a perforated wellbore. Also, it should be mentioned that the curve corresponding to sample 1-4 in Figure 8 shows that the fracture has not been initiated at the intersection point of the perforation and wellbore, but at a distance away inside the perforation hole.

The break down pressure (BDP) in sample 1-4 was 21.16 MPa. According to the results shown in Figure 8, when the wellbore pressure reaches the BDP, it appears that some additional fracture planes have been initiated along the perforation tunnel: this is because the BDP is larger than the FIPs at some other sections of the perforation hole. This has resulted in multiple fracturing, which was observed in this test. From Figure 8 the FIP for test 1-5 is 5.3 MPa which is close to the experimental and numerical results (i.e. 6.82 and 6.2 MPa). In addition, this figure shows that the fracture was initiated at the intersection of the perforation hole and wellbore wall.

Based on the analytical model, the difference between FIP and BDP in sample 1-5 is less pronounced than that of sample 1-4, which resulted in observing less multi-fractures created in various sections of the perforation tunnel. Instead, a more planar fracture has been formed along the perforation tunnel. This is similar to what was observed from the numerical model of sample 1-5, where a fracture was initiated on top and bottom sides of the perforation, and was along the perforation axis.

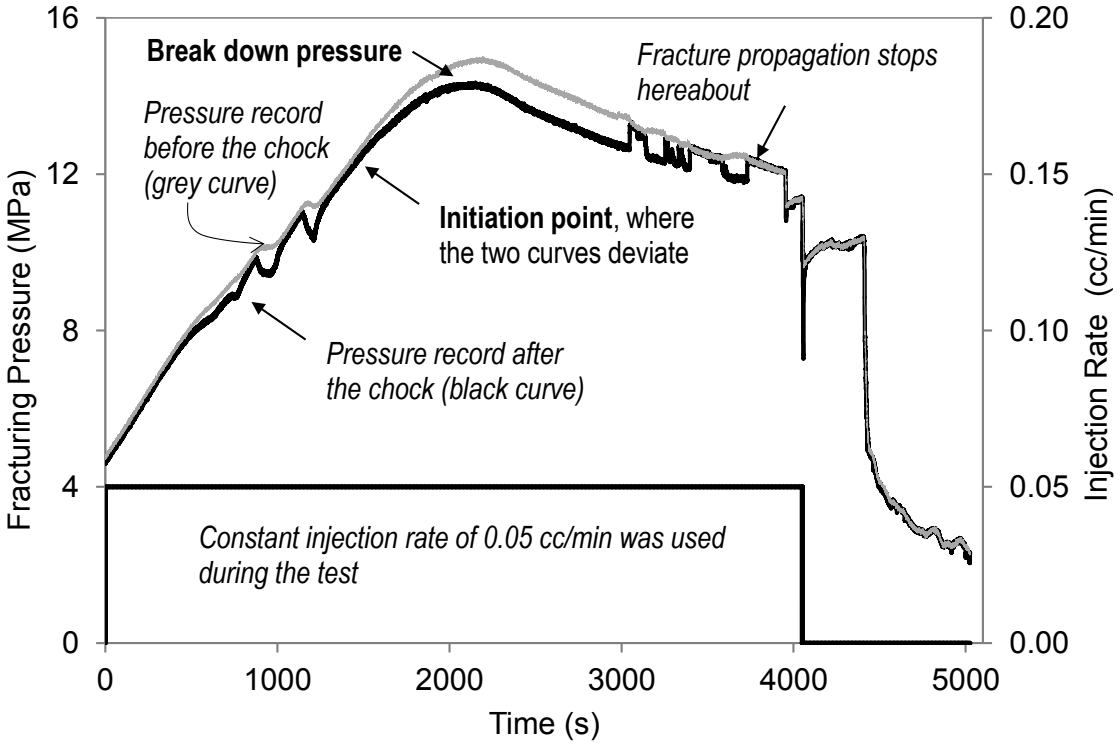

Figure 6. A pressure-time curve, showing various pressures during a fracturing test.

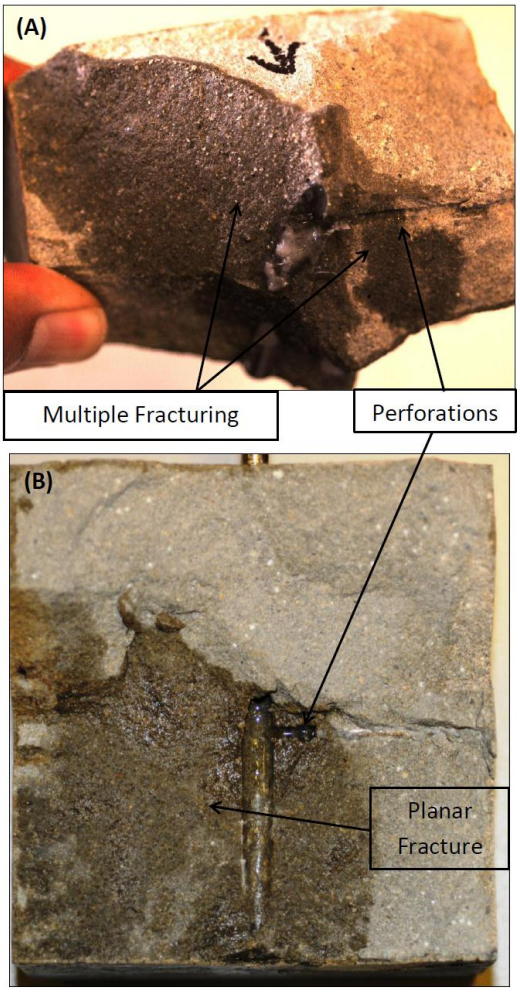

Figure 7. (A) Multiple fracture planes and fracture turning in sample 1-4, (B) development of a planar fracture in sample 1-5.

This would lead to a planar fracture, because the initiated fracture was in the PFP. As a conclusion, from the above findings, it appears that the lower the differences between FIP and BDP, the less chance for having multi-fracturing.

The effect of stress anisotropy was also found to be noticeable in the modelling and experiments performed in this study. It was generally observed that when stress anisotropy increases, larger initiation and break down pressures are expected. Samples 1-4 and 2-2 have the same perforation orientation relating to the applied stresses. A comparison between the fracturing pressures of these two samples shows that sample 2-2 has experienced a lower fracturing pressure, because of lower stress contrast.

Very similar results are obtained from the analytical calculations. Figure 8 shows a pressure of 13 MPa as the FIP in sample 2-2, which is in good agreement with the experimental and analytical results (i.e. 12.41 and 12.1 MPa). As it is seen in Figure 8, in comparison to sample 1-4, sample 2-2 has lower FIP along the perforation tunnel; however samples 2-3 and 1-5 have almost the same FIPs. Similar results were obtained from the experiments and numerical modelling (Table 3). Comparing the fracturing pressures of samples 1-5 and 2-3 in Table 3, which have similar perforation orientation and fracture geometries (both have planar fractures), it is seen that they have very similar pressures, because their planar fractures are opened against the minimum stress direction, and the value of this stress is the same in both tests.

From the results obtained above, it is seen that, when the perforations are aligned with the intermediate stress direction, the stress anisotropy does not have a pronounced influence on fracturing pressures; however, when it is in the direction of minimum stress, stress anisotropy will have a great influence on fracturing pressures. In other words, depending on the perforation direction, if the stress anisotropy is associated with the values of those stress components, which are perpendicular to the axis of the perforation, the perforation stress distribution will be affected to some extent, thereby the fracturing pressure will also be influenced.

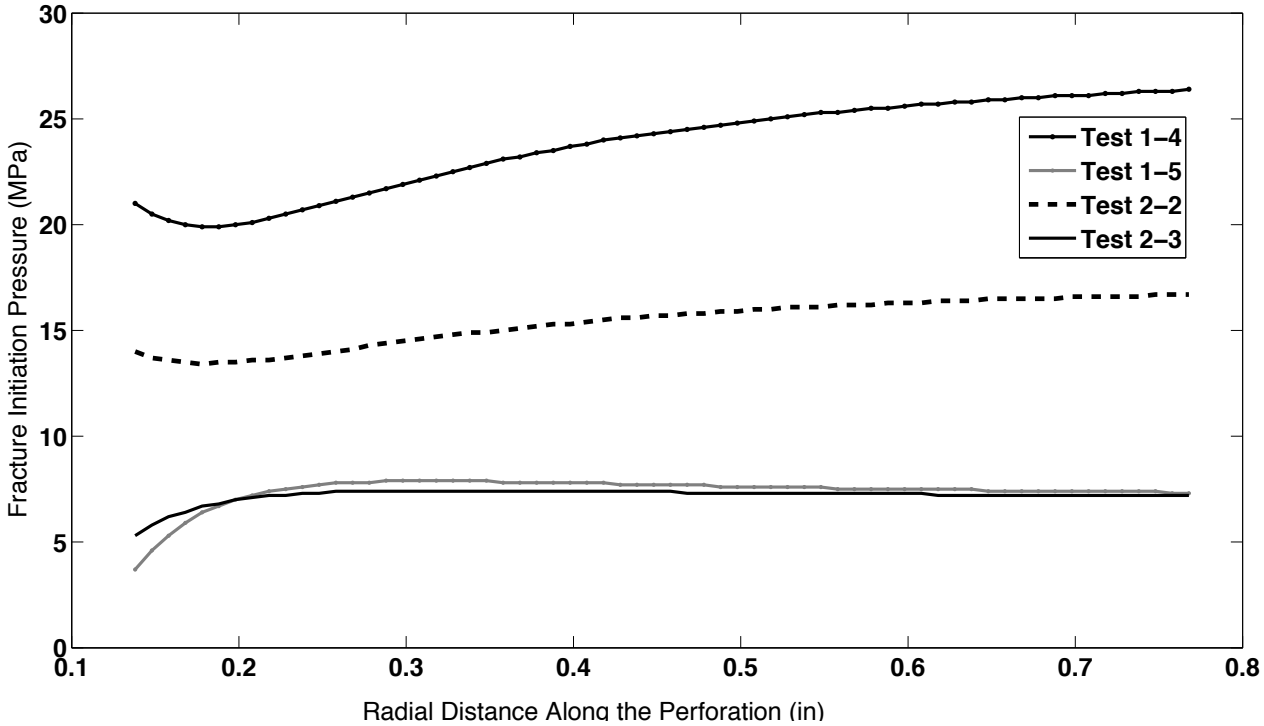

Figure 8. FIP along the perforation tunnel for four different tests obtained from the analytical modelling.

Pater (1999) found that an increase in stress anisotropy reduces the probability of the link-up of the initiated fractures from various perforations; however he has not mentioned anything about the effect of stress anisotropy on fracturing pressure.

The other important factor in a hydraulic fracturing operation is the orientation of the perforations. In sample 1-4 the perforation was aligned with the direction of minimum stress; therefore, the two other stresses were perpendicular to the axis of perforation tunnel. This caused a very high stress concentration around the perforation and, thereby, the fracturing pressures increased significantly. In sample 1-5, where the perforation was placed along the intermediate stress direction, the minimum and maximum stresses were perpendicular to the axis of perforation. This caused the fracture to be initiated and propagated at much lower pressures. The same results are obtained from the analytical and numerical simulations (see Fig. 8 and Table 3). An evaluation of the results of samples 2-2 and 2-3 yields similar conclusions. The fracture initiation pressure in sample 2-2, where the perforations are oriented towards the minimum stress direction, is 12.41 MPa, whereas it is 6.89 MPa for sample 2-3, in which the perforations are in the direction of intermediate stress.

CONCLUSIONS

In this paper a numerical model for analysing the mechanisms of fracture initiation and near wellbore fracture geometry is presented. This model is developed in a way to simulate the fracture initiation pressure in perforation tunnels of a borehole that is drilled in tight formations. The results of the numerical modelling are compared with some experimental fracturing tests and also an analytical simulator, with good agreement being observed. The results presented in this study show that in a perforated wellbore, which is drilled in a tight formation, an increase in the stress anisotropy will affect the fracturing pressures. The stress anisotropy generated from the stress components in the direction perpendicular to the perforation axis will influence the fracture initiation pressure, that is, the stress magnitude along the perforation tunnel is neutralised. The larger this anisotropy ratio the greater the initiation pressure will be.

The results of this study also indicate that the effect of the direction of a wellbore on the fracturing mechanism in a perforated wellbore should be analysed while the prevailing stress regime is considered. From the numerical modelling, laboratory tests and analytical results, it was observed that when the perforations are oriented in a direction such that the intermediate and maximum stresses are perpendicular to the axis of perforation, larger fracture initiation and break down pressures will be required compared to any other orientations chosen for the perforations. This, in turn, results in a higher chance for development of multiple fracturing planes around the perforation tunnel. Also, it was found that the lower the difference between FIP and BDP, the less the chance for having multiple fracturing. Additionally, it was observed that the direction of the perforation can affect the angle between the initiated fracture and the perforation axis.

REFERENCES

ABASS, H., BRUMLEY, J. AND VENDITTO, J., 1994—Oriented perforations - a rock mechanics view. SPE Annual Technical Conference and Exhibition, New Orleans, Louisiana, 25–28 September, SPE-28555-MS.

ATKINSON, C. AND EFTAXIOPOULOS, D., 2002—Numerical and analytical solutions for the problem of hydraulic fracturing from a cased and cemented wellbore. In: International journal of solids and structures, 39 (6), 1621–50.

AUD, W., WRIGHT, T., CIPOLLA, C. AND HARKRIDER, J., 1994—The effect of viscosity on near-wellbore tortuosity and premature screenouts. SPE Annual Technical Conference and Exhibition, New Orleans, Louisiana, 25–28 September, SPE-28492.

BEHRMANN, L. AND ELBEL, J., 1991—Effect of perforations on fracture initiation. In: Journal of Petroleum Technology 43 (5), 608–15.

BEHRMANN, L. AND NOLTE, K., 1999—Perforating requirements for fracture stimulations. In: SPE Drilling & Completion 14 (4), 228–34.

BUNGER, A.P., 2005—Near-surface hydraulic fracture, University of Minnesota. Major: Geological engineering.

CLEARY, M., JOHNSON, D., KOGSBØLL, H., OWENS, K., PERRY, K., PATER, C., ALFRED, S., HOLGER, S. AND MAURO, T., 1993—Field implementation of proppant slugs to avoid premature screen-out of hydraulic fractures with adequate proppant concentration. Low Permeability Reservoirs Symposium, Denver, Colorado, 26–28 April, SPE-25892-MS.

DAVIDSON, B., SAUNDERS, B., ROBINSON, B. AND HOLDITCH, S., 1993—Analysis of abnormally high fracture treating pressures caused by complex fracture growth. SPE Gas Technology Symposium, Alberta, Canada, 28–30 June, SPE-26154-MS.

FALLAHZADEH, S.H., RASOULI, V. AND SARMADIVALEH, M. 2013—Experimental Investigation of Hydraulic Fracturing in Vertical and Horizontal Perforated Boreholes. 47th American Rock Mechanics Association (ARMA) / Geomechanics Symposium, San Francisco, California, 23–26 June, 191953.

FALLAHZADEH, S.H. AND SHADIZADEH, S.R., 2013—A New Model for Analyzing Hydraulic Fracture Initiation in Perforation Tunnels. In: Energy Sources, Part A: Recovery, Utilization, and Environmental Effects 35 (1), 9–21.

FALLAHZADEH, S.H., SHADIZADEH, S.R. AND POURAFSHARY, P., 2010—Dealing with the challenges of hydraulic fracture initiation in deviated-cased perforated boreholes. Trinidad and Tobago Energy Resources Conference, Port of Spain, Trinidad, 27–30 June, SPE-132797.

FJAR, E., HOLT, R.M., RAAEN, A., RISNES, R. AND HORSRUD, P., 2008—Petroleum related rock mechanics. Hungary: Elsevier.

LEHMAN, L. AND BRUMLEY, J., 1997—Etiology of multiple fractures. SPE Production Operations Symposium, Oklahoma City, Oklahoma, 9–11 March, SPE 37406.

LHOMME, T.P.Y., 2005—Initiation of hydraulic fractures in natural sandstones. PhD, Delft University of Technology.

NELSON, E.B., 1990—Well cementing. Netherlands: Schlumberger.

PATER, C., 1999—Impact of perforations on hydraulic fracture tortuosity. In: Old Production & Facilities 14 (2), 117–130.

RASOULI, V., 2012—A true triaxial stress cell (TTSC) used for simulations of real field operations in the lab. In: True triaxial testing of rocks, 4, 311.

ROMERO, J., MACK, M. AND ELBEL, J., 1995—Theoretical model and numerical investigation of near-wellbore effects in hydraulic fracturing. SPE Annual Technical Conference and Exhibition, Dallas, Texas, 22–25 October, SPE-30506-MS.

SADD, M.H., 2009—Elasticity: theory, applications, and numerics. United States of America: Elsevier.

SARMADIVALEH, M., 2012—Experimental and Numerical Study of Interaction of a Pre Existing Natural Interface and an Induced Hydraulic Fracture. PhD, Curtin University.

THIERCELIN, M., DARGAUD, B., BARET, J. AND RODRIGUEZ, W., 1997—Cement design based on cement mechanical response. SPE Annual Technical Conference and Exhibition, San Antonio, Texas, 5–8 October, SPE-38598-MS.

WENG, X., 1993—Fracture initiation and propagation from deviated wellbores. SPE Annual Technical Conference and Exhibition, Houston, Texas, SPE 26597.

THE AUTHORS

Seyed Hassan Fallahzadeh is a PhD student at the Petroleum Engineering Department of Curtin University. His research focuses on hydraulic fracturing in perforated boreholes. The main objectives of his study are to analyse the mechanisms of fracture initiation and near wellbore propagation in a cased perforated wellbore. Seyed has also been involved in some other Petroleum Geomechanics projects with the Curtin Petroleum Geomechanics Group (CPGG). Seyed has received his BSc (2007) and MSc (2010) in Petroleum Engineering from Petroleum University of Technology. He was also awarded a master degree in petroleum well engineering from Curtin University, Perth in 2009.

s.hasan.fallah@gmail.com

Vamegh Rasouli is a Professor and Head of the Department of Petroleum Engineering at Curtin University in WA. He is a Chartered Professional Engineer (CPEng) and is a registered engineer with the National Professional Engineers Register (NPER) of Australia. Vamegh has received his PhD from Imperial College, London in 2002. In 2006, after joining Curtin University, he established Curtin Petroleum Geomechanics Group (CPGG) and in 2010 Curtin Drilling Research Group (CDRG). Vamegh is supervising a number of PhD students and involved in a number of research and consulting projects in the area of Geomechanics and drilling. He has done several projects related to Petroleum Geomechanics for various Companies and has also been a consulting engineer on various Geomechanics related projects with Schlumberger's Data and Consulting Services (DCS) in Perth.

v.rasouli@curtin.edu.au

Paper 5: *The Impacts of Fracturing Fluid Viscosity and Injection Rate on the Near Wellbore Hydraulic Fracture Propagation in Cased Perforated Wellbores.*

ARMA 15-645

The Impacts of Fracturing Fluid Viscosity and Injection Rate on the Near Wellbore Hydraulic Fracture Propagation in Cased Perforated Wellbores

Fallahzadeh, S.H.[a]
James Cornwell, A.[a]
Rasouli, V.[b]
Hossain, M.[a]
[a]*Curtin University, Perth, WA, Australia.*
[b]*University of North Dakota, USA*

This paper was prepared for presentation at the 49th US Rock Mechanics / Geomechanics Symposium held in San Francisco, CA, USA, 28 June-1 July 2015.

ABSTRACT: In this study, hydraulic fracturing tests were conducted on 150 mm synthetic cubic samples. The borehole drilled in the center of the sample was cased and perforations were created in the samples. A true tri-axial stress cell was used to simulate real far field stress conditions. In addition, dimensional analyses were performed to correspond the results of lab experiments to field-scale operations. Three different fracturing fluids with viscosities ranging from 20 to 600 Pa.s were used to investigate the effects of varying fracturing fluid viscosities and fluid injection rates on fracturing mechanism. The results indicated that by increasing the fracturing fluid viscosity and fluid injection rates, the fracturing energy rises, and consequently the fracturing pressures will increase. However, as the fracturing energy is transferred to the sample at a faster rate, the fracturing power increases, and accordingly the fracture initiation angle rises; this would lead to more curved fracture planes. It was evident that fractures would reorient perpendicular to the minimum principal stress direction despite the angle of initiation. Furthermore, it was observed that the presence of casing in the wellbore would influence the stress distribution around the casing in such a way that the fracture propagation tends to deviate from the wellbore vicinity.

1. INTRODUCTION

Hydraulic fracturing is commonly used as the most viable stimulation technique in order to improve the production rate and recovery factor of the oil and gas reservoirs. When performing a hydraulic fracturing operation in a cased perforated wellbore many problems may arise. These problems lead to high frictional pressure losses near the wellbore, and consequently would result in significant increase in the operation pressures and eventually premature screen-out [1-3]. Additionally, other issues such as multiple fracturing and near wellbore fracture tortuosity have been encountered during the implication of the hydraulic fracturing operation in cased perforated completions [4]. The quality of a hydraulic fracturing operation could be negatively impacted by these issues, and consequently the fracturing treatment may not improve the production of the wellbore effectively. Such kind of challenges are mainly due to the existence of the perforations cavities which complicate the fracture initiation and near wellbore propagation [5, 6].

Several researchers have conducted studies in order to investigate the mechanism of a hydraulic fracture creation in cased perforated wellbores [7-11]. They have shown that the wellbore inclination and azimuth as well as perforations spacing, phasing and orientations with respect to the in-situ stress directions play important roles in the process of fracture initiation and near wellbore propagation. Berhmann & Elbel [6] performed an experimental study and showed that when the perforation orientation is deviated more than 10° away from the direction of Preferred Fracture Plane (PFP), the fracture may not initiate from the perforation cavity. Later on, Romero et al. [12] built a theoretical and numerical model and recognized that when the orientation of the perforation gun is not properly designated, it could lead to a narrow fracture width close to the wellbore wall, which would be less than the width of the main body of the hydraulic fracture. This has been later investigated further and through an analytical study, it was indicated that when the perforation orientation is placed away from the direction of the tensile zone at the

wellbore circumference, the fracture initiation pressure will increase [9].

Several experimental studies have been carried out in order to physically model and analyze the mechanism of fracture creation in perforated boreholes [5, 6, 13]; however they have not scaled down the real field fracturing processes to experimental test samples. These sets of experimental research could have been greatly improved by the application of proper scaling analysis. Van de Ketterij and de Pater[14, 15], have developed and implemented the scaling laws in their fracturing experiments. They investigated the effects of fluid viscosity and injection rate on fracturing pressure; nevertheless, they only modeled a deviated wellbore with an azimuth of 60° and an inclination angle of 49°, and did not comprehensively analyzed the effects of these two parameters on fracture geometry.

This experimental study was performed to examine the effects of fracturing fluid viscosity and injection rate on the fracture initiation and break down pressures and near wellbore propagation geometry. Synthetic mortar samples with particular properties were made for the purpose of performing scaled hydraulic fracturing tests. Scaling analysis was conducted, and a true tri-axial stress cell (TTSC) was used to simulate the three in-situ principal stresses on 150 mm synthetic cubic samples. Three high viscous fluids were used as the fracturing fluid; these fluids included honey, and two different silicon oils. The fracturing fluids were used to conduct scaled hydraulic fracture experiments on nine synthetic samples. For each sample a particular fluid was injected with a specific flow rate ranging from 0.05 to 5 cc/minute. The fracturing fluid was injected through the casing and two perforations located at the center of the sample.

To properly analyze the tests' results, a new methodology was developed for predicting the fracture propagation time from the pressure-time curves. Accordingly, the fracture initiation and break down pressures are analyzed based on the particular fluid viscosity and injection flow rate implemented for each test. Two new parameters, namely fracturing energy and power, are introduced in order to improve the interpretation of the results. Subsequently, the near wellbore fracture propagation geometry is characterized by the initiation angle it makes at the perforation tunnel, and the propagation path it grows away from the wellbore. The geometries of fractures are then compared against the fracturing energies and powers of the corresponding tests. Consequently a new relationship is introduced to estimate the fracture initiation angle from the fracturing power. Moreover, the effects of the casing and its surrounding cement sheath properties on the fracturing process are discussed.

2. SAMPLE PREPARATION

In this section, the process of sample preparation is discussed. This process includes preparing appropriate cement and sand slurry mix and casting the slurry in cubic moulds. Then cased wellbore and perforations are created in the samples after casting and curing were completed. At the end of this section, the properties of the synthetic sample and fracturing fluid are presented.

2.1. Casting Cement Samples

To conduct scaled hydraulic fracturing tests, rock samples with particular hydro-mechanical properties are required. However, rock samples with desired properties are not readily available, as it is practically impossible to acquire a sufficiently large size intact sample from downhole. Additionally, the properties of rocks obtained from the outcrop (considering that they are a good representative of downhole rock samples) may not be homogeneous. Therefore, synthetic mortar samples were made to conduct these laboratory experiments, because it is possible to prepare these samples with reasonably homogenous properties [16].

The components of synthetic samples are cement, sands and water. Mechanical and hydraulic properties of any synthetic sample are significantly affected by the percentage of each individual component used in the cement slurry preparation. During sample preparation, it has been observed that a slight variation in the ratio of the components of the cement slurry could significantly alter the characteristics of the final concrete block. This emphasizes the importance of systematic selection of the cement, water and sand ratios. In addition, the sand grain size distribution influences the sample properties. Figure 1 shows the grain size distribution used to prepare the samples.

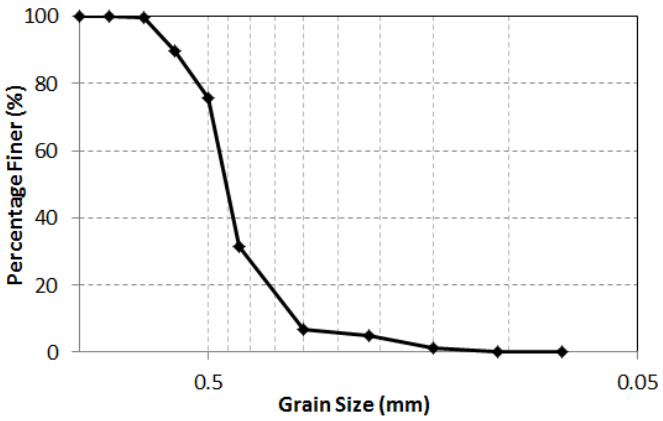

Figure 1: Grain size distribution for synthetic sample preparation.

Grain sizes were carefully chosen to be in the range of 200 to 850 μm in order to have a low permeable final mortar block. Low permeability will reduce fracturing

fluid leak off, which is suitable for scaling analysis. This is explained in more details in section 4.

The synthetic samples prepared in this study were produced based on the procedure presented by Sarmadivaleh and Rasouli [17]. The proposed cement slurry mixture consisted of Portland cement-sand and water-cement weight ratios of 1 and 0.4, respectively. Initially dry sand and cement were adequately mixed and then water was added to the mixture. The cement, sand and water were gradually mixed together using a heavy duty mixing equipment in a way that it reduced the volume of the air bubbles entering the slurry whilst also producing a homogenous mixture. The optimum mixing time was found to be 15 minutes at which point a uniform grain distribution was achieved.

To simulate the real field in-situ stress conditions, the experiments were planned to be carried out on cube-shaped samples, where three independent stresses could be applied. Therefore, standard concrete cubic moulds were used to make 150 × 150 × 150 mm mortar blocks. The cement slurry was poured into the cubic moulds which were slightly overfilled to compensate for the slight shrinkage of the cement. After filling the moulds the samples were placed on a vibration plate so that the air bubbles present within the slurry moved their way to the surface. It was found that the optimum vibration time was around 10 minutes. This was a sufficient time for air bubbles to graduate from the slurry with no separation of particles within the mixture due to its relatively high viscosity. Finally, around an hour after the casting, in which time the cement samples had partially shrunk, the top side of the samples were flattened using a wet trowel. The samples were then allowed to set for a day after which time they were removed from their moulds and placed in a water bath for 28 days. This allowed the cement to cure and reach its ultimate compressive strength [18].

2.2. Preparing Cased Perforated Samples

As the next step, the wellbore had to be drilled into the sample with its entire length being cased. This is mainly because the existence of the casing could significantly affect the wellbore stress distribution, and consequently the fracturing pressure and near wellbore fracture geometry would be affected [19]. Stainless steel tubing with an outer diameter of 12.7 mm, that could withstand a maximum internal pressure of 48.3 MPa, was selected to be used as the casing.

A wellbore was drilled directly through the center of each sample. The hole was drilled at 650 rpm through the entire length of the sample with a 14 mm masonry drill bit. The slow rate of penetration ensured maximum cutting efficiency. The hole was drilled as soon as the sample was removed from the water bath to reduce the risk of micro cracks forming around the wellbore.

The hole was then cleaned and a 400 mm long piece of the aforementioned tubing was cut to be glued in the wellbore; 150 mm length of the tubing was accommodated in the wellbore and the rest of the tubing was considered for connection purposes to the fracturing fluid chamber: this will be explained in more details in section 3.2. As the OD of the tubing was 12.7 mm and the wellbore diameter was 14 mm, a narrow annulus of only 0.65 mm wide was considered for the placement of the adhesive. Such narrow annulus was designed to minimize the effect of the adhesive on casing and wellbore stress distribution, for the time when the cubic sample would be under stress. However, some difficulties arose, due to this narrow annulus, when gluing the tubing in the hole, because the adhesive material was quite viscous and it could not easily fill and seal the annulus between the casing and the wellbore. To resolve this problem, initially the tubing was plugged at one end by an 8 mm OD steel rod, and it was slightly roughened to provide a better bond between the casing, glue and cement. Then one side of the wellbore was placed on a rubber sheet and enough adhesive was carefully poured into the wellbore from the other side. At this stage, the plugged end of the tubing was inserted in the wellbore and firmly pushed against the adhesive at the bottom of the hole. While enough force was applied and the rubber sheet was sealing the bottom side of the wellbore, the adhesive flowed upward in the annulus and filled the whole space. This upward flow of the adhesive ensured that no air bubble was left in the narrow annulus and consequently guaranteed the sealing of the dried adhesive.

It is noteworthy that the first tubing was glued in the wellbore using Selleys Liquid Nails adhesive; however, the rest of the samples were prepared using Super Strength Araldite adhesive. This was mainly because the former glue did not demonstrate enough strength and the fracturing fluid could break through it, when the fracturing test was in progress; this will be discussed further in 5.2. The strength properties of these adhesives are presented in Table 1.

The wellbore glue was allowed to cure for three days at which point two perforations were drilled into each sample. Each one was drilled at the center of the two parallel faces of the sample, perpendicular to the wellbore and orientated so that the perforations were facing directly opposite each other. The perforations were drilled through to the casing with a 4 mm masonry bit and a 4 mm general purpose drill bit through the steel casing. Each perforation was then cleaned and plugged with 35 mm of 3.75 mm steel rod using Araldite. The samples were allowed to cure for another 3 days after which they were cleaned up using a variety of files and sandpapers to guarantee that each surface of the sample was completely level and ensure a completely uniform

stress distribution being applied to each face when under stress.

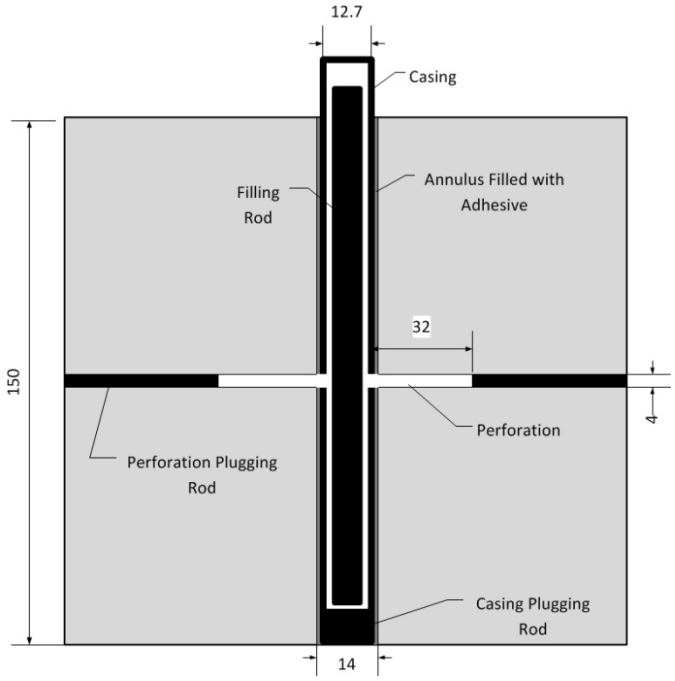

Figure 2: A schematic of 150 mm cubic sample with a cased wellbore at the center and two 4 mm perforations that are perpendicular to the axis of the wellbore and at an angle of 180° from each other (all dimensions are in mm).

Before the sample was placed inside the TTSC a 380 mm length of 6.2 mm OD steel rod was placed inside the wellbore to minimize the volume of the wellbore and hence reduce the wellbore filling time once the test had commenced. The other benefit of having this rod was to reduce the dead volume of the fracturing fluid. As a result, when the fracturing test was in progress, less compressed fracturing fluid will be present inside the hole at the time of fracture break down; therefore the fracture propagation could be better controlled.

The completed samples were now representative of a cased and perforated wellbore, with the perforations being aligned perpendicular to the maximum horizontal stress in the TTSC in order to promote fracture initiation. Figure 2 shows a schematic of the cased perforated block.

2.3. Sample and Fluid Properties

To perform scaling analysis for hydraulic fracturing experiments, samples' physical and mechanical properties as well as fracturing fluids' viscosity are needed. Sarmadivaleh and Rasouli [17] conducted conventional lab experiments including rock mechanics tests on core plugs to estimate some hydro-mechanical properties of the samples. Table 1 presents a summary of the physical and mechanical properties of the samples as well as the adhesives' strength properties.

3. EXPERIMENTAL SET-UP

3.1. True Tri-Axial Stress Cell (TTSC)

For conducting the fracturing tests three independent stresses should be applied on each cubic mortar sample to simulate the underground in-situ stresses. To achieve this objective, a true tri-axial stress cell (TTSC) was implemented [20]. The TTSC is capable of applying three independent orthogonal stresses in three directions on a sample. These stresses are applied to a sample using a series of hydraulic rams which are powered by three separate syringe pumps.

Table 1: Properties of the synthetic sample and the adhesives used for sample preparation.

Mechanical Properties		**Value**	**Unit**	**Testing Methodology**
UCS	Uni-axial compressive strength	79.5	MPa	Unconfined compression test*
T_o	Tensile strength	3.5	MPa	Brazilian tensile test*
K_{IC}	Fracture Toughness	0.78	MPa$\sqrt{m}$	Semi-Circular bend test*
Elastic Properties				
ν	Poisson's ratio	0.19	-	Unconfined compression test*
E	Young's Modulus	27.74	GPa	Unconfined compression test*
Adhesives Shear Strength				
τ_o	Selleys Liquid Nails	1.1	MPa	Sandblasted aluminum lap shear**
τ_o	Super Strength Araldite	26	MPa	Sandblasted aluminum lap shear**
Physical Properties				
ρb	Bulk density	2047	Kg/m^3	Density measurement test
ρg	Grain density	2500	Kg/m^3	Density measurement test
ϕ	Porosity	13.5	%	Two Boyle's cells
K	Permeability	0.019	mD	Transient gas flooding

*Presented by Sarmadivaleh and Rasouli [17].

**Provided by manufacturer.

Each syringe pumps is capable of providing a maximum pressure of 9500 psi at a maximum injection rate of 107 mL/min. The TTSC is designed in such a way that it could accommodate cubic samples of up to 300 mm in size. However, with the aid of a number of aluminum spacer blocks the TTSC could also be employed for testing a variety of smaller cubic sized samples. In this particular study, six 145 × 145 × 75 mm spacers were applied to properly accommodate the prepared samples at the center of the TTSC. The face of each spacer, which comes into contact with the face of the sample, is 5 mm smaller on each side; this is to ensure that the adjacent spacers would not come into contact with each other when there is some displacement in the sample. Figure 3 shows a top view of the TTSC and the syringe pumps, which were used for applying the stresses, and also a 150 mm sample accommodated in the cell using the spacer blocks.

As it was mentioned in the introduction section, the main goal of this study was to investigate the effects of the fracturing fluid viscosity and flow rate on the fracture initiation and near wellbore propagation geometry; therefore, a particular stress regime was considered to be applied on all samples in this study. This would have ensured that the stress regime would not influence the tests' results. Consequently, a maximum principal stress (σ_1) of 13.8 MPa (2000 psi), an intermediate principal stress (σ_2) of 10.3MPa (1500 psi), and a minimum principal stress (σ_3) of 6.9 MPa (1000 psi) were applied on each sample. Such stress components would represent a normal in-situ stress regime where $\sigma_1 > \sigma_2 > \sigma_3$.

In ideal circumstances it is expected that a hydraulic fracture initiate and propagate in a plane known as preferred fracture plane (PFP), which is perpendicular to the minimum principal stress direction. Therefore, all testing samples were placed in the cell in such a way that the perforations were along the direction of the intermediate principal stress, and the maximum principal stress was set along the wellbore axis. This would facilitate and ease the fracture to be developed in PFP.

It is noteworthy that the principal stresses were applied in three stages. Initially, all three stresses were concurrently increased to the minimum principal stress magnitude. At this point, the corresponding minimum stress syringe pump was set on a constant pressure mode to simulate the minimum in-situ stress perpendicular to the direction of the perforations. Then the other two stresses were increased to the intermediate principal stress, and at this stage the intermediate stress was kept constant. At the final stage, the maximum principal stress was increased to its required value and then its corresponding pump was set on constant pressure mode. This stress path was consistently applied to all samples tested in this study.

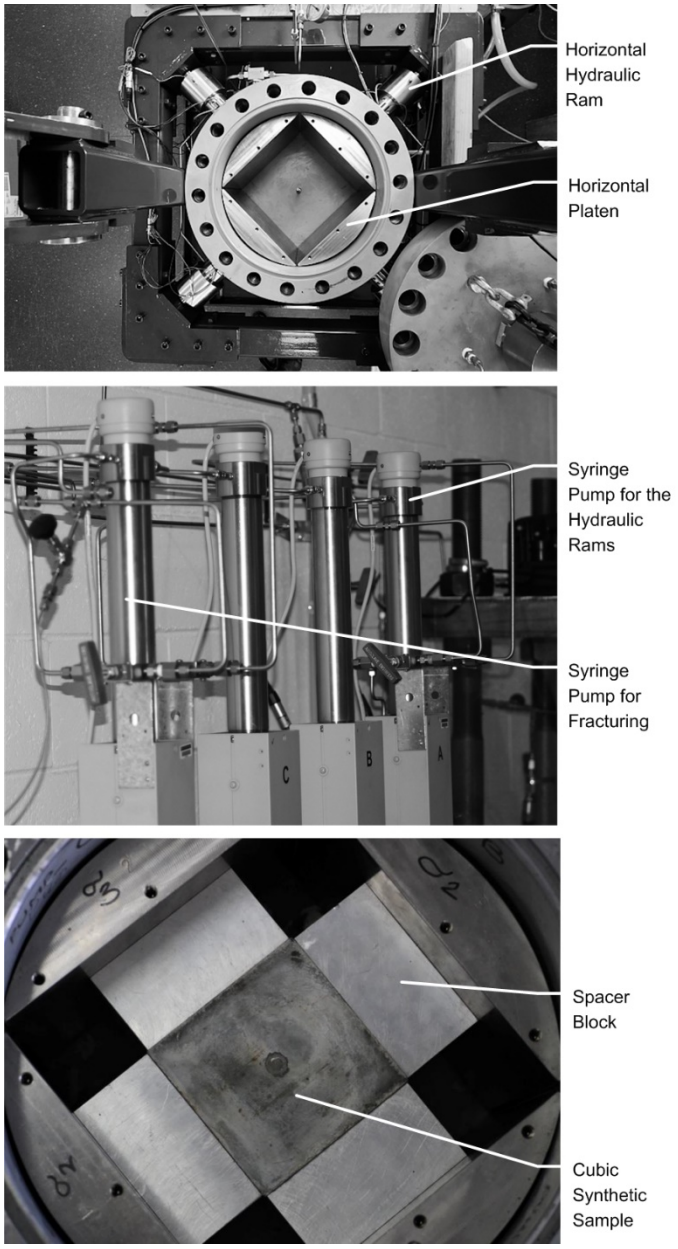

Figure 3: A view of the TTSC with the horizontal platen and the horizontal hydraulic rams (top), syringe pumps for the hydraulic rams and fracturing fluid injection (Middle), a synthetic sample accommodated in the TTSC using the spacer blocks (Bottom).

3.2. Fracturing Fluid Injection

Three high viscous fluids were used as the fracturing fluid to examine the effects of viscosity on fracturing pressures and propagation geometry. These fluids included honey, and two different silicon oils; the properties of which are listed in Table 2. The fracturing fluids were used to hydraulically fracture nine synthetic samples, and for each sample a particular fluid was injected with a specific flow rate ranging from 0.05 to 5 cc/minute.

Table 2: Fracturing fluid physical properties.

Fracturing Fluid	Viscosity (Pa.s)	Specific Density	Compressibility (1/psi)
Honey	20	1.36**	1.00×10^{-4}**
Poly DMS-T51	97.7*	0.977	$< 9.43 \times 10^{-5}$
Poly DMS-T56	586.8*	0.978	$< 9.43 \times 10^{-5}$

* Viscosities reported at 34.5 MPa by producer

** Obtained from [21].

A displacement chamber with a total volume of 120 cc was used along with a syringe pump to inject the high viscous fracturing fluid into the wellbore. The chamber was carefully cleaned and filled with the desired fracturing fluid before each set of tests. This process was strictly followed to make sure that no air bubbles could enter the fluid. Since air bubbles can easily get trapped in the high viscous fracturing fluids resulting in a detrimental effect on the fracturing experiment. This is due to the fact that air is much more compressible than the fracturing fluid. Therefore, when the wellbore is pressurizing with the fracturing fluid, the air bubbles shrink, while maintaining the same pressure as the wellbore. Once the fracture initiates in the sample, some new volume would be created and as a result some wellbore pressure reduction is expected. This variation in the wellbore pressure will be interpreted later to analyse the fracturing pressures and geometries. However, with the presence of compressed air bubbles, they could easily expand and compensate for the new created volume; consequently the wellbore pressure would not reduce much and the fracturing process may be misinterpreted. In addition, the expansion of the air bubbles could provide sufficient pressure to propagate the fracture very quickly to the boundary of the sample (i.e. uncontrolled fracture propagation), which is not favorable.

As three different fracturing fluids were used for these experiments, testing required the fluid chamber to be filled with the three different fluids. The nature of these fluids, particularly their high viscosity made this filling process to become a cumbersome and time consuming task. An alternative and more efficient approach was to first fill a larger chamber with a capacity of 750cc, then allowing the viscous fluid to settle in the chamber, and finally pressurising the chamber and slowly releasing the pressure so that all the air bubbles were removed from the fluid. The fracturing fluid was then displaced into the smaller fluid chamber before testing took place.

In order to inject the fracturing fluid into the wellbore, the fluid chamber should have been connected to the tubing of the sample. As it is seen in Figure 3, there is a hole at the bottom of the cell which is designed for the sample's casing to pass through. The top side of the casing, (located underneath the cell), is at the point where the fracturing fluid chamber was connected. Once testing commenced, the fracturing fluid was injected into the borehole of the sample from beneath the TTSC and the pre and post choke injection pressures were measured and recorded using two pressure transducers. These transducers were installed as close to the sample as possible and separated by a partially opened needle valve which acted as a choke (flow restrictor).

The choke helped to restrict and regulate the flow of the fracturing fluid which enabled more precise controlling of fracture growth [22]. If we consider the moment at which the wellbore is pressurized enough so that a fracture initiates from the perforation(s); some new volume is expected to develop which leads to a reduction in wellbore pressure. Therefore, the pressurized fluid, which is in the fracturing fluid chamber, would naturally flows at a higher flow rate towards the wellbore to compensate for this pressure reduction. This would consequently provide higher pressure in the wellbore and the initiated fracture would propagate uncontrollably and quickly towards the boundary of the sample. Such fast fracture growth in the laboratory-scale could not be reasonably compared with field-scale fracture propagation. Hence, the chock could control the flow of compressed fracturing fluid into a newly initiated fracture and accordingly would control the fracture propagation speed. Figure 4 shows a schematic of the fracturing fluid injection set-up. It should be noted that each synthetic sample was initially accommodated in the TTSC (Figure 3) and then it was connected to the fracturing fluid injection line.

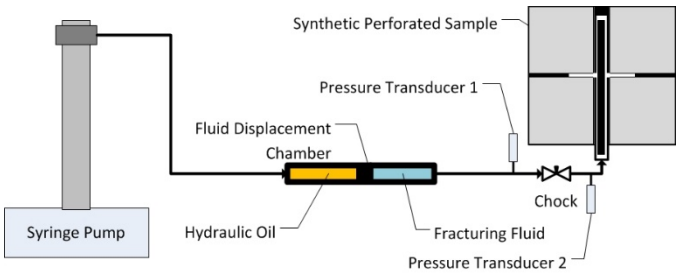

Figure 4: A schematic of fracturing fluid injection set-up.

4. SCALING ANALYSIS

In order to reasonably compare the results of laboratory scale hydraulic fracturing experiments to field scale operations, it is fundamentally important that scaling laws are applied. Scaling laws are simply the dimensional analysis involving the energy dissipation

during fracture growth. Known information such as sample size, wellbore dimensions and the hydro-mechanical properties of the sample are normally used as the inputs into the scaling model. This enables the output variables such as fluid viscosity, injection rate and total fracture propagation time, to be properly calculated and aided in the design of the laboratory hydraulic fracturing test [23].

At a laboratory scale, the majority of previous experimental works were conducted without the consideration of scaling laws [24]. As a consequence experimental parameters such as fluid viscosity and injection rates were based on the values used in real field operations. This resulted in very low fluid viscosities and highly exaggerated injection rates being used in the laboratory. However in order to properly monitor and analyze the fracture initiation and propagation in a small sample at lab scale, fracturing fluids with significantly higher viscosities are often required as well as drastically reduced injection rates. This ensures that the fracture is contained within the sample and allows fracture growth to be monitored without being affected by boundary conditions.

During hydraulic fracturing the time at which the wellbore pressurization rate reaches its maximum value is recognized as the fracture initiation point. Therefore, in this study, the fracture initiation time was considered as the reference point for scaled time. Conversely fracture breakdown is usually defined as the time at which the wellbore pressure reaches its maximum value, and fracture initiation typically occurs before this breakdown point [25]. Therefore the scaling period of a laboratory experiment starts with fracture initiation and runs through to the final stage of the fracture propagation.

Over the course of a hydraulic fracturing operation in the field, the initiation and propagation of the real fracture is influenced by three essential boundaries of viscosity, toughness and leak-off dominated regimes [22]. In these tests the permeability of the samples was around 0.019 mD and therefore the effect of leak off and the leak off regime could be regarded as negligible. During the majority of field fracturing operations, fracture growth is predominately toughness dominated throughout fracture initiation, however as the fracture develops it rapidly becomes viscous dominated [26]. Furthermore for a radial fracture the regime becomes more toughness dominated during the final stage of the fracture growth [27]. In this study scaling laws developed by de Pater et al [23] were applied whilst also validating our interpretations against more recent studies [22, 25, 27] to ensure that the majority of the fracture growth is viscous dominated similar to what happens in the field fracturing. In order to have viscous dominated fracture propagation the following equation should be satisfied [23]:

$$\kappa_{IC} < 2P_n\sqrt{\frac{r_f}{\pi}} \tag{1}$$

Here, K_{IC} is the fracture toughness, P_n is net fracture pressure and r_f is fracture radius. Considering the hydro-mechanical properties and dimensions of the samples used in this study, and based on the study done by Sarmadivaleh [28], the right hand side of Eq. 1 is always larger than the synthetic sample's fracture toughness; this is valid for the range of injection rates and fluid viscosities considered for this study. However, the injection time is different for each set of fracturing fluid viscosity and flow rate; this is more explained in the section 5.1.

In order to have a viscous dominated propagation regime, the dimensionless toughness parameter of a Penny-Shaped fracture can be calculated using following equation [27];

$$\kappa = K'\left(\frac{t^2}{\mu'^5 Q_0'^3 E'^{13}}\right)^{1/18} \tag{2}$$

In this equation t is the time of the experiment and Q_o' is the flow rate. In theory, based on Eq 2, the fracture propagation will be viscous dominated if κ is less than one, whereas if κ is greater than four the propagation will be toughness dominated [27]. It must be noted that the dimensionless toughness number, κ is time dependent; hence the fracture regime may change as time evolves. Other parameters are as follows:

$$K' = \left(\frac{32}{\pi}\right)^{1/2} K_{IC} \tag{3}$$

$$E' = \frac{E}{1-\nu^2} \tag{4}$$

$$\mu' = 12\mu \tag{5}$$

where, μ is fracturing fluid viscosity, E is rock's Young's modulus, and v is the Poisson's ratio. Using the samples' hydro-mechanical properties (Table 1), along with the fracturing fluid viscosities (Table 2) plus the range of the flow rates, which were used in this study, the dimensionless toughness numbers (κ) were calculated and presented in Table 3. As is seen in this table, all κ values are less than one, confirming that the conducted experiments in this study are viscous dominated fracture propagation.

It is noteworthy that the time of the experiment is 1000 s, which was selected based on the previous experimental experiences. However, it was observed that in some of the experiments, the propagation time were

less than 1000 s, which again would result in a κ value smaller than one, as κ is directly proportional to the propagation time.

Table 3: Dimensionless toughness number for each fracturing fluid flowing at a particular flow rate.

Fracturing Fluid	Viscosity (Pa.s)	Flow Rate (cc/min)	Dimensionless Toughness
Honey	20	1	0.65
Honey	20	2	0.58
Honey	20	5	0.49
Poly DMS-T51	97.7	0.05	0.69
Poly DMS-T51	97.7	0.1	0.61
Poly DMS-T51	97.7	1	0.42
Poly DMS-T56	586.8	0.1	0.37
Poly DMS-T56	586.8	1	0.25

5. RESULTS AND DISCUSSION

During this investigation hydraulic fracturing tests were conducted on nine 150 mm cubic concrete samples. The tests involved the use of three different fracturing fluids and a range of injection rates from 0.05 mL/min to 5 mL/min. The samples were prepared with significant levels of caution and care to ensure that the stress distribution being applied to each face of the sample was uniform. Further to this, the internal structure of the sample (i.e. the wellbore and perforations) were prepared with repeatability to make sure that the stress distribution applied by the high pressure fracturing fluid would be near identical in each sample.

This allowed control of the majority of the variables present in the experiment, and the accurate monitoring and study of the effects of varying the fracturing fluid viscosity and fluid injection rate. A normal stress regime was maintained throughout the testing on all nine samples, where σ_1 = 13.8 MPa, σ_2 = 10.3 MPa, and σ_3 = 6.9 MPa. Table 4 presents the fracturing tests' parameters and the fracture initiation and break down pressures for each test.

As previously mentioned, two pressure transducers were used to record the pre (P1) and post (P2) choke pressures, just at the entrance of the wellbore (see Figure 4), while the fracturing fluid was being injected into the wellbore. Due to the fact that the length of the wellbore was relatively short and the injection rates were quite low, this means that there was very little frictional pressure drop across its length and hence it could be neglected in the calculations. As the frictional pressure loss was negligible, the post choke pressure reading could be considered as the fracturing pressure (i.e. the wellbore pressure). However, the pre choke pressure reading was used as a means to estimate the initiation and breakdown pressures.

Figure 5 shows a pressure-time curve corresponding to test SL-1. In this figure, the pre and post chock pressures (P1 and P2) are shown as well as the wellbore pressurization rate. In addition, the difference between P1 and P2 is calculated and displayed versus time. This would greatly help in predicting the moment of fracture initiation as well as predicting the fracture propagation time.

As it is seen in Figure 5, over the first 550 seconds of the injection time, the pressure recording did not increase much, because the fracturing fluid was just filling the wellbore and the perforations. After the wellbore was completely filled, the two pressures started to build up and as a result the wellbore was pressurized.

The initiation pressure could be estimated as the point where the pre and post choke pressure readings begin to deviate from each other, whereas the breakdown

Table 4: Fracturing tests' parameters and main results.

Test No.	Fluid Viscosity (cP)	Injection Rate (cc/min)	Initiation Pressure (MPa)	Breakdown Pressure (MPa)	Propagation Time (s)
H-1	20000	1.00	8.96	9.10	----
H-2	20000	1-2.0	12.82	14.19	320
H-3	20000	2.00	10.69	11.41	669
H-4	20000	5.00	15.24	18.68	636
SL-1	97700	1.00	18.40	19.96	340
SL-2	97700	0.10	17.44	18.19	936
SL-3	97700	0.05	7.98-14.37	8.16-14.65	499
SH-1	586800	1.00	32.75	35.65	364
SH-2	586800	0.10	28.27	32.72	460

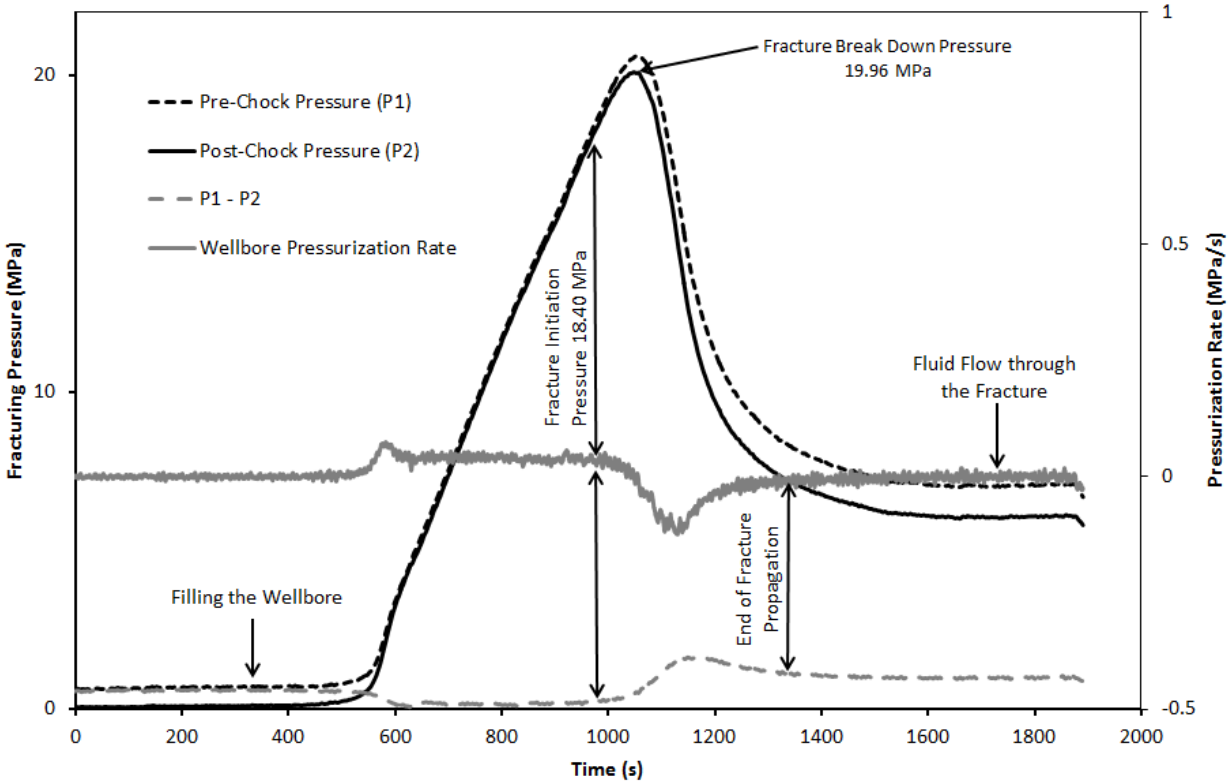

Figure 5: Fracturing pressures recording and wellbore pressurization rate for test SL-1.

pressure is taken as the maximum wellbore pressure. In essence as the wellbore is being pressurized, both the pre and post choke pressures would be increasing, however when the fracture initiates, micro fractures are created and hence the rate of increase of the wellbore pressure reduces. This is due to the fact that the pressurized fracturing fluid in the wellbore expands to fill the volume of the newly initiated flaws and consequently the wellbore pressure decreases. However, because of the presence of the chock, the pre choke transducer does not sense this reduction in pressure and increases more than that of post choke pressure, therefore the point at which the difference between the two pressures increases indicates the fracture initiation (see Figure 5).

The other evidence to mark the fracture initiation point is the reduction in the wellbore pressurization rate. This is basically due to the fact that as a fracture initiates, the wellbore pressure reduces and consequently the pressurization rate would decrease. This reduction in the pressurization rate along with the increase in the difference between the pre and post chock pressures were implemented in all these tests to precisely specify the moment of fracture initiation.

At the conclusion of each test, the in-situ stresses were reduced at a constant rate back down to atmospheric pressure. The sample was then taken out of the TTSC, at which point it was carefully broken apart along the induced fracture planes. The fracture planes were then photographed to aid analyzing the fracture geometries, whilst the pressure-time curves were used to interpret the initiation and breakdown pressures, as well as near wellbore fracture geometry. Table 5 presents a brief description of the fracture geometries.

5.1. Predicting Fracture Propagation Time

In laboratory fracturing experiments, fracture propagation time is generally considered as the time interval it takes for an initiated fracture to grow from the wellbore (or the perforations) all the way to the boundary of the experimental sample. This time interval is critically important in such experimental studies, because when the fracture propagates and the fracture tip gets close to the boundary of the sample and eventually intersects it, the last moments of fracture propagation may be influenced by the sample's boundary conditions. Therefore, the very last stages of the fracturing process may not appropriately represent the real field fracturing mechanism. In addition, any further injection of the fracturing fluid after the fracture has reached the boundary may resemble real hydraulic fracture propagation and mislead the experiment's interpretations.

Such issue is marked and shown in Figure 5, where after the fracture reached the sample boundary, the rest of the pressure recording data was just showing the fracturing fluid flowing through the created fracture all the way to the boundary of the sample. It should be noted that such

Table 5: Brief description of the fracture geometries.

Test No.	Test Description and Fracture Geometry
H-1	The fracturing Fluid (honey) created several fractures in the solid adhesive, which had filled the annulus between the casing and the wellbore; eventually the fractures reached the bottom of the annulus and the fluid leaked out.
H-2	This sample was initially intended to be fractured by a flow rate of 1 cc/min; however after 3105 s of injection, no fracture was initiated; therefore, the flow rate was then increased to 2 cc/min. Consequently the wellbore pressure increased and eventually a vertical, almost planar, fracture perpendicular to the direction of minimum stress was initiated and propagated from each perforation tunnel. The two fractures did not linked up at the vicinity of the wellbore, probably due to high stress concentration around the wellbore.
H-3	From each perforation a two-wing fracture was propagated along the perforation axis; however, the initiated fractures were not vertical at the perforation wall, and had an angle of about 35˚ with respect to the vertical plane. Both fractures propagated downwards and upwards in the sample in a curved path, and in a distance away from the wellbore they turned towards the vertical plane (PFP).
H-4	Similar to the previous test, curved fractures were initiated from the perforations, and then turned towards the PFP. The lower wing of the fracture in this test made an angle of about 80˚ with respect to the vertical plane; however, it turned towards a plane where less normal stress was applied.
SL-1	Almost similar to the two previous tests, from each perforation a two-wing fracture was created in an angle of 65˚ with respect to the vertical plane, and then in some distance away from the wellbore, the fractures turned towards the PFP.
SL-2	An almost planar fracture, making an angle of 3˚ with respect to PFP, was developed from both perforations, and propagated mostly towards the bottom of the sample.
SL-3	This test exhibited multiple fracturing; in addition a two-wing fracture was developed almost against the maximum stress, initiating from one of the perforations, and then one of its wing propagated and changed its direction towards a vertical plane, which was nearly perpendicular to the minimum stress. The other perforation just initiated a small fracture.
SH-1	A two-wing fracture was developed almost against the maximum stress, initiating from one of the perforations, and then one of its wing propagated and turned towards the PFP.
SH-2	An almost planar vertical fracture, making an angle of 25˚ with respect to PFP, was propagated from one of the perforations. The other perforation created a fracture which also developed towards the vertical plane and perpendicular to the minimum stress direction.

pressure behavior is very similar to hydraulic fracture propagation in the field, where the wellbore pressure remains almost constant. Therefore, it is critically important to consider a methodology in order to properly detect the end of the fracture propagation and disregard the rest of the pressure curve.

As it is explained in Section 4, the fracture propagation time (injection time) could be obtained using theoretical scaling analysis. Nevertheless, because the scaling analysis are based on some assumptions such as a penny shaped fracture propagation, and all these assumptions may not be valid in the case where a real hydraulic fracturing test is in progress; therefore, the estimated required injection time may not match the real one. For instance, when a fracture is initiated from a perforation and it is propagated along a curved path, due to the concentrated stress distribution around the wellbore and the perforation, it is not actually a penny shaped fracture. Therefore, as it is contradicting the assumptions of the scaling laws, such curved fracture propagation may not be accurately matched with scaling analysis.

In order to address this problem, a new methodology was developed in this study to interpret the fracturing pressures, so that the real propagation time (or its corresponding injection time) could be directly estimated from the pressure recordings. This methodology is based on the concept of fluid flow through a fracture. When a fluid with a constant viscosity and under isothermal

condition is flowing through a fracture, the frictional pressure loss along the fracture would not change over time. This means that when the fracture tip reaches the boundary of the sample, the rest of the wellbore pressure curve would present an almost constant pressure behavior versus time, meaning that the wellbore pressurization rate would become almost zero.

Conversely, one stage earlier, when the fracture initiates and propagates through the sample, as the tip of the fracture is growing, new volume is created and consequently the fracturing fluid would expand to fill this volume, and as a result the wellbore pressure would decrease. However, this pressure reduction pulse would take a short while to pass across the fluid restrictor (the chock); therefore the pre chock pressure (P1) may not decrease simultaneously. Accordingly, the pressure difference ($\Delta P = P1-P2$) would increase (see Figure 5). However, after a short while, the pre chock pressure would also decrease as a result of sensing the pressure pulse, and would accordingly support the wellbore pressure. Nevertheless, as the fracture is growing, more and more volume would be generated and the wellbore pressure keeps decreasing, especially after the fracture breaks down. This is indicated in Figure 5, where the wellbore pressurization rate is decreasing after the fracture break down point; simultaneously, the difference between the two pressures (ΔP) is still increasing.

Once some fracture length is created, the rate of fracture propagation would stabilize, because the tip of the fracture is moving far from the wellbore and perforation stressed zone, and it is approaching a less stressed region (concurrently, the wellbore pressure is now less than break down pressure, therefore less pressure is provided in the fracture for the purpose of its propagation). As a result the wellbore pressure would decrease less and this means that the pressurization rate would approach zero. Similarly, ΔP would firstly stabilize and then decrease.

As the fracture tip hits the boundary of the sample, the fluid can flow out of the sample. This means that the wellbore pressure is now equal to the fracturing fluid frictional pressure loss along the created fracture, and because this pressure loss does not change over time, the wellbore pressure would stabilize. This is the point where the pressurization rate becomes zero and ΔP would also stabilize. This point could practically be considered as the end of the fracture propagation, and the rest of the pressure-time data would represent the fluid flowing in the fracture (see Figure 5). This methodology has been implemented for all the tests in this study, and the fracture propagation of every test is presented in Table 4.

To illustrate the fracture propagation time, tests H-2 and H-3 could be compared. As it is presented in Table 4, honey was used as the fracturing fluid to conduct these two experiments. Test H-2 was initially intended to be fractured under a flow rate of 1 cc/min; however, after 3105 s of injection, no fracture was initiated (based on the pressure-time curve); therefore, the flow rate was then increased to 2 cc/min. Test H-3 was also performed using a flow rate of 2 cc/min. Nevertheless, when the corresponding fracturing pressure curves were analyzed using the aforementioned method; it was detected that the fracture propagation time of test H-2 was 320 s, while the other test had a fracture propagation time of 669 s.

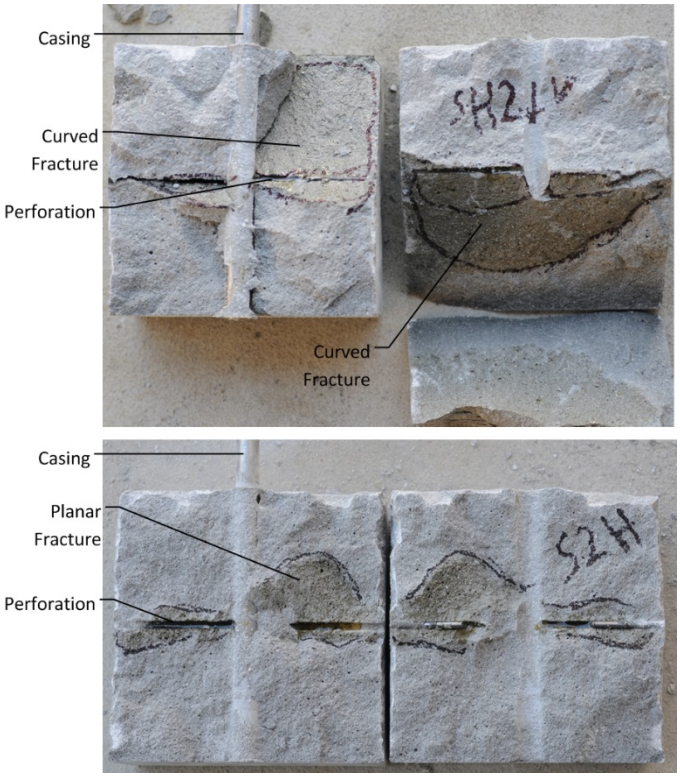

Figure 6: Test H-3 (top) and H-2 (Bottom) fracture geometries.

Referring to Figure 6, where the fracture geometries of these two tests are shown, it is seen that in Tests H-2 a planar fracture was propagated, and the fracture tip reached the side boundary of the sample, before the fracture has propagated much in vertical direction. This has resulted in a relatively small propagation time and consequently a small fracture plane. While test H-3 experienced a curved fracture geometry which has turned away from the wellbore and aligned itself almost with PFP before the tip of the fracture has reached the top boundary of the sample. As a result a larger fracture plane was created in test H-3 in comparison to that of test H-2 and this confirms the longer fracture propagation time in test H-3, as it has been predicted from its pressure-time curve.

5.2. *Cement Sheath Strength Effect*

A common practice in completion of an oil or gas wellbore is to cement the production casing in the open wellbore across the pay zone. This is achieved by pumping cement slurry, with some particular rheological properties down the hole and then the slurry would flow upwards in the annulus between the casing and the wellbore wall, and eventually the drilling engineers will wait for a fraction of a day or a few days for the cement to set, before they move on to the next operation [29]. From the drilling engineer point of view, the set cement should support the weight of the casing and for this reason it should reach a minimum strength of 34.5 MPa (5000 psi) [30]. This would be equivalent to a tensile strength of 3.4 MPa.

Such low strength properties might be sufficient to support the weight of the casing for wellbore drilling purposes; however, later on over the life of the wellbore, if the production engineer hydraulically pressurizes the wellbore and perforations, the fracturing fluid may propagate a fracture through the cement sheath rather than the formation rock. This is what was observed in the first test, where the pressurized fracturing fluid created multiple fractures through the solid adhesive (which was essentially used as the cement slurry to bond the casing to wellbore wall), and consequently no fracture was developed in the sample.

Figure 7 shows the fracturing pressure curve and a view of the sample in test H-1, which was broken by hammer after the test. As it is demonstrated by the pressure-time behavior, one may conclude that multiple fractures were initiated and propagated in the sample; because the curve does not reveal any point that could indicate the failure of the adhesive. However, when the sample was inspected after the test, it was realized that the fracturing fluid had actually created a micro-annulus and had leaked out of the sample just next to the casing. A further analysis, which was done after the sample was split apart using a hammer and a chisel, showed that no fracture was initiated within the sample, though both perforations had been pressurized by the fracturing fluid.

The same issue may happen in a real hydraulic fracturing operation, where the pressurized fracturing fluid could break through a low strength cement sheath in the annulus of the wellbore, while its pressure-time graph on the surface may appear to be very similar to a proper hydraulic fracture propagation in the formation. It is noteworthy that, in such condition, where the fracturing fluid has created a fracture in the cement sheath, it is more likely that the fracture would propagate upwards, because less stress would be applied to the tip of the fracture at shallower depths. Consequently, this may negatively impact the integrity of the wellbore. Therefore, it is crucial to investigate the cement strength properties before any hydraulic fracturing operation be performed in a cased perforated wellbore.

To prevent this problem in the rest of the samples, in contrary to sample H-1, which was glued using Selleys Liquid Nails adhesive with shear strength of 1.1 MPa (see Table 1), the rest of the samples were prepared using Super Strength Araldite adhesive. This latter glue offered a shear strength of 26 MPa, and had appropriately sealed the annulus in the rest of the tests with no instance of mico-annulus incident.

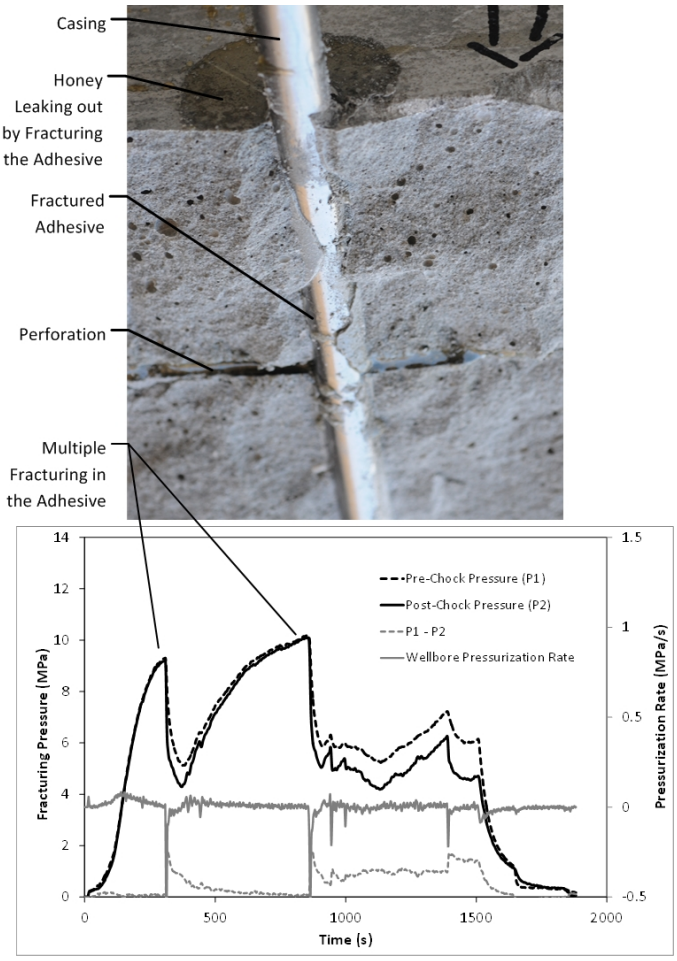

Figure 7: A view of the broken sample H-1 after the test, where fracturing fluid has propagated a fracture in the adhesive (top), and the corresponding fracturing pressure graph which shows a typical multi-fracturing mechanism (bottom).

5.3. *The Effects of Viscosity and Flow Rate*

According to the scaling analysis presented in Section 4, to conduct a scaled hydraulic fracturing experiment, the use of a very high fracturing fluid viscosity is necessary. This is basically to properly simulate the real physical phenomena taking place over the course of a field hydraulic fracturing process to laboratory experiments [23]. The other important parameter that is involved in the fracturing process is the injection flow rate. Typically, in laboratory experiments, when a very high viscous fluid is used, the injection flow rate should be

much lower than the field operation injection rates [24] . In this study, three different fracturing fluids were used, and in each test a particular injection flow rate ranging from 0.05 to 5 cc/minute was considered to investigate the impacts of these two important parameter on fracturing pressure, propagation and near wellbore geometry.

Because every test had a specific flow rate and viscosity, the product of flow rate and viscosity ($Q \times \mu$) is considered in order to ease the tests' results comparison and simplify the analysis. Considering the unit of flow rate (m^3/s) and the unit of viscosity ($N.s/m^2$), it is realized that the unit of the product of flow rate and viscosity will be N.m. This means that this product is representing the energy which is supplied for hydraulic fracturing. Such fracturing energy concept is later used to better interpret the tests' results.

Fracturing Pressures

Fracture initiation and break down pressures are the two most critical parameters of a fracturing operation, especially in cased perforated wellbore. Analyzing the fracture initiation and break down pressures presented in Table 4 along with their corresponding fracturing fluid viscosities and flow rates would reveal that as the product of flow rate and viscosity increases, generally higher pressures are experienced.

For instance, test SL-3, was performed using silicon oil as the fracturing fluid with a viscosity of 97700 cp, and the injection flow rate was 0.05 cc/min. This sample exhibited multiple fracturing and the first fracture was initiated at a pressure of 7.98 MPa and its break down pressure was 8.16 MPa. This first fracture did not propagate much and the wellbore pressure increased again and the second fracture was initiated at a wellbore pressure of 14.37 MPa and at this time the break down pressure was recorded to be 14.65 MP. Comparing this test with test SH-1, in which silicon oil viscosity was 586800 cp and the injection flow rate was 1 cc/min, it is observed that the latter test demonstrated a much larger fracturing pressures; where the initiation and break down pressures were 32.75 MPa and 35.65 MPa, respectively.

Similarly, comparing tests SH-1 and SH-2 would lead to the same result. These two tests were both conducted using silicon oil with a viscosity of 586800 cp; however, the injection flow rate in test SH-2 was one tenth of the flow rate in test SH-1. Consequently, in test SH-2, the fracture was initiated at a pressure of 28.27 MPa, while it was 32.75 MPa in test SH-1. The break down pressures also showed a difference of almost 3 MPa between the two tests. These comparisons highlight that a larger product of injection flow rate and viscosity would lead to higher fracturing pressures.

This is mainly because as a viscous fracturing fluid is injected at a higher flow rate, more energy is supplied to the wellbore. Consequently, the wellbore pressurization rate increases, this makes the fracturing process more dynamic, and as a result larger fracture initiation and break down pressures would be required to create a fracture. Physically, when a rock or concrete sample is loaded dynamically, it would exhibit larger strength parameters [31]; the same concept appears to be valid for a hydraulic fracturing test.

Fracture Geometry

The geometry of the hydraulic fracture (specifically near the wellbore) plays an important role during the fracturing operation. A more planar fracture plane would result in a wider fracture with lesser frictional pressure loss, and additionally, the chance of proppant bridging over a planar fracture plane is lower. Moreover, a planar fracture plane is favorable for hydrocarbon production, because oil and gas could flow through such fracture with less pressure reduction.

A description of fracture geometries for every sample is presented in Table 5; analyzing these fracture geometries along with the experimental parameters (see Table 4) would demonstrate how the injection flow rate and fluid viscosity may influence the near wellbore fracture geometry. Generally, because every sample had two perforations parallel to the direction of intermediate stress (maximum horizontal stress), it was expected that a two-wing fracture plane would be initiated from the top and bottom side of each perforation, and propagate vertically, perpendicular to the direction of minimum stress. However, most of the fractures were initiated in an angle with respect to the vertical plane (herein preferred fracture plane), and propagated in a curved path away from the wellbore and eventually the tip of the fractures grew towards the vertical plane.

Figure 6 shows the fracture geometries of the samples fractured in tests H-2 and H-3. As it is seen in this figure, in test H-2 almost a vertical fracture (along PFP) was developed; however, test H-3 resulted in a curved fracture plane, where the fracture was initiated from the perforations in an angle with respect to PFP, but each wing of fracture propagated in a curved path towards the PFP. As it is described in Table 5, tests H-4, SL-1, SL-3, and SH-1 also experienced curved fracture planes; however, the angles (with respect to PFP) at which the fractures were initiated from the perforations, as well as the curvature of the fracture planes were not the same in all these tests.

For instance, as it is shown in Figure 8, in test H-4 two-wing fractures were initiated from each perforation. However, the bottom fracture was initiated at a larger initiation angle than the top fracture. Moreover, the bottom fracture propagated almost in the horizontal plane, which is perpendicular to the vertical stress, while the top wing grew in a curved path towards the PFP.

Test SL-1 also resulted in two-wing fractures; however, the fracture initiation angle for this test is less than that of test H-4. Additionally, the top and bottom fractures in test SL-1 experienced less curvature in comparisons to the fractures in test H-4.

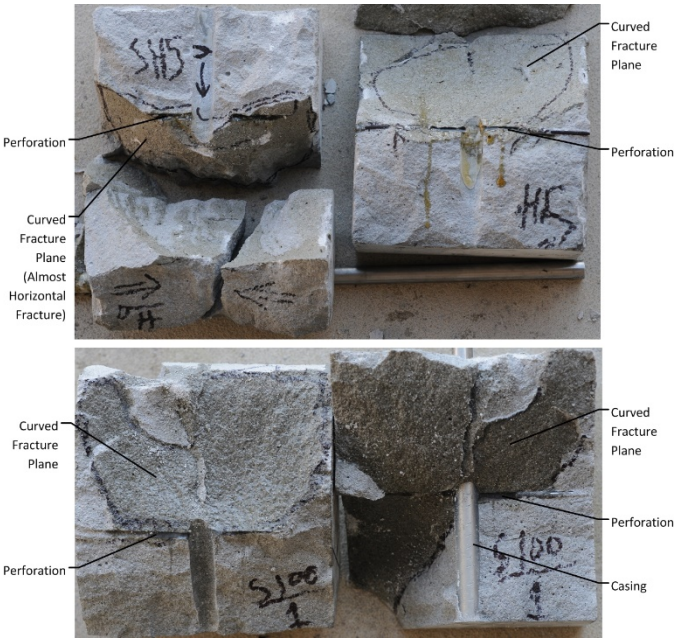

Figure 8: Fracture geometries of tests H-4 (top) and SL-1 (Bottom).

In order to recognize the relationship between fracture initiation angle and propagation geometry with the injection flow rate and viscosity, it is helpful to recall the product of these two parameters ($Q \times \mu$). The product of injection flow rate and viscosity is calculated for each test and presented in Table 6. As it is mentioned earlier, although by increasing the product value, higher initiation and break down pressures were recorded, it appears that some of the tests have the same product values, while their fractures' geometries are different. For instance, tests H-4 and SL-1 have almost the same product value (see Table 6); however, their fracture geometries are not the same.

To clarify this controversy, it is worthwhile to remember that the product of injection flow rate and viscosity represents the amount of energy applied to pressurize the wellbores and create the fractures. However, because every test had a particular injection rate and fluid viscosity, the wellbore pressurization time was not the same for all tests. For example, sample H-4 was pressurized with a flow rate of 5 cc/min using honey with a viscosity of 20 Pa.s, while sample SL-1 was tested using silicon oil with a viscosity of 97.7 Pa.s and a flow rate of 1 cc/min. Hence, sample H-4 was pressurized much faster than sample SL-1, as much less viscous fluid was injected into its wellbore at a higher flow rate. This is while both samples had almost the same level of fracturing energy ($Q \times \mu$), but sample H-4 had received this energy at a faster rate. Therefore, it would be significantly helpful to divide the fracturing energy by the time interval at which this energy was supplied to each sample. Energy divided by time would introduce a new parameter which is considered to be the fracturing power as given below:

$$P_{fracturing} = \frac{Q \times \mu}{t} \tag{6}$$

The time interval t is considered to be the wellbore pressurization time in each test. This time interval starts with the moment when the wellbore begins to pressurize and ends when the fracture breaks down.

Table 6 summarizes the fracturing energy, pressurization time, and fracturing power as well as the characteristics of fracture geometry for each test, excluding test H-1 in which no fracture was developed in the sample. Each fracture geometry is characterized by an initiation angle, which is the angle at which the fracture was initiated from the perforation with respect to the PFP. Additionally, the fracture propagation plane is also generally characterized as either planar or curved.

Comparing the fracturing powers of tests H-4 and SL-1 indicates why the fracture geometry in test H-4 had a larger initiation angle and a more curved fracture plane (see Figure 8), although they have almost equal fracturing energy of about 16×10^{-7} N.m. The same result is concluded when comparing the fracturing power and geometries in the other tests. For example, test SH-1experienced a fracturing power of almost 140×10^{-10} N.m/s, and as a result a curved fracture with an initiation angle of 75 degrees was created in this test.

In contrary, tests H-2, SL-2 and SH-2 had very low fracturing powers, and subsequently an almost planar fracture was initiated from their perforations and propagated in the vertical direction, along PFP. Thus, generally, it is concluded that the fracturing energy could not be directly related to the fracture initiation and propagation geometry. Nevertheless, the fracturing power could be associated with the fracture geometry very well.

Basically, as it is demonstrated in Figure 9, by increasing the fracturing power supplied to the sample, the wellbore pressurization rate increases, and consequently the fracture initiation angle increases. This means that at higher fracturing power, fractures could be initiated from the perforations in a direction which is perpendicular to higher stress components (herein vertical stress), and accordingly the fracture propagation would have a longer curved path so that it could get aligned with the PFP (the plane to which the minimum stress is perpendicular).

Table 6: Fracturing tests' energy, pressurization time, power, and fracture geometry characteristics.

Test No.	Injection Rate (m^3/s)×10^{-8}	Fluid Viscosity (Pa.s)	Q × μ (Fracturing Energy) (N.m) ×10^{-10}	Pressurization Time (s)	Fracturing Power (N.m/s) ×10^{-10}	Fracture Initiation Angle (°)	Fracture Propagation geometry
H-2	1.67	20.0	3763	3100	1.2	5	Planar
H-3	3.33	20.0	6667	900	7.4	35	Curved
H-4	8.33	20.0	16667	70	238.1	80	Curved
SL-1	1.67	97.7	16283	500	32.6	65	Curved
SL-2	0.17	97.7	1628	3200	0.5	3	Planar
SL-3	0.08	97.7	814	14000	0.06	0 - 70	Curved
SH-1	1.67	586.8	97800	700	139.7	75	Curved
SH-2	0.17	586.8	9780	4400	2.2	25	Almost Planar

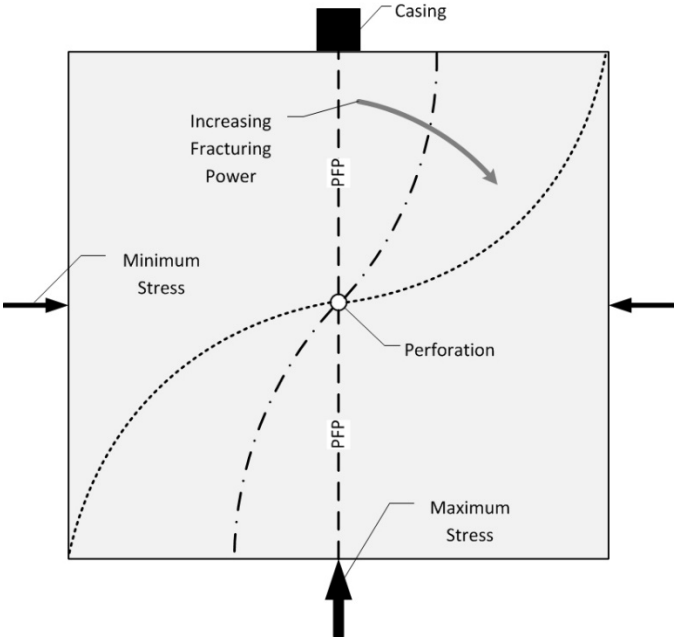

Figure 9: A schematic of the fracture initiation angle and propagation geometry in response to variation in the fracturing power.

A graph of fracture initiation angle versus fracturing power shows that there is a linear relationship between these two parameters on a semi-log plot (Figure 10). Such relationship could introduce the following general equation;

$$\lambda = a \log P_f + b \qquad (7)$$

where λ is the initiation angle, P_f is the fracturing power, and a and b are the constants of the equation, that may depend on sample's properties and the applied principal stresses. Further experiments and analysis are required to justify this equation and to include the effects of fracturing power on the fracture propagation curvature, because the curvature of the fracture appears to be closely related to its initiation angle.

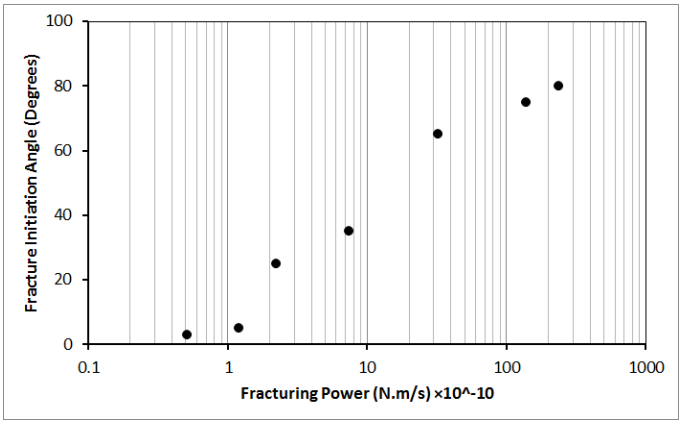

Figure 10: The relationship between the fracture initiation angle and the fracturing power.

It should be noted that test SL-3 had the lowest fracturing power of 0.06×10^{-10} N.m/s; however in this test a single fracture was not developed. The injection flow rate was as low as 0.05 cc/min; such low flow rate which was applied to a high viscous fracturing fluid (97.7 Pa.s) resulted in very long pressurization time (14000 s). Consequently, a very low fracturing power was supplied to the sample, which led to multiple fracturing over the course of wellbore pressurization. This is in good agreement with the results obtained in the experimental study conducted by Van de Ketterij [14]; while they only considered the product of injection flow rate and viscosity and did not indicate the influence of fracturing power. Therefore, test SL-3 is the only test that appears not following the relationship between the fracturing power and the fracture propagation geometry, and this is due to very low power that led to multiple fracturing.

Casing Effect

As it was mentioned earlier, in most of the tested samples, the fractures were initiated form the perforations in an angle with respect to vertical plane (PFP). Then the tip of the fracture turned towards the

PFP in some distance away from the wellbore wall. The fracturing power is now believed to be the main reason for the curvature of the fractures; however, the existence of the casing also played an important role. The steel casing has different elastic moduli with respect to synthetic sample; generally the elastic Young's modulus of the casing is larger than that of the sample.

Therefore, if one compares a pressurized open wellbore with a pressurized cased wellbore, assuming that both of them are at the same pressure; the open wellbore would experience larger radial stress on the wellbore wall. This is due to the fact that when the casing is pressurized, the whole fluid pressure would not be transferred to the surrounding wellbore's material because casing would have less radial displacement in comparison to the open wellbore [19]. As a result, less radial stress would be transferred to the wellbore wall. Lower radial stress would accordingly lead to higher tangential stress. So the casing can affect the wellbore and accordingly the perforation stress distribution. Consequently, the fracture initiation and break down pressures would be affected.

Authors have previously conducted some fracturing experiments on the same synthetic samples [32]; however, in the previous study there was no casing and the perforations were drilled in the openhole. It is noteworthy that the diameter of the perforations in the aforementioned study was 2 mm larger than the current study. However, based on the elastic stress distribution equation for the analysis of the stress profile around a circular cavity[31], the radius of the perforation does not have an effect on its stress distribution. Therefore, the results of the two experimental studies could be compared with each other.

A comparison between the fracture initiation and break down pressures of the planar fracture in this study with those of similar fracture geometries in the previous study reveals that the existence of the casing has significantly increased the fracturing pressures. As an example, in test SL-2, where a planar vertical fracture was propagated, the fracture initiation and break down pressure were 17.44 MPa and 18.19 MPa respectively. Similar planar vertical fracture geometry in the previous study (test 2-3 in [32]) was developed at an initiation pressure of 6.89 MPa and the corresponding break down pressure was 7.62 MPa. This comparison clearly illustrates the impact of the casing on wellbore and perforation stress distributions, and consequently the increase in the fracturing pressures.

6. CONCLUSIONS

In order to analyze the fracturing pressure-time curves a new methodology is introduced in this study to predict the fracture propagation time directly from the pressure-time curves. This has helped to indicate the time at which the fracture tip reached the boundary of the sample, and accordingly the rest of the pressure data after this time would be considered as representing the flow of the fracturing fluid through the propagated fracture. Therefore, this methodology could improve the results' interpretations.

Experimental results demonstrated that as the product of viscosity and injection flow rate increases, higher fracture initiation and break down pressure would be recorded. This product value has the same dimension as energy; therefore, it is considered to represent an energy term, named as fracturing energy. Hence, as the fracturing energy increases the fracturing pressures would increase accordingly.

Nevertheless, it was observed that the fracture initiation angle and near wellbore propagation geometry may not be directly related to fracturing energy. Therefore, a new parameter has been introduced by dividing the fracturing energy by the wellbore pressurization time, named as fracturing power (Eq.6). It is observed that as the fracturing power rises, the fracture initiation angle increases and a more curved fracture plane would be propagated.

It is also observed that casing has a significant effect on the wellbore and perforation stress distribution. As a result, larger fracture initiation and break down pressures would be expected in a cased perforated completion, in comparison to a perforated openhole wellbore. Additionally, casing would cause a vertical fracture to deviate from the wellbore and propagate in a curved path toward the PFP.

The strength properties of the cement sheath play an important role in the hydraulic fracturing mechanism in a cased perforated wellbore. Low shear strength cement sheath may result in creation of micro-annulus. Accordingly, the hydraulic fracture would propagate in the annulus between the casing and the wellbore wall, and as a result the wellbore pressure would decrease and consequently there would be no or little chance of the creation of hydraulic fracture in the formation.

7. REFERENCES

1. Aud, W., et al. *The effect of viscosity on near-wellbore tortuosity and premature screenouts*. in *SPE Annual Technical Conference and Exhibition*. 1994.

2. Cleary, M., et al. *Field implementation of proppant slugs to avoid premature screen-out of hydraulic fractures with adequate proppant concentration*. in *Low Permeability Reservoirs Symposium*. 1993.

3. Davidson, B., et al. *Analysis of abnormally high fracture treating pressures caused by complex fracture growth*. in *SPE Gas Technology Symposium*. 1993.
4. Lehman, L. and J. Brumley. *Etiology of multiple fractures*. in *SPE Production Operations Symposium*. 1997.
5. Abass, H., J. Brumley, and J. Venditto. *Oriented perforations-a rock mechanics view*. in *SPE Annual Technical Conference and Exhibition*. 1994.
6. Behrmann, L. and J. Elbel, *Effect of perforations on fracture initiation.* Journal of Petroleum Technology, 1991. **43**(5): p. 608-615.
7. Atkinson, C. and D. Eftaxiopoulos, *Numerical and analytical solutions for the problem of hydraulic fracturing from a cased and cemented wellbore.* International journal of solids and structures, 2002. **39**(6): p. 1621-1650.
8. Behrmann, L. and K. Nolte, *Perforating requirements for fracture stimulations.* SPE Drilling & Completion, 1999. **14**(4): p. 228-234.
9. Fallahzadeh, S.H., S.R. Shadizadeh, and P. Pourafshary. *Dealing with the challenges of hydraulic fracture initiation in deviated-cased perforated boreholes*. in *Trinidad and Tobago Energy Resources Conference*. 2010.
10. Gulrajani, S.N. and J. Romero. *Evaluation and modification of fracture treatments showing near-wellbore effects*. in *European Petroleum Conference*. 1996. Society of Petroleum Engineers.
11. Hossain, M., M. Rahman, and S. Rahman, *Hydraulic fracture initiation and propagation: roles of wellbore trajectory, perforation and stress regimes.* Journal of Petroleum Science and Engineering, 2000. **27**(3): p. 129-149.
12. Romero, J., M. Mack, and J. Elbel. *Theoretical model and numerical investigation of near-wellbore effects in hydraulic fracturing*. in *SPE Annual Technical Conference and Exhibition*. 1995.
13. Daneshy, A., *Experimental investigation of hydraulic fracturing through perforations.* Journal of Petroleum Technology, 1973. **25**(10): p. 1201-1206.
14. van de Ketterij, R.G., *Optimisation of the near-wellbore geometry of hydraulic fractures propagating from cased perforated completions*. 2001.
15. Van Ketterij, R. and C. De Pater, *Impact of perforations on hydraulic fracture tortuosity.* SPE production & facilities, 1999. **14**(02): p. 117-130.
16. Perkins, T. and J. Weingarten. *Stability and Failure of Spherical Cavities in Unconsolidated Sand and Weakly Consolidated Rock*. in *SPE Annual Technical Conference and Exhibition*. 1988. Society of Petroleum Engineers.
17. Sarmadivaleh, M. and V. Rasouli, *Test Design and Sample Preparation Procedure for Experimental Investigation of Hydraulic Fracturing Interaction Modes.* Rock Mechanics and Rock Engineering, 2014: p. 1-13.
18. Mindess, S., J.F. Young, and D. Darwin, *Concrete*. 2003.
19. Fallahzadeh, S. and V. Rasouli. *The Impact of Cement Sheath Mechanical Properties On Near Wellbore Hydraulic Fracture Initiation*. in *ISRM International Symposium-EUROCK 2012*. 2012. International Society for Rock Mechanics.
20. Rasouli, V., *A true triaxial stress cell (TTSC) used for simulations of real field operations in the lab.* True triaxial testing of rocks, 2012. **4**: p. 311.
21. Min, S., S. Sastry, and V. Balasubramaniam, *Compressibility and density of select liquid and solid foods under pressures up to 700MPa.* Journal of food engineering, 2010. **96**(4): p. 568-574.
22. Bunger, A.P., *Near-surface hydraulic fracture*. 2005, University of Minnesota, 2005. Major: Geological engineering.
23. De Pater, C., et al., *Experimental verification of dimensional analysis for hydraulic fracturing.* SPE Production and Facilities (Society of Petroleum Engineers);(United States), 1994. **9**(4).
24. Weijers, L., *The near-wellbore geometry of hydraulic fractures initiated from horizontal and deviated wells.* 1995.
25. Lhomme, T.P.Y., *Initiation of hydraulic fractures in natural sandstones*. 2005, Delft University of Technology.

26. Mack, M.G. and N. Warpinski, *Mechanics of hydraulic fracturing*, in *Reservoir Stimulation*. 2000. p. 6-1.
27. Detournay, E., *Propagation regimes of fluid-driven fractures in impermeable rocks.* International Journal of Geomechanics, 2004. **4**(1): p. 35-45.
28. Sarmadivaleh, M., *Experimental and Numerical Study of Interaction of a Pre Existing Natural Interface and an Induced Hydraulic Fracture*, in *Petroleum Engineering*. 2012, Curtin University.
29. Bourgoyne, A.T., et al., *Applied drilling engineering.* 1986.
30. Nelson, E.B., *Well cementing*. 1990: Elsevier Science.
31. Fjar, E., et al., *Petroleum related rock mechanics*. Vol. 53. 2008: Elsevier.
32. Fallahzadeh, S., V. Rasouli, and M. Sarmadivaleh, *An Investigation of Hydraulic Fracturing Initiation and Near-Wellbore Propagation from Perforated Boreholes in Tight Formations.* Rock Mechanics and Rock Engineering: p. 1-12.